DOCTORAL THESIS

Presented to the Department of Pharmacy,
Graduate School of Pharmaceutical Science

The University of Naples Federico II
For the Degree of

DOCTOR OF PHILOSOPHY

CORE-SHELL SUSTAINED
RELEASE NANOSYSTEMS FOR THE INTRAVENOUS
DELIVERY OF ANTICANCER DRUGS

by

CLAUDIA CONTE

APPROVED BY

Supervisor: Fabiana Quaglia, PhD
PhD Program Coordinator: Maria Valeria D'Auria, PhD

University of Naples Federico II, Naples, Italy
April, 2013

RINGRAZIAMENTI

Ed eccoci giunti ad un altro traguardo…

Non potevano mancare i ringraziamenti…

Il primo e più grande ringraziamento và alla professoressa Quaglia, che mi ha consentito di iniziare questo cammino meraviglioso, trasmettendomi giorno dopo giorno l'amore e la passione per la ricerca. La ringrazio particolarmente per avermi continuamente stimolata ed avermi dato la possibilità di fare tante esperienze formative che mi hanno arricchita non solo scientificamente ma anche personalmente.

L'Associazione Italiana per la Ricerca sul Cancro che ha finanziato il mio Dottorato di Ricerca e ha reso possibile tutte le sperimentazioni.

A tutto il gruppo di Tecnologia Farmaceutica con il quale ho lavorato, in particolare a Francesca Ungaro che è stata una seconda guida per me, sempre disponibile e pronta ad aiutarmi.

Ringrazio i ragazzi ed i professori dell'Università di Santiago de Compostela, María José Alonso, Marcos Garcia-Fuentes, Noemi Csaba e Maria de la Fuente, che mi hanno ospitata nei loro laboratori facendomi sentire a casa e dandomi l'opportunità di seguire un progetto di ricerca eccezionale.

Ringrazio tutti coloro che hanno collaborato con me per portare avanti la nostra ricerca, il Dott. Mazzaglia, il Dott. Arra, il Prof. Maglio e la Prof. Ianaro. In particolare Pasquale Tirino, Giuseppe Palma, Antonio Barbieri ed Elisa Panza che mi hanno insegnato che la ricerca non si fà da sola, ma ha bisogno di persone unite dallo stesso spirito investigativo per poter raggiungere dei risultati importanti.

Tutti i dottorandi come me, i ricercatori ed i professori che ho conosciuto alle scuole dottorali ed ai congressi, che hanno contribuito ad ampliare la mia conoscenza scientifica, trasmettendomi l'energia e la curiosità giusta per continuare il mio percorso.

I miei *Amici*-colleghi di laboratorio che hanno lavorato al mio fianco ogni singolo giorno di questi anni diventando a poco a poco la mia famiglia. Con loro ho imparato il significato di lavorare *in gruppo!*

Concetta, tu mi hai trasmesso le basi di questo lavoro ed insegnato i primi trucchi del mestiere!! Senza di te il dottorato non lo avrei mai sognato!

Ivana, sei stata e continui ad essere il mio modello da seguire! Ne devo fare ancora di strada per diventare brava come te!!

Ovidio, tu mi hai aiutata tantissimo! Sei stato il mio punto di riferimento in tanti momenti e senza di te questi anni sarebbero stati molto più complicati! Quando non c'eri in laboratorio, non solo la scienza si fermava, ma mi sentivo sola! Burbero come un orso ma sono riuscita anche a rubarti qualche abbraccio!

Giusy… bhè non ci sono parole… anche se sei in un altro continente ti sento sempre accanto a me!

I miei studenti, Valentina, Annalisa, Francesco, Gabriella ed Elisabetta che mi hanno seguita, sostenuta e talvolta anche ammirata. Spero con il cuore di aver contribuito alla vostra crescita e trasmesso l'importanza di ciò che stavamo imparando insieme! In particolare Gabriella che in questi ultimi mesi mi hai incoraggiata ed aiutata moralmente nella scrittura di questa tesi…. Senza di te non sarebbe stato facile concentrarmi!

A tutti i ragazzi che in questi anni sono stati in laboratorio che in un modo o nell'altro hanno arricchito le mie giornate!

Alle mie amiche italo-spagnole, Elisa, Angela, Sofia, Virgina ed Anna, che hanno reso la mia ricerca estera indimenticabile.

Ai miei amici di sempre, Davide, Francesca, Carmine, Luca e Francesco che mi hanno incoraggiata e spronata a non mollare mai in tanti momenti difficili.

Alla mia famiglia per aver creduto sempre in me ed accompagnata anche verso questo traguardo…

Tutti voi avete contribuito a rendere questa fantastica esperienza possibile ed indimenticabile!

Grazie a tutti!

<div align="right">Claudia Conte</div>

TABLE OF CONTENTS

ABCG2	ATP-binding cassette sub-family G member 2
AK	Actinic keratosis
AIF	Apoptosis-inducing factor
ALA	Aminolevulinic acid
AlPcS	Sulfonated aluminium phthalocyanines
ALPcTS	Chloroaluminum-tetrasulfophthalocyanine
AMD	Age-related macular degeneration
AP-1	Activator protein 1
AT-II	Angiotensin II
ATMPn	9-Acetoxy-2,7,12,17-tetrakis-(-methoxyethyl)-porphycene
AUC	Area under the curve
BCC	Basal Cell Carcinoma
BSA	Bovine Serum Albumin
BPD-MA	Benzoporphyrin derivative monoacid ring A
CAM	Chorioallantoic membrane
CDAMPs	Cell death-associated molecular patterns
COX-2	Cyclooxygenase-2
DAMPs	Damage-associated molecular patterns
DCs	Dendritic cells
DSPE	Distearoyl-phosphatidyl ethanolamine
DTX	Docetaxel
EGFR	Epidermal growth factor receptor
EPR	Enhanced Permeability and Retention Effect
ER	Endoplasmic reticulum
ERK	Extracellular signal-regulated kinases
FGR	Fluorescence-guided resection
FRET	Fluorescence resonance energy transfer
HIF	Hypoxia-inducible factor
Hp	Hematoporphyrin
HpD	Hematoporphyrin derivate
HPPH	2-(1hexyloxyethyl)-2 devinylpyropheophorbide-alpha
HSP	Heat shock proteins
ICAM	Intracellular cell adhesion molecule
ICG	Indocyanine green
IFN	Interferons
IL	Interleukin

1

MAPK	Mitogen-activated protein kinase
MDR	Multiple drug resistance
MeSo	Melting-sonication
MMPs	Metalloproteinases
MOMP	Mitochondria outer membrane permeabilization
MPM	Malignant pleural mesothelioma
MPS	Mononuclear phagocytic system
NF-κB	Nuclear factor κB
NPe6	Mono-L-aspartyl-chlorin e6
NP	Nanoparticle
Nrf 2	Nuclear factor-like 2
NSCLC	Non-small cell lung cancer
PAA	Poly(acrylic acid)
PCL	Poly(ε−caprolactone)
PD	Photodetection
PDLLA	Poly(D,L-lactide)
PDT	Photodynamic therapy
PEG	Poly(ethyleneglycol)
PGA	Poly(glycolide)
PLA	Poly(lactide)
PLGA	Poly(lactic-co-glycolic acid)
PS	Photosensitizing agent
PSMA	Prostate-specific membrane antigen
QD	Quantum dots
RCT	Randomized controlled trial
RES	Reticuloendothelial system
RIP	Receptor interacting protein
ROS	Reactive oxygen species
SCC	Squamous cell carcinoma
siRNA	Small interfering RNA
SnET$_2$	Tin ethyl etiopurpurin
SOD	Superoxide dismutase
THPC	Tetrakis(hydroxymethyl)phosphonium chloride
THPP	Tetra(hydroxyphenyl) chlorin
TLR	Toll-like receptor
TMPyP	Tetra(p-toluenesulfonate)

TNF	Tumour necrosis factor
TP	Two-photon
TPPS	Tetrasodium-meso-tetraphenylporphinesulfonate
VCAM	Vascular cell adhesion molecule
VEGF	Vascular endothelial growth factor
ZnPc	Zinc (II) phthalocyanine
$ZnPcS_4$	Tetrasulfonated zinc phthalocyanine

BACKGROUND

Over the past two decades enormous progress in the comprehension of the pathogenesis of cancer has been made. Cancer is a lethal disorder characterized by the development of abnormalities in cells causing uncontrollable and fast growth and division due to a combination of mutagenic stages. As a consequence of these mutations, cancer cells get a battery of specific properties such as limitless proliferation potential, self-sufficiency in growth signals and resistance to growth inhibitory signals, as well as evasion from apoptotic cues, which, in a normal situation, would contain their growth. Besides, tumors have developed diverse methods to attain further support through interactions with surrounding stromal cells, promoting their angiogenesis, tissue invasion and metastasis to distant organs, along with evasion from immune detection.

To date, the most common therapies in the fight against cancer are radiotherapy and chemotherapy. Although many advances have been achieved in conventional treatments, bioaccessibility of these drugs to tumor tissue is limited, large doses are required, leading to high toxicity to normal cells along with an increased incidence of MDR. Therefore, there has been an enormous interest in the research of more efficient therapeutic strategies that has prompted toward the development of novel cancer therapies over recent years.

Nanotechnology offers a great opportunity in cancer treatment based on the concept that a drug formulated in NPs can alter its pharmacokinetics enhancing the treatment ability to target and kill cells of diseased tissues/organs while affecting as few healthy cells as possible. Depending on the properties of the carrier, large variations in drug pharmacokinetics with major clinical implications may occur. In particular, sterically stabilized nanocarriers with a biomimetic coating (stealth nanocarriers) show an increased blood circulation and potential to accumulate predominantly in pathological sites with compromised leaky vasculature. Defective vascular architecture coupled with poor lymphatic drainage is common to many kinds of solid tumors and has been exploited to promote drug accumulation in tumor site (the so-called "EPR effect"). The further development of the concept of pharmaceutical biomimetic nanocarriers implies exploitation of differences between cancer and normal cells. Surface engineering of nanocarriers with specific ligands able to interact with cell surface structures overexpressed in cancer cells (particular antigens, peptide receptors, folate, transferring and integrin surface receptors) or tumor vasculature is a fascinating option for improving the specificity of anticancer treatments. Another advantage of the NP-based approach relies on the prolongation of drug half-life in the circulation and at target site, which could in theory reduce the number of administrations with consequent improvement

7

of the patient compliance. It has been suggested also that drug accumulation and slow release inside tumor cells can be useful to circumvent MDR. With the aim to increase treatment efficacy, combination chemotherapy has long been adopted as the standard of care against many cancer types. It is generally acknowledged that through the proper drug combination the treatment can promote synergistic actions, improve target selectivity and reduce the development of MDR.

PDT has emerged as a popular adjuvant therapy for cancer and has been approved as a primary treatment option for certain neoplastic conditions including inoperable esophageal tumors, head and neck cancers, and microinvasive endo-bronchial non-small cell lung carcinoma. PDT is also being investigated in preclinical and clinical studies for other cancer types including breast, prostate and ovarian cancers. PDT aims at selectively targeting neoplastic lesions by the combined action of a PS and visible light, which generally produces reactive oxygen species (mainly singlet oxygen). Selectivity is achieved partly by the accumulation of the PS in the malignant cells/tissue, and partly by restricting the application of the incident light to the desired area. PDT offers various treatment options in cancer management and has been used for localized superficial or endoluminal malignant and premalignant conditions. Its application has also been recently expanded to solid tumors. At present, regulatory approval for PDT has been obtained for selected tumors using for example Photofrin®, Foscan®, Levulan® and most recently Metvix®. There are several technical issues hampering the application of PDT in a wide range of diseases. First it is a difficult undertaking to prepare pharmaceutical formulations that enable parenteral administration of PS since most of them are hydrophobic and aggregate easily under physiological conditions. Secondly, the selective accumulation to diseased tissues is often not high enough for clinical use. In order to improve photodynamic-based treatments, several combination regimens, in which PDT has been associated with both traditional and innovative therapeutic approaches for cancer treatment have been proposed to increase the therapeutic effectiveness and to eradicate completely the tumor.

CHAPTER 1: INTRODUCTION

1.1 Nanotechnology in biomedical field

Nanotechnology is defined by the National Nanotechnology Initiative (http://www.nano.gov) as research and technology development at the atomic, molecular, or macromolecular scale leading to the controlled creation and use of structures, devices, and systems with a length scale of approximately 100 nm (Figure 1).
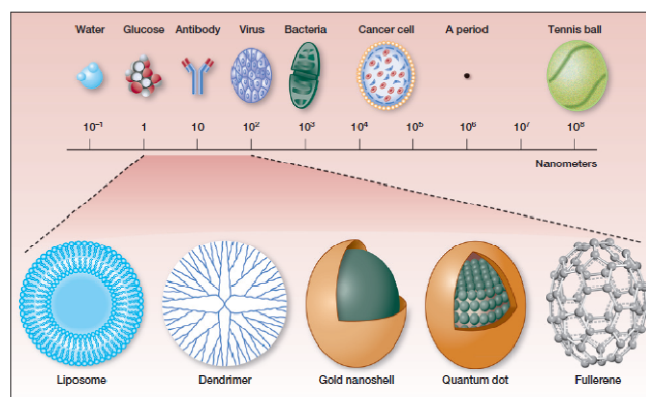
Figure 1. Examples of nanotechnology platforms used in drug development[1].

The term "nanomedicine" refers to the application of nanotechnologies to the biomedical field for controlled drug delivery as well as for diagnostic purposes. In the past 30 years, the explosive growth of nanotechnology has burst into challenging innovations in pharmacology, which is in the process of revolutionizing the delivery of biologically active compounds. Thus, several reviews aimed to analyze and to discuss the impact of nanotechnology in pharmacology to improve treatments of various diseases considered as the major health threats (cancer, infections, metabolic diseases, etc.) have been published [2,3,4,5,6,7,8,9]. Treatments of these severe diseases generally involve

---

[1]W. C. Zamboni, V. Torchilin, A. K. Patri, J. Hrkach, S. Stern, R. Lee, A. Nel, N. J. Panaro, and P. Grodzinski, "Best practices in cancer nanotechnology: perspective from NCI nanotechnology alliance," *Clin.Cancer Res.* 18, no. 12 (2012).

[2]S. Bamrungsap, Z. Zhao, T. Chen, L. Wang, C. Li, T. Fu, and W. Tan, "Nanotechnology in therapeutics: a focus on nanoparticles as a drug delivery system," *Nanomedicine.(Lond)* 7, no. 8 (2012).

[3]P. Couvreur and C. Vauthier, "Nanotechnology: intelligent design to treat complex disease," *Pharm.Res.* 23, no. 7 (2006).

[4]T. L. Doane and C. Burda, "The unique role of nanoparticles in nanomedicine: imaging, drug delivery and therapy," *Chem.Soc.Rev.* 41, no. 7 (2012).

[5]O. M. Koo, I. Rubinstein, and H. Onyuksel, "Role of nanotechnology in targeted drug delivery and imaging: a concise review," *Nanomedicine.* 1, no. 3 (2005).

highly toxic compounds for healthy tissues, where the use of traditional pharmaceutical formulations is considerably limited by the occurrence of sometime dramatic side effects.

Currently, several nanosized carriers, made of different materials such as lipids, polymers, metals, inorganic materials have been proposed in the biomedical field as diagnostic and therapeutic tools. In drug delivery technologies, nanocarriers are designed (i) to protect a drug from in vivo degradation; (ii) to enhance drug absorption by facilitating diffusion through epithelium; (iii) to modify pharmacokinetics and drug tissue distribution profile; (iv) to improve intracellular penetration and subcellular distribution. Furthermore, surface modification of pharmaceutical nanocarriers is normally used to control their biological fate in a desirable fashion and touse them simultaneously as therapeutic or diagnostic platform (theranostics). The most important results of such modification include an increased stability and half-life of nanocarriers in the circulation, passive or active targeting into the required pathological zone, responsiveness to local physiological stimuli such as pathology-associated changes in local pH and/or temperature, and ability to serve as imaging/contrast agents for various imaging modalities.

1.1.1 Nanocarriers as an emerging platform for cancer therapy

Cancer is a major cause of mortality: more than ten million people are diagnosed with the disease annually. Cancer is known to develop via a multistep carcinogenesis process entailing numerous cellular physiological systems, making it a highly incomprehensible and complex disease[10,11]. Initially, cancers start as localized diseases, but they are prone to spread to distant sites within the body, which makes cancers still incurable in several occasions.

---

[6]Y. Liu, H. Miyoshi, and M. Nakamura, "Nanomedicine for drug delivery and imaging: a promising avenue for cancer therapy and diagnosis using targeted functional nanoparticles," *Int.J.Cancer* 120, no. 12 (2007).

[7]J. Paradise, G. M. Diliberto, A. W. Tisdale, and E. Kokkoli, "Exploring emerging nanobiotechnology drugs and medical devices," *Food Drug Law J.* 63, no. 2 (2008).

[8]R. A. Petros and J. M. Desimone, "Strategies in the design of nanoparticles for therapeutic applications," *Nat.Rev.Drug Discov.* 9, no. 8 (2010).

[9]S. K. Sahoo and V. Labhasetwar, "Nanotech approaches to drug delivery and imaging," *Drug Discov.Today* 8, no. 24 (2003).

[10]A. Gupta, P. Avci, M. Sadasivam, R. Chandran, N. Parizotto, D. Vecchio, W. C. de Melo, T. Dai, L. Y. Chiang, and M. R. Hamblin, "Shining light on nanotechnology to help repair and regeneration," *Biotechnol.Adv.* (2012).

[11]A. Juarranz, P. Jaen, F. Sanz-Rodriguez, J. Cuevas, and S. Gonzalez, "Photodynamic therapy of cancer. Basic principles and applications," *Clin.Transl.Oncol.* 10, no. 3 (2008).

More harrowing is the fact that several significant achievements towards the treatment of the disease have failed to profoundly impact patient survival. The last century witnessed the maturation of chemotherapy as a viable, adjuvant therapeutic modality for the treatment of cancer. An enhanced understanding of the underlying mechanisms of tumorigenesis bursted the discovery and development of highly specific agents capable of exerting their effects on individual proteins or pathways either overexpressed or aberrant within tumors.

Despite many advances in conventional treatment options such as chemotherapy, surgery and radiation, cancer therapy is still far from optimal because it is plagued by some drawbacks. Frequent challenges encountered by current cancer therapies include non specific systemic distribution of antitumor agents, inadequate drug concentrations reaching the tumor site, limited ability to monitor therapeutic responses and development of MDR. These sobering facts indicate that to make further progress, it is necessary to put an emphasis on other existing but still under appreciated therapeutic approaches.

An increased interest is being focused on nanotechnological approaches in cancer treatment based on the concept that pharmacokinetics of an anticancer drug can be usefully altered in the body to promote drug accumulation predominantly in pathological sites[12,13,14]. Such a strategy is aimed to improve the treatment ability to target and to kill cells of diseased tissues/organs while affecting as few healthy cells as possible. Several reviews, indeed, have focused on the potential of nanotechnology in cancer and discussed how different nanoparticulate drug-delivery systems perform in this field[15,16,17,18,19,20,21,22,23,24,25].

[12]J. R. Heath and M. E. Davis, "Nanotechnology and cancer," *Annu.Rev.Med.* 59 (2008).

[13]K. K. Jain, "Advances in the field of nanooncology," *BMC.Med.* 8 (2010).

[14]D. Peer, J. M. Karp, S. Hong, O. C. Farokhzad, R. Margalit, and R. Langer, "Nanocarriers as an emerging platform for cancer therapy," *Nat.Nanotechnol.* 2, no. 12 (2007).

[15]Z. Gao, L. Zhang, and Y. Sun, "Nanotechnology applied to overcome tumor drug resistance," *J.Control Release* 162, no. 1 (2012).

[16]N. T. Huynh, E. Roger, N. Lautram, J. P. Benoit, and C. Passirani, "The rise and rise of stealth nanocarriers for cancer therapy: passive versus active targeting," *Nanomedicine.(Lond)* 5, no. 9 (2010).

[17]C. L. Waite and C. M. Roth, "Nanoscale drug delivery systems for enhanced drug penetration into solid tumors: current progress and opportunities," *Crit Rev.Biomed.Eng* 40, no. 1 (2012).

[18]M. Talekar, J. Kendall, W. Denny, and S. Garg, "Targeting of nanoparticles in cancer: drug delivery and diagnostics," *Anticancer Drugs* 22, no. 10 (2011).

[19]E. C. Dreaden, L. A. Austin, M. A. Mackey, and M. A. El-Sayed, "Size matters: gold nanoparticles in targeted cancer drug delivery," *Ther.Deliv.* 3, no. 4 (2012).

[20]H. Zhang, "Multifunctional nanomedicine platforms for cancer therapy," *J.Nanosci.Nanotechnol.* 12, no. 5 (2012).

[21]S. P. Egusquiaguirre, M. Igartua, R. M. Hernandez, and J. L. Pedraz, "Nanoparticle delivery systems for cancer therapy: advances in clinical and preclinical research," *Clin.Transl.Oncol.* 14, no. 2 (2012).

[22]M. Tiwari, "Nano cancer therapy strategies," *J.Cancer Res.Ther.* 8, no. 1 (2012).

The therapeutic effects of many anticancer drugs could be significantly improved if delivery of the drug occurs specifically to tumors (cancer cells) or preferably inside specific organelles inside cells and reduction of drug toxic side effects is achieved. In so doing, a multifunctional construct based on novel nanomaterials can be delivered directly to the tumor site and eradicate cancer cells selectively. An appropriate design allows nanoconstruct to improve drug efficacy (activity at lower doses) as compared with the free-drug treatment, which in turn gives a wider therapeutic window and lower side effects. Furthermore, NP carriers are also capable of addressing several drug delivery problems, which could not be effectively solved in the past and include overcoming MDR phenomenon and penetrating cellular barriers that may limit device accessibility to intended targets, such as the blood–brain barrier, among others.

There has been intense interest in identifying NP characteristics that are best suited for oncology applications. Pharmacokinetics of the NPs is crucial and depends on several physiochemical characteristics of the carrier such as size, surface charge, shape, nature and density of coating, composition, stability, steric stabilization, deformability, dose and route of administration[26,27].

Regarding their composition and structure, nanocarrier platforms for cancer can be categorized as organic-based, inorganic-based or a hybrid combination of the aforementioned. Organic nanoplatforms include polymeric nanocarriers, lipid-based nanocarriers (e.g., liposomes and nanoemulsions), dendrimers, and carbon-based nanocarriers (e.g., fullerenes and carbon nanotubes). Inorganic nanoplatforms include metallic nanostructures, silica NPs, and QDs.

1.1.2 *Polymeric nanomedicines for cancer*

Over the past few decades, several polymer-based nanocarriers have been developed as effective drug delivery devices[28]. The drug of interest is either dissolved, entrapped, adsorbed, covalently attached or encapsulated in the

---

[23]C. Heneweer, S. E. Gendy, and O. Penate-Medina, "Liposomes and inorganic nanoparticles for drug delivery and cancer imaging," *Ther.Deliv.* 3, no. 5 (2012).

[24]R. Misra, S. Acharya, and S. K. Sahoo, "Cancer nanotechnology: application of nanotechnology in cancer therapy," *Drug Discov.Today* 15, no. 19-20 (2010).

[25]S. Kolhe and K. Parikh, "Application of nanotechnology in cancer: a review," *Int.J.Bioinform.Res.Appl.* 8, no. 1-2 (2012).

[26]M. Wang and M. Thanou, "Targeting nanoparticles to cancer," *Pharmacol.Res.* 62, no. 2 (2010).

[27]S. E. Gratton, P. A. Ropp, P. D. Pohlhaus, J. C. Luft, V. J. Madden, M. E. Napier, and J. M. Desimone, "The effect of particle design on cellular internalization pathways," *Proc.Natl.Acad.Sci.U.S.A* 105, no. 33 (2008).

[28]A. Lamprecht, N. Ubrich, H. Yamamoto, U. Schafer, H. Takeuchi, P. Maincent, Y. Kawashima, and C. M. Lehr, "Biodegradable nanoparticles for targeted drug delivery in treatment of inflammatory bowel disease," *J.Pharmacol.Exp.Ther.* 299, no. 2 (2001).

nanocarrier. The advantages of using polymer-based nanocarriers for drug delivery result from their two main basic properties. First, the use of biodegradable materials for nanocarrier preparation allows an improved stability in the body and sustained drug release within the target site over a period of days or even weeks. Second, because of their small size, nanocarrier can penetrate through smaller capillaries and be taken up by cells, thus allowing efficient drug accumulation at the target sites.

Biodegradable polymers are materials widely used in the preparation of controlled release systems intended for innovative parenteral dosage forms. Their wide application in this field is due to their extensive degradation by chemical or enzymatic processes in water-soluble low molecular weight compounds that enter the normal metabolic pathways of the organism. Polymeric nanomedicines such as polymeric NPs, polymer micelles, polymersomes and polymer-drug conjugates currently developed for solid tumor treatment have proved to be efficacious cancer therapeutics (Figure 2).
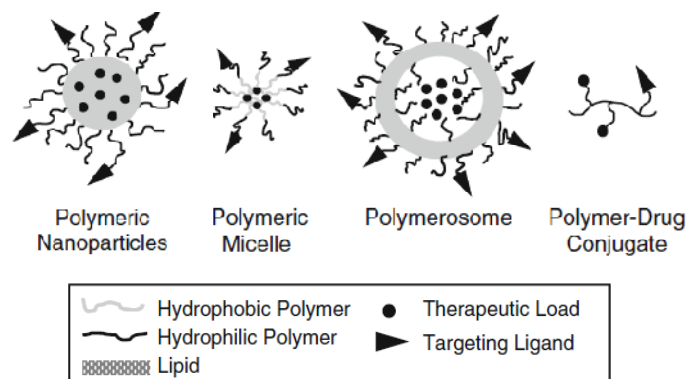
Figure 2. Polymeric nanoplatforms for drug delivery[29].

Polymeric NPs may be defined as colloidal systems generally made of polymers (biodegradable or not). According to the process used for the preparation of NPs, nanospheres or nanocapsules can be obtained (Figure 3).

Nanocapsules differ from nanospheres in that they are vesicular systems with reservoir structure, which is liquid or semisolid at room temperature. In the case of nanocapsules, the core is composed of oil hence allowing a high payload of a hydrophobic drug whereas nanocapsules with an aqueous core

---

[29]F. Alexis, E. M. Pridgen, R. Langer, and O. C. Farokhzad, "Nanoparticle technologies for cancer therapy," *Handb.Exp.Pharmacol.*, no. 197 (2010).

enable to encapsulate water-soluble compounds. Generally, the polymer shell surrounding the liquid core is formed either due to polymerization taking place at the interface between the dispersed and continuous phase of the emulsion or by precipitation of a preformed polymer at the surface of emulsion droplets. Nanospheres are matrix particles, i.e. particles where entire mass is solid. To remain well dispersed in a liquid, NPs, like all types of colloids, need to be stabilized using amphiphilic molecules or colloid protecting agents. Drugs can be either entrapped inside the NPs or adsorbed on their surface.
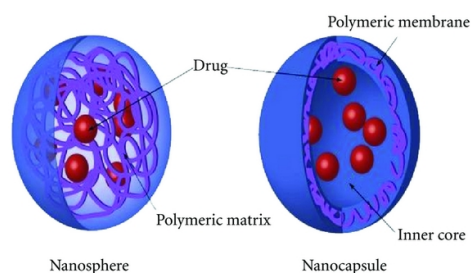
Figure 3. The two main types of polymeric NPs known as nanosphere (matrix system) and nanocapsule (reservoir system) with different drug-loading modalities.

Biodegradable NPs can be prepared from a variety of materials such as proteins, polysaccharides and synthetic biodegradable polymers, depending on many factors such as i) size of the desired NPs, ii) properties of the drug to be encapsulated (aqueous solubility, stability, etc.), iii) surface characteristics and functionality, iv) degree of biodegradability and biocompatibility, and v) drug release profile of the final product. The methods to prepare NPs can be classified in 1) dispersion of preformed polymers, 2) polymerization of monomers and 3) ionic gelation method for hydrophilic polymers. Production of NPs have been recently reviewed in the light of pharmaceutical technology by Benoit et al [30] especially focusing on the formation of NPs on nano-emulsion templates. Today, numerous examples of original methods to form NPs entrapping lipophilic and hydrophilic molecules are available[31,32]. For

---

[30]N. Anton, J. P. Benoit, and P. Saulnier, "Design and production of nanoparticles formulated from nano-emulsion templates-a review," *J.Control Release* 128, no. 3 (2008).

[31]C. Perez, A. Sanchez, D. Putnam, D. Ting, R. Langer, and M. J. Alonso, "Poly(lactic acid)-poly(ethylene glycol) nanoparticles as new carriers for the delivery of plasmid DNA," *J.Control Release* 75, no. 1-2 (2001).

[32]A. Taden, K. Landfester, and M. Antonietti, "Crystallization of dyes by directed aggregation of colloidal intermediates: a model case," *Langmuir* 20, no. 3 (2004).

example, working on the intrinsic solubility and melting point (T_m) of a polymer without the use of an organic solvent, a new method named 'MeSo' has been developed in our laboratories[33]. The method consists in the nano-emulsification of a fluid, non water-miscible copolymer at T >T_m by sonication in water. Cooling at room temperature then hardens the copolymer and, spherical non-aggregated particles are formed.

Micelles are self-assembling nanosized colloidal particles which form spontaneoulsy under certain concentrations and temperatures from amphiphilic or surface-active molecules, which consist of two clearly distinct regions with opposite affinities towards a given solvent. The formation of micelles is driven by the decrease of free energy in the system because of the removal of hydrophobic fragments from the aqueous environment and the re-establishing of hydrogen bond network in water. Hydrophobic segments of amphiphilic molecules form the core of a micelle, while hydrophilic fragments form the micelle shell. When used as drug carriers in aqueous media, micelles solubilize molecules of poorly soluble non polar pharmaceuticals within the micelle core[34]. Micelles based on biodegradable polyesters are now considered as a very promising injectable delivery system.

Polymersomes are polymer-based vesicular shells that form upon hydratation of amphiphilic block copolymers. As the nanocapsules, polymersomes are indeed vesicular systems in which the drug is confined to a reservoir or within a cavity surrounded by a polymer coating. In particular, the core of this vesicle is an aqueous phase while the surrounding coating is a polymer bilayer composed of amphiphilic copolymers. Accurate selection of polymer MW, hydrophilic/hydrophobic ratio and chemistry impart polymersomes with a broad and tunable range of carrier properties. These systems are capable of encapsulating a large range of therapeutically water soluble active molecules and biomolecules, with considerable work being done to engineer the release of those encapsulants at the desired place and time[35].

Finally, polymer–drug conjugates are macromolecular prodrugs where a drug is covalently bound to a water soluble polymeric carrier, normally via a biodegradable linker. Amphiphilic polymer-drug conjugates in aqueous

---

[33]F. Quaglia, L. Ostacolo, Rosa G. De, M. I. La Rotonda, M. Ammendola, G. Nese, G. Maglio, R. Palumbo, and C. Vauthier, "Nanoscopic core-shell drug carriers made of amphiphilic triblock and star-diblock copolymers," *Int.J.Pharm.* 324, no. 1 (2006).

[34]V. P. Torchilin, "Micellar nanocarriers: pharmaceutical perspectives," *Pharm.Res.* 24, no. 1 (2007).

[35]D. E. Discher and F. Ahmed, "Polymersomes," *Annu.Rev.Biomed.Eng* 8 (2006).

solution can form micelles or micelle-like nanoassemblies in which the lipophilic drug is confined in the internal core of the system[36].

1.1.3 Administration routes for nanoparticles

Multiple biological barriers exist for drugs to successfully reach their intended target in the body [37]. Oral drugs need to have high stability in the gastrointestinal tract and the ability to penetrate intestinal epithelium to achieve high systemic bioavailability. Similarly, skin, nasal, and pulmonary drug delivery requires efficient transport of drugs across the epithelium. While most new drug formulations for small molecules are intended for the oral route, with drug chemistry directed towards optimization of absorption extent, intravenous (iv) administration remains the most direct and efficient route to deliver drugs like peptides, proteins, large molecules, and fragments of nucleic acids.

Several nanocarrier systems have been designed and developed as pharmaceutical formulations for different administration routes. For example, significant research has been done using NPs as oral[38] and pulmonary[39] drug delivery vehicles. Oral delivery of peptides and proteins using NPs has been shown to be far superior to the delivery of free drugs in terms of bioavailability, residence time, and biodistribution. The bioavailability of these molecules is limited by the epithelial barriers of the gastrointestinal tract and they may also be susceptible to gastrointestinal degradation by digestive enzymes. For this reason, the advantage of using polymeric NPs is to allow encapsulation of bioactive molecules and protect them against enzymatic and hydrolytic degradation. The administration of small peptides can occur also through the nasal route. This is due to the greater permeability and lower enzymatic activity of the nasal mucosa as compared to the intestinal mucosa. However, as in the case of the oral route, the transport of particles across the nasal epithelium has been considered as a defence event, strictly related to the nose-associated lymphoid tissue. Nevertheless, the activity generated over the last few years in the design of transmucosal drug carriers has led to the conclusion that the surface composition of NPs affects the crossing of the

---

[36]X. Hu and X. Jing, "Biodegradable amphiphilic polymer-drug conjugate micelles," *Expert.Opin.Drug Deliv.* 6, no. 10 (2009).

[37]A. Chrastina, K. A. Massey, and J. E. Schnitzer, "Overcoming in vivo barriers to targeted nanodelivery," *Wiley.Interdiscip.Rev.Nanomed.Nanobiotechnol.* 3, no. 4 (2011).

[38]EP. Herrero , MJ. Alonso , N. Csaba, "Polymer-based oral peptide nanomedicines," *Ther Deliv.* (2012).

[39]F. Ungaro , I. d'Angelo , A. Miro , MI. La Rotonda , F. Quaglia, "Engineered PLGA nano- and micro-carriers for pulmonary delivery: challenges and promises," *J Pharm Pharmacol.*(2012).

epithelium and the intensity of this transport[40]. For example, it was recently demonstrated that chitosan NPs accumulate in the first layers of the epithelium from where they can release their cargo[41].

In the treatment of specific disease, such as cancer, the field of injectable nanocarriers has matured to include a wide range of strategies incorporating many different materials. Taking advantages of the abnormal organization and structure of the tumor vasculature, that will be described in the following, a great part of the research efforts in the field of advanced pharmaceutical technologies were focused on the design of an enormous number of nanoscopic delivery systems for iv administration, in order to improve efficacy and specificity of anticancer treatments.

1.1.4 Injectable nanoparticles for cancer

Injectable nanocarriers have received much attention due to their vast range of structures and ability to contain multiple functional groups, both within the bulk material and on the surface of the particles. In general, an effective nanomedicine should have high therapeutic loading, controlled drug release along with efficient targeting ability. Nevertheless, multiple obstacles must be overcome in order to have an effective injectable drug delivery system[42]. The major challenges include overcoming clearence in the body, increasing cellular uptake into target tissue/cells, and endosomal escape that is especially important for nucleic acid fragments.

1.1.4.1 Elimination by renal clearance and RES

Natural elimination processes include both renal clearance and MPS uptake.

Renal clearance of intravascular agents is a process involving glomerular filtration, tubular secretion and finally elimination of the molecule through urinary excretion. Filtration of particles through the glomerular capillary wall is highly dependent on molecule size and is referred to as the filtration-size threshold. Molecules with a diameter of less than 6 nm are typically filtered, while those more than 8 nm are not typically capable of glomerular filtration[43].

---

[40]N. Csaba , M. Garcia-Fuentes , MJ. Alonso, " Nanoparticles for nasal vaccination,"*Adv Drug Deliv Rev.* (2009).

[41] M. Garcia-Fuentes , MJ. Alonso, "Chitosan-based drug nanocarriers: where do we stand?," *J Control Release.* (2012).

[42]D. M. Webster, P. Sundaram, and M. E. Byrne, "Injectable nanomaterials for drug delivery: Carriers, targeting moieties, and therapeutics," *Eur.J.Pharm.Biopharm.* (2013).

[43]H. S. Choi, W. Liu, P. Misra, E. Tanaka, J. P. Zimmer, Ipe B. Itty, M. G. Bawendi, and J. V. Frangioni, "Renal clearance of quantum dots," *Nat.Biotechnol.* 25, no. 10 (2007).

MPS uptake proceeds quickly and must be avoided in order to have an acceptable circulation time for nanocarrier. The MPS, also referred to as the RES, is the main natural clearance system for particles not filtered by the kidneys acting via phagocytosis. Recognition by the MPS is aided by opsonization, which consists in the binding of blood opsonins to nanocarrier surface thus inducing its phagocytosis and accumulation in the liver (Kuppfer cells). The liver acts as a reservoir toward nanocarriers conditioning their rapid first-phase disappearance from the blood and, in case of biodegradable systems, their second-phase release in the body under degraded and excretable form. This biodistribution can be of benefit for the chemotherapeutic treatment of MPS localized tumors (e.g. hepatocarcinoma or hepatic metastasis arising from digestive tract or gynecological cancers, bronchopulmonary tumors, myeloma and leukemia). Multiple methods have been investigated to avoid opsonin binding, thus increasing circulation time and increasing the carrier's ability to reach its target cell for internalization. Ideally, an injectable NP has to be smaller than 100 nm to avoid internalization by the MPS. The surface charge also helps increase cellular uptake and avoid self-aggregation between NPs, also resulting in lowered MPS recognition (-10 mV to +10 mV). Particles with hydrophobic surfaces, in fact, will preferentially be taken up by the liver, followed by the spleen and lungs, while particles with longer circulation times should be 100 nm or less in diameter and have a hydrophilic surface in order to reduce clearance by macrophages[44].

1.1.4.2   *Long circulating nanocarriers (Stealth)*

In order to overcome the opsonization of nanocarriers, a number of widely used and effective methods have been investigated to make nanocarriers "invisible" to the immune system, creating long-circulating NPs, known also as stealth NPs (Figure 4). Interestingly, by coating the NP surface with hydrophilic polymers, such as PEG, poloxamers, or hydrophilic polysaccharides, it is possible to create a hydrated water barrier that provides good steric hindrance to the attack of phagocytes. Indeed, the presence of such macromolecules allows the prevention of opsonization thanks to this protective hydrophilic and flexible layer, preventing their interaction with blood components[45,46]. Furthermore, a steric stabilization limits also aggregation

---

[44] D. E. Owens, III and N. A. Peppas, "Opsonization, biodistribution, and pharmacokinetics of polymeric nanoparticles," *Int.J.Pharm.* 307, no. 1 (2006).

[45] S. M. Moghimi and J. Szebeni, "Stealth liposomes and long circulating nanoparticles: critical issues in pharmacokinetics, opsonization and protein-binding properties," *Prog.Lipid Res.* 42, no. 6 (2003).

[46] S. M. Moghimi, A. C. Hunter, and J. C. Murray, "Long-circulating and target-specific nanoparticles: theory to practice," *Pharmacol.Rev.* 53, no. 2 (2001).

between particles themselves in the blood and contribute to system stability in biological environments. In so doing, NPs exhibit decreased levels of uptake by the MPS and, consequently, an increased circulation time in the blood, and accumulate in solid tumors passing through their leaky vasculature (*passive targeting*). In particular, it was demonstrated that NPs decorated with PEG can circulate for a longer time as compared to non-pegylated NPs, and normally exhibit a circulation half-life of 2-24h in mice and rats, and as long as 45h in humans. PEGylation simply refers to the decoration of a particle surface by the covalent surface grafting, or adsorption of PEG chains. Some research has directly shown that particles with covalently bound PEG chains exhibit longer blood circulation half-lives than similar particles with only surface adsorbed PEG.

Gref et al[47] were the first to report the advantages of PEGylation on PLGA-PEG NPs, resulting in a substantial increase in blood residence time. The chain length, shape, and density of PEG on the particle surface have been shown to be the main parameters affecting NP surface hydrophilicity and phagocytosis. Most research indicates that a PEG chain with molecular weight of 2000 Da or greater is required to achieve increased MPS-escape. This minimum MW is most likely due to the loss in flexibility of shorter PEG chains. Also, it has been shown that as molecular weight is increased above 2000, the blood circulation half-life of the PEGylated particles is also increased, which may be due in part to the increased chain flexibility of higher MW PEG polymers. In addition to chain molecular weight, surface chain density and conformation are also critical factors to achieve improved stealth characteristics, although these two aspects are much more interrelated [48]. For instance, at low surface coverage, the PEG chains have a larger range of motion and will typically take on what is termed a "mushroom" configuration, where on average they will be located closer to the surface of the particle. Very low surface coverage can also lead to gaps in the PEG protective layer where opsonins can freely bind to the NP surface. On the other hand, at high surface coverage the PEG chains range of motion will be greatly restricted and they will most often exhibit a semi-linear or "brush" configuration. Although a high surface coverage ensures that the entire surface of NP is covered, this method also decreases the mobility of the PEG chains and thus decreases the steric hindrance properties of the PEG

[47] R. Gref , M. Lück , P. Quellec , M. Marchand , E. Dellacherie , S. Harnisch , T. Blunk , RH. Müller, "Stealth' corona-core nanoparticles surface modified by polyethylene glycol (PEG): influences of the corona (PEG chain length and surface density) and of the core composition on phagocytic uptake and plasma protein adsorption," *Colloids Surf B Biointerfaces.* (2000).

[48] S. I. Jeon and J. D. Andrade, "Protein-Surface Interactions in the Presence of Polyethylene Oxide II. Effect of Protein Size," *J. Colloid Interface Sci.* 1991, 142, 159-166.

layer. Interestingly, a threshold of 1-2 nm space between the PEG chains was estimated for minimal protein absorption.
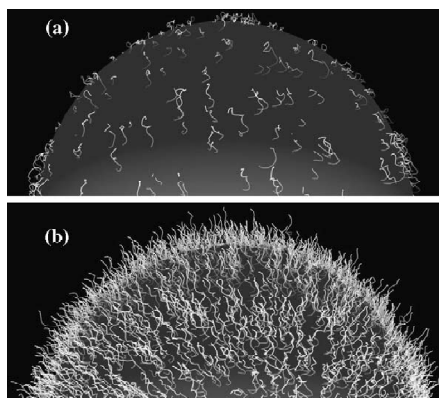
Figure 4. Schematic diagrams of PEG configurations on the upper hemisphere of a polymeric NP. In (a), the low surface coverage of PEG chains leads to the "mushroom" configuration where most of the chains are located closer to the particles surface. In (b), the high surface coverage and lack of mobility of the PEG chains leads to the "brush" configuration where most of the chains are extended away from the surface[49].

1.1.5   Principles of drug targeting to tumors

Ideally, for anticancer drugs to be effective in cancer treatment, they should first (after administration) be able to reach the desired tumor tissues through the penetration of barriers in the body with minimal loss of activity in the bloodstream. Second, after reaching the tumor tissue, drugs should have the ability to selectively kill tumor cells without affecting normal cells and extend their effect along time. These two basic strategies are also associated with improvements in patient survival and quality of life, by simultaneously increasing the intracellular concentration of drugs and reducing dose-limiting toxicities. In principle, NP delivery of anticancer drugs to tumor tissues can be achieved by either passive or active targeting (Figure 5).

Passive targeting refers to the accumulation of a drug or a drug carrier system at a desired site owing to physico-chemical or physiological factors. It takes

---

[49] D.E. Owens III and N.A. Peppas, "Opsonization, biodistribution, and pharmacokinetics of polymeric nanoparticles," *Int. J. Pharm*. 307, no. 1 (2006).

advantage of the size of NPs and the unique properties of tumor vasculature and microenvironment.

For further growth and enlargement, tumors need to form new blood vessels, via the angiogenesis process, in order to obtain nutrients and sustain their growth.
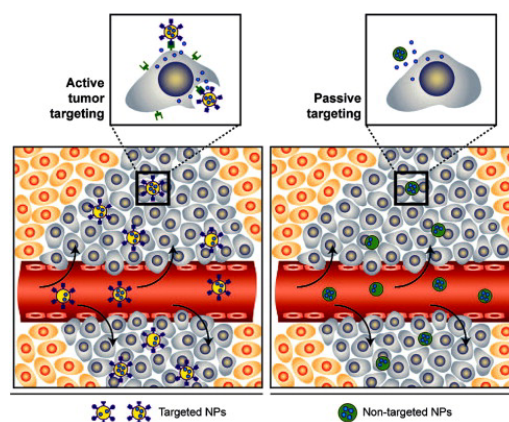
Figure 5. Passive *vs* active targeting. (Right) NPs tend to passively (by their biophysicochemical properties) extravasate through the inflammated vasculature; (Left) Once NPs have extravasated in the target tissue, the presence of targeting ligands (e.g. proteins) on the NP surface can result in active targeting of NPs to receptors that are present on target cell or tissue resulting in enhanced accumulation and cell uptake through receptor-mediated endocytosis[50].

Tumor vessels are generally abnormal and have aberrant branching, blind loops of twisted shape, which are characterized by architectural defectiveness and a high degree of vascular density. The newly formed tumor blood vessels usually present an abnormal architecture too, including defective endothelial cells with wide fenestrations, irregular vascular alignment, lack of a smooth muscle layer or innervation, wide lumen and impaired functional receptors for AT-II. Blood flow behavior, such as direction of blood flow, is also irregular or inconsistent in these vessels. When compared with normal vessels, tumor vessels are "leaky", owing to basement membrane abnormalities and a decreased number of pericytes lining the rapidly proliferating endothelial cells. Indeed, the pore size of tumor vessels varies from 100 nm to almost 1 mm in diameter, depending upon the anatomic location of the tumors and the stage of tumor growth. In comparison, the tight endothelial junctions of normal vessels

---

[50]M. Mahmoudi, S. Sant, B. Wang, S. Laurent, and T. Sen, "Superparamagnetic iron oxide nanoparticles (SPIONs): development, surface modification and applications in chemotherapy," *Adv.Drug Deliv.Rev.* 63, no. 1-2 (2011).

are tipically of 5-10 nm in size. The leaky and defective architecture of tumor vasculature might be due to elevated levels of vascular mediators such as bradykinins, nitric oxide, VEGF, basic fibroblast growth factor, prostaglandins and so on. Moreover, solid tumors are also characterized by an impaired and lack lymphatic network that decreases the clearance of macromolecules giving, consequently, extended retention times in the tumor interstitium[51,52]. The unique pathophysiologic characteristics of tumor vessels coupled with poor lymphatic drainage (Figure 6) induces the *EPR* effect, which enables macromolecules, including NPs, to extravasate through these gaps into extravascular spaces and accumulate inside tumor tissues.
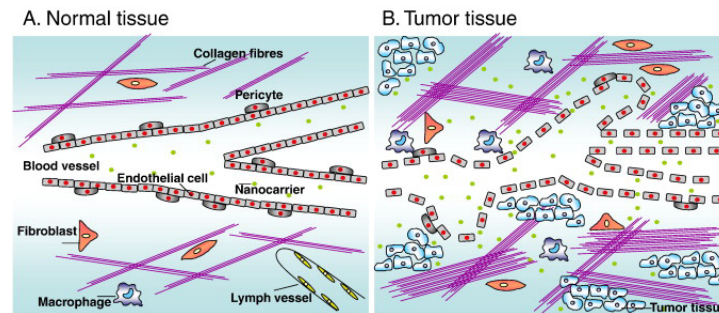
Figure 6. Differences between normal and tumor tissues that explain the passive targeting of nanocarriers by the EPR. A. Normal tissues contain linear blood vessels maintained by pericytes. Collagen fibres, fibroblasts and macrophages are in the extracellular matrix. Lymph vessels are present. B. Tumor tissues contain defective blood vessels with many sac-like formations and fenestrations. The extracellular matrix contains more collagen fibres, fibroblasts and macrophages than in normal tissue. Lymph vessels are lacking[53].

The EPR effect reported by Matsumura and Maeda in 1986[54] was commented by Torchilin[55] as a molecular weight-dependent phenomenon: particles larger than 40 kDa, which is the threshold for renal clearance, show a prolonged

---

[51]H. F. Dvorak, J. A. Nagy, J. T. Dvorak, and A. M. Dvorak, "Identification and characterization of the blood vessels of solid tumors that are leaky to circulating macromolecules," *Am.J.Pathol.* 133, no. 1 (1988).

[52]J. A. Nagy, A. M. Dvorak, and H. F. Dvorak, "Vascular hyperpermeability, angiogenesis, and stroma generation," *Cold Spring Harb.Perspect.Med.* 2, no. 2 (2012).

[53]F. Danhier, O. Feron, and V. Preat, "To exploit the tumor microenvironment: Passive and active tumor targeting of nanocarriers for anti-cancer drug delivery," *J.Control Release* 148, no. 2 (2010).

[54]Y. Matsumura and H. Maeda, "A new concept for macromolecular therapeutics in cancer chemotherapy: mechanism of tumoritropic accumulation of proteins and the antitumor agent smancs," *Cancer Res.* 46, no. 12 Pt 1 (1986).

[55]V. Torchilin, "Tumor delivery of macromolecular drugs based on the EPR effect," *Adv.Drug Deliv.Rev.* 63, no. 3 (2011).

circulation time (thus, a much increased half-life) and hence very slow clearance from the body, with a higher AUC. Thus, these molecules permeate gradually tumors in a selective fashion.

In addition, accumulated macromolecular drugs remain in tumors for a relatively long time (e.g., several days). Molecular weight is not the only determinant of the EPR effect; other factors such as the surface charge and an in vivo surveillance system for macromolecules (i.e., scavenger receptors of the RES) are quite important. The vascular endothelial luminal surface is known to carry a negative charge, so basic proteins with positive charges or cationic polymers rapidly bind to vascular endothelial cells, which results in a lower AUC, shorter plasma half-life, and a consequently reduced tumor drug accumulation by means of the EPR effect. Acidic or neutral particles are thus expected to have a longer plasma half-life. However, the RES in the liver and spleen showed faster uptake of negatively charged NPs than that of neutral particles.

PEGylation thus benefits EPR-based targeting of drugs to tumors. Certain PEG-modified particles are also now understood to have a slower uptake into tumor cells than non-PEGylated molecules. Developing suitable PEGylation strategies to achieve a longer plasma half-life, as well as better intracellular trafficking, is of utmost importance. The EPR effect will drive the particles into tumor tissue but the ultimate goal is access of active drugs to target sites. Therefore, the release rate of the drug from the carrier at the target must be optimal (e.g., 3–10% per day), because too slow a release results in insufficient concentrations of active drugs at sites of action. Release that is too rapid would lead to a high concentration of free drug in circulation but no drug accumulation in the tumor, the results thus being a considerably lower therapeutic effect and undesired systemic toxicity.

On the basis of this scenario, the vast majority of nanomedicines developed for drug targeting to tumors rely on the EPR effect. These primarily include long-circulating liposomes, polymers and micelles. Examples of passively targeted nanomedicines approved for clinical use are Myocet®, Doxil®, Daunoxome®, Abraxane® and Genexol-PM®. Several additional passively tumor-targeted nanomedicines are currently in clinical trials, and a large number of other ones are in early- and late-stage preclinical development.

Targeting cancer cells using the EPR effect is not feasible in all tumors because the degree of tumor vascularization and porosity of tumor vessels can vary with the tumor type and status. One approach to overcome this limitation is to attach targeting moieties to the NP surfaces, thus forming an "active nanocarrier". Active targeting of nanomedicines provides the additional

targeting mechanism of receptor-mediated binding of NPs to surface receptors expressed on tumor cells or blood vessels, such as αβ-integrins, folic acid, and prostate-specific membrane antigen. Research has been conducted on several targeting ligands, including antibodies, aptamers, peptides, and small molecules. Efficient binding and internalization requires that receptors are expressed exclusively on target sites relative to normal cells. At present, several targeted delivery systems are under clinical trials, such as transferrin receptor targeted cytotoxic platinum-based oxaliplatin in a liposome (MBP-426), transferrin receptor targeted cyclodextrin-containing NPs with siRNA payload (CALAA-01), or PSMA targeted polymeric NPs containing DTX (BIND-014). To date, however, in spite of significant advances made at the preclinical level with regard to active targeting, only antibody-based nanomedicines, such as Zevalin, Mylotarg, Ontak and Bexxar have been approved for clinical use.

The observation that actively targeted 'classical' nanomedicines so far largely failed to demonstrate benefit at the preclinical level can likely be mostly attributed to the fact that after leaving the highly leaky tumor vasculature, there are quite a number of anatomical and physiological barriers that need to be overcome before antibody- or peptide-targeted formulations can bind to (and enter) cancer cells. These include the presence of pericyte-, smooth muscle cell- and fibroblast-based cell layers between endothelial and tumor cells, the high cellular density within solid malignancies, and the high interstitial fluid pressure that is typical of tumors. Therefore, and also because of the binding-site barrier, which further limits the penetration of actively targeted nanomedicines into the tumor interstitium, actively targeted nanomedicines tend to have problems finding their target cells, and they generally fail to demonstrate an advantage over passively targeted formulations[56].

The possibility to engineer a NP surface with a wide range of functional groups allowed to design and develop multifunctional nanostructures (Figure 7). Multifunctional nanocarriers can combine a specific targeting agent (usually an antibody or peptide) with NPs for imaging (such as QDs or magnetic NPs), a cell-penetrating agent (e.g. the polyArg peptide TAT), a stimulus-sensitive element for drug release, a stabilising polymer to ensure biocompatibility (PEG most frequently) and two or more therapeutic compounds. This approach can be used for example for simultaneously tumor imaging, diagnosis and treatment. Combining diagnosis and therapy in one process is an emerging biomedical method referred to as theranostic. Several

---

[56]F. Danhier, O. Feron , V. Préat, "To exploit the tumor microenvironment: Passive and active tumor targeting of nanocarriers for anti-cancer drug delivery," *J Control Release,* (2010).

recent reviews have discussed engineering designs, physiochemical characteristics and biomedical applications of magnetic NPs that can simultaneously act as diagnostic molecular imaging agents and as drug carriers[57,58,59].
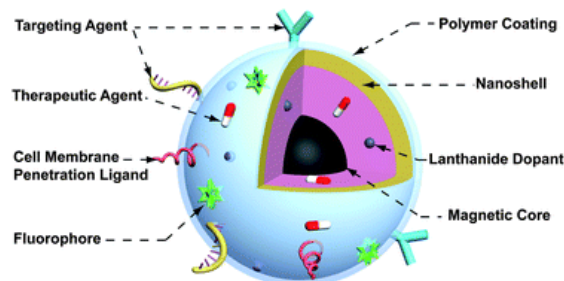
Figure 7. Example of multifunctional nanoplatform.

1.1.6 *PEGylated nanocarriers in clinical use*

As previously described, the circulation time of nanocarriers intended for iv administration and directed passively to solid tumors is widely increased by the inclusion of surface bound hydrophilic molecules such as PEG. Whereas free drugs are usually cleared from circulation within minutes of iv administration, PEGylated nanostructures can circulate for hours and accumulate in sites of leaky vasculature, carrying along the entrapped drug. The use of PEG has been shown to increase circulation times of different nanocarriers such as liposomes and polymeric NPs. To date, several stealth and PEGylated nanocarriers or drugs are already on the market and others are still under clinical trials and studied in animals. Table 1 summarizes the most relevant examples.

---

[57]K. Y. Choi, G. Liu, S. Lee, and X. Chen, "Theranostic nanoplatforms for simultaneous cancer imaging and therapy: current approaches and future perspectives," *Nanoscale.* 4, no. 2 (2012).

[58] P. Prabhu and V. Patravale, "The upcoming field of theranostic nanomedicine: an overview," *J.Biomed.Nanotechnol.* 8, no. 6 (2012).

[59] N. Ahmed, H. Fessi, and A. Elaissari, "Theranostic applications of nanoparticles in cancer," *Drug Discov.Today* 17, no. 17-18 (2012).

Table 1. PEGylated nanomedicines for cancer approved or under clinical and preclinical research.

Name	Formulation	Drug	Indication	Status
Liposomes				
Doxil® (Caelyx® in EU)	PEGylated	Doxorubicin	Breast and ovarian cancer, multiple myeloma, Kaposi's sarcoma	Market
Lipoplatin	PEGylated	Cisplatin	Various malignancies	Phase III
S-CKD602	PEGylated	CKD-602	Various malignancies	Phase I/II
NL CPT-11	PEGylated	Irinotecan (CPT-11)	Glioma	Phase I
MCC-465	Human antibody (GAH)-PEG	Doxorubicin	Gastric cancer	Phase I
Thermodox™	Heat-activated PEGylated	Doxorubicin	Liver cancer, breast cancer	Phase III
-	DSPE-mPEG$_{2000}$	Paclitaxel	Enhanced antitumor effect in human breast cancer bearing nude mice	Preclinical
-	DSPE-mPEG$_{5000}$	Paclitaxel	Long circulation time and decrease in drug uptake in MPS-containing organs	Preclinical
Polymeric micelles				
Genexol-PM®	PEG-PLA	Paclitaxel	Breast cancer, lung cancer, ovarian cancer	Market/Phase II
Nanoxel	mPEG-PDLLA	Docetaxel	Breast cancer	Market/Phase I
NK911	PEG-PAA	Doxorubicin	Various solid malignancies	Phase III
NK105	PEG-PAA	Paclitaxel	Gastric cancer	Phase II
NC-6004 (Nanoplain™)	PEG-polyglutamic acid	Cisplatin	Pancreatic cancer	Phase I/II
NK012	PEG-PGA	SN-38	Various solid malignancies	Phase II

28

Polymeric NPs

Name	Polymer	Drug	Description	Phase
BIND-014	PEG-PLGA	Docetaxel	Various solid malignancies	Phase I
CRLX101	Cyclodextrin-PEG	Camptothecin	Various malignancies	Phase II
CALAA-01	Cyclodextrin-PEG-transferrin	Anti-RRM2 siRNA	Various solid malignancies	Phase I
-	mPEG-PLGA	Cisplatin	Decrease of tumor volume and higher survival rate in HT-29 tumor-bearing SCID mice than free drug	Preclinical
-	PCL-PLA-PEG-PCL-PLA	Camptothecin	Superior antitumor effect and extended retention time in the blood of murine sarcoma-bearing mice	Preclinical
-	PEG-PLA	Paclitaxel	Higher half-life and AUC than Taxol	Preclinical
-	PEG-PCL	Docetaxel	NPs inhibited tumor growth and achieved high concentration in tumors in tumor-bearing mice	Preclinical
-	PEG-PLGA	Paclitaxel	Remarkable tumor growth inhibition and increased survival rate of transplantable liver tumor-bearing mice compared to Taxol	Preclinical
-	PEG-PLGA	Docetaxel	Drug biological half-life increased and tumor accumulation higher than Taxotere on C26 tumor-bearing mice	Preclinical
-	PEG-PLGA	Doxorubicin	Decrease in cardiotoxicity	Preclinical

Nanoassembly of polymer conjugates

Name	Polymer	Drug	Description	Phase
Oncaspar®	PEG-drug	L-asparaginase	Leukaemia	Market
Pegamotecan	PEG-drug	Camptothecin	Gastric cancer	Phase II
PegIntron	PEG-drug	IFN2α/-IFN2β	Melanoma, leukaemia	Phase II
NKTR-102	PEG-drug	Irinotecan	Breast cancer, ovarian cancer, colorectal	Phase III

1.1.7 Amphiphilic block copolymers

In the field of injectable PEGylated nanomedicines for cancer, amphiphilic block copolymers have attracted a great deal of attention due to their ability to form various types of self-assembling NPs. These polymers are obtained by the polymerization of more than one type of monomer, typically one hydrophobic and one hydrophilic, so that the resulting molecule is composed of regions that have opposite affinities for an aqueous solvent. These materials are generally composed of biocompatible, biodegradable hydrophobic polymer blocks such as polyesters covalently bound to a biocompatible hydrophilic block, typically PEG. To date, numerous block copolymers have been synthesized, not only with a variety of block combinations, but also varying hydrophilic and hydrophobic block lengths.

Block copolymers are classified into several types by sequential arrangement of component segments (Figure 8).
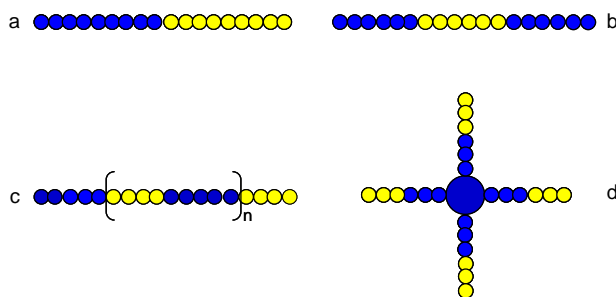
Figure 8. Types of block copolymers: a) AB type diblock, b) ABA type triblock, c) AB_n type multiblock, d) $(AB)_n$ star block.

The simplest block copolymer is AB-type block copolymer, which is composed of one segment of homopolymer A linked to one segment of homopolymer B. In the second type of copolymer, both terminals of B unit is connected at the terminal of A unit, and thus, it is referred to as an ABA type block copolymer. In the third type of block copolymers, A and B segments are connected n times and referred to as a multiblock copolymer. The fourth type of block copolymer has a star block architecture. In this last family, unit A has multi-arm functionality and copolymerizes with B blocks giving a star-like

shape. The number of arms of the star block copolymer depends on the number of functional groups on block A.

The literature abounds with studies using amphiphilic block copolymers of different compositions that produce,by different preparation techniques, core-shell nanoassemblies referred to as micelles (spherical, worm-like, crew-cut), nanospheres, nancapsules and polymersomes.

The selection of an appropriate hydrophobic core-forming material is considered of utmost importance in order to attain a physically stable delivery system. Poly(alpha-hydroxesters), such as PDLLA, PGA, and PCL, remain the most widely employed polymers for core-shell nanostructures to target hydrophobic drugs, given their biocompatibility and biodegradability.

1.1.7.1   Poly-ε-caprolactone

PCL (Figure 9) is an aliphatic polyester of considerable interest in the design of amphiphilic block copolymer.
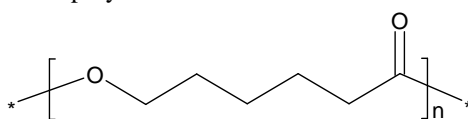
Figure 9. PCL.

PCL is a semi-crystalline polymer with a low glass transition temperature (Tg -60 °C) and a melting temperature between 59 and 64 °C related closely to the crystalline nature of the material. It is slowly biodegradable in vivo by chemical and enzymatic reactions. It was used for the preparation of sustained release systems of oral contraceptives (Capronor®)[60]. Recently, the process of degradation in vivo was studied by implanting the low molecular weight poly(ε-caprolactone[14]C) in rats and by measuring the radioactivity in urine, feces, exhaled air and the residual activity in the implant site. A complete bioabsorption was observed in 60 days and the presence of ε-hydroxycaproic acid, produced by complete hydrolysis of the polymer, as well as tritiated water as metabolites. While studying the mechanism of bioabsorption, studied by electron microscopic analysis of the tissue at the implantation site, the presence of intracellular polymeric particles was detected, demonstrating the

---

[60]C. G. Pitt, M. M. Gratzl, G. L. Kimmel, J. Surles, and A. Schindler, "Aliphatic polyesters II. The degradation of poly (DL-lactide), poly (epsilon-caprolactone), and their copolymers in vivo," *Biomaterials* 2, no. 4 (1981).

role of phagocytosis in the final stage of polymer degradation[61]. The cell and tissue biocompatibility of PCL was demonstrated but also an extensive inflammatory reaction in the muscle probably due to increased vascularity of the tissue and a larger amount of implanted material was evidenced. The inflammation may be due to a high local concentration of degradation products and to a potential transport of the polymer with subsequent activation of neutrophils. The rapid activation of neutrophils by microsphere-based PCL, after intramuscular injection, was confirmed from the measurement of the superoxide anion generated from the material. Finally, studies of flow cytometry to assess the effect of PCL microspheres on apoptosis and cell cycles were conducted. Results revealed that the material exhibits excellent cytocompatibility[62].

Due to its high reactivity and ability to polymerize in not drastic conditions for the presence of the terminal -OH groups, PCL represents an excellent candidate for the synthesis of amphiphilic block copolymers. Furthermore, due to a marked lipophilic character PCL is considered an excellent material to prepare self-assembling systems, being prone to form a lipophilic core where poorly water-soluble drugs can be entrapped.

1.1.7.2   *Amphiphilic block copolymers of PCL-PEG and anticancer drugs*

PCL-PEG copolymers are important biomedical materials with amphiphilicity, controlled biodegradability and good biocompatibility. They have great potential in the fields of nanotechnology, tissue engineering, pharmaceutics, and medicinal chemistry.

Generally, amphiphilic block copolymers composed of hydrophilic and hydrophobic segments can form a micelle-like structure with a hydrophobic inner core and a hydrophilic outer shell in selective solvent[63,64]. In PCL-PEG polymeric micelles, hydrophobic core formed by PCL is surrounded by water-soluble polar groups of PEG that extend into an aqueous medium. Therefore, drugs with a hydrophobic character can be easily incorporated into NP core by

---

[61]V. R. Sinha, K. Bansal, R. Kaushik, R. Kumria, and A. Trehan, "Poly-epsilon-caprolactone microspheres and nanospheres: an overview," *Int.J.Pharm.* 278, no. 1 (2004).

[62]Q. Luo, J. Chen, and K. Dai, "[Study on the cytocompatibility of biodegradable poly(epsilon-caprolactone) microspheres in vitro]," *Sheng Wu Yi.Xue.Gong.Cheng Xue.Za Zhi.* 20, no. 1 (2003).

[63]D. Lemoine, C. Francois, F. Kedzierewicz, V. Preat, M. Hoffman, and P. Maincent, "Stability study of nanoparticles of poly(epsilon-caprolactone), poly(D,L-lactide) and poly(D,L-lactide-co-glycolide)," *Biomaterials* 17, no. 22 (1996).

[64]E. Piskin, "Biodegradable polymers as biomaterials," *J.Biomater.Sci.Polym.Ed* 6, no. 9 (1995).

covalent binding or non-covalent hydrophobic interactions in aqueous media[65,66,67].

Micro/NPs from PCL-PEG copolymers are successfully employed to improve the aqueous solubility of hydrophobic drugs. With this purpose, micelles containing small drugs such as indomethacin[68], rapamycin[69], honokiol[70], cyclosporine A[71] and fenofibrate[72] were prepared. Spontaneously self-assembled micelles encapsulating ketoprofen and furosemide were obtained using PCL-PEG modified with trimethylene carbonate PEG-P(CL-co-TMC)[73] whereas micelles containing risperidone were studied for oral delivery[74]. Invaluable insight in the delivery of hydrophobic drugs for cancer chemotherapy has been gained through the research on polymeric NPs. Hydrophobic drugs such as hydroxycamptothecin[75], paclitaxel[76] and DTX[77,78]

[65]Y. I. Jeong, M. K. Kang, H. S. Sun, S. S. Kang, H. W. Kim, K. S. Moon, K. J. Lee, S. H. Kim, and S. Jung, "All-trans-retinoic acid release from core-shell type nanoparticles of poly(epsilon-caprolactone)/poly(ethylene glycol) diblock copolymer," *Int.J.Pharm.* 273, no. 1-2 (2004).

[66]J. Ryu, Y. I. Jeong, I. S. Kim, J. H. Lee, J. W. Nah, and S. H. Kim, "Clonazepam release from core-shell type nanoparticles of poly(epsilon-caprolactone)/poly(ethylene glycol)/poly(epsilon-caprolactone) triblock copolymers," *Int.J.Pharm.* 200, no. 2 (2000).

[67]S. Singh and M. S. Muthu, "Preparation and characterization of nanoparticles containing an atypical antipsychotic agent," *Nanomedicine.(Lond)* 2, no. 2 (2007).

[68]K. Letchford, R. Liggins, and H. Burt, "Solubilization of hydrophobic drugs by methoxy poly(ethylene glycol)-block-polycaprolactone diblock copolymer micelles: theoretical and experimental data and correlations," *J.Pharm.Sci.* 97, no. 3 (2008).

[69]J. A. Yanez, M. L. Forrest, Y. Ohgami, G. S. Kwon, and N. M. Davies, "Pharmacometrics and delivery of novel nanoformulated PEG-b-poly(epsilon-caprolactone) micelles of rapamycin," *Cancer Chemother.Pharmacol.* 61, no. 1 (2008).

[70]C. Gong, X. Wei, X. Wang, Y. Wang, G. Guo, Y. Mao, F. Luo, and Z. Qian, "Biodegradable self-assembled PEG-PCL-PEG micelles for hydrophobic honokiol delivery: I. Preparation and characterization," *Nanotechnology.* 21, no. 21 (2010).

[71]H. M. Aliabadi, A. Mahmud, A. D. Sharifabadi, and A. Lavasanifar, "Micelles of methoxy poly(ethylene oxide)-b-poly(epsilon-caprolactone) as vehicles for the solubilization and controlled delivery of cyclosporine A," *J.Control Release* 104, no. 2 (2005).

[72]K. K. Jette, D. Law, E. A. Schmitt, and G. S. Kwon, "Preparation and drug loading of poly(ethylene glycol)-block-poly(epsilon-caprolactone) micelles through the evaporation of a cosolvent azeotrope," *Pharm.Res.* 21, no. 7 (2004).

[73]D. J. Latere, L. Rouxhet, M. E. Brewster, V. Preat, and A. Arien, "Spontaneously self-assembled micelles from poly(ethylene glycol)-b-poly(epsilon-caprolactone-co-trimethylene carbonate) for drug solubilization," *Pharmazie* 63, no. 3 (2008).

[74]F. Mathot, Beijsterveldt L. van, V. Preat, M. Brewster, and A. Arien, "Intestinal uptake and biodistribution of novel polymeric micelles after oral administration," *J.Control Release* 111, no. 1-2 (2006).

[75]J. Zhang, L. Q. Wang, H. Wang, and K. Tu, "Micellization phenomena of amphiphilic block copolymers based on methoxy poly(ethylene glycol) and either crystalline or amorphous poly(caprolactone-b-lactide)," *Biomacromolecules.* 7, no. 9 (2006).

[76]M. Shahin and A. Lavasanifar, "Novel self-associating poly(ethylene oxide)-b-poly(epsilon-caprolactone) based drug conjugates and nano-containers for paclitaxel delivery," *Int.J.Pharm.* 389, no. 1-2 (2010).

[77]Q. Liu, R. T. Li, H. Q. Qian, M. Yang, Z. S. Zhu, W. Wu, X. P. Qian, L. X. Yu, X. Q. Jiang, and B. R. Liu, "Gelatinase-stimuli strategy enhances the tumor delivery and therapeutic efficacy of docetaxel-loaded poly(ethylene glycol)-poly(varepsilon-caprolactone) nanoparticles," *Int.J.Nanomedicine.* 7 (2012).

were formulated into NPs with high encapsulation efficiency and kept stable in aqueous media. In addition, PCL-PEG NPs containing hydrophilic drug such as doxorubicin were also prepared to modulate drug release profile [79]. Noticeably, some published work relies on the attachment of folate groups as targeting moiety for NPs[80]. Superparamagnetic iron oxide and doxorubicin were also co-encapsulated within folate-conjugated PCL-PEG micelles[81].

Other specific applications of PCL-PEG NPs such as multimodal carriers for drugs and imaging agents were reported. PCL-PEG NPs co-encapsulating a hydrophobic vitamin (beta-carotene) and an inorganic colloid for imaging (Au) were obtained[82]. PCL-PEG copolymers were also intensively studied for their potential in non-viral gene carriers[83,84] and for their ability to self-assemble in polymersomes for hydrophilic drugs[85].

[78]F. Ungaro, C. Conte, L. Ostacolo, G. Maglio, A. Barbieri, C. Arra, G. Misso, A. Abbruzzese, M. Caraglia, and F. Quaglia, "Core-shell biodegradable nanoassemblies for the passive targeting of docetaxel: features, antiproliferative activity and in vivo toxicity," Nanomedicine. 8, no. 5 (2012).

[79] A. K. Yadav, P. Mishra, S. Jain, P. Mishra, A. K. Mishra, and G. P. Agrawal, "Preparation and characterization of HA-PEG-PCL intelligent core-corona nanoparticles for delivery of doxorubicin," J.Drug Target 16, no. 6 (2008).

[80] E. K. Park, S. Y. Kim, S. B. Lee, and Y. M. Lee, "Folate-conjugated methoxy poly(ethylene glycol)/poly(epsilon-caprolactone) amphiphilic block copolymeric micelles for tumor-targeted drug delivery," J.Control Release 109, no. 1-3 (2005).

[81]X. Yang, W. Deng, L. Fu, E. Blanco, J. Gao, D. Quan, and X. Shuai, "Folate-functionalized polymeric micelles for tumor targeted delivery of a potent multidrug-resistance modulator FG020326," *J.Biomed.Mater.Res.A* 86, no. 1 (2008).

[82] M. E. Gindy, A. Z. Panagiotopoulos, and R. K. Prud'homme, "Composite block copolymer stabilized nanoparticles: simultaneous encapsulation of organic actives and inorganic nanostructures," *Langmuir* 24, no. 1 (2008).

[83] T. K. Endres, M. Beck-Broichsitter, O. Samsonova, T. Renette, and T. H. Kissel, "Self-assembled biodegradable amphiphilic PEG-PCL-lPEI triblock copolymers at the borderline between micelles and nanoparticles designed for drug and gene delivery," *Biomaterials* 32, no. 30 (2011).

[84]T. Kanazawa, K. Sugawara, K. Tanaka, S. Horiuchi, Y. Takashima, and H. Okada, "Suppression of tumor growth by systemic delivery of anti-VEGF siRNA with cell-penetrating peptide-modified MPEG-PCL nanomicelles," *Eur.J.Pharm.Biopharm.* 81, no. 3 (2012).

[85]D. E. Discher and F. Ahmed, "Polymersomes," *Annu Rev Biomed Eng.* (2006).

1.2   Photodynamic Therapy

With advances in the early diagnosis of cancer and increased interest in the conservation of normal tissue during cancer surgery, the rising demands for non-invasive or minimally invasive therapeutic methods for cancer have led to the accelerated development of medical technologies such as radiation therapy, ultrasound treatment, cryotherapy and PDT. PDT is a clinically approved, minimally invasive procedure that can exert a selective cytotoxic activity toward malignant cells. The procedure involves administration of a PS followed by irradiation at a wavelength corresponding to an absorbance band of the PS. In the presence of oxygen, a series of events lead to direct tumor cell death, damage to the microvasculature, and induction of a local inflammatory reaction. Clinical studies reveal that PDT can be curative, particularly in early stage tumors, can prolong survival in patients with inoperable cancers and significantly improve quality of life. Minimal normal tissue toxicity, negligible systemic effects, greatly reduced long-term morbidity, lack of intrinsic or acquired resistance mechanisms and excellent cosmetic as well as organ function-sparing effects of this treatment make it a valuable therapeutic option for combination treatments. With a number of recent technological improvements, PDT has the potential to become integrated into the mainstream of cancer treatment.

1.2.1   Principles of PDT

Photodynamic effectiveness is based on photochemical reactions between light and tumor tissue with exogenous PS. These components, tolerated singly by the diseased cells, generate cytotoxic oxygen-based molecular species in proper dosage and concentration. Mechanistically it consists in three phases: excitation of PS, generation of toxic oxygen and cell death (Figure 10). In the first phase, irradiated light of an appropriate wavelength, usually visible or near-infrared, excites the PS molecules in the ground or singlet state, characterized by two electrons with opposite spins in a low energy molecular orbital. Following the absorption of light in the form of photons, one of these electrons is boosted into a high-energy orbit, but keeps its spin from the first short-live excited singlet state. The light is usually chosen to coincide with the maximum absorption wavelength of the drug molecules. In common with many other fluorescent molecules, PS can, at this stage, decay to the native state with concomitant emission of light in the form of fluorescence. However, the excited singlet state PS may also undergo a process known as intersystem crossing whereby the spin of the excited electron inverts to form a relatively

more stable and long-lived excited triplet-state that has electrons which spin in a parallel conformation. A high quantum efficiency for this transition is a key characteristic of a good PS. The PS in triplet state can either decay radiation to the ground state or transfer its energy to molecular oxygen (O_2) in the surroundings, which is unique in being a triplet in its ground state. This step leads to the formation of singlet oxygen ($^1O_2$), which initiates oxidation of susceptible substrates, and the reaction is referred to as a Type II process. A Type I process can also occur whereby the PS reacts directly with an organic molecule in a cellular microenvironment, acquiring a hydrogen atom or electron to form a radical. Subsequent autoxidation of the reduced PS produces a superoxide anion radical (O^{-2}). Dismutation or one electron reduction of O^{-2} gives hydrogen peroxide (H_2O_2), which in turn can undergo one-electron reduction to a powerful and virtually indiscriminate oxidant hydroxyl radical (HO^-).
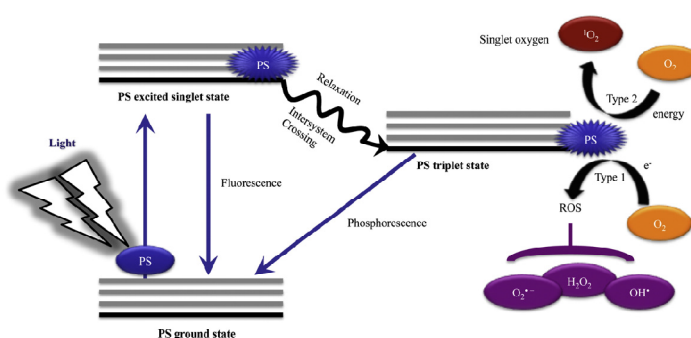
Figure 10. Schematic illustration of a photodynamic reaction. The PS initially absorbs a photon that excites it to the short-lived singlet state. This can lose energy by fluorescence, internal conversion to heat, or by intersystem crossing to the long-lived triplet state. This triplet PS can interact with molecular oxygen in two pathways, type 1 and type 2, leading to the formation of ROS and singlet oxygen ($^1O_2$) respectively[86].

Both Type 1 and Type 2 reactions can occur simultaneously and competitively, and the ratio between these processes depends on the type of PS used, as well as the concentrations of substrate and oxygen. Type II reaction, however, appears to play a central role in cytotoxicity, because of the highly efficient interaction of the $^1O_2$ species with various biomolecules. Singlet oxygen, in

---

[86]A. Gupta, P. Avci, M. Sadasivam, R. Chandran, N. Parizotto, D. Vecchio, W. de Melo, T. Dai, L. Y. Chiang, M. R. Hamblin, "Shining light on nanotechnology to help repair and regeneration," *Biotechnology Advances,* (2012).

fact, is believed to be the main cytotoxic agent in PDT[87].Singlet oxygen species have a lifetime of less than 3.5 μs and can diffuse only 0.01 to 0.02 μm during this period. Therefore, the initial extent of the damage is limited to the site of concentration of the PS.This is usually the mitochondria, plasma membrane, Golgi apparatus, lysosomes, endosomes and ER. The nucleus and nuclear membrane are usually spared and DNA damage is rare.

In addition to direct damage to neoplastic cells, vascular damage plays an important role in tumor eradication. In PDT, oxygen radicals induce changes in both tumor and surrounding normal vasculature, decreasing the barrier function of endothelial cells and depriving neoplastic cells of nutrients[88].

1.2.2 Light sources and Light Delivery

No single light source is ideal for all PDT indications, even with the same PS. The choice of light source should therefore be based on PS absorption, disease, cost, and size. Furthermore, the clinical efficacy of PDT is dependent on complex dosimetry: total light dose, light exposure time, light delivery mode (single vs fractionated or even metronomic) and fluence rate (intensity of light delivery).

The effective excitation light magnitude is determined by the combination of optical absorption and scattering properties of the tissue. Absorption is largely due to endogenous tissue chromophores such as hemoglobin, myoglobin and cytochromes (Figure 11). The optical scattering of tissue decreases with wavelength. For the spectral range of 450–1,750 nm, tissue scattering is, in general, more prevalent than absorption, although for the range of 450–600 nm, melanin and hemoglobin provide significant absorption, while water plays a similar role for $l > 1,350$ nm. Therefore, the optimal optical window for PDT, as well as for optical imaging, is in the near-infrared spectral region (600–1,300 nm), where the scattering and absorption by tissue are minimized and, therefore, the longest penetration depth can be achieved. Within this optical window, the longer the wavelength is, the deeper is the penetration depth. However, light up to only approximately 800 nm can generate $^1O_2$, because longer wavelengths have insufficient energy to initiate a photodynamic reaction[89].

---

[87]P. Agostinis, K. Berg, K. A. Cengel, T. H. Foster, A. W. Girotti, S. O. Gollnick, S. M. Hahn, M. R. Hamblin, A. Juzeniene, D. Kessel, M. Korbelik, J. Moan, P. Mroz, D. Nowis, J. Piette, B. C. Wilson, and J. Golab, "Photodynamic therapy of cancer: an update," *CA Cancer J.Clin.* 61, no. 4 (2011).

[88]R. Schmidt, "Photosensitized generation of singlet oxygen," *Photochem.Photobiol.* 82, no. 5 (2006).

[89]J. L. Sandell and T. C. Zhu, "A review of in-vivo optical properties of human tissues and its impact on PDT," *J.Biophotonics.* 4, no. 11-12 (2011).

The light source for PDT must exhibit suitable spectral characteristics that coincide with the maximum absorption wavelength range of the PS applied in order to generate enough ROS to produce a cytotoxic effect. Currently approved PS absorb in the visible spectral regions below 700 nm, where light penetration into the skin is only a few millimeters, clinically limiting PDT to treating topical lesions. Different light sources have been usedin clinical and experimental PDT. Laser systems are widely used for treatment of dermatological conditions[90].

The gold vapor laser (628 nm), the argon ion-pumped dye laser (630 or 635 nm), and the copper vapor-pumped dye laser constitute the most popular systems.These systems allow the selection of a wavelength that has a maximal effective tissue penetration of approximately 10 mm, and have been used in combination with all types of PS.The laser beams can be launched into an optical fiber applicator, enabling light to be delivered directly into internal tumors. However, these techniques are relatively expensive, require specialized supporting staff and are space-consuming.
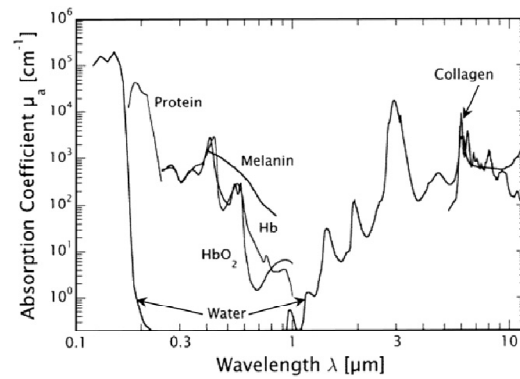
Figure 11. Optical absorption coefficients of principal tissue chromophores in the human body[91].

It is probable that such systems will eventually be replaced by laser diode arrays which are very convenient since they can be easily moved, require only a single phase supply and also being relatively inexpensive. Commercially

---

[90]D. Barolet, "Light-emitting diodes (LEDs) in dermatology," *Semin.Cutan.Med.Surg.* 27, no. 4 (2008).

[91]D. K. Chatterjee, L. S. Fong, and Y. Zhang, "Nanoparticles in photodynamic therapy: an emerging paradigm," *Adv.Drug Deliv.Rev.* 60, no. 15 (2008).

available incoherent light sources, such as incandescent or arc lamps, have been used in topical PDT by several groups mainly for treatment of large lesions[92]. Because coherence of light is not necessary for PDT, such sources offer the advantage of being less expensive and easier to handle. The most popular of them is the filtered slide projector, which excludes light below 600 nm with glass filters, minimizing the emission of shorter wavelengths, which by being strongly absorbed by hemoglobin, could lead to the production of heat-induced erythema. Despite this, unfiltered white light has also been employed, and recently, professional incoherent lamp like PDT 1200 lamp has been developed for PDT.

1.2.3   Photosensitizing agents

Most of the PS used in cancer therapy are based on a heterocyclic tetrapyrrole structure, similar to that of the protoporphyrin contained in hemoglobin.
There are many properties which an ideal PS should possess:
- ✓ stable composition;
- ✓ easily synthesized or readily available;
- ✓ minimal self-aggregation tendency;
- ✓ not highly hydrophobic or encapsulated inside appropriate carriers;
- ✓ non-toxic in the absence of light exposure;
- ✓ photostable;
- ✓ absorbance in the red region of spectrum with high extinction molar coefficient;
- ✓ target specificity;
- ✓ quickly cleared from the body.

Each of the currently commercially available PS has specific characteristics, but none of them is an ideal agent. For example, most of the PS are hydrophobic and can aggregate very easily in aqueous media which can affect their photophysical, chemical and biological properties[93].

PS are generally classified as porphyrins and non-porphyrins. Amid porphyrin-based PS first, second, and third generation PS are reported.

The first generation agent, Hp, was isolated from hemoglobin of dried blood using concentrated sulfuric acid in 1841 by Scherer. Purification and solubilization of Hp are the chemical processes leading to the preparation of HpD, a very complex mixture of several components, of which approximately

---

[92] C. B. Warren, L. J. Karai, A. Vidimos, and E. V. Maytin, "Pain associated with aminolevulinic acid-photodynamic therapy of skin disease," *J.Am.Acad.Dermatol.* 61, no. 6 (2009).

[93] R. R. Allison and C. H. Sibata, "Oncologic photodynamic therapy photosensitizers: a clinical review," *Photodiagnosis.Photodyn.Ther.* 7, no. 2 (2010).

50% is identifiable as oligomeric ematoporphyrins and protoporphyrins, which have a low *in vivo* photosensitizing activity. Further chemical purification yielded to the preparation of porfimer sodium (Photofrin®), a lyophilized concentrated form of monomeric and oligomeric ematoporphyrin derivatives, clinically approved in the treatment of early- and late-stage lung cancers, esophageal cancer, bladder cancer, malignant and nonmalignant skin diseases and early-stage cervical cancer. It is also being considered as a potential therapy against Kaposi's sarcoma, Barrett's esophagus with high-grade dysplasia, psoriasis and cancers of the head, brain, neck and breast.

Photofrin® is characterized by an absorption maximum of 630 nm (corresponding to a penetration of about 5–10 mm) and a low molar extinction coefficient which in turn demands high concentrations of Photofrin® and light to obtain an adequate tumor eradication, and a long half-life of 452 h, causing long-lasting photosensitivity. The time delay between drug delivery and the time it takes to maximize the tumor to normal cell uptake within the target tissue determines the correct time for light application. Photofrin®-mediated PDT involves iv administration of PS followed by irradiation (100– 200 J/cm^2 of red light) 24-48 h later. During this period Photofrin is cleared from a number of tissues and remains concentrated at target site[94].

Various chemical modifications of the tetrapyrrolic ring of the porphyrins characterize the different groups of the *'second-generation'* PS. They have high absorption coefficients and quantum yields as well as absorption peaks in the far red (660–700 nm) or near infrared (700–850 nm) regions. The serum half-life of the second-generation PS is short and tissue accumulation is selective and quick (within 1–6 h after injection). Thus the treatment can be carried out on the same day as the administration of the drug. In addition, the risk of burns by accidental sun exposure is low because clearance from normal tissues is rapid. Toxicity to skin and internal organs in the absence of light (so-called 'dark' toxicity) is absent or minimal. Many PS currently under investigation belong to two chemical groups: the chlorins and the cyanines. The joining of four benzenes or naphthalene rings to the β-pyrrolic positions of porphyrins and the substitution of the methine-bridge carbons with nitrogen produce phthalocyanines and naphthalocyanines, respectively. The presence of aluminium, zinc(II), silicon(IV) and other ions gives hexacoordination and guarantees a satisfactory yield of singlet oxygen generation.

Chlorins are reduced porphyrins such as NPe6 and chlorin e6, hydrophilic compounds with some amphiphilicity and similar photobiological properties.

---

[94]R. R. Allison, V. S. Bagnato, and C. H. Sibata, "Future of oncologic photodynamic therapy," *Future.Oncol.* 6, no. 6 (2010).

They have been found effective in treating BCC and SCC. $SnET_2$ and m-THPC are hydrophobic and their use for dermatological indications has been investigated extensively. Finally, bacteriochlorins might be particularly useful for the PDT of pigmented tumors.

Phthalocyanines are second-generation PS, containing a diamagnetic metal ion, which have shown high photodynamic efficiency in the treatment of animal tumors, as well as reduced phototoxic side effects. AlPcS are chemically stable, readily soluble in water, and have a strong absorption in the red part of the spectrum. ALPcTS has been used in clinical studies of BCC, Kaposi's sarcoma and lung cancer. In addition, other PS with different modifications of the porphyrin structure are available. Porphycenes, synthetic porphyrins, and isomers of porphines, are efficient generators of singlet oxygen and of tumor regression. ATMPn is a chemically pure substance with fast pharmacokinetics and superior photodynamic properties *in vitro* and *in vivo* as compared to Photofrin II®. Texaphyrins are synthetic, water-soluble expanded-ring porphyrin analogues, in which a phenyl ring replaces one pyrrole ring. They can be easily complexed with large metal cations, such as Ln(III) or Lu(III), to give metal complexes that are photoactive *in vivo* with high selectivity and an efficient generation of $^1O_2$ with an absorption peak near 732 nm. The lack of significant persistent skin phototoxicity is another outstanding characteristic of these compounds. Photosensitivity lasts up to 6 weeks but strict avoidance of sunlight is needed only for the first 2 weeks. TPPS is a hydrophilic substituted porphyrin that is 25–30 times more effective than HpD and Photofrin[95,96].

Second generation PS show lower toxicity, but most of them exhibit poor solubility in aqueous media, preventing iv delivery into the bloodstream and affecting their efficacy and tumor selectivity. Thus, it becames important to develop more performing compounds with improved deliverability. Currently, research efforts have been focused on the development of third generation PS, characterized by more specificity to the target cells, resulting in minimized accumulation in healthy tissues. Conjugating a targeting component, such as an antibody (directed against the tumour antigens), PS allows the drug to localize, accumulate and bind selectively at the diseased site[97,98]. The PS

[95] A. E. O'Connor, W. M. Gallagher, and A. T. Byrne, "Porphyrin and nonporphyrin photosensitizers in oncology: preclinical and clinical advances in photodynamic therapy," *Photochem.Photobiol.* 85, no. 5 (2009).

[96] P. G. Calzavara-Pinton, M. Venturini, and R. Sala, "Photodynamic therapy: update 2006. Part 1: Photochemistry and photobiology," *J.Eur.Acad.Dermatol.Venereol.* 21, no. 3 (2007).

[97] R. Hudson, M. Carcenac, K. Smith, L. Madden, O. J. Clarke, A. Pelegrin, J. Greenman, and R. W. Boyle, "The development and characterisation of porphyrin isothiocyanate-monoclonal antibody conjugates for photoimmunotherapy," *Br.J.Cancer* 92, no. 8 (2005).

bioconjugate is then able to (specifically) photodynamically inactivate in tumour cells expressing the tumour-associated antigen, minimizing healthy cell localization and concomitant damage. An alternative approach would be to use a colloidal carrier such as a liposome or targeted NPs. For example BPD-MA, also known as Verteporfin (Visudyne®, Novartis AG), is a semisynthetic porphyrin derived from protoporphyrin. It has poor water solubility but can be formulated successfully either in liposomes or emulsions.

Non-porphyrin derivates include hypericin, a naturally occurring compound from *Hypericum* plants that shows maximum absorption in the ultraviolet (330 nm) and visible (550 and 588 nm) light range, high singlet oxygen production, minimal dark toxicity, and high clearance from the body, after administration. Hypocrellins, methylene blue, azure C, methylene violet, thionine, methylene green, Nile blue A, and rhodamine 123 are potential PS for PDT.

1.2.4   *Changes in cell signaling after PDT*

PDT treatment is connected to the modification of different signal transduction cellular pathways, in relation to calcium expression levels, lipid metabolism effects, tyrosine kinase expression, cell adhesion molecules and cytokines. In particular, there is an acute stress reaction leading to changes in cellular metabolism following PDT treatment which may result in apoptosis, necrosis or cell survival.

1.2.4.1   *Calcium and lipid metabolism*

PDT performed on cancer cells in vitro has been shown to raise the levels of total intracellular calcium via the influx of Ca^{2+} through ion channels, release of Ca^{2+} stored in internal stores in the endoplasmic reticulum and mitochondria, and/or activation of ion exchange mechanisms, and this has been associated with cell death, and in certain occasions and conditions, with cell survival[99]. In many cases, the rapid release of arachidonic acid metabolites due to the activation of phospholipase A2 (a membrane enzyme activated by Ca^{2+}) and the increase of intracellular ceramide levels after PDT treatment have been observed. Ceramide has been shown to activate a number of enzymes involved in stress signaling cascades including both protein kinases

---

[98]C. Staneloudi, K. A. Smith, R. Hudson, N. Malatesti, H. Savoie, R. W. Boyle, and J. Greenman, "Development and characterization of novel photosensitizer : scFv conjugates for use in photodynamic therapy of cancer," *Immunology* 120, no. 4 (2007).

[99]D. Nowis, M. Makowski, T. Stoklosa, M. Legat, T. Issat, and J. Golab, "Direct tumor damage mechanisms of photodynamic therapy," *Acta Biochim.Pol.* 52, no. 2 (2005).

and phosphatases regulating diverse cellular processes including apoptosis, cell senescence, cell cycle, and cellular differentiation.

1.2.4.2 Tyrosine kinases

The MAPK signaling pathways play an important role in signal transduction within eukaryotic cells, whereby they modulate many cellular events including ERK-1/2. It has been found that after PDT treatment of cells, ERK's expression is significantly decreased in relation to an increase in cell death and so it can be assumed that the two processes are connected. Furthermore, many studies on cancerous cell lines have found that PDT can induce the complete loss of the EGFR on the cell membrane, inducing anti-proliferative responses and apoptosis.

1.2.4.3 Cellular adhesion and cytokines

PDT causes the damage of adhesion molecules located within the cell membranes, such as integrins, immunoglobulin G superfamily, selectins, cadherins, ICAM-1 and VCAM-1. For this reason, the alterations in the attachment of cancer cells to the substratum induces a decrease in cellular adhesion as well as a decrease in their metastatic potential. Moreover, it was widely demonstrated that in most cases PDT may induce over- or under-expression of cytokines, which often relates to tumor regression and possible eradication.

1.2.4.4 Hypoxia and angiogenesis

Tumor hypoxia is associated with malignant progression, resistance to chemotherapy, PDT and radiotherapy together with increased metastasis and poor prognosis. There are some current reports that suggest that hypoxia derived from antiangiogenic effects might promote the selection of aggressive tumor cell phenotypes and that therefore these treatment do not result always in clinical benefits[100]. The HIF is a master transcriptional activator of oxygen-regulated genes, which are involved in anaerobic energy metabolism, angiogenesis, cell survival, cell invasion, and MDR. Since PDT is capable of rapidly consuming significant amounts of tissue oxygen and also shutting down blood that delivers oxygen supply to the tumor region, the treatment itself may produce severe levels of hypoxia. Therefore, high levels of HIF

---

[100]S. J. Conley, E. Gheordunescu, P. Kakarala, B. Newman, H. Korkaya, N. Heath, S. G. Clouthier, and M. S. Wicha, "Antiangiogenic agents increase breast cancer stem cells via the generation of tumor hypoxia," *PNAS* (2012).

expression are often associated with a poor overall cellular response to PDT treatment, so further investigation is warranted in order to understand and overcome this phenomenon[101].

1.2.5   Pathways of PDT-mediated tumor destruction

Three distinct mechanisms have been recognized which contribute to the observed reduction (and frequent disappearance) of tumors when treated with PDT (Figure 12).
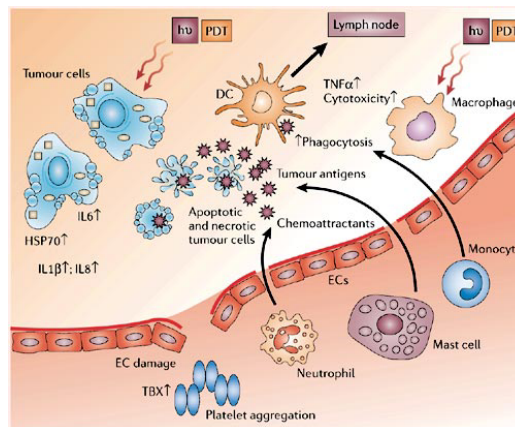
Figure 12. Consequences of PDT. Damage to endothelial cells activates a cascade of events that lead to local inflammation, vessel dilatation and platelet aggregation[102].

In the first case, the ROS that is generated by PDT can kill tumor cells directly by apoptosis and/or necrosis if the PS has been taken up by tumor cells. Alternatively, PDT also damages the tumor-associated vasculature, which can lead to tumor death via lack of oxygen and nutrients. Lastly, the acute inflammation and release of cytokines and stress response proteins induced in the tumor by PDT can lead to an invasion of leukocytes that can both contribute to tumor destruction as well as stimulate the immune system to recognize and destroy tumor cells even at isolated locations. These three mechanisms can also influence each other. The relative importance of each

[101]C. A. Robertson, D. H. Evans, and H. Abrahamse, "Photodynamic therapy (PDT): a short review on cellular mechanisms and cancer research applications for PDT," *J.Photochem.Photobiol.B* 96, no. 1 (2009).
[102]A. P. Castano, P. Mroz, and M. R. Hamblin, "Photodynamic therapy and anti-tumour immunity," *Nat.Rev.Cancer* 6, no. 7 (2006).

mechanism for the overall tumor response is yet to be defined and so requires further research. It is clear, however, that the combination of all these components in PDT is required for optimum long-term tumor regression, especially of tumors that may have metastasized.

1.2.5.1 Mechanisms of cell death in PDT

Although PDT can induce many cellular and molecular signaling pathway events in cells, its main purpose is to induce cell death. In particular, PDT can evoke the three main cell death pathways: apoptotic, necrotic, and autophagy-associated cell death (Figure 13).
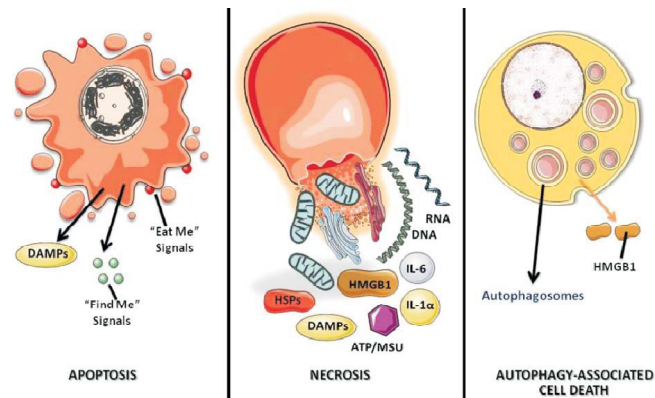
Figure 13. Three Major Cell Death Morphotypes[103].

The concentration, physiochemical properties and subcellular location of the PS, the concentration of oxygen, the appropriate wavelength and intensity of the light, as well as the cell type specific properties may all influence the mode and extent of cell death. In general, it is believed that lower doses of PDT lead to more apoptotic cells, while higher doses lead to proportionately more necrotic cells.

Apoptosis is a generally major cell death modality in cells responding to PDT for the activation of the pro-apoptotic family of proteins Bcl. MOMP after

---

[103]P. Agostinis, K. Berg, K. A. Cengel, T. H. Foster, A. W. Girotti, S. O. Gollnick, S. M. Hahn, M. R. Hamblin, A. Juzeniene, D. Kessel, M. Korbelik, J. Moan, P. Mroz, D. Nowis, J. Piette, B. C. Wilson, and J. Golab, "Photodynamic therapy of cancer: an update," *CA Cancer J.Clin.* 61, no. 4 (2011).

photodynamic injury is controlled by Bcl-2 family members and thought to be largely p53-independent.

With mitochondria-associated PS, photodamage to membrane-bound Bcl-2 can be a permissive signal for MOMP and the subsequent release of caspase activators such as cytochrome c and Smac/DIABLO, or other proapoptotic molecules, including AIF.

High proportions of cell death occur after PDT when there is strong evidence of caspase 3 and 9 being present within the cell lysate, indicating that PDT must activate them within the cellular death pathway. Lysosomal membrane rupture and leakage of cathepsins from photo-oxidized lysosomes induces Bid cleavage and MOMP.

Phototoxicity is not propagated only through caspase signaling but involves other proteases, such as calpains, as well as non apoptotic pathways. Typically, inhibition orgenetic deficiency of caspases only delays phototoxicity or shifts the cell death modality toward necrotic cell death. The molecular mechanisms underlying programmed necrosis are still elusive, but certain events including activation of RIP kinase, excessive mitochondrial ROS production and lysosomal damage are recurrently involved. Severe inner mitochondria membrane photodamage or intracellular Ca2þ overload could promote mitochondrial permeability transition, an event that may favor necrotic rather than apoptotic phototoxicity. It has been suggested that apoptosis and necrosis share common initiation pathways and that the final outcome is determined by the presence of an active caspase. This implies that apoptosis inhibition re-orients cells to necrosis, so that cells sufficiently damaged by PDT are destroyed, regardless of the mechanism involved.

Photodamage of cells can also lead to the stimulation of macroautophagy (hereafter referred to as autophagy) by various stress signals including oxidative stress. This process can have both a cytoprotective and a pro-death role after cancer chemotherapies, including those involving ROS as primary damaging agents. Recent studies delineate autophagy as a mechanism to preserve cell viability after photodynamic injury[104]. PS that photodamage the lysosomal compartment may compromise completion of the autophagic process, causing incomplete clearance of the autophagic cargo. Accumulation of ROS-damaged cytoplasmic components may then potentiate phototoxicity in apoptosis-competent cells. A better understanding of the interplay between autophagy, apoptosis, and necrosis and how these processes lead to improved

---

[104]J. J. Reiners, Jr., P. Agostinis, K. Berg, N. L. Oleinick, and D. Kessel, "Assessing autophagy in the context of photodynamic therapy," *Autophagy.* 6, no. 1 (2010).

tumor response will be a requisite to devise better therapeutic strategies in PDT[105].

1.2.5.2 *Cytoprotective mechanisms*

Numerous publications have reported cytoprotective mechanisms that cancer cells exploit to avoid the cytotoxic effects of PDT such as the production in cancer cells of antioxidant molecules (eg, some amino acids, glutathione,vitamin E) and the expression of enzymes that can detoxify ROS. For example, SOD overexpression or treatment with SOD mimetics have been shown to counteract the cytotoxic effect of PDT. The third cytoprotective mechanism involves proteins whose encoding genes are themselves induced by PDT. Many categories can be specified but most of them are part of signaling pathways that can regulate PDT-induced apoptosis or participate in the repair of lesions induced by oxidative stress. NFκB inhibition by overexpression of the Basuper-repressor or by the use of pharmacological inhibitors strongly sensitizes cancer cells to apoptosis induced by PDT. Other stress-related transcription factors induced by PDT include AP-1, HIF, or Nrf_2. PDT was shown to upregulate heme $oxygenase^{-1}$ expression, and the mechanism is dependent on Nrf_2 nuclear accumulation and on p38 MAPK and phosphoinositide 3-kinase activities. PDT was found to induce expression of various HSPs for which a protective role in PDT has been described[106]. For example, transfection of tumor cells with the HSP gene increased the survival of tumor cells after PDT. Similarly, increased HSP60 and HSP70 levels are inversely correlated with sensitivity to the photodynamic treatment. The simplest explanation for these observations is the ability of HSPs to bind to oxidatively damaged proteins. Moreover, the intracellular function of HSPs is not only restricted to protein refolding. Many HSPs ''client'' proteins play a critical role in the regulation of prosurvival pathways. PDT also leads to increased ubiquitination of carbonylated proteins, thereby tagging them for degradation in proteasomes, which prevents the formation of toxic protein aggregates.

1.2.5.3 *Antivascular Effects of PDT*

PDT has been known to cause microvasculature collapse leading to severe tissue hypoxia, eventual complete blood flow stasis, hemorrhage, and, in some

---

[105]D. Kessel, "Death pathways associated with photodynamic therapy," *Med.Laser Appl.* 21, no. 4 (2006).

[106]E. Buytaert, M. Dewaele, and P. Agostinis, "Molecular effectors of multiple cell death pathways initiated by photodynamic therapy," *Biochim.Biophys.Acta* 1776, no. 1 (2007).

larger vessels, the formation of platelet aggregates (Figure 14). The vascular effects of PDT can differ greatly based on the different PS and the drug-light interval administered. For example, PDT with Photofrin® changes vessel constriction and permeability, vessel leakage and leukocyte adherence, certain phthalocyanine derivatives cause vascular leakage and NPe6 results in blood flow stasis. Although microvascular damage and hypoxia after PDT contributes to greater tumor response, reduction in oxygen during treatment can limit tumor control by inducing the production of proangiogenic markers such as VEGF, COX-2, MMPs and other cytokines, creating enhanced environment for tumor recurrence. Many reports directly implicate the endothelium as a primary target for PDT in vivo; this stimulated research into the relative sensitivity of endothelial cells to PDT and the responses of endothelial cells that could initiate the various phenomena at the vessel level.
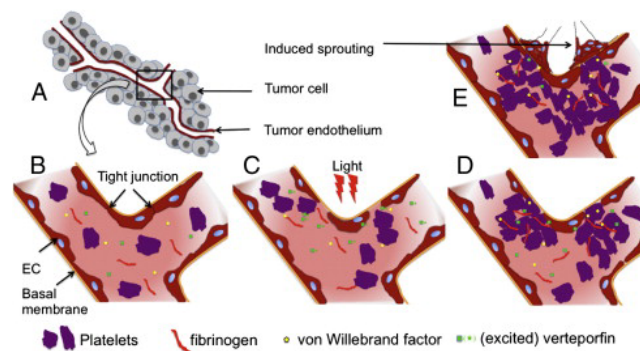
Figure 14. Tumor endothelial responses after PDT leading to blood flow stasis. (A) Tumor blood vessel before PDT. (B-E) Magnification of the junction of the tumor vessel. (B) Before PDT endothelial cells are tightly attached to the basement membrane of the vessel wall, lining the blood vessel. Endothelial cells are connected through tight junctions. (C) After injection of a PS and light exposure, cellular stress inside the endothelial cells results in disruption of tight junctions, partial retraction and detachment from the vessel wall. (D) Blood gets in contact with the vessel wall collagen and the clotting cascade is initiated, ultimately leading, through the interaction with fibrinogen, to the formation of a stabilized thrombus, leading to obstruction of the vessel. (E) Due to the angiogenic switch, endothelial cell proliferation, migration and sprout formation is observed[107].

Exponentially growing endothelial cells were significantly more sensitive than similarly proliferating tumor cells, and the difference in sensitivity was accompanied by greater PS accumulation in the endothelial cells. Endothelial

---

[107] A. Weiss, Bergh Hv den, A. W. Griffioen, and P. Nowak-Sliwinska, "Angiogenesis inhibition for the improvement of photodynamic therapy: the revival of a promising idea," *Biochim.Biophys.Acta* 1826, no. 1 (2012).

cell responses to sublethal doses of PDT may also contribute to vascular changes observed in tissue[108,109,110].

1.2.6   PDT and the Immune Response

Numerous preclinical and clinical studies have demonstrated that PDT can influence the adaptive immune response in different ways; some regimens result in potentiation of adaptive immunity, whereas others lead to immunosuppression. The precise mechanism leading to potentiation versus suppression is unclear; however, it appears as though the effect of PDT on the immune system is dependent upon the treatment regimen, the area treated, and the PS type. Recent reports have shown that clinical antitumor PDT also increases antitumor immunity[111].

First of all, PDT frequently provokes a strong acute inflammatory reaction observed as localized edema at the targeted site (Figure 15). This reaction starts with the generation of important alarm/danger signals, also called DAMPs or CDAMPs, at the treated site that can be detected by the innate immunity. As consequence, PDT induce oxidative stress which triggers a vast array of signal pathways via TLRs. This includes expression of HSPs, transcription factors such as NF-κB and AP-1. NF-κB and AP-1 can then induce expression of immunoregulatory and proinflammatory proteins such as IL (-1α, -1β, -2, -6, -8, -11, -12, -15), TNF, chemokines and IFN-α/β. Further, photooxidative degradation of membrane lipids and generation of arachidonic acid metabolites are themselves potent inflammatory mediators that cause a rapid and strong inflammatory reaction. These processes together with the release of histamine and serotonin from damaged vasculature cause infiltration of the tumor site by diverse populations of immune cells (neutrophils, mast cells and macrophages) that become activated and engaged in tumor cell destruction. However, a key event appears to be PDT induced complement activation.

Photosensitization induces the innate immunity response with subsequent development of adaptive immunity. In particular, PDT activates both humoral and cell-mediated antitumor immunity. PDT-induced acute local and systemic

---

[108]R. Bhuvaneswari, Y. Y. Gan, K. C. Soo, and M. Olivo, "The effect of photodynamic therapy on tumor angiogenesis," *Cell Mol.Life Sci.* 66, no. 14 (2009).

[109]V. H. Fingar, T. J. Wieman, S. A. Wiehle, and P. B. Cerrito, "The role of microvascular damage in photodynamic therapy: the effect of treatment on vessel constriction, permeability, and leukocyte adhesion," *Cancer Res.* 52, no. 18 (1992).

[110]V. H. Fingar, "Vascular effects of photodynamic therapy," *J.Clin.Laser Med.Surg.* 14, no. 5 (1996).

[111]K. Pizova, K. Tomankova, A. Daskova, S. Binder, R. Bajgar, and H. Kolarova, "Photodynamic therapy for enhancing antitumour immunity," *Biomed.Pap.Med.Fac.Univ Palacky.Olomouc.Czech.Repub.* 156, no. 2 (2012).

inflammation is postulated to culminate in the maturation and activation of DCs. Activated DCs then migrate to tumor draining lymph nodes, where they stimulate T-cell activation. Generation of CD8+ effector and memory T cells is frequently, but not always, dependent upon the presence and activation of CD4+T cells. PDT-induced antitumor immunity may or may not depend on CD4+ T cells and may be augmented by natural killer cells. Nevertheless, in some cases, certain PDT regimens have been shown to systemically suppress immune reactivity[112].
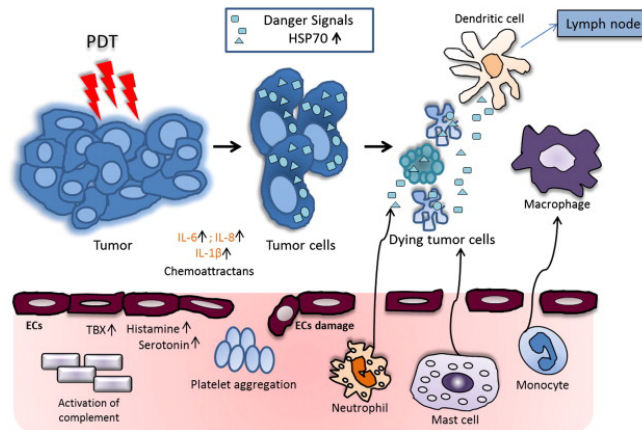
Figure 15. PDT induces an anti-tumor immunity response. PDT-treated dying cells produce danger signals including the expression of HSPs, cytokines, adhesion molecules, co-stimulatory molecules and immunologically important genes. These processes together with the release of histamine and serotonin from damaged vasculature induce an activation of complement, sequential arrival of neutrophils. DCs are activate by PDT sensing endogenous danger signals release by dying tumor cells, then they migrate to the tumor-draining lymph nodes and stimulate T-cell activation[113].

It was demonstrated for example that the cutaneous Photofrin-PDT and ALA-PDT cause suppression of the contact hypersensitivity reaction and the increase in levels of IL-10 expression in the sera of treated animals. It is

[112]S. O. Gollnick, D. A. Musser, A. R. Oseroff, L. Vaughan, B. Owczarczak, and B. W. Henderson, "IL-10 does not play a role in cutaneous Photofrin photodynamic therapy-induced suppression of the contact hypersensitivity response," *Photochem.Photobiol.* 74, no. 6 (2001).

[113]L. M. Sanabria, M. E. Rodríguez, I. Cogno, N. B. R. Vittar, M. F. Pansa, M. J. Lamberti, V. A Rivarola, "Direct and indirect photodynamic therapy effects on the cellular and molecularcomponents of the tumor microenvironment," *Biochimica et Biophysica Acta,* (2013).

50

known that IL-10 suppresses cell-mediated immune response via its ability to inhibit activation of Th1 cells by APC. Nevertheless, the major effector cell in CHS is the IFN-γ secreting CD8+ (Tc1) cell. Therefore, it is possible that PDT induces a defect in thedevelopment of Th1 and Tc1 cells. Another potential suppressor of Th1 and Tc1 development, and thus CHS, is IL-4, often inducted by PDT treatment[114].

1.2.7   *Clinical PDT for cancer*

PDT has been utilized for pre-neoplastic and neoplastic diseases in a wide variety of organ systems, including skin, genitourinary, esophagus, prostate, bile duct, pancreas, head and neck, and brain. Several medicines have been approved or are currently in clinical trials (table 2).

Several types of skin cancers and precancers are among the first to be studied in PDT due to their accessibility to PS and external light. In the definitive setting, PDT is currently approved for the treatment of AK, BCC and SCC.

Successful results for PDT of nonhyperkeratotic AK have been achieved with systemically administered porfimer sodium as well as topically applied ALA and methyl-ALA (MAL). Twenty-eight RCTs that reported the use of PDT in the treatment of AK have been identified[115] and aggregated data indicate better rates of complete response and better cosmetic results with PDT than with the other treatments[116].

Thirteen RCTs on superficial and nodular BCC have been reported, comparing ALA-PDT with surgical excision, cryotherapy or placebo. In particular, for superficial BCC, the outcome after PDT appears similar to surgery or cryotherapy, whereas for nodular (deep) BCC, PDT is less effective than surgery for lesion clearance. Finally, PDT can substantially reduce the size of large SCC tumors reducing morbidity and increasing overall curative response[117].

Regarding ophthalmic disease, the only clinically PDT treatment is Verteporfin (Visudyne®) approved for AMD worldwide since 2000. Its

---

[114]S. O. Gollnick, B. Owczarczak, and P. Maier, "Photodynamic therapy and anti-tumor immunity," *Lasers Surg.Med.* 38, no. 5 (2006).

[115]D. Fayter, M. Corbett, M. Heirs, D. Fox, and A. Eastwood, "A systematic review of photodynamic therapy in the treatment of pre-cancerous skin conditions, Barrett's oesophagus and cancers of the biliary tract, brain, head and neck, lung, oesophagus and skin," *Health Technol.Assess.* 14, no. 37 (2010).

[116]C. A. Morton, S. B. Brown, S. Collins, S. Ibbotson, H. Jenkinson, H. Kurwa, K. Langmack, K. McKenna, H. Moseley, A. D. Pearse, M. Stringer, D. K. Taylor, G. Wong, and L. E. Rhodes, "Guidelines for topical photodynamic therapy: report of a workshop of the British Photodermatology Group," *Br.J.Dermatol.* 146, no. 4 (2002).

[117]G. Jeremic, M. G. Brandt, K. Jordan, P. C. Doyle, E. Yu, and C. C. Moore, "Using photodynamic therapy as a neoadjuvant treatment in the surgical excision of nonmelanotic skin cancers: prospective study," J.Otolaryngol.Head Neck Surg. 40 Suppl 1 (2011).

therapy involves iv administration of verteporfin followed by activation through an ophthalmoscope equipped with a 690 nm diode laser while the PS is still in the general circulation. Several RCTs are currently under way to evaluate the efficacy of AMD PDT for use with other PS, such as SnET$_2$, motexafin lutetium, and Npe6[118].

In the field of head and neck cancer, over 1500 patients have been treated with PDT[119] with Photofrin, 5-ALA, Foscan and Photoclor by systemic delivery; in particular, Foscan® was approved in Europe in 2001 for the palliative treatment of patients with advanced head and neck cancer who have exhausted other treatment options. Furthermore, various formulations of porfimer sodium, ALA and temeporfin are currently undergoing intensive clinical investigation as an adjunctive treatment for brain tumors, such as glioblastoma multiforme, anaplastic astrocytoma, malignant ependymomas or meningiomas, melanoma and lung cancer brain metastasis, and recurrent pituitary adenomas [120]. Currently, PS are being evaluated both as intraoperative diagnostic tools by means of PD and FGR as well as during PDT as an adjunctive therapeutic modality. The most recently published trials that employed PD, FGR, and PDT provided additional encouraging results, but the initial delay in tumor progression did not translate to extended overall survival[121]. PDT is increasingly being used to treat cancers of the airways and other tumors in the thoracic cavity, especially NSCLC[122]. Different RCTs based on talaporfin or porfimer sodium-mediated PDT showed good results and complete response rate in patients with early stage lung cancer or for whom surgery is not feasible[123].

[118]J. I. Lim, "Photodynamic therapy for choroidal neovascular disease: photosensitizers and clinical trials," Ophthalmol.Clin.North Am. 15, no. 4 (2002).

[119]M. A. Biel, "Photodynamic therapy of head and neck cancers," *Methods Mol.Biol.* 635 (2010).

[120]H. Kostron, "Photodynamic diagnosis and therapy and the brain," *Methods Mol.Biol.* 635 (2010).

[121] S. Eljamel, "Photodynamic applications in brain tumors: a comprehensive review of the literature," *Photodiagnosis.Photodyn.Ther.* 7, no. 2 (2010).

[122]C. B. Simone, J. S. Friedberg, E. Glatstein, J. P. Stevenson, D. H. Sterman, S. M. Hahn, and K. A. Cengel, "Photodynamic therapy for the treatment of non-small cell lung cancer," *J.Thorac.Dis.* 4, no. 1 (2012).

[123]D. J. Minnich, A. S. Bryant, A. Dooley, and R. J. Cerfolio, "Photodynamic laser therapy for lesions in the airway," *Ann.Thorac.Surg.* 89, no. 6 (2010).

Table 2. PS for PDT.

Trade name	PS	Structure	Excitation λ (nm)	Cancer indication (Approvals)
Clinically approved Ps [a]				
Levulan	5-ALA	Porphyrin precursor	635	AK (Canada, USA)
Metvix, Metvixia	Methylester of 5-ALA	Porphyrin precursor	635	AK (Canada, USA)
Photofrin	Porfimer sodium	Porphyrin	630	BCC (EU), SCC in situ (EU), Bladder cancer (Canada)
Foscan	m-THPC	Chlorin	652	Cervical cancer (Japan), Esophagus cancer and dysplasia (Canada, EU, USA, Japan), Gastric cancer (Japan), Lung cancer (Canada, EU, Japan, USA)
Laserphyrin	Taporfin sodium (Talaporfin), MACE, NPe6, LS11	Chlorin	664	Head and neck cancer (EU), Lung cancer (Japan)
Fotolon	Chlorine6 +	Chlorin	660	Skin, vulva, cervix, oral cancer (Russia)
Fotoditazin	Chlorin e6 + chlorin p6	Chlorin	660	Skin cancer (Russia, S. Korea)
Photosense	AlPcS	Phthalocyanine	675	Skin, vulva, oral, esophagus and stomach; breast metastases (Russia)

PS in clinical trials[b]

Hexvix; Benzvix	ALA esters (hexyl-ALA/benzyl-ALA)	Porphyrin precursor	635	Bladder, gastrointestinal, and skin
Verteporfin	BPD-MA	Porphyrin	690	BCC; (also approved as Visudyne™ for AMD, a non-cancer condition)
Photochlor	HPPH	Chlorin	665	BCC, esophagus, head and neck, and lung
Purlytin	$SnEt_2$	Chlorin	664	Breast, prostate, Kaposi's sarcoma and skin cancer
Lutex	Lutetium texaphyrin/ Motexafin lutetium	Texaphyrin	732	Brain, breast, cervical and prostate
Pc 4	Silicon phthalocyanine 4	Phthalocyanine	675	Cutaneous T cell lymphoma
Tookad	Padoporfin	Bacteriochlorin	762	Prostate cancer
WST-11	Padeliporfin	Bacteriochlorin	753	Prostate cancer

[a] Compounds, diseases, and countries in which clinical uses for each disease indication are fully approved.

[b] Compounds in the lower table are still investigational. Also, note that many clinically-approved PS in the upper table are being investigated beyond their originally approved indications.

Another interesting application of PDT is in the MPM[124].

In gastroenterology, endoscopically accessible premalignant or malignant lesions located within the esophagus, the stomach, the bile duct, or the colorectum with a high surgical risk have become suitable targets of endoscopic PDT [125]. Photofrin-PDT has been approved for obstructing esophageal cancer, early-stage esophageal cancer, and Barrett's esophagus in several countries, as an alternative to esophagectomy because these are superficial and large mucosal areas that are easily accessible for light. Recent pilot studies have demonstrated that endoscopic Photofrin-PDT is also effective in the palliative treatment of hilarcholangiocarcinoma[126], PDT for early duodenal and ampullary cancers and advanced adenomas.

Due to advances in light applicators, the interstitial PDT is now becoming a practical option for solid lesions, including those in parenchymal organs such as the liver and pancreas[127]. Talaporfin-mediated PDT may have efficacy in treating hepatocellular carcinoma, whereas Foscan looked promising in the treatment of pancreatic cancer[128]. In the case of prostate cancer, Foscan, Tookad, and Lutex looked minimally-invasive alternatives to surgery or radiotherapy, reducing the risk of the post-surgical side effects of incontinence and impotence. Bladder cancer tends to be a superficial condition, and for this reason it is proposed that a superficial treatment mediated with ALA or its ester derivatives, by intravesical instillation, may be a preferable means for local therapy[129].

The last PDT application is based on the treatment of gynecological cancers. For cervical intraepithelial neoplasia, PDT based on chlorine e6 (Fotolon) or hexyl-ALA offers a nonscarring alternative to cone biopsy. For vulvar intraepithelial neoplasia, use of Foscan or ALA may ameliorate the need for radical mutilating surgery. Similarly, penile intraepithelial neoplasia and anal intraepithelial neoplasia have been treated with ALA-based PDT, sometimes

---

[124] J. S. Friedberg, "Photodynamic therapy for malignant pleural mesothelioma: the future of treatment?," *Expert.Rev.Respir.Med.* 5, no. 1 (2011).

[125] M. W. Wiedmann and K. Caca, "General principles of photodynamic therapy (PDT) and gastrointestinal applications," *Curr.Pharm.Biotechnol.* 5, no. 4 (2004).

[126] M. A. Ortner, "Photodynamic therapy for cholangiocarcinoma," *Lasers Surg.Med.* 43, no. 7 (2011).

[127] T. J. Vogl, K. Eichler, M. G. Mack, S. Zangos, C. Herzog, A. Thalhammer, and K. Engelmann, "Interstitial photodynamic laser therapy in interventional oncology," *Eur.Radiol.* 14, no. 6 (2004).

[128] S. G. Bown, A. Z. Rogowska, D. E. Whitelaw, W. R. Lees, L. B. Lovat, P. Ripley, L. Jones, P. Wyld, A. Gillams, and A. W. Hatfield, "Photodynamic therapy for cancer of the pancreas," *Gut* 50, no. 4 (2002).

[129] A. P. Berger, H. Steiner, A. Stenzl, T. Akkad, G. Bartsch, and L. Holtl, "Photodynamic therapy with intravesical instillation of 5-aminolevulinic acid for patients with recurrent superficial bladder cancer: a single-center study," *Urology* 61, no. 2 (2003).

with complete clearance. Extramammary Paget's disease responds to PDT with porfimer sodium or ALA[130].

1.2.8   Combined PDT

At present, combination of different chemotherapeutic drugs in a chemotherapy regimen is an attractive strategy for effective anticancer treatment. In a clinical setting the treated patients were found to fail the experiences of single agent chemotherapy, because it is limited to act on specific cancer survival pathways and showed low response rates and relapse of tumor. The major limiting factors associated with poor prognosis of cancer following single agent chemotherapeutic treatment in cancer patients are: MDR, significant toxicity and undesirable side effects. To improve the therapeutic potential of cancer chemotherapy, it is essential to establish an alternative approaches that could provide a solution to the problems involved in single drug chemotherapy. To this end, much attention has been given to combination approaches for a better long-term prognosis and to decrease side effects associated with high doses of single drug treatment. Unlike single agent therapy, combination therapy can modulate different signaling pathways, maximizing the therapeutic effect by overcoming toxicity and, moreover, can overcome the mechanisms of MDR associated with cancer treatment. The use of combination therapy for cancer treatment has been well established in recent years and its advantages applied to cancer therapy are illustrated below. One of the prime benefits of combination therapies is the potential for providing synergistic effects. In combination therapy the overall therapeutic benefit of the drugs in combination were found to be greater than the sum of the effects of the drugs individually. These advantages have driven drug discovery efforts toward the search for combination therapies. The best drug combination with maximal antitumor efficacy can be calculated by multiple drug effect/combination index isobologram analysis, an effective way to demonstrate that drugs are working synergistically. The prime mechanism of synergistic effect following combinational drug treatment could act on the same or different signaling pathways to achieve more-favorable outcomes at a lower dose with equal or increased efficacy[131,132]. Combinations of various

---

[130]S. Anand, B. J. Ortel, S. P. Pereira, T. Hasan, and E. V. Maytin, "Biomodulatory approaches to photodynamic therapy for solid tumors," *Cancer Lett.* 326, no. 1 (2012).

[131]P. Parhi, C. Mohanty, and S. K. Sahoo, "Nanotechnology-based combinational drug delivery: an emerging approach for cancer therapy," *Drug Discov.Today* 17, no. 17-18 (2012).

[132]J. Lehar, A. S. Krueger, W. Avery, A. M. Heilbut, L. M. Johansen, E. R. Price, R. J. Rickles, G. F. Short, III, J. E. Staunton, X. Jin, M. S. Lee, G. R. Zimmermann, and A. A. Borisy, "Synergistic drug combinations tend to improve therapeutically relevant selectivity," *Nat.Biotechnol.* 27, no. 7 (2009).

therapeutic modalities with non overlapping toxicities are among the commonly used strategies to improve the therapeutic index of treatments in modern oncology. Two general approaches may increase the antitumor effectiveness of PDT: 1) sensitization of tumor cells to PDT and 2) interference with cytoprotective molecular responses triggered by PDT in surviving tumor or stromal cells. Any interactions between PDT and PDT-sensitizing agents will be confined to the illuminated area. Therefore, the potentiated toxicity of the combinations is not systemic. This should be of special importance in elderly or debilitated patients who tolerate more intensive therapeutic regimens poorly. Moreover, considering its unique $^1O_2$-dependent cytotoxic effects, PDT can be safely combined with other antitumor treatments without the risk of inducing cross-resistance[133]. There have been few studies on combinations of PDT with standard antitumor regimens published to date. PDT can be used in combination with surgery as a neoadjuvant, adjuvant, or repetitive adjuvant treatment, preferably image-guided fluorescence to confine illumination to the most suspicious lesions. PDT has also been successfully combined with radiotherapy and chemotherapy[134,135].

Another approach to promote PDT efficacy involves increased PS delivery or impaired loss from tumor cells. The first approach involves conjugation of PS to various tumor-targeting molecules. This may be important in the treatment of tumors where large surface areas are illuminated and hence increased tumor selectivity is desired. The use of compounds that impair PS efflux has also been demonstrated to effectively sensitize tumor cells to PDT, although such approaches seem to be limited to those PS that are the substrates of outward transport systems such as ABCG2[136]. The development of novel target-specific antitumor drugs has enabled examination of a number of concept-based combinations that in various molecular mechanisms sensitize tumor cells to the

[133] D. Kessel and C. Erickson, "Porphyrin photosensitization of multi-drug resistant cell types," *Photochem.Photobiol.* 55, no. 3 (1992).

[134] J. Golab, D. Nowis, M. Skrzycki, H. Czeczot, A. Baranczyk-Kuzma, G. M. Wilczynski, M. Makowski, P. Mroz, K. Kozar, R. Kaminski, A. Jalili, M. Kopec', T. Grzela, and M. Jakobisiak, "Antitumor effects of photodynamic therapy are potentiated by 2-methoxyestradiol. A superoxide dismutase inhibitor," *J.Biol.Chem.* 278, no. 1 (2003).

[135] A. Szokalska, M. Makowski, D. Nowis, G. M. Wilczynski, M. Kujawa, C. Wojcik, I. Mlynarczuk-Bialy, P. Salwa, J. Bil, S. Janowska, P. Agostinis, T. Verfaillie, M. Bugajski, J. Gietka, T. Issat, E. Glodkowska, P. Mrowka, T. Stoklosa, M. R. Hamblin, P. Mroz, M. Jakobisiak, and J. Golab, "Proteasome inhibition potentiates antitumor effects of photodynamic therapy in mice through induction of endoplasmic reticulum stress and unfolded protein response," *Cancer Res.* 69, no. 10 (2009).

[136] W. Liu, M. R. Baer, M. J. Bowman, P. Pera, X. Zheng, J. Morgan, R. A. Pandey, and A. R. Oseroff, "The tyrosine kinase inhibitor imatinib mesylate enhances the efficacy of photodynamic therapy by inhibiting ABCG2," *Clin.Cancer Res.* 13, no. 8 (2007).

cytotoxic effects of PDT. Proteins are major targets for oxidative reactions because they constitute nearly 70% of the dry weight of cells. Oxidized proteins can be refolded by molecular chaperones such as HSPs. Inefficient restoration of their structure leads to accumulation of misfolded proteins and their aggregation, which precipitates cell death. Accumulation of damaged or misfolded proteins within ER triggers a process called ER stress, which can be ameliorated by unfolded protein response or can lead to cell death. Therapeutic approaches that interfere with refolding or removal of oxidized proteins can be used to sensitize tumor cells to PDT. For example, modulation of HSP function with geldanamycin, a HSP90 inhibitor, sensitizes tumor cells to PDT[137]. Bortezomib, a proteasome inhibitor successfully used in the treatment of hematological disorders, potentiates the cytotoxic effects of PDT by aggravation of ER stress. Moreover, several apoptosis-modulating factors such as rapamycin, Bcl-2 antagonists, ursodeoxycholic acid, or ceramide analogues have been shown to increase PDT-mediated cancer cell death[138](table 3).

---

[137]A. Ferrario, N. Rucker, S. Wong, M. Luna, and C. J. Gomer, "Survivin, a member of the inhibitor of apoptosis family, is induced by photodynamic therapy and is a target for improving treatment response," *Cancer Res.* 67, no. 10 (2007).

[138] M. F. Zuluaga and N. Lange, "Combination of photodynamic therapy with anti-cancer agents," *Curr.Med.Chem.* 15, no. 17 (2008).

Table 3. Combinations of PDT and various therapeutic modalities in cancer treatment.

DRUG OR TREATMENT MODALITY	OUTCOME/RESULTS
CHEMOTHERAPEUTICS AND NOVEL ANTICANCER DRUGS	
Anthracyclines	Doxorubicin improves PDT-mediated tumor growth control in mice
Platinum compounds	Cisplatin potentiates antitumor activity of PDT in mice
Antimetabolites	Methotrexate enhances in vitro cytotoxicity of PDT with ALA by upregulation of protoporphyrin IX production
Microtubule inhibitors	Vincristine administered prior to or immediately after PDT improves its antitumor activity in mice
DNA methyltransferase inhibitors	5-azadeoxycytidine prolongs survival of PDT-treated animals and improves tumor growth control
Proteasome inhibitors	Bortezomib enhances PDT-mediated ER stress in cancer cells in vitro and significantly delays post-PDT tumor regrowth in mice
RADIOTHERAPY	Two-way enhancement of antitumor effects: PDT sensitizes cancer cells to radiotherapy and radiotherapy increases anticancer efficacy of PDT, prolonged tumor growth control induced by combined treatment
DRUGS MODULATING ARACHIDONIC ACID CASCADE	
COX-2 inhibitors	COX-2 inhibitors (such as NS-398, nimesulide, or celecoxib) potentiate antitumor effects of PDT, possibly through indirect antiangiogenic effects
LOX inhibitors	MK-886 sensitizes tumor cells to PDT-mediated killing
AGENTS INCREASING PS ACCUMULATION IN TUMOR CELLS	
Vitamin D	Increases ALA-induced protoporphyrin IX accumulation and thus potentiates PDT cytotoxicity in vitro
Imatinib	Increases intracellular accumulation of second-generation PS and thus potentiates PDT cytotoxicity in vitro

59

Lipid-lowering drugs	Lovastatin improves in vitro LDL binding and porfimer sodium uptake by cancer cells
Salicylate	Enhancement of PDT efficacy via increased PS uptake by tumor cells

APPROACHES INCREASING OXYGEN DELIVERY TO TUMOR CELLS

EPO	EPO improves chemotherapy-induced anemia and restores antitumor efficacy of PDT in mice; however, EPO might also inhibit direct PDT-mediated cytotoxicity toward certain cancer cells
Hyperbaric oxygen	Increased antitumor effects of PDT in mice and in advanced pleural tumors in humans
Hyperthermia	In various treatment regimens, hyperthermia potentiates antitumor efficacy of PDT in vitro and in animal models the short time interval between these two treatment modalities might increase normal tissue injury via vascular effects

TARGETING CYTOPROTECTIVE MECHANISMS AND INCREASING OF RADICAL FORMATION IN CANCER CELLS

Distruption of heme degradation pathway	Targeting of HO^{-1} with selective inhibitors and siRNA as well as an siRNA-mediated knockdown of ferrochelatase or chelation of iron ions potentiate antitumor effects of PDT
Inhibition of SOD 2	2-methoxyestradiol, a natural SOD inhibitor, enhances PDT cytotoxicity in vitro and improves antitumor effects of PDT in mice
NO synthase inhibition	Improved tumor response to PDT in mice
HSP90 modulation	Interference with HSP90 client proteins binding using a geldanamycin derivative improves responsiveness to PDT both in vitro and in vivo

TARGETING OF TUMOR VASCULATURE

Antiangiogenic treatment	Anti-VEGF or anti-VEGFR monoclonal antibodies, matrix MMP inhibitor (prinomastat), TNP-470, and other antiangiogenic agents as well as adenovirus-driven IL-12 expression potentiate antitumor effects of PDT in mice

60

1.3   NPs in PDT

A PDT treatment can be considered to be selective in that the toxicity to tumor tissue is induced by the local activation of the PS, while normal tissue not exposed to light are spared. In spite of this, several drawbacks limit the clinical application of PDT.

Firstly, several organs or tissues exposed to environmental light can suffer some phototoxicity following PS administration. For example, patients treated with PDT using porphyrins as PS exhibit some degree of cutaneous photosensitivity on exposure to solar radiation which persists for several weeks. This side effect is caused by the accumulation and prolonged retention of the PS in the skin. Secondly, the low extinction coefficients of PS require the administration of relatively large amounts of drug to obtain a satisfactory therapeutic response. Furthermore, the adsorption maximum is at a relatively short wavelength leading to a poor tissue penetration of light. Finally, most of the PS are hydrophobic. This lipophilic nature may be an important factor affecting the preferential accumulation in cellular hydrophobic loci since these molecules must be able to get into the cells by crossing lipid membranes. However, due to their minute solubility in water, iv treatment is greatly hampered. Thus, it is necessary to develop suitable delivery systems such as oil-dispersions, liposomes, polymeric NPs or hydrophilic polymer-PS conjugates.

The ideal drug delivery system should enable the selective accumulation of the PS within the diseased tissue and the delivery of therapeutic concentrations of PS to the target site with little or no uptake by non-target cells. The carrier should be able also to incorporate the PS without loss or alteration of its activity. Another reason for using vehicles is to provide an environment where the PS can be administered in a monomeric form. In fact, due to their chemical structure, most PS tend to aggregate in aqueous media. This state is one of the determining factors, which can hinder the efficacy of the drug in vivo by decreasing its bioavailability and limiting its capacity to absorb light.

Nanocarriers for the delivery of PS for PDT can be divided into passive and active based on the presence or the absence of a targeting molecule on the surface. Passive carriers can be sub-classified by material composition into biodegradable polymer-based NPs and non-polymer based NPs. Active NPs can be sub-classified by mechanism of activation.

1.3.1 Passive NPs

1.3.1.1 Biodegradable NP carriers

Biodegradable polymeric NPs have received tremendous attention as a possible means of delivering antineoplastic conventional agents, as well as PS for their capacity to lie in high drug loading, the possibility of controlling the drug release, and the existence of a large variety of materials and manufacturing processes. Investigation into biodegradable polymeric NPs for use in PDT began as early as 1990 with efforts to enhance carrier capacity and control drug release.

In 1991, Labib et al reported the encapsulation of $ZnPcS_4$ or AlPc into poly(isobutylcyanoacrylate) or poly(ethylbutylcyanoacrylate) 'nanocapsules' or 'nanospheres'[139]. Almost all subsequent research have utilized PLA/PLGA NPs. In a series of studies p-THPP was encapsulated into sterile sub-150nm biodegradable NPs based on PLGA and PLA[140,141].

At the same time, m-THPP was incorporated in biodegradable modified chitosan NPs and in vitro photocytotoxicity and cellular uptake investigated[142].

In order to further investigate these p-THPP loaded PLGA NPs, the efficacy of the encapsulated drug was assessed on the chick embryo CAM model[143]. It was proven that PDT-induced vascular occlusion of p-THPP is enhanced when encapsulated into NP delivery systems, due to a longer residence time inside the vasculature. In another study, the in vitro and in vivo photodynamic activities of verteporfin-loaded PLGA NPs intended to be intravenously injected were investigated[144]. In particular, two types of verteporfin loaded PLGA NPs (167 and 370 nm in diameter) were prepared. A higher photocytotoxic effect was evident in the case of smaller sized NPs for their higher intracellular uptake. Furthermore, in vivo studies on

---

[139]A. Labib, V. Lenaerts, F. Chouinard, J. C. Leroux, R. Ouellet, and J. E. van Lier, "Biodegradable nanospheres containing phthalocyanines and naphthalocyanines for targeted photodynamic tumor therapy," *Pharm.Res.* 8, no. 8 (1991).

[140]Y. N. Konan, M. Berton, R. Gurny, and E. Allemann, "Enhanced photodynamic activity of meso-tetra(4-hydroxyphenyl)porphyrin by incorporation into sub-200 nm nanoparticles," *Eur.J.Pharm.Sci.* 18, no. 3-4 (2003).

[141]Y. N. Konan, R. Cerny, J. Favet, M. Berton, R. Gurny, and E. Allemann, "Preparation and characterization of sterile sub-200 nm meso-tetra(4-hydroxylphenyl)porphyrin-loaded nanoparticles for photodynamic therapy," *Eur.J.Pharm.Biopharm.* 55, no. 1 (2003).

[142]Saboktakin M. Reza, R. M. Tabatabaie, A. Maharramov, and Ramazanov M. Ali, "Synthesis and in vitro studies of biodegradable modified chitosan nanoparticles for photodynamic treatment of cancer," *Int.J.Biol.Macromol.* 49, no. 5 (2011).

[143]A. Vargas, B. Pegaz, E. Debefve, Y. Konan-Kouakou, N. Lange, J. P. Ballini, H. van den Bergh, R. Gurny, and F. Delie, "Improved photodynamic activity of porphyrin loaded into nanoparticles: an in vivo evaluation using chick embryos," *Int.J.Pharm.* 286, no. 1-2 (2004).

[144]Y. N. Konan-Kouakou, R. Boch, R. Gurny, and E. Allemann, "In vitro and in vivo activities of verteporfin-loaded nanoparticles," *J.Control Release* 103, no. 1 (2005).

rhabdomyosarcoma-bearing DBA/2 mice demonstrated that verteporfin-loaded small NPs effectively controlled tumour growth for 20 days in the mice with early light irradiation times following drug administration. In yet another study based on PLGA NPs, Ricci-Junior et al reported the preparation, characterization and results of the phototoxicity assay of PLGA NPs containing ZnPc for PDT use. This system showed a strong phototoxicity on P388-D1 cells[145]. Following, another PLGA nanosystem entrapping ZnPc was developed and tested on tumor-bearing mice[146]. Other PS that have been experimented include ICG[147] and Hypericin[148]. These compounds have the potential to be used for both diagnostic and therapeutic purposes. In particular, ICG-entrapped PLGA NPs and hypericin-loaded PLA-NPs were investigated. Recently, hypocrellin was entrapped in PLGA NPs and used for PDT treatment of SCCVII growing subcutaneously in syngeneic mice[149]. Temoporfin-loaded core-shell PEG-PLGA NPs were prepared and in vivo activity assessed on athymic nude-Foxn1 mice[150]. Another novel drug delivery system for hydrophobic PS was accomplished using PEG–PCL micelles containing protoporphyrin IX[151].

1.3.1.2   Non-biodegradable NP carriers

Non-biodegradable NPs have a different role in PDT than the biodegradable ones. They are not traditionally used for drug delivery because of their inability to degrade and release drugs in controlled amounts. However, unlike other drugs, PS are not by themselves toxic to the targeted cells; rather, they act like catalysts to create toxic products from non-toxic dissolved oxygen. Like catalysts, they are themselves not destroyed by the process, and can be used repeatedly with proper activation. In such a scenario, non-biodegradable

[145]E. Ricci-Junior and J. M. Marchetti, "Zinc(II) phthalocyanine loaded PLGA nanoparticles for photodynamic therapy use," *Int.J.Pharm.* 310, no. 1-2 (2006).

[146]M. Fadel, K. Kassab, and D. A. Fadeel, "Zinc phthalocyanine-loaded PLGA biodegradable nanoparticles for photodynamic therapy in tumor-bearing mice," *Lasers Med.Sci.* 25, no. 2 (2010).

[147]V. Saxena, M. Sadoqi, and J. Shao, "Polymeric nanoparticulate delivery system for Indocyanine green: biodistribution in healthy mice," *Int.J.Pharm.* 308, no. 1-2 (2006).

[148] M. Zeisser-Labouebe, N. Lange, R. Gurny, and F. Delie, "Hypericin-loaded nanoparticles for the photodynamic treatment of ovarian cancer," *Int.J.Pharm.* 326, no. 1-2 (2006).

[149]M. Korbelik, R. Madiyalakan, T. Woo, and A. Haddadi, "Antitumor efficacy of photodynamic therapy using novel nanoformulations of hypocrellin photosensitizer SL052," *Photochem.Photobiol.* 88, no. 1 (2012).

[150]M. Rojnik, P. Kocbek, F. Moret, C. Compagnin, L. Celotti, M. J. Bovis, J. H. Woodhams, A. J. Macrobert, D. Scheglmann, W. Helfrich, M. J. Verkaik, E. Papini, E. Reddi, and J. Kos, "In vitro and in vivo characterization of temoporfin-loaded PEGylated PLGA nanoparticles for use in photodynamic therapy," *Nanomedicine.(Lond)* 7, no. 5 (2012).

[151]B. Li, E. H. Moriyama, F. Li, M. T. Jarvi, C. Allen, and B. C. Wilson, "Diblock copolymer micelles deliver hydrophobic protoporphyrin IX for photodynamic therapy," *Photochem.Photobiol.* 83, no. 6 (2007).

carriers can be used as carriers to circumvent problems of usage of the free drug. To be effective, NPs must be small enough to have a volume of distribution roughly parallel to that of the free drug. This requires stringent control on size, with a maximum allowable diameter less than 100 nm, and preferably in the sub-50 nm range.

Ceramic-based NPs, non-covalently doped with PS, hold several advantages over organic polymeric particles like ambient temperature conditions in the preparative processes, stability, exquisite control over size, shape and porosity, very low sizes (less than 50 nm), immunity to changes in pH and microbial attack. Possibly, the first paper on the use of ceramic-based NPs as a novel drug-carrier system for PDT used silica-based spherical particles encapsulating the anticancer drug HPPH[152]. Covalent bonding of the PS molecules into organically modified silica (ORMOSIL) NPs creates more stable formulations[153]. ORMOSIL was also used later by this group for TP dye encapsulation[154]. Wieder et al reported the development of a delivery system based on gold NPs, whereby a phthalocyanine is bound to the surface of the NP. In this study a significant improvement in PDT efficiency was evident as compared to the free PS[155]. TP dyes have received attention lately because of their ability to convert absorbed low-energy radiation to higher energy emissions. Dyes which can direct by transfer the higher energy to molecular oxygen for generation of singlet oxygen can be very useful in PDT because they can be activated in deep tissues. The first report in this direction used microemulsion to incorporate the TP dye porphyrin TMPyP into polyacrylamide NPs[156]. Organically modified silica NPs were used to co-encapsulate HPPH and an excess amount of BSA and TP sensitization of singlet oxygen in an aqueous dispersion was demonstrated. NPs were taken up by tumor cells and cytotoxic effect under TP irradiation was demonstrated.

---

[152]I. Roy, T. Y. Ohulchanskyy, H. E. Pudavar, E. J. Bergey, A. R. Oseroff, J. Morgan, T. J. Dougherty, and P. N. Prasad, "Ceramic-based nanoparticles entrapping water-insoluble photosensitizing anticancer drugs: a novel drug-carrier system for photodynamic therapy," *J.Am.Chem.Soc.* 125, no. 26 (2003).

[153]T. Y. Ohulchanskyy, I. Roy, L. N. Goswami, Y. Chen, E. J. Bergey, R. K. Pandey, A. R. Oseroff, and P. N. Prasad, "Organically modified silica nanoparticles with covalently incorporated photosensitizer for photodynamic therapy of cancer," *Nano.Lett.* 7, no. 9 (2007).

[154]S. Kim, T. Y. Ohulchanskyy, H. E. Pudavar, R. K. Pandey, and P. N. Prasad, "Organically modified silica nanoparticles co-encapsulating photosensitizing drug and aggregation-enhanced two-photon absorbing fluorescent dye aggregates for two-photon photodynamic therapy," *J.Am.Chem.Soc.* 129, no. 9 (2007).

[155]M. E. Wieder, D. C. Hone, M. J. Cook, M. M. Handsley, J. Gavrilovic, and D. A. Russell, "Intracellular photodynamic therapy with photosensitizer-nanoparticle conjugates: cancer therapy using a 'Trojan horse'," *Photochem.Photobiol.Sci.* 5, no. 8 (2006).

[156]D. Gao, R. R. Agayan, H. Xu, M. A. Philbert, and R. Kopelman, "Nanoparticles for two-photon photodynamic therapy in living cells," *Nano.Lett.* 6, no. 11 (2006).

1.3.2   Active NPs

1.3.2.1   Quantum dots

QDs are nanoparticulate imaging probes with high quantum yields, high photostability and fluorescent emission properties which can be tunable by size. QDs can transfer energy to surrounding O_2, with consequent toxicity to cells. Several recent papers have explored their potential as PS in their own. In probably the first paper to mention this possibility, while investigating the two-step energy-transfer mechanism from CdSe QDs to the attached PS. The authors discovered that semiconductor QDs alone can generate $^1O_2$ without a mediating PS molecule in toluene probably because of the intercalation of dissolved O_2 molecules with the TOPO layer at the QD surface [157]. To circumvent the inefficiency of QDs alone to generate singlet oxygen, several attempts have been made to covalently conjugate PSs to CdSe/ZnS via organic bridges [158] or by electrostatic interactions. For example, recently, AlPcSs, conjugated with amine-dihydrolipoic acid coated QDs by an electrostatic binding, was able to destroy the most cancer cells via FRET mediated PDT[159].

1.3.2.2   Self-lighting NPs

Self Lighting PDT is a new approach to cancer treatment through a combination of radiation therapy and PDT. Upon exposure to ionising radiation such as X-rays, scintillation luminescence will emit from the NPs and activate the PS; as a consequence, singlet oxygen is produced to enhance the killing of cancer cells by ionizing radiation. Supplementing conventional radiation therapy (that can damage healthy tissues as well) with PDT will enable the use of lower doses of radiation. When the NPs have persistence luminescence, e.g. $BaFBr:Eu^+$, Mn^+ NPs, short X-ray exposures are followed by prolonged PS excitation. The period of afterglow is increased in vivo because of higher ambient temperatures [160]. However, direct application in biological systems have not been reported yet.

---

[157] A. C. Samia, X. Chen, and C. Burda, "Semiconductor quantum dots for photodynamic therapy," *J.Am.Chem.Soc.* 125, no. 51 (2003).

[158] L. Shi, B. Hernandez, and M. Selke, "Singlet oxygen generation from water-soluble quantum dot-organic dye nanocomposites," *J.Am.Chem.Soc.* 128, no. 19 (2006).

[159] L. Li, J. F. Zhao, N. Won, H. Jin, S. Kim, and J. Y. Chen, "Quantum Dot - Aluminum phthalocyanine Conjugates perform photodynamic reactions to kill cancer cells via fluorescence resonance energy transfer (FRET)," *Nanoscale.Res.Lett.* 7, no. 1 (2012).

[160] W. Chen and J. Zhang, "Using nanoparticles to enable simultaneous radiation and photodynamic therapies for cancer treatment," *J.Nanosci.Nanotechnol.* 6, no. 4 (2006).

1.3.2.3   *Upconversion NPs*

Luminescent materials with triplet excitation states (phosphors) emit light of higher energy than exciting radiation (Anti-Stokes emission) by different mechanisms, including upconversion and simultaneous TP absorption[161]. Simultaneous TP absorption requires a single entity where the transition from ground to an excited electronic state is brought about by simultaneous absorption of two low energy photons whose combined energy is sufficient to induce the transition. Quantum mechanically, this takes place through the attainment of a virtual intermediate state on absorption of the first photon. Upconversion relies on sequential discrete absorption and luminescence steps where at least two metastable entities (usually ions) are involved, the first serving as an excitation reservoir, and the second as the emitting state. It is generally a more efficient process, does not require coherent radiation and involves real (as opposed to virtual) intermediate states. Anti-Stokes emissions for upconversion processes are found to exceed excitation energies by 10–100 times kT. Since both the mechanisms allow excitation with low energy light and since this is known to penetrate tissues deeply, NPs excited by each process have been used to activate PS. The common advantage is in extending the reach of PDT to tumor sites several centimeters below the skin/mucosal surface. The role of the NPs here can be likened to a nanotransducer. NPs are by themselves unable to generate singlet oxygen species from dissolved oxygen, and require the attachment of an appropriate PS with an excitation band matching the emission of the NPs. Upconversion NPs are modified nanometer-sized composites which generate higher energy light from lower energy radiation, usually near-infrared or infrared, through the use of transition metal, lanthanide, or actinide ions doped into a solid state host. A variety of core materials and dopants have been demonstrated for upconversion particles with actual/possible biological applications.

The first reported use of upconversion NPs in PDT used NaYF4:Yb3+, Er3+ NPs coated with a porous, thin layer of silica doped with merocyanine-540 PS and functionalized with a tumor targeting antibody[162]. Then, upconversion ZnPc/PEI/NaYF4 NPs were developed. The ability to observe the emission from the NPs to some depth within tissues can have enormous impact on the diagnosis and monitoring of some tumors. NIR light, for example, can penetrate to a considerable extent in soft fibro-fatty tissues like breast, and the

---

[161]F. Auzel, "Upconversion and anti-Stokes processes with f and d ions in solids," *Chem.Rev.* 104, no. 1 (2004).

[162]P. Zhang, W. Steelant, M. Kumar, and M. Scholfield, "Versatile photosensitizers for photodynamic therapy at infrared excitation," *J.Am.Chem.Soc.* 129, no. 15 (2007).

upconversion NPs can potentially be used for therapy as well as monitoring of tumors over time.

1.3.3   NPs in combined PDT

The idea to combine two drugs with different mechanism of action and pharmacokinetics in a nanocarrier with well-tailored properties can allow a control over anticancer drug/PS biological fate and promote co-localization in the same area of the body[163]. This approach is rather recent and demonstrated to be a promising strategy to overcome tumor drug resistance in a mouse tumor model treated with doxorubicin in combination with the PS methylene blue[164]. In particular, surfactant-polymer hybrid NPs formulated using an anionic surfactant, Aerosol-OT, and a naturally occurring polysaccharide polymer, sodium alginate, were used for synchronized delivery of the two drugs. Balb/c mice bearing syngeneic JC tumors (mammary adenocarcinoma) were used as a drug-resistant tumor model. NP-mediated combination therapy significantly inhibited tumor growth and improved animal survival. NP-mediated combination treatment resulted in enhanced tumor accumulation of both doxorubicin and methylene blue, significant inhibition of tumor cell proliferation, and increased induction of apoptosis. Moreover, a study of combination of PDT with chemotherapy using as a model tumor mammary adenocarcinoma was conducted; the results showed that this combination may result in a decrease in resistance of the tumor .

---

[163]G. Palumbo, "Photodynamic therapy and cancer: a brief sightseeing tour," *Expert.Opin.Drug Deliv.* 4, no. 2 (2007).

[164]A. Khdair, D. Chen, Y. Patil, L. Ma, Q. P. Dou, M. P. Shekhar, and J. Panyam, "Nanoparticle-mediated combination chemotherapy and photodynamic therapy overcomes tumor drug resistance," *J.Control Release* 141, no. 2 (2010).

AIM OF THE WORK

The goal of the project was to design and develop biodegradable nanocarriers for the combined delivery of a conventional cytotoxic drug and a PS for PDT with the aim to potentiate anticancer effect and attenuate toxicity profile of both drugs. To this purpose, we developed iv nanoassemblies with different structures and able to deliver both hydrophilic and hydrophobic molecules.

The knowledge of the state of the art has encouraged us to focus on nanocarriers based on amphiphilic PCL-PEO block copolymers developed from the group of Prof. Maglio at Department of Chemistry - University of Napoli Federico II. PCL-PEO block copolymers with different architectures were synthesized according to well established procedures and by novel "core first" - "coupling onto" strategies based on ROP polymerization followed by coupling of different segments performed with condensation or "click" chemistry reactions.

DTX and the highly lipophilic phtalocyanine ZnPc were selected as conventional chemotherapeutic and PS, respectively, to obtain "the proof of concept".

DTX, a semisynthetic taxane (Figure 16) analogue of Paclitaxel, is one of the most widely used chemotherapeutic agents in solid tumors, with efficacy against advanced breast, non-small lung cancers, head and neck, ovary, prostate, stomach and urothelium cancers[165,166]. The anticancer mechanism of DTX as a potent inhibitor of cancer cell replication is related to its ability to block cancer cells in the late G2-mitotic phase of the cell cycle by stimulating microtubule polymerization and suppressing their dynamics. In analogy to many other anticancer drugs, DTX suffers for severe toxicity related to myelosuppression whereas neutropenia is usually considered as dose-limiting factor. Nevertheless, asthenia and peripheral neuropathy can limit continued administration of weekly DTX[167]. Furthermore, DTX is sparingly soluble in water and thus difficult to formulate in dosage forms intended for iv delivery.

In recent years, a conspicuous number of controlled release systems were developed to deliver DTX, improving its antitumor activity as well as reducing its toxicity profile (see table 1).

---

[165]F. Calabro and C. N. Sternberg, "New drugs and new approaches for the treatment of metastatic urothelial cancer," *World J.Urol.* 20, no. 3 (2002).

[166]S. J. Clarke and L. P. Rivory, "Clinical pharmacokinetics of docetaxel," *Clin.Pharmacokinet.* 36, no. 2 (1999).

[167]P. E. Kintzel, L. B. Michaud, and M. K. Lange, "Docetaxel-associated epiphora," *Pharmacotherapy* 26, no. 6 (2006).
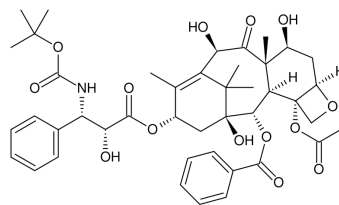
Figure 16. Chemical structure of DTX.

ZnPc is a second generation PS, not yet approved in therapy, able of producing cytotoxic singlet oxygen with high yield [168, 169]. Structurally related to porphyrins (Figure 17), it is characterized by a high molar extinction coefficient (25000 $M^{-1}cm^{-1}$) and a maximum absorption peak between 670 and 770 nm in the red region of the spectrum. The presence of the central atom of Zn provides a high yield of singlet oxygen with long half-life of the triplet state. This highly hydrophobic molecule localizes exclusively in mitochondria and after irradiation induces direct damage to cellular organelles. It was demonstrated that ZnPc is able to bind lipoproteins and serum albumin depending on the vehicle used for administration. Hydrophobic character of ZnPc hinders its systemic administration but, on the contrary, facilitates its encapsulation in many drug delivery systems as liposomes[170,171], polymeric micelles[172,173] and NPs[174].

[168]C. Fabris, G. Valduga, G. Miotto, L. Borsetto, G. Jori, S. Garbisa, and E. Reddi, "Photosensitization with zinc (II) phthalocyanine as a switch in the decision between apoptosis and necrosis," *Cancer Res.* 61, no. 20 (2001).

[169]A. Juarranz, J. Espada, J. C. Stockert, A. Villanueva, S. Polo, V. Dominguez, and M. Canete, "Photodamage induced by Zinc(II)-phthalocyanine to microtubules, actin, alpha-actinin and keratin of HeLa cells," *Photochem.Photobiol.* 73, no. 3 (2001).

[170]C. A. de Oliveira, L. K. Kohn, M. A. Antonio, J. E. Carvalho, M. R. Moreira, A. E. Machado, and F. B. Pessine, "Photoinactivation of different human tumor cell lines and sheep red blood cells in vitro by liposome-bound Zn(II) Phthalocyanine: Effects of cholesterol," *J.Photochem.Photobiol.B* 100, no. 2 (2010).

[171]G. H. Rodal, S. K. Rodal, J. Moan, and K. Berg, "Liposome-bound Zn (II)-phthalocyanine. Mechanisms for cellular uptake and photosensitization," *J.Photochem.Photobiol.B* 45, no. 2-3 (1998).

[172]W. M. Sharman, J. E. van Lier, and C. M. Allen, "Targeted photodynamic therapy via receptor mediated delivery systems," *Adv.Drug Deliv.Rev.* 56, no. 1 (2004).

[173]C. F. van Nostrum, "Polymeric micelles to deliver photosensitizers for photodynamic therapy," *Adv.Drug Deliv.Rev.* 56, no. 1 (2004).

[174]Soares M. da Volta, M. R. Oliveira, E. P. dos Santos, Gitirana L. de Brito, G. M. Barbosa, C. H. Quaresma, and E. Ricci-Junior, "Nanostructured delivery system for zinc phthalocyanine: preparation, characterization, and phototoxicity study against human lung adenocarcinoma A549 cells," *Int.J.Nanomedicine.* 6 (2011).
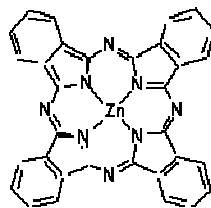
Figure 17. Chemical structure of ZnPc.

Specific tasks of the work can be outlined as follow:

T1) Development of PCL-PEO nanoassemblies to deliver hydrophilic molecules

Design and production of nanostructures able to deliver hydrophilic compounds is a challenging task, especially when using PCL-PEO copolymers. To this purpose we investigated the ability of different PCL-PEO block copolymers to self-assemble in water forming nanostructures for the entrapment of hydrophilic molecules. Thus, we prepared nanocapsules with an inner aqueous core for the sustained release of hydrophilic molecules through a novel emulsion melting-sonication technique.

T2) Development of intravenous nanoassemblies to deliver DTX

We focused on biodegradable block copolymers of PCL-PEO with two different architectures (diblock and triblock), as base material. Block copolymers were assembled in core-shell NPs entrapping DTX by the MeSo method. Formulation studies were mainly devoted to obtain nanocarriers which are stable in biological environments, entrap high amounts of drug and deliver it at controlled rates. Thanks to the collaboration with Dr Caraglia (Department of Biochemistry - Second University of Napoli) and Dr Arra (Tumor Institute Pascale), we were able to assess toxicity of NPs in several cancer cell lines and in mice as a preliminary step for further activity studies.

72

T3) Development of multifunctional nanoparticles entrapping ZnPc and DTX for combined photodynamic and conventional therapy of cancer

Nanocarriers were developed with the aim to combine two drugs with different pharmacokinetics in a nanocarrier with well-tailored properties which can allow a control over anticancer drug/PS biological fate and promote their co-localization in the same area of the body. Combined NPs containing both DTX and ZnPc were prepared again by MeSo employing the same amphiphilic materials. Overall properties, stability, and *in vitro* biological behavior of NPs as well as fluorescence behavior were evaluated. Cell culture studies aimed to clarify the cellular biofate encompassing both mechanisms involved in cellular uptake and molecular events controlling cellular response were carried out. Finally, in vivo activity of these systems in an ortothopic mice model of amelanotic melanoma was investigated.

CHAPTER 2: Nanocapsules Based on Linear and Y-Shaped 3-Miktoarm Star Block PEO-PCL Copolymers as Sustained Delivery System for Hydrophilic Molecules

Nanocapsules Based on Linear and Y-Shaped 3-Miktoarm Star Block PEO-PCL Copolymers as Sustained Delivery System for Hydrophilic Molecules

Giovanni Maglio,† Fabio Nicodemi,† Claudia Conte,‡ Rosario Palumbo,†
Pasquale Tirino,†Elisabetta Panza,§ Angela Ianaro,§ Francesca Ungaro,‡ and
Fabiana Quaglia‡

†Department of Chemistry "Paolo Corradini", ‡Department of Pharmaceutical and
Toxicological Chemistry, and §Department of Experimental Pharmacology, University
of Naples Federico II, Naples, Italy

76
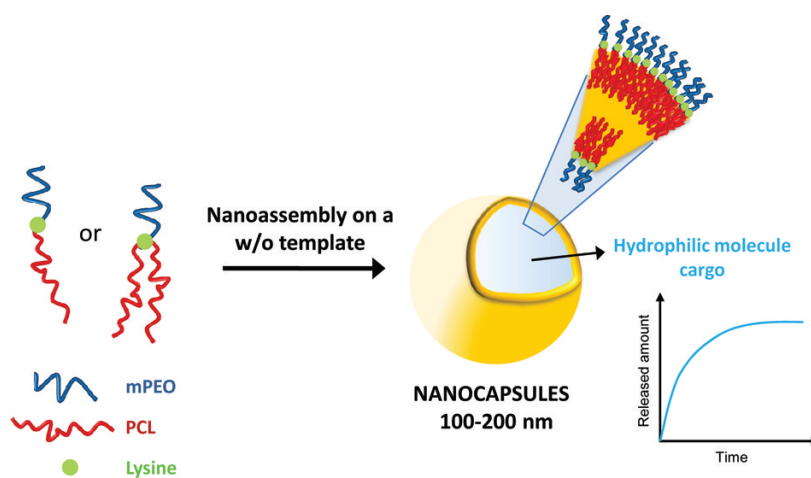
Abstract

Well-defined amphiphilic Y-shaped miktoarm star block copolymers of PEO and PCL were synthesized by ring opening polymerization of ε-caprolactone initiated by a PEO bound lysine macroinitiator. The copolymers were characterizedby ^{1}H NMR, SEC, DSC, and WAXD techniques. Separate PCL and PEO crystalline phases occur in melt-crystallized copolymers when their segmental lengths were comparable and the PCL content was ≤80 wt %. Self-assembling of these copolymers in aqueous medium led to nanoaggregates with low critical aggregation concentration values (0.35 to 1.6 mg·L^{-1}) and size depending on composition. Despite the fact that copolymers were not prone to self-organize in vesicles, once processed by a novel w/o emulsion-melting/sonication technique, they gave nanocapsules with a water core and a hydrophilic surface. A macromolecular fluorescent dye was effectively loaded and released at sustained rate by optimizing nanocapsule formulation. The results demonstrate that amphiphilic block copolymers can be assembled in different kinds of nanomorphologies independently of their hydrophilic/hydrophobic balance and architecture through specifically designed preparation techniques.

Introduction

Materials, such as protein, oligonucleotides (ODNs) and siRNA represent forthcoming treatments of cancer and viral infections. Thus, for optimal activity, the ideal carrier system would be hydrophilic molecules entrapped within the internal core of polymeric nanocapsules wall [1] or polymersomes [2-4] in order to mask them and to protect them from interactions with proteins.

Amphiphilic block copolymers (ABCs) have received increasing interest because they can aggregate in aqueous medium, leading to different nanomorphologies, mainly dictated by block copolymer composition and molecular geometry[1,2].

Much interest has concerned miktoarm star-block copolymers, branched systems with three or more arms, at least two of which are chemically different. Their structure is thereby characterized by the presence of different building blocks linked to the same junction point.[3-8] Several synthetic strategies such as atom transfer or nitroxide-mediated radical polymerization (ATRA, NMP), reversible addition–fragmentation chain transfer (RAFT), and "click chemistry" reactions have been successfully employed in the synthesis of miktoarm star-block copolymers with well-defined macromolecular building blocks and architecture[9-13]. Many ABCs contain as hydrophilic component blocks of poly(ethylene oxide) (PEO) that impart structure stability and biomimetic properties to formed nanostructures[14]. Poly(ε-caprolactone) (PCL) has been frequently used to form the core of self-assembling ABC systems owing to its high hydrophobicity, propensity to aggregation, as well as low glass transition temperature that ensures a partial rubbery core. PEO-PCL copolymers are currently investigated as base materials for different drug delivery systems[15,16] although the most promising application remains in the field of anticancer drug delivery[17,18]. In fact, nanocontainers of PEO-PCL with core-shell structures consisting in a core of hydrophobic blocks surrounded by an hydrated flexible fringe of hydrophilic blocks have been intensively investigated in the past few years as delivery system for lipophilic drugs[19-23]. Linear di- and triblock systems have been extensively employed as drug nanocarriers; also, branched PCL-*g*-PEO and multiarm star-shaped PEO-PCL diblock copolymers have attracted attention and synthetic procedures to obtain star architectures with different numbers have been developed[24-30]. Nevertheless, it has been recognized that hydrophilic/lipophilic balance is a key factor controlling the type of aggregate formed (micelle, worm, vesicles) as well as stability in biological media[31-33]. Much more complicated is to obtain

nanostructures based on PEO-PCL copolymers able to deliver hydrophilic compounds. In this research area, some work has been done to develop tailor made ABC able to self-organize in vesicles, that is, the so-called polymersomes[34,35]. Again, hydrophobic–hydrophilic balance inspires the organization and morphology of the ABCs, and the nature and the length of the blocks determine their stability, size, drug-loading capacity, and release rate.[32] Nevertheless, PEO-PCL polymersomes spontaneously evolve to micelles in an aqueous environment, rapidly delivering their drug cargo.[36] Prompted by these considerations, here we try to design PEO-PCL NPs able to entrap efficiently hydrophilic molecules and release them at sustained rates. To this purpose, we developed a novel emulsion/melting-sonication technique based on copolymer hardening on a w/o emulsion template. Both linear and Y-shaped 3-miktoarm star-block PEO-PCL copolymers were employed in the study to understand the suitability of the technique on different PEO-PCL architectures. Miktoarm copolymers were obtained through a straightforward synthetic strategy based on the combination of coupling reactions and ring-opening polymerization (ROP) using lysine as a core molecule. Self-organization properties were investigated and compared with those of a linear diblock PEO-PCL copolymer of similar composition, with the aim to evaluate the influence of copolymer architecture on self-aggregation both in aqueous environment and using the emulsion-melting sonication technique. Rhodamine-dextran was selected as a model hydrophilic macromolecule and its encapsulation in and release from nanocapsules investigated. Finally, toxicity toward red blood cells and melanoma cell lines was tested.

Experimental part

Materials

α-OCH$_3$,ω-NH$_2$ poly(ethylene oxide) with Mn =2.0 kDa (mPEO$_{2.0k}$-NH$_2$, Aldrich) was dried by distillation of the water–toluene azeotrope. ε-Caprolactone (CL, Aldrich) was dried over CaH$_2$ at room temperature for 48 h and then distilled under vacuum before use. Stannous-(2-ethylhexanoate)$_2$ (Sn(oct)$_2$, Aldrich) and pyridine (Fluka) were purified by vacuum distillation before use. N-Hydroxysuccinimide (NHS) and succinic anhydride (SA) (Fluka) were dried under high vacuum. N,N-diisopropylethylamine (DIPEA), $N\alpha,N\varepsilon$-di-Z-lysine (di-Z-lys), N,N'-dicyclohexylcarbodiimide (DCCI), and 4-dimethylaminopyridine (DMAP), all provided by Fluka, and Pd/C (Pd 10 wt % by Aldrich) were used without further purification. Potassium phosphate dibasic and potassium phosphate monobasic,sodium azide, sodium chloride, Span 80, polyethylene glycol (PEG, Mw 400 Da), rhodamine B isothiocyanate-Dextran (RhDex, Mw 10kDa), and 3-[4,5-dimethyltiazol-2yl]-2,5 diphenyl tetrazolium bromide (MTT) were from Sigma-Aldrich. Sodium hydroxide was from Delchimica Scientific Glassware. Miglyol 812 (capryl/caprylictriglycerides) was from Farmalabor (Italy). Normal hexane, methylenechloride (DCM), and chloroform (CHCl$_3$) of analytical grade were purchased from Carlo Erba Reagenti (Milan, Italy). Analytical grade DCM and CHCl$_3$ were dried according to literature methods.

Synthesis of the macroinitiator Lys-mPEO$_{2.0\ k}$ (1). A two-steps procedure was used in the synthesis of the macroinitiator after a preliminary activation of the –COOH group of di-Z-Lys with NHS, performed in a CHCl$_3$ solution using DCCI as condensing agent and DMAP as catalyst.

(a) A solution of mPEO$_{2.0k}$-NH$_2$ (1.02 g, 0.51 mmol) and activated di-Z-Lys (0.255 g, 0.50 mmol) in 12 mL of DCM was stirred at r.t. for 24 h. The crude product recovered removing the solvent was washed with a diethyl ether/methanol mixture (3:1 v:v), then purified by column chromatography on silica gel to eliminate unreacted mPEO$_{2k}$-NH$_2$ using a CHCl$_3$/CH$_3$OH mixture as eluent, with a linear gradient of 2, 4, 8 wt% of CH$_3$OH. Di-Z-Lys-mPEO$_{2.0k}$ was recovered removing the solvents under vacuum (1.01 g,70% yield): ^{1}H–NMR (CDCl$_3$, ppm): 7.35 (10H, aromatic H of Z group); 5.40 (1H, -CH$_2$-NH-CO-O-CH$_2$-$\varnothing$); 5.20-5.00 (5H, -CO-O-CH_2-$\varnothing$ + -CH-NH-CO-O-CH$_2$-$\varnothing$); 3.70-3.60 (176H, -CH$_2$OCH$_2$-); 3.45 (2H, -CO-NH-CH_2-PEO); 3.36 (3H, -OCH$_3$); 3.20 (2H, -CH$_2$-CH_2-NH-CO-O-$\varnothing$); 2.00-1.00 (6H, -CH-(CH_2)$_3$-CH$_2$-NH-CO-O-CH$_2$-$\varnothing$).

80

(b) Pd/C (0.266 g) was added to a solution of di-*Z*-Lys-PEO$_{2.0k}$ (1.498 g) in 35 mL of methanol and hydrogen was bubbled for 6 h at 30°C. The reaction mixture was then centrifuged to eliminate Pd/C and the supernatant solution was filtered through a celite layer. Methanol was removed under vacuum to give 1.11 g (85% yield) of Lys-*m*PEO$_{2.0k}$ (**1**) (η_{inh} 0.15 dL·g^{-1}, 80 % yield). ^{1}H–NMR (CDCl$_3$, ppm): 3.70-3.60 (176H, -CH$_2$OCH$_2$-); 3.45 (2H, -Lys-CO-NH-C*H*$_2$-PEO); 3.36 (3H, -OCH$_3$); 3.20 (2H, -CH-CH$_2$-CH$_2$-CH$_2$-C*H*$_2$-NH-*Z*); 1.0-2.0 (6H,-CH-(C*H*$_2$)$_3$-CH$_2$-NH-Lys.

Synthesis of (Lys-mPEO$_{2.0\,k}$)-(PCL$_{2.1\,k}$)$_2$ (2a) and (Lys-mPEO$_{2.0\,k}$)-(PCL$_{6.15\,k}$)$_2$(2b), AB$_2$ block copolymers (A=PEO, B=PCL). A 50 mL flask was charged under nitrogen with (1) (0.94 g, 0.45 mmol) and CL (1.90 g, 16.7 mmol). The mixture was stirred at 80 °C for 24 h, then Sn(Oct)$_2$ (3.7 mg, 9.1 µmol) was added to the mixture and the polymerization was carried out at 120 °C for 24 h. After cooling, the product was dissolved in 6 mL of CHCl$_3$ and precipitated in chilled diethylether (300 mL). The precipitate was collected and dried in a vacuum oven to give 2.41 g of (2a). (ηinh = 0.18 dL·g^{-1}, 85% yield, Mw/Mn = 1.48). ^{1}H–NMR (CDCl$_3$, ppm): 4.05 (72H, -CH$_2$-OCO-, PCL); 3.65 (178H, -CH$_2$-O-, PEO, + 4H, -CH$_2$-CH$_2$-OH, PCL); 3.45 (2H, -Lys-CO-NH-CH$_2$-, PEO);3.36 (3H, -OCH$_3$, PEO); 2.3 (72-CH$_2$-CO-, PCL); 1.8-1.3 (224H, -O-CH$_2$-[CH$_2$-]$_3$-CH$_2$CO-, PCL, + -[CH$_2$]$_3$-CH$_2$-NH-, Lys). (Lys-mPEO$_{2.0k}$)-(PCL$_{6.15k}$)$_2$, (2b), was obtained according to the above procedure using a monomer to initiator molar ratio of 112. (ηinh = 0.30 dL·g-1, 87% yield, Mw/Mn = 1.64).

Synthesis of the A(BA)$_2$ block copolymer (Lys-PEO$_{2.0,k}$)-(PCL$_{6.15\,k}$-PEO$_{2.0\,k}$)$_2$. The synthesis was carried out through a two-steps procedure:
(a) (Lys-PEO$_{2.0k}$-(PCL$_{6.15k}$)$_2$, (**2b**), (1.55 g, 0.11 mmol) dissolved in 8 mL of CHCl$_3$ was reacted with 0.068 g (0.68 mol) of SA and 0.004 g of pyridine (50.6 mmol) for 48 h at 60 °C. The solution was poured in 400 mL of a diethylether/methanol mixture (5:2 v:v) and the precipitated (Lys-PEO$_{2.0\,k}$)-(PCL$_{6.15\,k}$-COOH)$_2$ was collected and dried in a vacuum oven (1.41 g, 90% yield). (b) NHS (21 mg, 0.18 mmol), DCC (37 mg, 0.18 mmol) and DMAP (4.0 mg, 3.3 mmol) were added to a solution of (Lys-PEO$_{2.0k}$)-(PCL$_{6.15k}$-COOH)$_2$ (0.643g, 45.0 µmol) in 6 mL of CH$_2$Cl$_2$. The reaction was carried out for 24 h at r.t. under stirring. Then, after filtration to remove the precipitated dicyclohexylurea, the solution was poured in 300 mL of a diethylether/methanol mixture (5:2 v:v). The precipitate was collected and dried under vacuum at 30°C (0.579 . Activated (Lys-PEO$_{2.0k}$)-(PCL$_{6.15k}$-

COOH)$_2$ (0.579 g 0.04 mmol) and 0.217 g (0.11 mmol) of mPEO$_{2.0k}$-NH$_2$ were dissolved in 10 mL of DCM. After addition of DIPEA (0.021 g, 0.23 mmol), the reaction was carried out at r.t. for 24 h. The reaction mixture was poured in 300 mL of a diethylether/methanol mixture (5:2 v:v) and the precipitate was collected and dried under vacuum (0.685 g, 86% yield, η_{inh} = 0.36 dL·g^{-1}, M_w/M_n =1.48).

Synthesis of the AB diblock copolymer PEO$_{2.0k}$-PCL$_{4.3k}$. A linear AB diblock copolymer was prepared by ROP of CL at 120 °C for 24 h using α-methoxy,ω-hydroxyl-PEO (M_n = 2.0 kD) as initiator and Sn(Oct)$_2$ as catalyst; CL: initiator molar ratio = 38 (η_{inh} = 0.28 dL·g^{-1}, 88% yield, M_w/M_n = 1.16).

Polymer Characterization

^{1}H NMR spectra were recorded at 25 °C on a Varian-Gemini spectrometer at 200 MHz using CDCl$_3$ as asolvent and TMS as internal reference. Differential scanning calorimetry (DSC) analyses were carried out under nitrogen on 5 to 6 mg samples using a Mettler-Toledo 30 instrument with a 2 °C·min^{-1} scanning rate in the temperature range 0–80 °C. Inherent viscosities were measured at 25 °C in CHCl$_3$ using an Ubbelhode viscometer (c = 0.5 g·dL^{-1}). Wide-angle X-ray diffraction spectra (WAXS) were recorded with a Philips PW-1711 diffractometer using a Ni-filtered Cu K α radiation; the crystallinity degree was evaluated subtracting the contribution of the amorphous part from the total scattering. Size-exclusion chromatography (SEC) was performed on a Jasco PU-1580 system equipped with a refractive index detector, using polystyrene standards as reference. Samples were eluted in tetrahydrofuran at 25 °C through three Polymer Laboratories Phenogel columns connected in series.

Copolymers Self-Assembly

Critical aggregation concentration (CAC) of the copolymers was determined by a fluorescence spectroscopy method, as previously reported.[29] In brief, copolymers were stirred for 24 h in water at 60 °C. The dispersion was cooled at room temperature and filtered to eliminate undissolved polymer. Polymer solubility was assessed by weighing the sample after freeze-drying. A pyrene solution in acetone was added in 2 mL flasks to provide a final concentration of 6 × 10^{-7} M. Acetone was evaporatedand replaced with aqueous polymer solutions at different concentrations ranging from 0.084 to 42 μg/mL for AB to 0.23–615 μg/mL for Y-shaped copolymers. Samples were heated to 65 °C for 1 h,cooled to room temperature, and analyzed at 25°C on a Shimadzu RF-1501

spectrofluorimeter. Excitation spectra were registered at $\lambda_{em} = 390$ nm, and the ratio $I334/I331$ was plotted against polymer concentration. CAC was extrapolated from the linear part of the graph. The size of aggregates was evaluated on the above samples and determined by photon correlation spectroscopy using a N5 submicrometer particle size analyzer (Beckman-Coulter). Dispersion was diluted in Milli-Q water at the intensity between 104 and 106counts/s, and measurements were performed at 25 °C on 90° angle.

Nanocapsule Preparation

Nanocapsules with an inner aqueous core were prepared by an emulsion-melting/sonication procedure. A vial containing 10 mg of copolymer and 2 mL of a 2% (w/v) solution of Span 80 in Miglyol 812 was placed in a water bath heated to 75 ± 1°C to allow copolymer melting. Then, 0.2 mL of water or a water/PEG$_{400}$ 1:1 v/v solution containing RhDex (0.2 mg) was added to the previously warmed mixture and allowed to equilibrate at the same temperature. The sample was sonicated for 10 min at 3W (Sonicator 3000, Misonix) by a microtip probe. Nanocapsules were finally cooled and allowed to harden under magnetic stirring at room temperature. Nanocapsules were washed four times (twice with hexane and twice with distilled water) by ultracentrifugation at 137,000 *g* for 30 min to remove the external oily phase and the unloaded molecules. Then, nanocapsules were freeze-dried without the help of cryoprotectant and kept at 4 °C. Recovery yield of nanocapsules was evaluated, weighting the solid residue after freeze-drying. Results are expressed as the ratio of the actual nanoparticles weight to the theoretical polymer weight × 100.

Nanocapsule Characterization

The hydrodynamic diameter and polydispersity index of nanocapsules were determined by photon correlation spectroscopy (PCS) using a N5 submicrometer particle size analyzer (Beckman-Coulter). Nanocapsules dispersion was dilutedin Milli-Q water at the intensity between 104 and 106 counts/s, and measurements were performed at 25 °C on 90° angle. Each sample was analyzed in triplicate. Zeta potential was determined by analyzing a dispersion of nanocapsules in water on a Zetasizer Nano Z (Malvern Instruments). Results are reported as the mean of three separate measurements on three different batches ± standard deviation.

The morphology of nanocapsules was assessed by TEM on a Leo 912 AB microscope (Zeiss). A dispersion of nanocapsules in water was placed on a copper grid and stained with uranile acetate (2% w/v). ^{1}H NMR spectra of a

nanocapsule dispersion in D_2O were recorded at 25 °C on a Varian-Gemini spectrometer at 200 MHz.

RhDex Loading and Release from Nanocapsules

RhDex loading inside nanocapsules was assessed by treating 1 mg of freeze-dried nanocapsules in 1 mL of methylene chloride and extracting RhDex in 1 mL of water under vortex mixing. Phase separation was accomplished by centrifugation at 5000 rpm and 4 °C for 1 min (Universal 16R, Hetting Zentrifugen). The amount of RhDex in the aqueous phase was measured by spectrofluorimetry at λ_{ex} = 556 nm and λ_{em}= 573 nm (RF-1501, Shimadzu). To verify a possible interference of copolymers, we treated an amount of unloaded nanocapsule by the same method and analyzed it. The linearity of response was verified in the concentration range 0.1 to 2 μg/mL (R^2 =0.996, LOD = 0.001 μg/mL, LOQ = 0.002 μg/mL). Results are expressed as actual loading percent (mg of RhDex encapsulated per 100 mg of nanocapsules) and encapsulation efficiency (ratio of actual to theoretical loading).

Release profile of RhDex from nanocapsules was evaluated by placing 0.5 mL of a nanocapsule dispersion (2 mg/mL) in a dialysis sac (molecular weight cutoff 50 000 Da, Spectra/Por), which was placed in 5 mL of a 10 mM phosphate buffer at pH 7.4 and 37 °C. At predetermined intervals, 1 mL of medium was withdrawn and replaced by the same amount of fresh buffer. As a control, the release profile of free RhDex was evaluated. RhDex in the release medium was quantified according to the previously described method.

Hemolysis

Human blood freshly collected in EDTA-containing tubes was washed three times with isotonic 10 mM phosphate buffer saline (PBS) solution (pH 7.4) by centrifugation at 880g for 5 min (Universal 320R, Hettich Zentrifugen), and the pellet, containing red blood cells (RBCs), was finally diluted 1:10 v/v with 10 mM PBS. RBC suspension (0.1 mL) was added to 0.9 mL of a nanocapsuledispersion at concentration ranging from 0.01 to 1.0 mg/mL of copolymer. After incubation at 37 °C for 30 min, the sample wascentrifuged at 1000g for 10 min to remove nonlysed RBC. The supernatant was collected and analyzed for hemoglobin release by spectrophotometric determinations at 416 nm. To obtain 0 and 100% hemolysis, 0.1 mL of RBC suspension was added to 0.9 mL of PBS and distilled water, respectively. The degree of hemolysis was determined by the following equation: hemolysis (%) =(ABS $-$ ABS$_0$)/(ABS$_{100}-$ ABS$_0$) $\times$ 100, where ABS$_{100}$ and ABS$_0$ are the absorbances of the solution at 100 and 0% hemolysis, respectively.

Cytotoxicity Assay

The human melanoma cell lines A375 and the normal human epidermal melanocytes (NHEMs) (PromoCell, Germany) were tested. NHEMs were grown in melanocyte growth medium 2 (PromoCell), whereas A375 were grown in complete Dulbecco's modified Eagle's medium (DMEM), supplemented with 10% fetal bovine serum (FBS), 2 mM glutamine, 25 mM HEPES, 100 units/mL penicillin, and 100 μg/mL streptomycin at 37 °C in a humidified incubator under 5% CO_2. Cell proliferation was measured by the MTT assay.[35] The cells were seeded on 96-well plates (1×10^4cells/well) and treated with nanocapsules (0.1 to 1 mg/mL) for 24–48 h before adding 25 μL of MTT (5 mg/mL in saline). Cells were thus incubated for additional 3 h at 37 °C. After this time interval, cells were lysed, and dark-blue crystals were solubilized with a solution containing 50% (v/v) *N,N*-dimethyl formamide and 20% (w/v) sodium dodecylsulfate with a pH adjusted to 4.5. The OD of each well was measured with a microplate spectrophotometer (Titertek Multiskan MCC/340) equipped with a 620 nm filter.

Results and Discussion

Synthesis and Characterization of Copolymers

Well defined miktoarm star-block AB_2 and $A(BA)_2$ copolymers (A=PEO, B=PCL) were synthesized via a combination of segment coupling and ROP of CL. *Nα,Nε*-di-Z-lysine (di-Z-lys) was used as a multifunctional core molecule with a carboxyl group and two carbobenzyloxy (Z)-protected functional amino groups available for sequential reactions. The reaction pathway is displayed in Scheme 1.
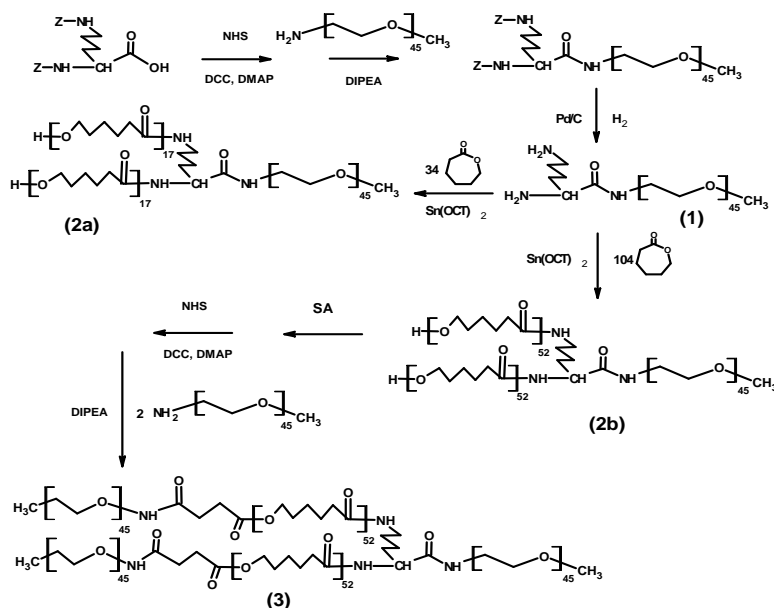
Scheme 1. Synthetic Pathways for Miktoarm Y-Shaped PEO-PCL Block Copolymers.

First, *α*-methoxy,*ω*-amino-PEO with *M*n=2 kDa (*m*PEO$_{2.0k}$-NH$_2$) was reacted with a di-Z-Lys previously activated with NHS converting the carboxyl group into a succinimidylester group. Then, deprotection of the amino groups by catalytic hydrogenation leads to product (1), containing a single *m*PEO chain and two −NH$_2$ groups, which was used as a macroinitiator of the bulk ROP of CL in the presence of a catalytic amount of Sn(oct)$_2$. The molecular weight of PCL blocks was controlled varying the CL/initiator molar ratio in the feed.

Two different Mn values, 2.0 and 6.0 kDa, were selected for the PCL segments, yielding two AB$_2$ copolymers, mPEO$_{2.0k}$-(PCL$_{2.1k}$–OH)$_2$ (2a) and mPEO$_{2.0k}$-(PCL$_{6.15k}$–OH)$_2$ (2b). The copolymer (3), with the A(BA)$_2$ architecture, was obtained by coupling of two mPEO$_{2k}$-NH$_2$ chains to the PCL segments of 2b, after conversion of PCL hydroxyl end groups into carboxyl groups subsequently activated by NHS. The molecular structures of the macroinitiator and copolymers were investigated by ^{1}H NMR spectroscopy. The coupling of mPEO$_{2k}$-NH$_2$ to di-Z-Lys was detected monitoring the appearance in the spectrum of 1 of a resonance at 3.46 ppm attributed to –O–CH_2–CH_2–NH–CO–end groups of linked PEO chains (Supporting Information, Figure S1). A reaction degree ≥90% was estimated by comparing the resonance integral of –CH$_2$–O–CH$_2$– units of PEO at 3.6 to 3.7 ppm with those relative to CH$_2$ and aromatic –CH– protons of benzyl-protecting groups of di-Z-Lys at 5.20 and 7.35 ppm, respectively. The quantitative deprotection of –NH$_2$ groups in the Lys moiety by hydrogenation was assessed, monitoring the disappearance of the resonances due to the Z group. The average PCL chain length in the AB$_2$ copolymers was evaluated from the relative intensity of the α-hydroxy methylene protons of –CH_2–OH chain ends at 3.64 ppm and the inner methylene protons –CH_2–O–CO– of the main chain at 4.07 ppm (Supporting Information, Figure S2). The experimental Mn values found by ^{1}H NMR were close to those calculated from the monomer/initiator molar ratio in the feed. Unimodal and rather sharp molecular weight distributions were found by SEC analysis (Supporting Information, Figure S3). Direct evidence of the successful coupling of two mPEO$_{2.0k}$ segments to mPEO$_{2.0k}$-(PCL$_{6.15k}$-OH)$_2$ in the synthesis of the A(BA)$_2$ copolymer was found evaluating by ^{1}H NMR the enrichment of PEO in the (3) copolymer compared with the (2B) precursor. Accordingly, the SEC diagram of (3) displays a single sharp peak (PDI = 1.48) with a shift toward higher molecular weight with respect to that of A$_{2.0k}$(B$_{6.15k}$)$_2$, as shown in Figure 1. A corresponding increase in the inherent viscosity was also observed.
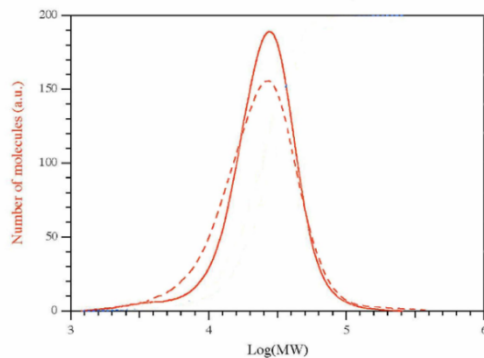
Figure 1. Molecular weight distributions of $A_{2k}(B_{6.1k})_2$ (solid line) and $A_{2k}(B_{6.1k}-A_{2k})_2$ (dashed line) obtained by SEC.

The characterization results for the Y-shaped copolymers are reported in Table 1, together with those of a linear mPEO$_{2.0k}$-PCL$_{4.3k}$. diblock copolymer having the same composition and molecular weight of mPEO$_{2.0k}$(PCL$_{2.1k}$)$_2$, for the sake of comparison. A lower viscosity was found for the latter copolymer, as expected because of the branched architecture. The slightly broader molecular weight distributions observed for Y-shaped copolymers are likely related to the multistep synthetic procedures.

Table 1. Characterization data of a linear AB and Y-shaped miktoarm PCL-PEO block copolymers (A=PEO, B=PCL).

Copolymer	PCL (wt-%)	M_n[a] (kDa)	M_w[b] (kDa)	PDI[c]	η_{inh}[d] (dL·g^{-1})
A_{2k}-$B_{4.3k}$	68	6.3	10.9	1.16	0.28
$A_{2k}(B_{2.1k})_2$	68	6.2	7.9	1.48	0.18
$A_{2k}(B_{6.1k})_2$	86	14.2	16.4	1.64	0.33
$A_{2k}(B_{6.1k}-A_{2k})_2$	67	18.2	19.6	1.48	0.36

[a] Number average molecular weight evaluates by ^{1}H-NMR.
[b] Molecular weight obtained by SEC.
[c] Molecular weight polydispersity index obtained by SEC.
[d] Inherent viscosity in CHCl$_3$ at 25°C, c = 0.5 g/dL.

Crystallization Behavior

DSC and WAXS techniques were used to gain insight into the self-organization and the crystallization behavior of the copolymers in bulk. Since PCL and PEO have close melting temperatures, the melt crystallization behavior is rather complex, especially underdynamic conditions, because coincident crystallization of both components may occur and the crystallization of one block may affect the crystallization of the second block.[37,38]A low scanning rate (2 °C/min) in the cooling run may promote the formation of well-separate exotherms for different blocks, provided that the crystallization from the melt occurs in the presence of a microphase-separated structure.[39] Thermograms relative to crystallization from the melt and to second melting runs are shown in Figure 2, and the results are summarized inTable 2.
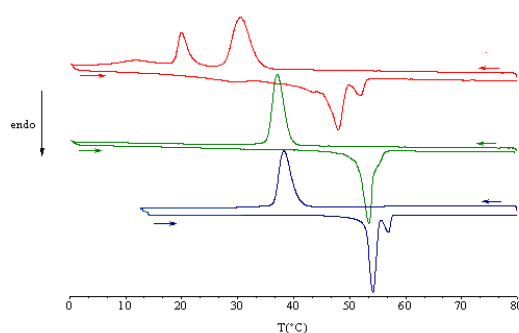
Figure 2. DSC thermograms of $A_{2k}(B_{2.1k})_2$ (red), $A_{2k}(B_{6.1k})_2$ (green),and $A_{2k}(B_{6.1k}\text{-}A_{2k})_2$ (blue) copolymers.

Single melting and crystallization peaks were observed in the DSC traces of $A_{2.0k}(B_{6.15k})_2$. Because the competition in crystallization between PCL and PEO blocks mainly depends on the PEO-PCL weight ratio as well as on the relative segmental lengths,[40,41] the peaks were attributed to the PCL component considering the low weight fraction of PEO and the high segmental length of PCL blocks (6.15 kDa) compared with the PEO block (2.0 kDa). The powder WAXS diagram of $A_{2.0k}(B_{6.15k})_2$ displayed characteristic diffraction maxima of crystalline PCL at $2\theta = 21.5°$, $23.9°$, whereas those related to PEO at $2\theta=19.2°$, $23.4°$ were not detected, in agreement with the DSC results (Supporting Information, Figure S4).

Table 2. Thermal behaviour and crystallinity of a linear AB and Y-shaped miktoarm PCL-PEO block copolymers (A=PEO, B=PCL).

Copolymer	$T_m^{a,b}$ (°C)		$\Delta H_m^{a,b}$ (J·g^{-1})		ΔH_c^{a} (J·g^{-1})		T_c^{a} (°C)		X_c^{c} (%)	
	A	B	A	B	A	B	A	B	A	B
$A_{2k}B_{4.3k}$	46.6	53; 57	11	50	16	52	26.8	34.3	18 (15)	47 (52)
$A_{2k}(B_{2.1k})_2$	43.0	47.9	20	42	15	40	20.0	30.5	20 (25)	40 (42)
$A_{2k}(B_{6.1k})_2$	-	56.4	-	62	-	58	-	38.8	-	55 (51)
$A_{2k}(B_{6.1k}A_{2k})_2$	-	54.2	-	48	-	47	-	38.3	-	40 (43)

[a] Crystallization and melting temperatures determined by DSC.
[b] Second heating run.
[c] % crystallinity calculated from WAXS spectra and from ΔH_m (in brackets).

The crystallization of PCL chains as first, in fact, provides strong restrictions to PEO chains that hinder their crystallization. Evidence of a PEO crystalline phase was not found, both by DSC and WAXS analyses, also for $A_{2k}(B_{6k}A_{2k})_2$, despite the higher content of PEO (35% by wt). Tm and Tc of PCL were not affected by the increased PEO content, while lowering of melting and crystallization enthalpies were found. These findings emphasize the relevance of segment length in the organization of separate crystalline domains. The double melting endotherms of PCL may be ascribed to a melting recrystallization process of less-ordered crystallites and reflects a more complex crystallization process related to the increased number of outer short PEO blocks. In the case of $PEO_{2k}(PCL_{2k})_2$ and $PEO_{2k}(PCL_{4k})$, with identical length of PEO segments and 2:1 PCL/PEO weight ratio, the coexistence of two crystalline phases was suggested by the presence of well separate crystallization and melting peaks. The WAXS diagrams displayed characteristic diffraction maxima for both PCL and PEO crystalline phases, in agreement with a double-crystalline morphology suggested by DSC. The relative intensities of the PCL and PEO crystalline diffraction peaks support the attribution to PCL of high-temperature crystallization and melting peaks with crystallization of PEO blocks occurring inside a preformed crystalline PCL environment. The crystallinity degree of PCL and PEO evaluated by WAXS are consistent with the melting enthalpies found by DSC, evidencing in

90

the branched copolymer a limited Xc lowering for PCL blocks balanced by a corresponding increase in Xc for PEO blocks.

Self-Assembly in Aqueous Solution

The aggregation of ABCs in aqueous environment is an enthalpy-driven process resulting from replacement of unfavorable water/hydrophobic-B-block contacts in the unimer dispersed state with favorable B−B contacts within the solvent-free core in core−shell structures. Therefore, the aggregate stability, assessed by low CACs and negative free-energy values, $\Delta G° = RT \ln(\text{XCAC})$ (XCAC = ABC molar fraction at CAC), is mainly controlled by the chemical nature and length of hydrophobic block. Self-assembly of copolymers in aqueous environment was followed by a steady-state fluorescent spectroscopic method using pyrene as a probe (Figure 3). The CAC and $\Delta G°$ values are reported in the table inserted in Figure 3. The low CAC values are indicative of a fair thermodynamic stability in aqueous medium. With respect to the linear diblock A_{2k}-$B_{4.3k}$, the star-block $A_{2k}(B_{2.1k})_2$ counterpart showed a small free-energy penalty associated with the localization of 3 arms in A-B junctions at the core/corona interface with consequent loss of conformational freedom. As expected, the size of aggregates formed by block copolymers with low MW is smaller than 100 nm (D_H for $A_{2k}B_{4.3k}$ and $A_{2k}(B_{2.1k})_2$ were 40 and 67 nm, respectively), whereas larger D_H, in the rangeof 180–200 nm, with broad size distributions was found for aggregates based on high MW copolymers. Therefore, $A_{2k}B_{4.3k}$ and $A_{2k}(B_{2.1k})_2$ were selected as model ABCs for the preparation of nanocapsules.

91

Figure 3. $I334/I331$ of pyrene in aqueous copolymer solutions at different concentrations. In the table, calculated CAC and $\Delta G°$ are reported.
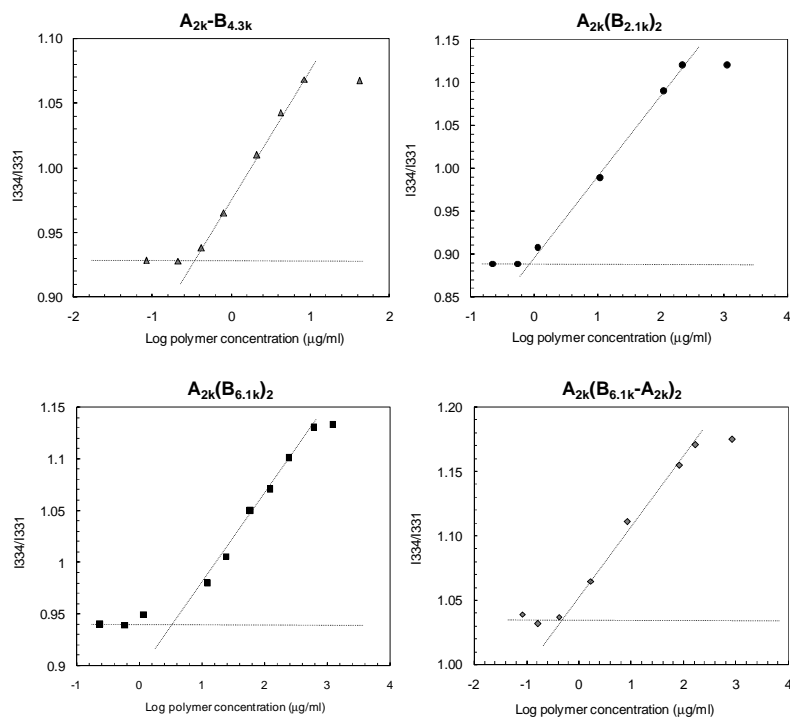
Copolymer	CAC (mg·L^{-1})	CAC (mol·L^{-1})	$\Delta G^{\bullet}$ (kJ·mol^{-1})
A_{2k}-$B_{4.3k}$	0.30	$4.76 \cdot 10^{-8}$	-52.1
$A_{2k}(B_{2.1k})_2$	0.69	$1.11 \cdot 10^{-7}$	-49.6
$A_{2k}(B_{6.1k})_2$	3.50	$2.46 \cdot 10^{-7}$	-47.6
$A_{2k}(B_{6.1k}-A_{2k})_2$	0.41	$2.25 \cdot 10^{-8}$	-53.9

Preparation and Characterization of RhDex-Loaded Nanocapsules

Assembly of ABCs of PCL is generally suited to deliver lipophilic drugs with the advantage to improve greatly their water solubility and to exert a spatial and temporal control over the delivered drug dose. The efficient delivery of

hydrophilic drugs is indeed much more complicate to attain. As expected, RhDex, selected as a model hydrophilic macromolecule,could not be efficiently entrapped during copolymer self-assembly through conventional methods reported in the literature such as dialysis or melting-sonication in water[27,42] (encapsulation efficiency of RhDex was <2%). This suggested that spontaneous organization of copolymers in nanostructures able to entrap hydrophilic molecules as a consequence of slow solvent removal (dialysis) or hardening in water from a melted phase (melting-sonication) was not a suitable strategy. Therefore, we tried to design a general procedure suitable to give nanocapsules with the aim to: (i) employ materials with different architectures not necessarily designed to form vesicles; (ii) efficiently entrap hydrophilic compounds; and (iii) release them at controlled rates.

Options available in the literature to prepare nanocapsules with an aqueous core from preformed copolymers are very scarce.[43] This prompted us to develop an alternative method of preparation based on the idea that copolymer hardening can occour at the interface of a w/o emulsion nanotemplate. In fact, it has been recently demonstrated that PEO-PCL diblock copolymers can act as an emulsifier and stabilize o/w emulsions forming a polymeric interface.[44] The technique developed in this study, indicated as emulsion/melting-sonication (EMeSo), consists of (i) melting the copolymer in Miglyol 812 at a temperature about 10 °C higher than copolymer Tm; (ii) adding the aqueous inner phase with the dissolved active principle, which may or may not contain a stabilizer (PEG$_{400}$); (iii) apply sonication to generate a w/oemulsion; and (iv) cool the mixture at room temperature to promote copolymer hardening. In this way, molten copolymer forms a skin around aqueous droplets, giving nanocapsules with an inner aqueous core. The oily nanocapsules suspension is then purified by washing with hexane and then redispersed in water to allow freeze-drying. Two copolymer architectures and different formulation conditions were employed to prepare nanocapsules, as reported in Table 3. PEG$_{400}$ was added in the aqueous phase of the emulsion to promote phase separation of PEO-PCL nanocapsule wall. In all the experimental conditions tested, nanocapsules were formed except for ABA copolymer, where the absence of PEG$_{400}$ destabilizes the formulation causing copolymer precipitation. Recovery yield was similar and satisfactory for all formulations.

Table 3. Properties of RhDex-loaded nanocapsules.

Formulation code[a]	AB-W	AB-WP	AB$_2$-W	AB$_2$-WP
Copolymer	A$_{2k}$B$_{4.3k}$	A$_{2k}$B$_{4.3k}$	A$_{2k}$(B$_{2.1k}$)$_2$	A$_{2k}$(B$_{2.1k}$)$_2$
Yield(% ± SD)	80±1	85±1	82±2	80±1
Mean D$_H$(nm ± SD)	110±5	100±2	100±1	201±1
P.I.	0.347	0.206	0.369	0.177
Zeta Potential (mV ± SD)	-30±0.3	-16.3±1	-30±0.8	-18±1
RhDex actual loading[b] (mg/100 mg nanocapsules ± SD)	0.882±0.010	1.175±0.035	0.799±0.036	1.141±0.028
RhDex enc. efficiency[c] (% ± SD)	45±1.0	59±2.2	40±0.7	57±1.4

[a] Code W refers to nanocapsules with water as aqueous core whereas code WP refers to nanocapsules with water/PEG$_{400}$ 1:1 by wt as aqueous core.
[b] Actual loading is expressed as amount of RhDex encapsulated per 100 mg of nanocapsules.
[c] Ratio between actual and theoretical loading x 100. Theoretical loading was 2%.

Nanocapsules were spherical and not-aggregated, as demonstrated by TEM (Figure 4), showing a capsular structure consistent with the presence of an inner core surrounded by an external polymer wall.
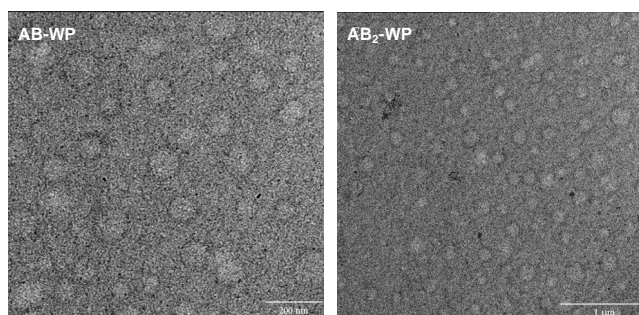
Figure 4. Transmission electron microscopy images of nanocapsules prepared according to compositions reported in Table 3.

D_H evaluated by PCS were in the range100–250 nm, in agreement with TEM, which is a size interval suitable for administration also via intravenous injection. Theformation of a PEO coating at the surface of nanocapsules was confirmed by analyzing ^{1}H NMR spectra of nanocapsules dispersed in D$_2$O at 25 °C (data not shown) that evidenced sharp resonances of PEO methylene

94

hydrogen atoms at 3.60 δ and broad resonances of low intensity relative to PCL units, indicating a reduced chain mobility of PCL segments in the nanocapsule wall. Encapsulation efficiency of RhDex was >50% and considered again to be satisfactory for a hydrophilic macromolecule in a nanosized system. Release rates of RhDex from nanocapsules (Figure 5) were characterized by an initialburst, followed by a slower diffusion/erosion phase. Burst effect and overall release trend for nanocapsules containing only water in the internal phase were similar. On the contrary, burst release strongly decreased as PEG_{400} was added in the internal aqueous phase, and release rate of RhDex was sustained for a time interval longer as compared with that observed for nanocapsules with a water core.
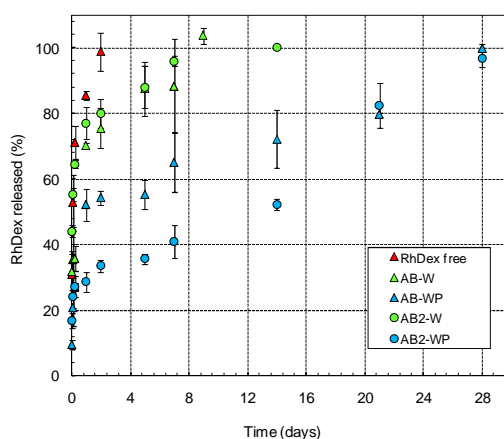
Figure 5. Release profile of RhDex from nanocapsules as evaluated by dialysis in 10 mM phosphate buffer at pH 7.4 and 37 °C. Dialysis of free RhDex is reported as control. Each point is the mean of four measurements ± SD.

This effect can be attributed to a lower molecule mobility in the hydrated core due to viscosizing properties of free PEG and its hindered diffusion in the external medium. The slowest release rate was observed for nanocapsules prepared with AB_2-WP, probably due to their size being larger than that of AB-WP. As compared with release obtained for other macromolecules from polymersomes made of diblock PEO-PCL with similar composition,[36] the delivery rate was very slow, which supports the hypothesis that no morphology transition occurs because of copolymer degradation. Hemolytic activity of nanocapsules on human RBC was investigated to verify their suitability via intravenous administration (Figure 6). A low hemolysis degree (<11%) was

observed with both AB-WP and AB$_2$-WP formulations independently on the nanocapsule concentration. According to several studies,[45] hemolysis values found for nanocapsules can be rated as "no concern" because they span in the 5−25% range. Because of a better control of release rate, which presumably should occur also in vivo, we focused on AB$_2$-WP formulations for further in vitro testing. To exclude a potential cytotoxic effect of nanocapsules, we investigated their activity on A375 proliferation. As shown in Figure 6, A375 growth was not affected by any of the concentration of AB$_2$-WP tested at all the time points considered. Similar results were obtained with the NHEM cell line (data not shown).
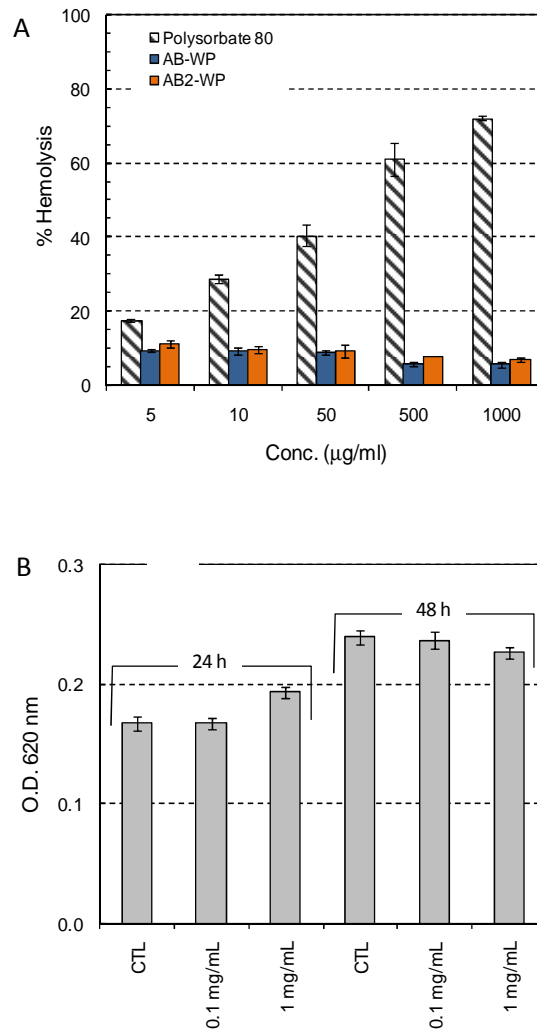
Figure 6. (A) Hemolytic activity of polysorbate 80 (positive control), AB-WP, and AB$_2$-WP nanocapsules. Each point is the mean of four measurements ± SD. (B) Cytotoxicity of AB$_2$-WP nanocapsules on A375 cell line. Each point is the mean of three measurements ± SD.

Conclusions

A straightforward synthetic pathway based on a combination of segment coupling and ROP steps was developed to obtain amphiphilic Y-shaped miktoarm PEO-PCL block copolymers. Y-shaped copolymers demonstrated a high self-assembling tendency in water comparable to that of linear counterparts, which suggests their use as nanocontainers for lipophilic drugs. We showed that it is otherwise possible to obtain nanocapsules for the sustained release of hydrophilic macromolecules by processing PEO-PCL copolymers through an emulsion/melting-sonication technique. Nanocapsules showed an excellent cell toxicity profile and thus represent a nanosystem of great potential in several drug delivery applications.

References

(1) Allen, C.; Maysinger, D.; Eisenberg, A. Nano-engineering block copolymer aggregates for drug delivery. *Colloids and Surfaces B: Biointerfaces* 1999, *16* (1-4), 3-27.

(2) Letchford, K.; Burt, H. A review of the formation and classification of amphiphilic block copolymer nanoparticulate structures: micelles, nanospheres, nanocapsules and polymersomes. *European Journal of Pharmaceutics and Biopharmaceutics* 2007, *65* (3), 259-269.

(3) Pispas, S.; Hadjichristidis, N.; Potemkin, I.; Khokhlov, A. Effect of architecture on the micellization properties of block copolymers: A(2)B miktoarm stars vs AB diblocks. *Macromolecules* 2000, *33* (5), 1741-1746.

(4) Rao, J.; Zhang, Y.; Zhang, J.; Liu, S. Facile preparation of well-defined AB2 Y-shaped miktoarm star polypeptide copolymer via the combination of ring-opening polymerization and click chemistry. *Biomacromolecules.* 2008, *9* (10), 2586-2593.

(5) Rahman, M. S.; Changez, M.; Yoo, J. W.; Lee, C. H.; Samal, S.; Lee, J. S. Synthesis of amphiphilic miktoarm star copolymers of poly(n-hexyl isocyanate) and poly(ethylene glycol) through reaction with the active methylene group. *Macromolecules* 2008, *41* (19), 7029-7032.

(6) Liu, H.; Xu, J.; Jiang, J. L.; Yin, J.; Narain, R.; Cai, Y. L.; Liu, S. Y. Syntheses and micellar properties of well-defined amphiphilic AB(2) and A(2)B Y-shaped miktoarm star copolymers of E-caprolactone and 2-(dimethylamino)ethyl methacrylate. *Journal of Polymer Science Part A-Polymer Chemistry* 2007, *45* (8), 1446-1462.

(7) Babin, J.; Taton, D.; Brinkmann, M.; Lecommandoux, S. Synthesis and self-assembly in bulk of linear and Mikto-arm star block copolymers based on polystyrene and poly(glutamic acid). *Macromolecules* 2008, *41* (4), 1384-1392.

(8) Zhang, H. H.; Huang, Z. Q.; Sun, B. W.; Guo, J. X.; Wang, J. L.; Chen, Y. Q. Y-shaped poly(ethylene glycol) and poly(trimethylene carbonate) amphiphilic copolymer: Synthesis and for drug delivery. *J. Polym. Sci. A Polym. Chem.* 2008, *46* (24), 8131-8140.

(9) Whittaker, M. R.; Urbani, C. N.; Monteiro, M. J. Synthesis of 3-miktoarm stars and 1st generation mikto dendritic copolymers by "living" radical polymerization and "click" chemistry. *Journal of the American Chemical Society* 2006, *128* (35), 11360-11361.

(10) Lutz, J. F. Solution self-assembly of tailor-made macromolecular building blocks prepared by controlled radical polymerization techniques. *Polymer International* 2006, *55* (9), 979-993.

(11) Sumerlin, B. S.; Vogt, A. P. Macromolecular Engineering through Click Chemistry and Other Efficient Transformations. *Macromolecules* 2010, *43* (1), 1-13.

(12) York, A. W.; Kirkland, S. E.; McCormick, C. L. Advances in the synthesis of amphiphilic block copolymers via RAFT polymerization: Stimuli-responsive drug and gene delivery. *Advanced Drug Delivery Reviews* 2008, *60* (9), 1018-1036.

(13) Cameron, D. J. A.; Shaver, M. P. Aliphatic polyester polymer stars: synthesis, properties and applications in biomedicine and nanotechnology. *Chem. Soc. Rev.* 2011, *40* (3), 1761-1776.

(14) Joralemon, M. J.; McRae, S.; Emrick, T. PEGylated polymers for medicine: from conjugation to self-assembled systems. *Chem. Commun.* 2010, *46* (9), 1377-1393.

(15) Wei, X. W.; Gong, C. Y.; Gou, M. Y.; Fu, S. Z.; Guo, Q. F.; Shi, S.; Luo, F.; Guo, G.; Qiu, L. Y.; Qian, Z. Y. Biodegradable poly(epsilon-caprolactone)-poly(ethylene glycol) copolymers as drug delivery system. *International Journal of Pharmaceutics* 2009, *381* (1), 1-18.

(16) Haag, R. Supramolecular drug-delivery systems based on polymeric core-shell architectures. *Angewandte Chemie-International Edition* 2004, *43* (3), 278-282.

(17) Mikhail, A. S.; Allen, C. Block copolymer micelles for delivery of cancer therapy: transport at the whole body, tissue and cellular levels. *J. Control Release* 2009, *138* (3), 214-223.

(18) Huynh, N. T.; Roger, E.; Lautram, N.; Benoit, J. P.; Passirani, C. The rise and rise of stealth nanocarriers for cancer therapy: passive versus active targeting. *Nanomedicine. (Lond)* 2010, *5* (9), 1415-1433.

(19) Torchilin, V. P. Nanocarriers. *Pharmaceutical Research* 2007, *24* (12), 2333-2334.

(20) Aliabadi, H. M.; Mahmud, A.; Sharifabadi, A. D.; Lavasanifar, A. Micelles of methoxy poly(ethylene oxide)-b-poly(epsilon-caprolactone) as vehicles for the solubilization and controlled delivery of Cyclosporine A. *Journal of Controlled Release* 2005, *104* (2), 301-311.

(21) Gaucher, G.; Dufresne, M. H.; Sant, V. P.; Kang, N.; Maysinger, D.; Leroux, J. C. Block copolymer micelles: preparation, characterization and application in drug delivery. *Journal of Controlled Release* 2005, *109* (1-3), 169-188.

(22) Gaucher, G.; Marchessault, R. H.; Leroux, J. C. Polyester-based micelles and nanoparticles for the parenteral delivery of taxanes. *J. Control Release* 2010, *143* (1), 2-12.

(23) Kim, S. Y.; Lee, Y. M. Taxol-loaded block copolymer nanospheres composed of methoxy poly(ethylene glycol) and poly(epsilon-caprolactone) as novel anticancer drug carriers. *Biomaterials* 2001, *22* (13), 1697-1704.

(24) Wei, J.; Huang, J. L. Synthesis of an amphiphilic star triblock copolymer of polystyrene, poly(ethylene oxide), and polyisoprene using lysine as core molecule. *Macromolecules* 2005, *38* (4), 1107-1113.

(25) Maglio, G.; Nese, G.; Nuzzo, M.; Palumbo, R. Synthesis and characterization of star-shaped diblock poly(epsilon-caprolactone)/poly(ethylene oxide) copolymers. *Macromol. Rapid Commun.* 2004, *25* (12), 1139-1144.

(26) Deng, M.; Chen, X.; Piao, L.; Zhang, X.; Dai, Z.; Jing, X. Synthesis of four-armed poly(+Á-caprolactone)-block-poly(ethylene oxide) by diethylzinc catalyst. *J. Polym. Sci. A Polym. Chem.* 2004, *42* (4), 950-959.

(27) Quaglia, F.; Ostacolo, L.; De Rosa, G.; La Rotonda, M. I.; Ammendola, M.; Nese, G.; Maglio, G.; Palumbo, R.; Vauthier, C. Nanoscopic core-shell drug carriers made of amphiphilic triblock and star-diblock copolymers. *International Journal of Pharmaceutics* 2006, *324* (1), 56-66.

(28) Wang, F.; Bronich, T. K.; Kabanov, A. V.; Rauh, R. D.; Roovers, J. Synthesis and evaluation of a star amphiphilic block copolymer from poly(epsilon-caprolactone) and poly(ethylene glycol) as a potential drug delivery carrier. *Bioconjugate Chemistry* 2005, *16* (2), 397-405.

(29) Quaglia, F.; Ostacolo, L.; Nese, G.; Canciello, M.; De Rosa, G.; Ungaro, F.; Palumbo, R.; La Rotonda, M. I.; Maglio, G. Micelles based on amphiphilic PCL-PEO triblock and star-shaped diblock copolymers: Potential in drug delivery applications. *Journal of Biomedical Materials Research Part A* 2008, *87A* (3), 563-574.

(30) Rieger, J.; Passirani, C.; Benoit, J. P.; Van Butsele, K.; Jerome, R.; Jerome, C. Synthesis of amphiphilic copolymers of poly(ethylene oxide) and poly(epsilon-caprolactone) with different architectures, and their role in the preparation of stealthy nanoparticles. *Advanced Functional Materials* 2006, *16* (11), 1506-1514.

(31) Lecommandoux, S.; Lazzari, M.; Liu, G. *An Introduction to Block Copolymer Applications: State-of-the-Art and Future Developments;* Wiley-VCH Verlag GmbH & Co. KGaA: 2006.

(32) Shen, H.; Eisenberg, A. Control of Architecture in Block-Copolymer Vesicles. *Angew. Chem.* 2000, *112* (18), 3448-3450.

(33) Qiu, L. Y.; Bae, Y. H. Polymer architecture and drug delivery. *Pharmaceutical Research* 2006, *23* (1), 1-30.

(34) Ahmed, F.; Discher, D. E. Self-porating polymersomes of PEG-PLA and PEG-PCL: hydrolysis-triggered controlled release vesicles. *Journal of Controlled Release* 2004, *96* (1), 37-53.

(35) Discher, D. E.; Ortiz, V.; Srinivas, G.; Klein, M. L.; Kim, Y.; David, C. A.; Cai, S. S.; Photos, P.; Ahmed, F. Emerging applications of polymersomes in delivery: From molecular dynamics to shrinkage of tumors. *Progress in Polymer Science* 2007, *32* (8-9), 838-857.

(36) Kim, Y. H.; Tewari, M.; Pajerowski, J. D.; Cai, S. S.; Sen, S.; Williams, J.; Sirsi, S.; Lutz, G.; Discher, D. E. Polymersome delivery of siRNA and antisense oligonucleotides. *Journal of Controlled Release* 2009, *134* (2), 132-140.

(37) Castillo, R. V.; Muller, A. J. Crystallization and morphology of biodegradable or biostable single and double crystalline block copolymers. *Progress in Polymer Science* 2009, *34* (6), 516-560.

(38) Hua, C.; Dong, C. M. Synthesis, characterization, effect of architecture on crystallization of biodegradable poly(epsilon-caprolactone)b-poly(ethylene oxide) copolymers with different arms and nanoparticles thereof. *Journal of Biomedical Materials Research Part A* 2007, *82A* (3), 689-700.

(39) An, J. H.; Kim, H. S.; Chung, D. J.; Lee, D. S.; Kim, S. Thermal behaviour of poly(epsilon-caprolactone)-poly(ethylene glycol)-poly(epsilon-caprolactone) tri-block copolymers. *Journal of Materials Science* 2001, *36* (3), 715-722.

(40) Bogdanov, B.; Vidts, A.; Schacht, E.; Berghmans, H. Isothermal crystallization of poly(epsilon-caprolactone-ethylene glycol) block copolymers. *Macromolecules* 1999, *32* (3), 726-731.

(41) Bogdanov, B.; Vidts, A.; Van Den Bulcke, A.; Verbeeck, R.; Schacht, E. Synthesis and thermal properties of poly(ethylene glycol)-poly(epsilon-caprolactone) copolymers. *Polymer* 1998, *39* (8-9), 1631-1636.

(42) Ungaro, F.; Conte, C.; Ostacolo, L.; Maglio, G.; Barbieri, A.; Arra, C.; Misso, G.; Abbruzzese, A.; Caraglia, M.; Quaglia, F. Core-shell biodegradable nanoassemblies for the passive targeting of docetaxel: features, antiproliferative activity and in vivo toxicity. *Nanomedicine.* 2011, *Sep 1 Epub ahead of print[1]].*

(43) Anton, N.; Benoit, J. P.; Saulnier, P. Design and production of nanoparticles formulated from nano-emulsion templates-a review. *J. Control Release* 2008, *128* (3), 185-199.

(44) Nam, Y. S.; Kim, J. W.; Shim, J.; Han, S. H.; Kim, H. K. Nanosized Emulsions Stabilized by Semisolid Polymer Interphase. *Langmuir* 2010, *26* (16), 13038-13043.

(45) Amin, K.; Dannenfelser, R. M. In vitro hemolysis: Guidance for the pharmaceutical scientist. *Journal of Pharmaceutical Sciences* 2006, *95* (6), 1173-1176.

CHAPTER 3: Core-shell biodegradable nanoassemblies for the passive targeting of docetaxel:features, antiproliferative activity and in vivo toxicity

Core-shell biodegradable nanoassemblies for the passive targeting of docetaxel: features, antiproliferative activity and in vivo toxicity

Francesca Ungaro, PhD[a], Claudia Conte, PharmD[a], Luisanna Ostacolo, PhD[a],
Giovanni Maglio, MChem[b], Antonio Barbieri, PhD[c],
Claudio Arra, MD[c], Gabriella Misso, PhD[d], Alberto Abbruzzese, MD[d],
Michele Caraglia, PhD[d], Fabiana Quaglia, PhD[a]

[a]Department of Pharmaceutical and Toxicological Chemistry,
University of Naples Federico II, Naples, Italy
[b]Department of Chemistry "Paolo Corradini," University of Naples Federico II,
Naples, Italy
[c]Experimental Pharmacology Unit, Department of Research, National Cancer Institute
Fondazione G. Pascale, Naples, Italy
[d]Department of Biochemistry and Biophysics, University of Naples Medical School,
Naples, Italy
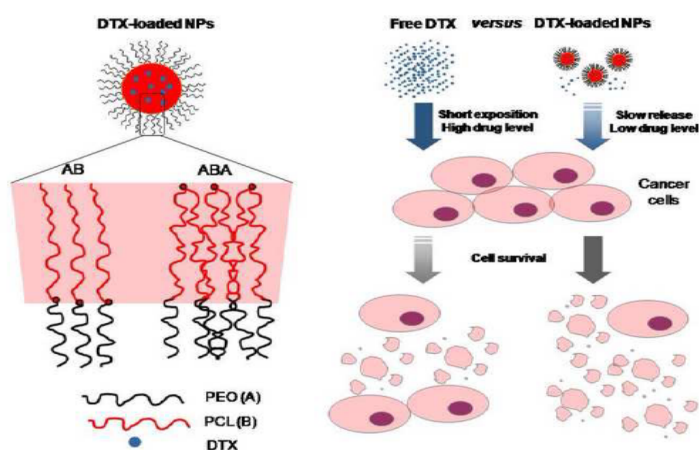
Abstract

Amphiphilic block copolymers of poly(☐-caprolactone) and poly(ethylene oxide) were assembled in core shell nanoparticles (NPs) by a melting-sonication technique (MeSo). The entrapment of the poorly water-soluble anticancer drug docetaxel (DTX), nanocarrier cytotoxicity toward different cells and toxicity in mice were investigated. The encapsulation mechanism was rationalized and related to copolymer properties such as crystallinity and drug solubility in the copolymer phase. DTX release from NPs occurred in two drug pulses over 30 days. DTX entrapment in NPs strongly decreased haemolysis of erythrocytes in comparison with a commercial DTX formulation. In comparison with free DTX, NPs were both more efficient in inhibiting cell growth of breast and prostate cancer cells and less toxic in experimental animal models. The results of this study indicate that MeSo is an interesting technique for the achievement of peculiar core-shell nanocarriers for the passive targeting and sustained release of poorly water-soluble anticancer drugs.

From the Clinical Editor: In this study, stealth nanoparticles of PEO/PCL block copolymers for passive targeting of docetaxel to solid tumors were developed using a novel technique. The studied properties of NPs suggest strong potential as anticancer drug-delivery system.

Key words: Nanoparticles; Amphiphilic block copolymers; Anticancer drugs; Docetaxel

Introduction

Nanotechnology offers a highly promising avenue in cancer treatment based on the concept that a drug formulated in nanoparticles (NPs) can alter its pharmacokinetics, enhancing the treatment ability to target and kill cells of diseased tissues or organs while negatively affecting as few healthy cells as possible[1,2]. Depending on the properties of the carrier, large variations in drug pharmacokinetics with major clinical implications may occur. Sterically stabilized nanocarriers with a biomimetic coating (stealth nanocarriers) show an increased longevity in the circulation and the potential to accumulate predominantly in pathological sites with compromised leaky vasculature, such as solid tumors. Direct correlations between the longevity of a nanocarrier in the circulation and its ability to reach the target have been observed on multiple occasions[3]. Furthermore, a number of reviews have amply illustrated how surface modification can be achieved by the use of poly(ethylene oxide) (PEO) to obtain longcirculating NPs[4,5]. It is established that PEO length and surface density can affect biomimetic properties of the nanocarrier, with special regard to opsonization process, and in vivo fate[6,7]. In recent years, the use of poly(ε-caprolactone) (PCL) has emerged overwhelmingly as the core material for NPs and micelles[8,9]. Due to its high hydrophobicity and crystallinity as well as low melting and glass transition temperatures, PCL is considered an excellent candidate to form the hydrophobic core of nanocarriers and deliver its drug cargo at controlled rates. In fact, it has been suggested that high core hydrophobicity can be of help in retaining the drug inside the carrier throughout circulation time, avoiding its premature release and erratic biodistribution[10]. Despite attractive properties, PEO/PCL NPs have been poorly investigated and never especially engineered (size, surface, drug release) for the purpose of passive targeting nor tested in depth for their biological potential[9].The easiest way to obtain core-shell nanocarriers is to assemble PEO/PCL amphiphilic block copolymers in core-shell nanostructures with micellar or nanosphere structure. Among PEO/PCL copolymers, diblock architecture is generally preferred due to a very simple synthetic pathway of the amphiphilic copolymer. Examples of core-corona micelles/NPs made of PEO (A) and PCL (B) blocks with AB[11] and BAB[12-14] structure for the delivery of hydrophobic anticancer drugs have been published recently. However, very little is known about the applicability of novel polymer architectures in giving core-shell nanocarriers for passive targeting of anticancer drug delivery, where they have the potential to offer a superior degree of NP coating. Recently, we have demonstrated that depending on copolymer architecture, PEO-PCL micelles behave very differently in

biological environments despite sharing very similarsize, surface properties, and release rates[15]. The most widely employed "bottom-up" method to prepare nanocarriers from these copolymers, such as the solvent displacement method, makes use of a nanoemulsion template[16,17]. In this case the manufacture of NPs irremediably involves the removal of the volatile, occasionally toxic solvent from the formulation, which causes polymer precipitation within the organic phase. Solvent removal can be performed by evaporation or diffusion shock, and of course the presence of solvent traces represents a limitation in pharmaceutical manufacturing. Recently, we proposed a simple method named "melting-sonication" (MeSo) to produce coreshell NPs based on PEO-PCL block copolymers without the use of toxic organic solvents[18]. Working on copolymer amphiphilic properties and low melting temperature, we successfully produced nanoassemblies of copolymers with ABA triblock architectures, demonstrating stealth properties and the ability to entrap lipophilic molecules. In this article we propose MeSo as technique suitable to produce NPs made of (PEO-PCL) block copolymers for the passive targeting of docetaxel (DTX) in solid tumors. NPs were produced by two copolymers with ABA and simple AB architecture and sharing similar lipophilic/hydrophilic ratio. Relevant properties of NPs were explored and related to in vitro/in vivo biological profiles in view of their application as an anticancer drug-delivery system.

Methods

Docetaxel (DTX) was purchased from Fluka (Sigma-Aldrich). Potassium phosphate dibasic and potassium phosphate monobasic, sodium azide and sodium chloride were from Sigma-Aldrich. Sodium hydroxide was from Delchimica Scientific Glassware. Ethanol 96°, phosphoric acid (85%) and acetonitrile were purchased from Carlo Erba Reagenti (Milan, Italy). α-Methoxy,ω-hydroxy-poly(ethyleneoxide) (mPEO$_{2000}$-OH) and α-methoxy,ω-amino-poly(ethyleneoxide) (mPEO$_{2000}$-NH$_2$) (Aldrich), were dried by azeotropic distillation from toluene. ε-Caprolactone, (CL) (Aldrich), was distilled over CaH$_2$ under vacuum before use. Tin(2-ethylhexanoate)$_2$, Sn(Oct)$_2$ (Aldrich), 4 (dimethylamino)pyridine (DMAP) (Fluka), N,N'-dicyclohexylcarbodiimide (DCCI) (Fluka), N-hydroxysuccinimide (NHS) (Fluka) and the sodium salt of 3-(trimethylsilyl)propionic- 2,2,3,3-d4 acid (TMSP) (Aldrich) were used as received.

Preparation of DTX-loaded NPs

PEO$_{2000}$-PCL$_{4100}$ diblock (AB) and PEO$_{2000}$-PCL$_{6800}$-PEO$_{2000}$ triblock copolymers (see Supplementary Material) were employed to prepare unloaded and DTX-loaded NPs. NPs were prepared by MeSo according to the procedure that we previously developed[18]. In this study 10 mg of copolymer were added to 2 mL of filtered water in a vial and then poured into a water bath at 75 ± 1°C to allow copolymer melting. DTX (0.5, 1 or 1.5 mg) was dissolved in 0.2 mL of ethanol and added to filtered water in the presence of melted copolymer, sonicated for 10 minutes at 6W (Sonicator 3000, Misonix) by a microtip probe and finally cooled at around 22°C under magnetic stirring. NPs were filtered through 0.45 μm filters (RC, Phenomenex, Bologna, Italy), and freeze dried. The recovery yield of the production process was evaluated weighting the solid residue after freeze-drying. Results are expressed as the ratio between the weight of NPs obtained and the initial (drug + polymer) weight × 100.

Characterization of NPs

The hydrodynamic diameter (D$_H$) and polydispersity index of NPs were determined by Photon Correlation Spectroscopy using a N5 Submicron Particle Size Analyzer (Beckman-Coulter Inc., Fullerton, California). A dispersion of NPs was diluted in Milli- Q water at an intensity between 104–106 counts/s and measurements were performed at 25°C on a 90-degree angle. The morphology of NPs was assessed by TEM on a Leo 912AB microscope (Carl Zeiss S.p.a., Milano, Italy). A dispersion of NPs in water was placed on a

110

copper grid and stained with uranile acetate (2% w/v). The evaluation of the amount of hydrated PEO chains located in NP corona was performed by ^{1}H-NMR (400 MHz) in D_2O at 25°C and 70°C, using TMSP as internal standard. NPs (4–5 mg) were suspended in 1 mL of a 1×10^{-5} M solution of TMSP in D_2O. The intensity ratio of the PEO resonance at $\delta = 3.6$–3.7 to the methyl resonance of TMSP at $\delta = 0$ was compared with that obtained after the addition of 1 mL of chloroform-d, which allows a complete dissolution of the copolymer. Zeta potential was determined by analyzing a dispersion of NPs in water on a Zetasizer Nano Z (Malvern Instruments Ltd., Malvern, United Kingdom). Results are reported as the mean of three separate measurements on three different batches ± Standard Deviation (SD). Differential scanning calorimetry (DSC) analyses were performed on a Mettler-Toledo-30 calorimeter under nitrogen using a 10°C/minute scan rate.

DTX loading and release

DTX loading was assessed by dissolving 1 mg of NPs in an acetonitrile-water mixture 50:50 (v/v). The sample was stirred overnight and filtered through a 0.45 μm filter (RC, Phenomenex). The amount of DTX dissolved was measured by HPLC on a Shimadzu (Shimadzu Italia s.r.l., Milano, Italy) apparatus equipped with a LC-10ADvp pump, a SIL-10ADvp autoinjector, a SPD-10Avp UV-Vis detector and a C-R6 integrator. The analysis was performed on a Phenosphere-NEXT 5μ, C18column (250 × 4.6 mm, 100 Å) (Phenomenex). The mobile phase was a 40:60 (v/v) mixture of 20 mM phosphate buffer at pH 4.5 with acetonitrile pumped at a flow rate of 1 mL/minute. The UV detector was set at 227 nm. A calibration curve for DTX in ethanol was constructed in the concentration range 0.820–82 μg/mL. The limits of quantitation (LOQ) and detection (LOD) were 0.105 and 0.0005 mg/mL. Release of DTX from NPs was assessed by dialysis in 10 mM phosphate buffer at pH 7.4 (PBS). NPs (1 mg) were added to 0.5 mL PBS and placed in a dialysis bag (MWCO= 3500 Da, Spectra/Por). The sample was poured in 5 mL of PBS (sink condition) and kept at 37°C. At selected time intervals, 1 mL of release medium was withdrawn and replaced with an equal volume of fresh medium. The concentration of DTX was determined by HPLC as described above. The release profiles of the NPs were compared with that of the commercial formulation Taxotere.

Hemolysis of DTX-loaded NPs

Human blood freshly collected in EDTA-containing tubes was washed 3 times with isotonic 10 mM phosphate buffer saline (PBS) solution (pH 7.4) by centrifugation at 880g for 5 minutes and the pellet, containing red blood cells (RBC), was finally diluted 1:10 v/v with 10 mM PBS. RBC suspension (0.1 mL) was added to 0.9 mL of a NP dispersion at concentration ranging from 0.01 to 2.0 mg/mL of DTX. After incubation at 37°C for 30 minutes, the sample was centrifuged at 1000g for 10 minutes to remove nonlysed RBC. The supernatant was collected and analyzed for hemoglobin release by spectrophotometric determinations at 416 nm. To obtain 0 and 100% hemolysis, 0.1 mL of RBC suspension were added to 0.9 mL of PBS and distilled water, respectively. The degree of hemolysis was determined by the following equation: Hemolysis (%) = $(ABS-ABS_0)/(ABS_{100}-ABS_0) \times 100$, where ABS_{100}, and ABS_0 are the absorbances of the solution at 100% and 0% hemolysis, respectively.

Cell cultures

Our experimental models consist of human prostate carcinoma DU145 and LnCaP cell lines, human breast cancer MDA-MB 231 and MCF-7 cell lines (American Type Tissue culture Collection, Rockville, Maryland). DU145, LNCaP and MDA-MB231 cells were grown in DMEM, and MCF-7 cells were grown in RPMI 1640, both supplemented with heat-inactivated 10% FBS, 20 mM HEPES, 100 μg/mL penicillin, 100 μg/mL streptomycin, 1% L-glutamine and 1% sodium pyruvate. Cells were grown in a humidified atmosphere of 95% air/5% CO_2 at 37°C.

Cell proliferation assay

Analysis of cell proliferation was performed in the presence of DTX, DTX-loaded NPs and empty NPs on cell lines seeded in 96-well plates at the density of $1-2 \times 10^3$ cells/well in serum containing media. After 24 hours of incubation at 37°C, the cells were treated with increasing concentrations of DTX and DTX-NPs (0.78 to 100 ng/mL of DTX) as well as empty NPs. Cells were incubated under these conditions for a time-course spanning 72 hours. Cell viability was assessed with MTT method as previously described[19]. All data are expressed as mean ± SD. Statistical analysis was performed by analysis of variance (ANOVA) with Neumann-Keul's multiple comparison or Kolmogorov-Smirnov tests where appropriate.

In vivo toxicity

Seven-week-old female BALB/c mice were obtained from Harlan (San Pietro al Natisone, Italy). Mice were housed 6 per cage and maintained on a 12-hours light :12-hours dark cycle (lights on at 7:00 a.m.) in a temperature-controlled room (22 ± 2°C) and with food and water ad libitum at all times. The experimental protocols were in compliance with the European Communities Council directive (86/609/EEC). After a 1-week acclimation to the housing conditions, maximum tolerated dose (MTD) was evaluated by lateral tail vein injection of DTX, DTX-loaded NPs and empty NPs. NPs were dispersed in a saline solution (0.9% NaCl). Survival experiments to define MTD were performed with 6 animals per group. Drug effects were determined by monitoring of body weight and survival. Mouse body weight was monitored 3 times per week up to 28 days. MTD was defined as the maximum dose that caused no drug related lethality while producing an animal body weight loss of less than 20% of original weight. A fatality within 2 weeks after the first drug treatment was defined as a drug-related death. Body weight loss greater than 30% was considered lethal. Statistical significance was calculated by ANOVA and Bonferroni-corrected P-value for multiple comparison tests.

Results

Preparation and characterization of NPs

Two amphiphilic block copolymers, a diblock PEO-PCL and a triblock PEO-PCL-PEO, both designed to have a similar PCL/PEO weight ratio close to 2/1 and PEO segments with the same length, were used to prepare AB and ABA based NPs by MeSo. Relevant properties of the synthesized copolymers are reported in Table 1, whereas overall characteristics of NPs are summarized in Table 2.

Table 1. Molecular characterization and thermal data of PCL-PEO block copolymers.

Block copolymer	Wt % of PCL	M_n of blocks [a] (kDa)		η_{inh} (dL/g)	PDI[b]	T_m [c] (°C)	ΔH_m [c] (J/g)	X_c [d] (%)
		PCL	PEO			PEO PCL	PEO PCL	PEO PCL
AB	67	4.1	2.0	0.28	1.16	41.3 56.2	10 50	12 54
ABA	63	6.8	2.0	0.38	1.27	39.0 56.8	11 43	13 48

[a] Number average molecular weight evaluates by ^{1}H-NMR.
[b] Molecular weight polydispersity index obtained by SEC.
[c] Melting temperature and enthalpy determined by DSC.
[d] Crystallinity calculated from wide angle X-ray spectra.

Table 2. Properties of unloaded and DTX-loaded NPs.

NP code	[a]DTX (mg)	D_H (nm ± SD)	PDI	ZP (mV ± SD)	[b]Actual loading	EE (% ±SD)	Yied (%)
AB	-	61 ± 4	0.174	−14.9 ± 2.5	-	-	72 ± 2
AB$_5$	5	56 ± 2	0.280	−14.5 ± 0.5	4.9 ± 0.3	85 ± 3	44 ± 1
AB$_{10}$	10	57 ± 2	0.213	−16.8 ± 2.0	8.7 ± 0.5	90 ± 5	79 ± 1
AB$_{15}$	15	53 ± 3	0.208	−18.6 ± 0.7	5.1 ± 0.1	41 ± 1	52 ± 6
ABA	-	93 ± 6	0.239	−12.2 ± 1.4	-	-	89 ± 2
ABA$_5$	5	87 ± 3	0.308	−11.2 ± 3.0	4.9 ± 0.1	98 ± 2	48 ± 6
ABA$_{10}$	10	74 ± 7	0.254	−10.9 ± 0.9	8.1 ± 0.2	91 ± 1	70 ± 3
ABA$_{15}$	15	83 ± 9	0.331	−12.3 ± 1.0	4.8 ± 1.2	44 ± 8	52 ± 3

[a]Approximate DTX amount per 100 mg of copolymer.
[b]Ratio between the actual amount of DTX entrapped and initial DTX amount employed × 100.
[c]Encapsulation efficiency.

A temperature approximately 20°C higher than copolymer melting temperature was adequate to give NPs with good yields. The incorporation of DTX did not significantly affect D_H, whereas a slight increase of PI was observed for NPs prepared from both copolymers. Both blank and loaded ABA NPs displayed greater D_H than the corresponding AB ones. The nearly spherical morphology of the NPs was clearly observed by TEM (Figure 1), which also evidenced the absence of aggregation phenomena and a size close to that obtained by PCS.
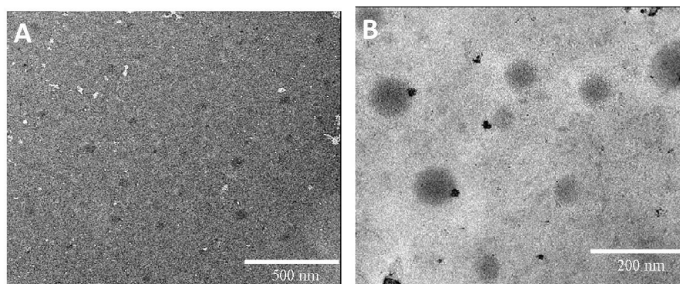
Figure 1. Transmission electron microscopy images of DTX-loaded AB_{10} (A) and ABA_{10} (B) NPs.

The core-shell structure of the NPs was verified by ^{1}H-NMR studies on unloaded NPs. Sharp peaks relative to PCL and PEO blocks were observed using chloroform-d as a solvent with high affinity with both segments. When NPs were dispersed in D_2O at 25°C, their spectra showed only the sharp peak of the PEO methylene groups at $\delta=3.60$-3.70, whereas resonances of PCL blocks were not observed even at high magnification. At 70°C, i.e., above melting temperature of the PCL, broad peaks attributed to PCL blocks were generated, in agreement with the formation of a viscous state of melted PCL chains in the core. To determine the amount of hydrated PEO chain located on the surface, a known amount of TMSP was used as internal standard in a D_2O dispersion of NPs at 25°C. The comparison of these spectra with those obtained after the addition of chloroform-d, a good solvent for both blocks, allowed the partition of PEO between the hydrated shell and the core to be calculated. It was found that, at 25°C, 80–90% of PEO was actually present in the corona for AB NPs and that its amount was significantly lower (≈50%) in the case of ABA NPs. Zeta potential was slightly negative for both unloaded and DTX-loaded AB and ABA NPs. AB NPs were more negative than ABA NPs regardless of the amount of DTX loaded (Table 2). DTX encapsulation efficiency in NPs was the highest at intermediate amount of DTX used, whereas a decrease in entrapment efficiency occurred at higher DTX amounts

115

initially employed. The maximum amount of DTX entrapped inside NPs was around 8 mg/100 mg NPs for both AB and ABA NPs. An amount as low as ≈ 5% of total DTX employed to prepare NPs was not entrapped in ABA_{10} NPs after MeSo, remaining free in the aqueous dispersion, whereas unencapsulated DTX increased to approximately 16% for AB_{10} NPs. DSC analysis evaluated the physical state of DTX inside NPs prepared at intermediate DTX loading, i.e., the highest DTX actual loading obtained. Figure 2 reports the heating thermograms of DTX-loaded AB_{10} and ABA_{10}, collected at 10°/minute scanning rate and compares them with that of a DTX control treated by MeSo in the same experimental conditions as those employed to produce NPs.
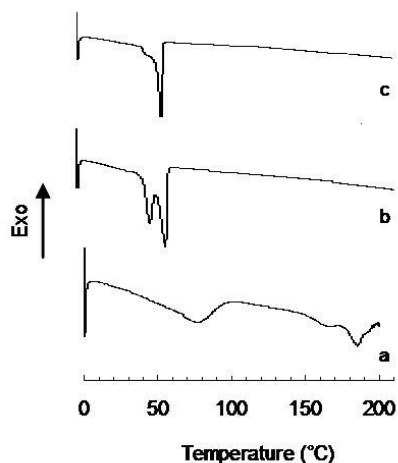
Figure 2. DSC thermograms of DTX treated by MeSo (a), AB_{10} NPs (b) and ABA_{10}NPs (c).

DTX curve showed a melting endotherm at about 186°C, in agreement with T_m of crystalline DTX, while a corresponding endotherm was not observed in the thermograms of loaded NPs. Moreover, the thermograms show melting endotherms of PCL and PEO blocks identical to those of unloaded systems and similar to DSC traces of copolymers, self-organized in bulk. Release profiles of DTX from NPs in PBS at pH 7.4 are reported in Figure 3.
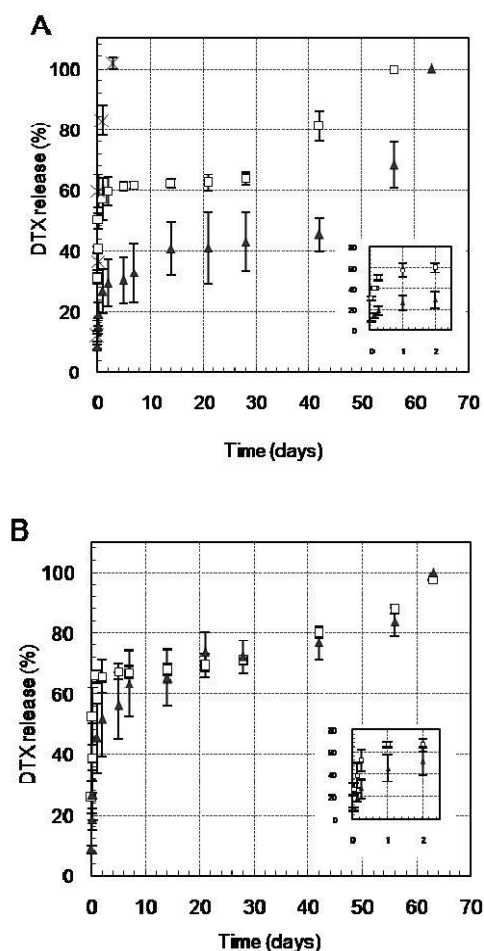
Figure 3. Release profile of DTX from NPs in 10 mM phosphate buffer at pH 7.4 and 37 °C.Panel A. Release profile of DTX from AB_5 (□) and ABA_5 (▲) NPs. Release of DTX fromTaxotere[R] (×) is reported for comparison. Panel B. Release profile of DTX from AB_{10} (□) and ABA_{10} (▲) NPs. Inset in A and B show release profiles of DTX in the initial stage. Eachpoint is the mean of four measurements±SD.

A two-pulse release was observed for both types of NPs and characterized by an initial fast release, a plateau and a second release stage. At the initial stage, drug release was dependent on copolymer type, due to a slower release rate for ABA NPs (see inset in Figure 3, A and B). Release profiles of DTX at low loadings show that control over DTX release rate in the initial stage is more efficient in the case of ABA NPs than for AB NPs.

117

In vitro cytotoxicity

Hemolytic properties of DTX-loaded NPs were evaluated and compared with those of Taxotere (Figure 4).
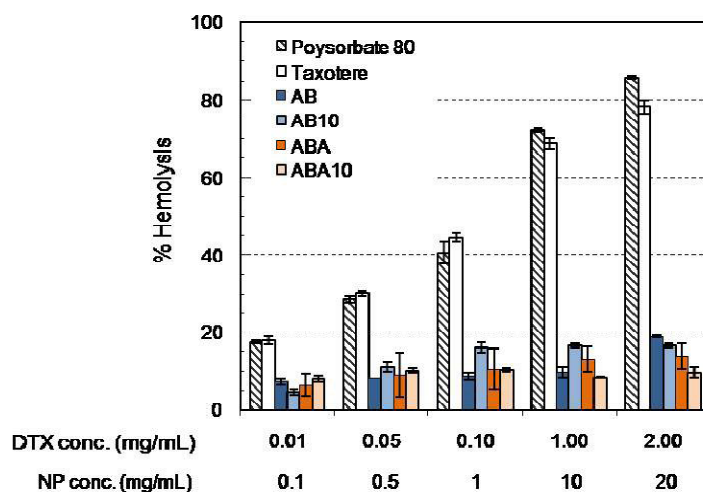
Figure 4. Hemolytic activity of Taxotere[R], polysorbate 80, DTX-loaded AB_{10} and ABA_{10} NPs, unloaded AB and ABA NPs. Polysorbate 80 is the surfactant present in the Taxotere[R] vehicle. Each point is the mean of four measurements±SD.

The results of the hemolysis test demonstrated that toxicity toward RBC of Taxotere could be mainly attributed to polysorbate 80, whereas DTX-loaded NPs were much less toxic to RBC at all concentrations tested. In vitro cytotoxicity of free DTX or DTX-loaded NPs was evaluated by incubating 5 human tumor cell lines derived from breast (MCF-7 and MDA-MB231) and prostate (LnCaP and DU145) cancer with increasing concentrations of free DTX, DTX-loaded AB_{10} and ABA_{10} NPs (0.78 to 100 ng/mL), and empty AB and ABA NPs for 72 hours (Figure 5).
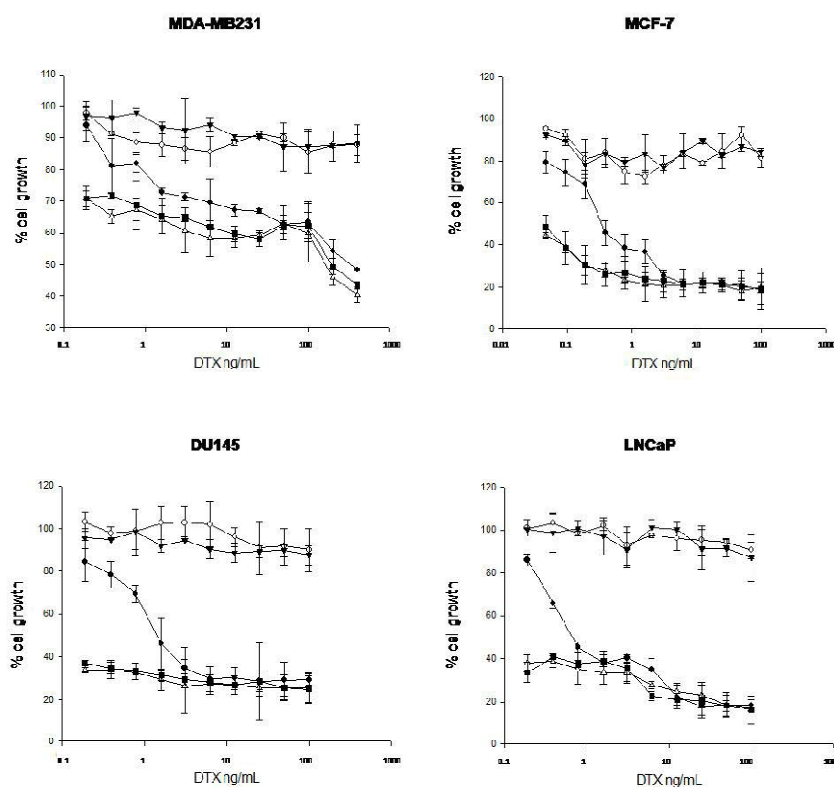
Figure 5. Growth inhibition of cells treated with free DTX or DTX-loaded NPs for 72 h, evaluated by MTT assay and expressed as percentage of untreated cells. Data are reported as mean of three independent experiments ± SD. Key legend: free DTX (▣), unloaded ABA ( ) and AB (▾) ○ NPs, DTX-loaded ABA_{10} (▴) and AB_{10} NPs ( ). Each point is the mean of four measurements ± SD.

Cell growth was then assessed by using the MTT assay as described in the Methods section. Empty NPs did not induce significant cell growth inhibition at every concentration and time interval tested. As expected, free DTX caused a significant cell growth inhibition after 72 hours of treatment in a range from 10 to 90%, and both dose/effect curves of both DTX-loaded AB_{10} and ABA_{10} NPs did not show a clear dose-dependent effect in all cell lines. Furthermore, we observed that both DTX-loaded AB_{10} and ABA_{10} NPs induced cell growth inhibition more forcefully than free DTX. In fact, the obtained data suggested that the DTX-loaded NPs caused a potent growth inhibition already at low DTX dosages, accounting for an anticancer activity ranging from 70 to 40% at

a DTX concentration of 0.78 ng/mL depending on the cell line used for the assays (Figure 5).

Moreover, the values of potentiating factor (PF) reported in Table 3 demonstrate that both types of DTX-loaded NPs potentiated the growth inhibition induced by free DTX, reaching a PF higher than 1.0 in cancer cell lines of different histogenesis (Table 3). Specifically, PF values define the specific contribution of DTX-loaded NPs evaluated as the ratio of the IC_{50} or IC_{25} of encapsulated DTX to the IC_{50} or IC_{25} of free DTX. The PF was higher for the IC_{25} than for the IC_{50} values (Table 3); in fact, the encapsulation of DTX appeared to potentiate the antiproliferative activity of DTX at lower concentrations whereas the growth inhibitory activity of the NPs resembled that of free DTX for higher concentrations.

Table 3. $IC_{50/25}$ values (ng/ml) of free DTX or DTX-loaded NPs in different cell lines.

		DTX	ABA$_{10}$	P.F.	AB$_{10}$	P.F.
DU145	IC_{50}	1.36 ± 0.04	$<0.195 \pm 0.003$	>7	$<0.195 \pm 0.003$	>7
	IC_{25}	0.55 ± 0.04	$<0.195 \pm 0.003$	>3	$<0.195 \pm 0.003$	>3
LNCaP	IC_{50}	0.700 ± 0.009	$<0.19 \pm 0.04$	>4	$<0.19 \pm 0.06$	>4
	IC_{25}	0.28 ± 0.02	$<0.19 \pm 0.04$	>1.5	$<0.19 \pm 0.06$	>1.5
MDA-MB231	IC_{50}	345.39 ± 0.04	164.60 ± 0.03	2.1	$>184.85 \pm 0.01$	1.9
	IC_{25}	1.413 ± 0.004	$<0.19 \pm 0.03$	>7	$<0.19 \pm 0.01$	>7
MCF-7	IC_{50}	0.35 ± 0.01	$<0.04 \pm 0.01$	>9	$<0.04 \pm 0.01$	>9
	IC_{25}	0.09 ± 0.05	$<0.04 \pm 0.01$	>2	$<0.04 \pm 0.01$	>2

In vivo toxicity

MTD for intravenously administered free DTX, DTX-loaded AB$_{10}$ and ABA$_{10}$ NPs (0.78 to 100 ng/ml) and empty AB and ABA NPs was determined in healthy 7-week-old BALB/c female mice. Survey experiments to define MTD were performed with 6 animals/group. DTX-loaded NPs were dispersed in a 0.9% NaCl solution. No severe side effects, sudden deaths or mean loss of more than 20% or 30% of the initial body weight were observed up to 28 days after drug administration with free DTX or DTX-loaded NPs at every concentration tested suggesting that MTD was never achieved with any treatment (Figure 6). However, either 35 or 50 mg/m^2 free DTX induced an about 25% decrease of the mean body weight of mice if compared with that of

the control group. This difference was statistically significant (*P<0.005) (Figure 6A). Lower dosages of free DTX did not cause any change in mean body weight compared with control mice. Similarly, at every used dosage, neither DBL-DTX nor TBL-DTX caused any significant change in the mean animal body weight compared with control mice (Figure 6B). These data suggested that neither NPs were toxic for mice and that they induced milder side effects than the highest dosage of free DTX induced.
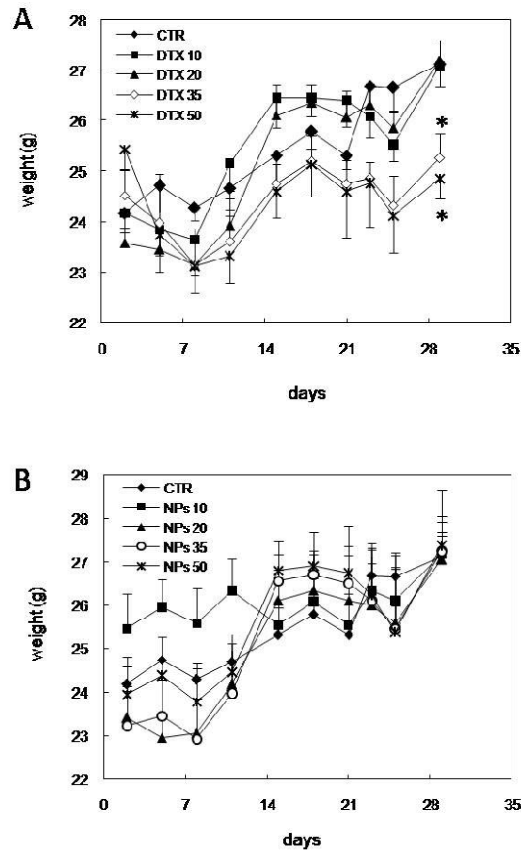
Figure 6. Effects of free DTX and DTX-loaded NPs on the body weight changes of mice. Mice were randomized and treated with (A) different doses (from 10 to 50 mg/kg as indicated in the figure) of either free DTX (DTX) and (B) DTX-loaded ABA_{10} NPs by intravenously administered in the tail veins of the animals. The body weight was determined three times a week for 4 weeks and the results were expressed as means (n=6) + SD. *p<0.005.

Discussion

MeSo is an interesting technique set up in our labs to produce core-shell NPs for drug delivery. The technique has been used here to prepare NPs from block copolymers of PCL and PEO with different architectures and to entrap the anticancer drug DTX. The formulation study aimed at understanding how copolymer physical-chemical properties affect those features of NPs that are relevant to the therapeutic response. Furthermore, the toxicity of NPs on RBC, different tumor cell lines and in mice was investigated to pinpoint the in vivo potential of the system. MeSo consists of the nanoemulsification of a fluid, nonwater-miscible copolymer at a temperature higher than T_m in water under sonication. The copolymer is then hardened by cooling at room temperature giving spherical nonaggregated NPs with a hydrophilic coating and a hydrophobic core. As indicated by the NMR results and zeta potential study, hydrated PEO segments with high chain mobility were located in the corona of NPs, and the PCL chains interact with each other, forming a solid-like compact semicrystalline core with strongly constrained motions. PEO was quantitatively distributed on the surface only for AB NPs, suggesting that a more regular core-shell structure was reached in the case of the diblock copolymer. This finding can be easily related to the structural differences between copolymers and especially to the presence of a single junction between PCL and PEO blocks in AB, which favors self-assembly in the MeSo process. Although the total amount of PEO found on the surface of ABA NPs was slightly lower than that found on AB NPs, zeta potential values suggested a different PEO organization with a more efficient shielding of the PCLcharge in the case of ABA NPs. It is conceivable that in the shell of ABA NPs, the presence of two PEO chains joined to the core by a single PCL chain ensures a higher surface density of PEO. Thus, PEO distribution on particle surface at a comparable hydrophilic/hydrophobic ratio might be modulated by chain flexibility of copolymers with different architectures. Nevertheless, such an organized PEO shell has previously been demonstrated to impart stealth properties to ABA NPs[18]. With regard to the drug-loading ability of NPs, the trend of actual loading at increasing DTX amount employed to obtain NPs suggests that the drug-to-copolymer ratio plays a key role in allowing efficient drug entrapment in the nano-structuring melted copolymer analogously to observations made for NPs prepared from other PCL copolymers by solvent displacement methods[20,21]. Behind the preparation of NPs by MeSo, complex multiple processes take place that strongly impact nanocarrier features. Nevertheless, some general indications on the process of nanocarrier formation can be affirmed based on our findings. Considering the very low solubility of

DTX in water, it can be reasonably hypothesized that drug incorporation within PCL phase is promoted when the copolymer is in a melted state, because it is hindered in preformed core-shell NPs. Thus, loading efficiency is critically affected by the solubility profile of the drug in the dispersing medium (water), which has to be low, taking into account the great difference in the solubility parameters δ of water and DTX (47.9 and 25.5 MPa1/2, respectively), and in the melted copolymer (δ of PCL = 18.2 MPa1/2), which displays higher miscibility with the drug. It can be hypothesized that at drug loading higher than intermediate, in which a sharpdecrease of encapsulation efficiency is experienced, DTX rapidly precipitates in the water phase losing the possibility to partition in melted copolymer and remain entrapped in NPs. The absence of crystalline order of DTX in the solid NPs also suggests that an efficient drug dispersion in the polymer can be reached. On the other hand, the presence of crystalline PEO and PCL domains indicates that MeSo technique does not hinder efficient phase separations of immiscible separate copolymer segments. Due to the semicrystalline nature of both copolymers, it is reasonable to assume that the drug is entrapped in the amorphous regions of the PCL core of the NPs. Accordingly, actual loading of AB_{10} and ABA_{10} seems to correlate well to copolymer crystallinity with the less crystalline ABA giving higher actual loading of DTX than AB bulk copolymer. DTX-loaded AB_{10} and ABA_{10} NPs could be freeze-dried without the help of any cryoprotectant and redisperded in PBS, giving the original hydrodynamic diameter and without displaying any aggregation. This feature is important from a pharmaceutical perspective because it promises a good shelf life of the formulation. The size of DTX-loaded NPs below 100 nm can be considered a cut-off value to achieve long-circulating properties in vivo[5]. Thus, an advantage of MeSo technique is the possibility to finely control this feature without the help of any surfactant. This aspect is important when considering that carrier distribution in different body compartments as well as extravasation in solid tumors are strongly affected not only by size[4,22] but also by the presence of surfactant on the surface[23].

Hemolytic potential is of critical importance for any intravenously administered drug because a negative interaction with blood components can strongly limit their applicability. This aspect is much more important when a hydrotropic vehicle is needed as in the case of Taxotere where polysorbate 80 and ethanol are added to solubilize DTX. It is well known that surfactants at high concentrations are responsible for toxic effects due to membrane penetration and saturation of surfactant unimers which solubilize membrane lipids and proteins[24,25]. The lower toxicity of DTX-loaded ABA_{10} NPs in

comparison with AB_{10} NPs at concentrations higher than 0.05 mg/mL (P<0.001) could be due to the presence of perfect core-shell micelles prone to dissociate and release unimers. Because CMC for AB is lower than that of ABA, it can be hypothesized that the formation of core-shell AB micelles during the fabrication of NPs is higher for AB in comparison with ABA. The presence of a greater amount of AB micelles results in a greater presence of AB unimers, which could exert a certain toxicity on RBC. Both types of developed NPs were found to have very peculiar release trends with a two-pulse profile. The finer control over DTX release rate in the initial stage in the case of ABA NPs can be reasonably ascribed to a lower PCL crystallinity in ABA, which promotes a more homogeneous distribution of DTX in the amorphous regions of NPs and its progressive delivery. At a higher DTX loading, an increased concentration gradient develops which increases delivery rate in the initial diffusive stage and speeds up release for both AB and ABA NPs. Again, the initial release of DTX was slower for ABA NPs, confirming the importance of reducing polymer crystallinity for an efficient modulation of release rate. In the plateau stage, which starts when all the diffusible drug molecules in the hydrating medium are over, DTX release stops; this is likely due to slow PCL degradation. The second drug pulse can be attributed to massive PCL degradation of the inner core allowing drug delivery from the polymer crystalline phase. Actually, drug pulse occurs at comparable times for both AB and ABA NPs, confirming that PCL degradation rate is the main determinant accounting for this effect and consistent with the two-step degradation mechanism, which has recently been suggested for PCL-PEO NPs in aqueous environment[26]. This release behavior could be of great interest in the treatment of solid tumors because it has been suggested that enhanced therapeutic efficacy of nanomedicines may be a function, in part, of this mechanism[27]. In fact, a controlled drug release rate in tumor interstitium can be of help in generating a drug concentration gradient in the tissue with major effects on the pharmacological effect of drugs and tumor resistance[28]. The experimental conditions realized in the in vitro release study could well simulate those induced in vivo by the dose-dense administration of DTX. The conventional high-dose chemotherapy is not very effective and is associated with high toxicity[29]. Dose-dense chemotherapy, in which one or more chemotherapeutic agent is administered at more frequent intervals, has shown efficacy in phase III RCTs[30,31]. It was, moreover, recently reported that the administration of paclitaxel (another taxane similar to DTX) on a weekly schedule (dosedense therapy), rather than the standard every-3-week schedule (conventional therapy), might produce greater tumor-cell death both in vitro

124

and in vivo[32]. It was reported that paclitaxel-induced apoptosis depends on the paclitaxel concentration and the duration of the exposure time. Therefore, it cannot be excluded that in our experimental conditions the continuous exposure of the tumor cells to DTX could elicit mechanisms of cell death (i.e., apoptosis) different from those caused by the addition of a single DTX pulse[33]. The different mechanisms of cell death induced by free Vs DTX-loaded NPs could account for the different antiproliferative effects observed in our experimental conditions. The different in vitro cytotoxicity of NPs versus free DTX was paralleled by a milder toxicity profile of DTX-loaded ABA_{10} NPs in an animal experimental model. Although the administration of scalar dosages of DTX both free or entrapped in NPs did not allow the achievement of a MTD, the highest dosages of free DTX caused a reduction in the body weight increase of the animals, whereas no effects were recorded with the corresponding dosages of DTX-loaded ABA_{10} NPs. This discrepancy could be due to the slow release of DTX in the blood circulation and the consequent elimination of the drug from the liver and kidney. These results strongly suggest the advisability of further development of these NP formulations in preclinical animal models of human cancers.

References

(1) Couvreur P, Vauthier C. Nanotechnology: intelligent design to treat complex disease. Pharm Res 2006;23:1417-50.

(2) Jabr-Milane LS, van Vlerken LE, Yadav S, Amiji MM. Multi-functional nanocarriers to overcome tumor drug resistance. Cancer Treat Rev 2008;34:592-602.

(3) Owens III DE, Peppas NA. Opsonization, biodistribution, and pharmacokinetics of polymeric nanoparticles. Int J Pharm 2006;307:93-102.

(4) Li SD, Huang L. Pharmacokinetics and biodistribution of nanoparticles. Mol Pharm 2008;5:496-504.

(5) Alexis F, Pridgen E, Molnar LK, Farokhzad OC. Factors affecting the clearance and biodistribution of polymeric nanoparticles. Mol Pharm 2008;5:505-15.

(6) Gref R, Luck M, Quellec P, Marchand M, Dellacherie E, Harnisch S, et al. 'Stealth' corona-core nanoparticles surface modified by polyethylene glycol (PEG): influences of the corona (PEG chain length and surface density) and of the core composition on phagocytic uptake and plasma protein adsorption. Colloids Surf B Biointerfaces 2000; 18:301-13.

(7) Kim D, El-Shall H, Dennis D, Morey T. Interaction of PLGA nanoparticles with human blood constituents. Colloids Surf B Biointerfaces 2005;40:83-91.

(8) Allen C, Maysinger D, Eisenberg A. Nano-engineering block copolymer aggregates for drug delivery. Colloids and Surfaces B-Biointerfaces 1999;16:3-27.

(9) Gaucher G, Marchessault RH, Leroux JC. Polyester-based micelles and nanoparticles for the parenteral delivery of taxanes. J Control Release 2010;143:2-12.

(10) Gaucher G, Dufresne MH, Sant VP, Kang N, Maysinger D. Leroux JC Block copolymer micelles: preparation, characterization and application in drug delivery. J Control Release 2005;109:169-88.

(11) Letchford K, Liggins R, Wasan KM, Burt H. In vitro human plasma distribution of nanoparticulate paclitaxel is dependent on the physicochemical properties of poly(ethylene glycol)-block-

poly(caprolactone) nanoparticles. Eur J Pharm Biopharm 2009;71:196-206.

(12) Gou M, Zheng L, Peng X, Men K, Zheng X, Zeng S, et al. Poly(epsilon-caprolactone)-poly(ethylene glycol)-poly(epsilon-caprolactone) (PCL-PEG-PCL) nanoparticles for honokiol delivery in vitro. Int J Pharm 2009;375:170-6.

(13) Gou M, Zheng X, Men K, Zhang J, Zheng L, Wang X, et al. Poly(epsilon caprolactone)/ poly(ethyleneglycol)/ poly(epsiloncaprolactone) nanoparticles: preparation, characterization, and application in doxorubicin delivery. J Phys Chem B 2009;113:12928-33.

(14) Feng N, Wu P, Li Q, Mei Y, Shi S, Yu J, et al. Oridonin- loaded poly(ε-caprolactone)- poly(ethyleneoxide)- poly(ε-caprolactone) copolymer nanoparticles: preparation, characterization, and antitumor activity on mice with transplanted hepatoma. J Drug Target 2008; 16:479-85.

(15) Ostacolo L, Marra M, Ungaro F, Zappavigna S, Maglio G, Quaglia F, et al. In vitro anticancer activity of docetaxel-loaded micelles based on poly(ethylene oxide)-poly(epsilon-caprolactone) block copolymers: Do nanocarrier properties have a role? J Control Release 2010;148: 255-63.

(16) Anton N, Benoit JP, Saulnier P. Design and production of nanoparticles formulated from nano-emulsion templates: a review. J Control Release 2008;128:185-99.

(17) Pinto RC, Neufeld RJ, Ribeiro AJ, Veiga F, Nanoencapsulation I. Methods for preparation of drug-loaded polymeric nanoparticles. Nanomedicine 2006;2:8-21.

(18) Quaglia F, Ostacolo L, De Rosa G, La Rotonda MI, Ammendola M, Nese G, et al. Nanoscopic core-shell drug carriers made of amphiphilic triblock and star-diblock copolymers. Int J Pharm 2006;324: 56-66.

(19) Caraglia M, Marra M, Giuberti G, D'Alessandro AM, Baldi A, Tassone P, et al. The eukaryotic initiation factor 5A is involved in the regulation of proliferation and apoptosis induced by IFNα and EGF in human cancer cells. J Biochem 2003;133:757-65.

(20) Aliabadi HM, Mahmud A, Sharifabadi AD, Lavasanifar A. Micelles of methoxy poly(ethylene oxide)-b-poly(epsilon-caprolactone) as vehicles for the solubilization and controlled delivery of cyclosporine A. J Control Release 2005;104:301-11.

(21) Cheon Lee S, Kim C, Chan Kwon I, Chung H, Young Jeong S. Polymeric micelles of poly(2-ethyl-2-oxazoline)-block-poly([epsilon]- caprolactone) copolymer as a carrier for paclitaxel. J Control Release 2003;89:437-46.

(22) Davis ME, Chen ZG, Shin DM. Nanoparticle therapeutics: an emerging treatment modality for cancer. Nat Rev Drug Discov 2008;7:771-82.

(23) Esmaeili F, Ghahremani MH, Esmaeili B, Khoshayand MR, Atyabi F, Dinarvand R. PLGA nanoparticles of different surface properties: preparation and evaluation of their body distribution. Int J Pharm 2008;349:249-55.

(24) Jones MN. Surfactants in membrane solubilisation. Int J Pharm 1999;177:137-59.

(25) Shalel S, Streichman S, Marmur A. Modeling surfactant-induced hemolysis by Weibull survival analysis. Colloids Surf B-Biointerfaces 2003;27:223-9.

(26) Shen CH, Guo SR, Lul CF. Degradation behaviors of monomethoxy poly(ethylene glycol)-b-poly(epsilon-caprolactone) nanoparticles in aqueous solution. Polym Adv Technol 2008;2008(19):66-72.

(27) Hori K, Nishihara M, Yokoyama M. Vital microscopic analysis of polymeric micelle extravasation from tumor vessels: macromolecular delivery according to tumor vascular growth stage. J Pharm Sci 2010;99: 549-62.

(28) Kyle AH, Huxham LA, Yeoman DM, Minchinton AI. Limited tissue penetration of taxanes: a mechanism for resistance in solid tumors. Clin Cancer Res 2007;13:2804-10.

(29) Nieto Y. The verdict is not in yet. Analysis of the randomized trials of highdose chemotherapy for breast cancer. Haematologica 2003;88:201-11.

(30) Kerbel RS, Kamen BA. The anti-angiogenic basis of metronomic chemotherapy. Nat Rev Cancer 2004;4:423-36.

(31) Citron ML, Berry DA, Cirrincione C, Hudis C, Winer EP, Gradishar WJ, et al. Randomized trial of dose-dense versus conventionally scheduled and sequential versus concurrent combination chemotherapy as postoperative adjuvant treatment of nodepositive primary breast cancer:

first report of Intergroup Trial C9741/Cancer and Leukemia Group B Trial 9741. J Clin Oncol 2003;21:1431-9.

(32) Mori T, Kinoshita Y, Watanabe A, Yamaguchi T, Hosokawa K, Honjo H. Retention of paclitaxel in cancer cells for 1 week in vivo and in vitro. Cancer Chemother Pharmacol 2006;58:665-72.

(33) De Souza R, Zahedi P, Moriyama EH, Allen CJ, Wilson BC, Piquette-Miller M. Continuous docetaxel chemotherapy improves therapeutic efficacy in murine models of ovarian cancer. Mol Cancer Ther 2010;9:1820-30.

CHAPTER 4: Biodegradable core-shell nanoassemblies for the delivery of docetaxel and Zn(II) phthalocyanine inspired by combination therapy for cancer

Biodegradable core-shell nanoassemblies for the delivery of docetaxel and Zn(II)-phthalocyanine inspired by combination therapy for cancer

C. Conte [a], F. Ungaro [a], G. Maglio [b], P. Tirino [b], G. Siracusano [c],
M.T. Sciortino [c], N. Leone [d], G. Palma [e], A. Barbieri [e], C. Arra [e],
A. Mazzaglia [f], F. Quaglia [a]

[a] Dip. di Farmacia, University of Napoli Federico II, Napoli, Italy;
[b] Dip. di Chimica Paolo Corradini, University of Napoli Federico II, Napoli, Italy;
[c] Dip. di Scienze della Vita, Sezione di Microbiologia, Genetica e Biologia Molecolare, University of Messina, Messina, Italy;
[d] CNR-IPCF Istituto per i Processi Chimico Fisici, Messina, Italy;
[e] Struttura Semplice Dipartimentale di Sperimentazione Animale, Istituto Nazionale dei Tumori - Fondazione "G. Pascale" - IRCCS, Napoli, Italy;
[f] CNR-ISMN Istituto per lo Studio dei Materiali Nanostrutturati UOS Palermo, c/o Dipartimento di Scienze Chimiche dell'Università di Messina, Messina, Italy
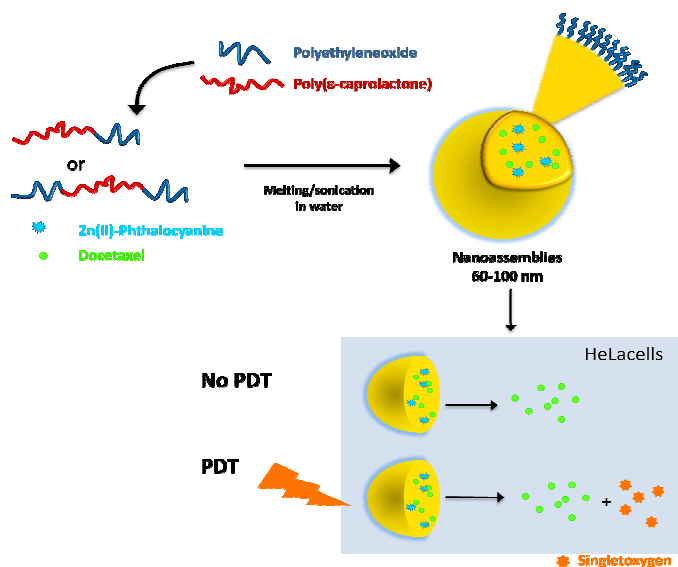
132

Abstract

Combination therapies for cancer aim to exploit either additive or synergistic effects arising from the action of two species with the final goal to maximize the therapeutic efficacy. In this work, we develop multifunctional nanoparticles (NPs) for co-delivery of the conventional anticancer drug docetaxel (DTX) and the second generation photosensitizer zinc-phthalocyanine (ZnPc) as potential dual carrier system for the combination of chemotherapy and photodynamic therapy (PDT). Biodegradable and amphiphilic block copolymers based on poly(ε-caprolactone) (PCL=B) and poly(ethylene oxide) (PEO=A), with AB and ABA architectures, were assembled in "core-shell" NPs and loaded with both DTX and ZnPc employing the melting/sonication method. Hydrodynamic diameters within the range 60–100 nm and low polydispersity indexes were obtained. Zeta potential was negative for all the formulations and unaffected by drug encapsulation. Concerning drug loading ability of NPs, the entrapment efficiency was related to initial ZnPc/DTX ratio. Steady-stationary and time-resolved emission fluorescence measurements pointed out the embedding of monomeric ZnPc in the NPs, excluding the presence of ZnPc self-supramolecular oligomers. The release of DTX was biphasic whereas ZnPc remained mainly associated with NPs. Singlet oxygen generation was observed when ZnPc-loaded NPs were irradiated at 610 nm within a 45 min time range, despite that ZnPc was not released in the medium. Stability of NPs in the presence of serum proteins and plasma was excellent and no toxicity toward red blood cells was found. NPs cytotoxicity was evaluated in HeLa cells irradiated for 30 min with a halogen lamp. After 72 h, viability of cells treated with ZnPc/DTX-loaded NPs strongly de- creased as compared to NPs loaded only with DTX, thus showing a combined effect of both DTX and ZnPc. Superior antitumor activity of ZnPc/DTX-loaded NPs as compared to DTX-loaded NPs wasconfirmed in an animal model of orthotopic amelanotic melanoma, thus pointing to the application of PEO–PCL NPs in the combined chemo-photodynamic therapy of cancer.

Keywords: Photodynamic therapy, Nanoparticles, Amphiphilic block copolymers, Poly(epsiloncaprolactone), Poly(ethyleneoxide), Docetaxel

Introduction

The concept of combining different treatment modalities is widely employed in modern oncology to improve the therapeutic response. Photodynamic therapy (PDT) is a non-invasive clinical treatment based on the administration of a photosensitizer (PS) that, after irradiation by a non-thermal light, photochemically reacts with tissue components, causing the formation of cytotoxic species and the following cell death through the initiation of apoptosis and necrosis[1]. Anticancer effects of PDT are ascribed to direct cytotoxic effects on tumor cells, damage to tumor vasculature, and induction of a severe inflammatory action, all acting in cooperation[2]. Tumor selectivity of PDT is ensured by the application of localized light to neoplastic areawithout affecting healthy tissues Nevertheless, induction of a systemic immune response, is a key aspect since it is foreseen as a strategy to treat metastatic cancer [2]. PDT has been combined with surgery, radiotherapy and chemotherapy and considered promising for the management of malignant and premalignant non-melanoma skin cancer, Barrett esophagus and non-resectable cholangiocarcinoma whereas its role in managing other type of tumors has not been unequivocally proven[2–5]. Acting by different mechanisms, cytotoxic drugs can act in concert with PS for tumor killing, achieving potentiated therapeutic outcome through an anticancer synergistic effect[6]. Under irradiation with light of appropriate wavelength, PS is promoted from its ground state to the first excited single state which results in a chain of further electronic transitions. Due to intersystem crossing, PS in the triplet state can transfer energy to molecular oxygen and generate singlet oxygen. Short singlet oxygen lifetime (around 3 μs) and resulting diffusion distance ($2^-4 \times 10^{-6}$ cm^2 s^{-1}) make PDT a highly selective treatment[7]. Amid second generation PS, phthalocyanines have attracted attention over the past two decades as very promising candidates for tumor PDT[7]. Due to the presence of a suitable coordinating atom (zinc, aluminum, silicon), they exhibit long-lived triplet state with high singlet oxygen production. Nevertheless, poor water solubility of phthalocyanines is highly beneficial to increase tumor to normal tissue ratio[8] but strongly limits intravenous administration, in analogy to highly lipophilic chemotherapeutic agents. To overcome these issues and alleviate PS accumulation in the body and post-PDT skin photosensitivity under exposure to environmental light, the so-called third generation of PS has been developed. It comprises second generation PS associated to a carrier able to promote PS accumulation at the target site as well as to minimize healthy cell localization and concomitant damage. On these bases, formulation of PS in different nanosized delivery systems has been attempted[9–12]. A variety of

photoactive NPs has been developed so far and found to alter PS pharmacokinetics as well as control side effects[12,13]. Research on third generation PS has been focused on uncoated biodegradable NPs made of PLGA[10,12–14] or poly(ε-caprolactone) (PCL)[15] which, due to recognition by the host's immune system, are rapidly uptaken in MPS and cannot be considered highly efficient in altering PS biodistribution[16]. Nevertheless, from the early attempts of PS incorporation in biomimetic stealth biodegradable NPs[17] to more recent findings[18], an improvement of tumor selectivity as well as reduction of drug/light interval, treatment times, normal tissue damage, cutaneous sensitivity and dose required has been found when employing PEGylated nanocarriers as compared to free drug. The idea to combine two drugs with different pharmacokinetics in a nanocarrier with well-tailored properties can allow a control over anticancer drug/PS biological fate and promote co-localization in the same area of the body[19]. This approach is rather recent and demonstrated to be a promising strategy to overcome tumor drug resistance in a mouse tumor model treated with doxorubicin in combination with the PS methylene blue[20]. Furthermore, design of nanosystems being stable in vivo and able to release slowly their drug cargo in the body can strongly resemble metronomic chemotherapy and allow chronic administration of chemotherapeutics at relatively low, minimally toxic doses, and with no prolonged drug-free breaks. The potential of this approach has been recently revised on the basis of clinical trials[21] and considered a very promising novel strategy also in cancer PDT[2]. On these basis and our previous experience in the delivery of the antimitotic lipophilic drug docetaxel (DTX) through core-shell biodegradable NPs[22,23], here we develop NPs of amphiphilic block copolymers of PCL and poly(ethylene oxide) (PEO) for co-delivery of DTX and zinc-phthalocyanine (ZnPc). NPs were made from PCL/PEO block copolymers with simple diblock (AB) and triblock (ABA) structure to highlight the role of copolymer architecture on NP overall properties. The combination of steady-stationary and time-resolved emission fluorescence measurements gave insights into the entrapment process of ZnPc in the NPs, pointing out the crucial function of its monomeric form in the generation of singlet oxygen. The chemo-phototherapeutic dual effect of DTX and ZnPc was investigated on cancer cells, providing also data to understand the real mechanism in which the apoptotic cell death constitutes the ultimate effect. Finally, the synergic effect of DTX and ZnPc was preliminarily evaluated after NP injection in an orthotopic mouse model of amelanotic melanoma so as to reinforce the translational potential of the NP-based combined approach in clinical practice.

Experimental part

Materials

Docetaxel (DTX, MW=807.88) was purchased from LC laboratories (USA). Zinc(II) phthalocyanine (ZnPc, MW=577.91), (2-hydroxypropyl)-β-cyclodextrin (DS 0.6), threalose, human serum albumin, Polysorbate 80, anthracene-9,10-dipropionic acid, potassium phosphate dibasic and potassium phosphate monobasic, sodium azide and sodium chloride were purchased from Sigma-Aldrich. Sodium hydroxide was provided from Delchimica Scientific Glassware. Ethanol 96°, phosphoric acid (85%), acetonitrile and tetrahydrofuran were purchased from Carlo Erba Reagenti (Milan, Italy). α-Methoxy,ω-hydroxy poly(ethylene oxide) with Mn=2.0 kDa, $mPEO_{2000}$-OH, (Aldrich) was dried by azeotropic distillation from toluene. ε-Caprolactone, CL, (Aldrich) was distilled over CaH_2 under vacuum before use. Tin(2-ethylhexanoate)$_2$, $Sn(Oct)_2$, (Aldrich), 4-(dimethylamino) pyridine,DMAP (Fluka), 1,3-dicyclohehylcarbodiimide, DCCI (Fluka), and N-hydroxysuccinimide, NHS (Fluka) were used as received.

Synthesis and characterization of block copolymers

A PEO_{2000}–PCL_{4300} diblock copolymer (AB) was prepared as previously described[23]. Briefly, $mPEO_{2000}$-OH and $Sn(Oct)_2$ were used as initiator and catalyst, respectively, in the bulk ring-opening polymerization (ROP) of CL at 120 °C; CL/initiator molar ratio=38 (ηinh= 0.28 $dL \times g^{-1}$ at 25 °C in chloroform; Mw/Mn=1.16). A PEO_{2000}–PCL_{6800}–PEO_{2000} triblock copolymer (ABA) was synthesized by a two-step procedure[23]. Briefly, α,ω-dihydroxy-PCL_{6800}, obtained by ROP of CL initiated by 1,4-butanediol under the experimental conditions above reported, was coupled in the second step with two $mPEO_{2000}$-COOH segments after activation of the carboxyl group with NHS. DCCI, as condensing agent, and DMAP as catalyst were used in the coupling step (ηinh=0.39 $dL \times g^{-1}$ at 25 °C in chloroform; Mw/Mn=1.32).

Preparation of NPs

AB and ABA copolymers were employed to prepare unloaded, DTX-loaded, ZnPc-loaded and ZnPc/DTX-loaded NPs by a slightly modified melting/sonication procedure (MeSo) previously described[23]. Ten mg of copolymer were added to 1.8 mL of filtered water in a vial that was poured in a water bath heated at 72±2 °C to allow copolymer melting. For ZnPc/DTX-loaded NPs, DTX (5% or 10% of copolymer weight) and ZnPc (0.2% of copolymer weight) were dissolved in 0.1 mL of ethanol or THF, respectively.

136

Drug solutions were mixed and added to water containing melted copolymer. The mixture was sonicated for 10 min at 3 W (Sonicator 3000, Misonix, USA) by a microtip probe and finally cooled at room temperature. The organic solvent was then completely removed by vacuum distillation using a rotary evaporator for 30 min. For NPs loaded with a single drug, the same procedure was employed (drug was dissolved in the correspondent solvent and the other solvent added to give a 1:1 ethanol/THF volume ratio). NPs were filtered through 0.45 μm filters (RC, Chemtek, Italy), freeze-dried for 24 h and kept at 4 °C. When needed, threalose or HPβCD were added as cryoprotectants at different mass ratio with NPs. Recovery yield of production process was evaluated on an aliquot of NP dispersion (without cryoprotectant) by weighting the solid residue after freeze-drying. Results are expressed as the ratio of the actual NPs weight to the theoretical polymer weight×100.

Size and zeta potential of NPs

The hydrodynamic diameter (D_H) and polydispersity index (PI) of NPs were determined by Photon Correlation Spectroscopy (PCS) using an N5 Submicron Particle Size Analyzer (Beckman-Coulter). An NP dispersion was diluted in Milli-Q water at intensity in the range 104–106 counts/s and measurements were performed at 25°C on 90° angle. Results are reported as mean D_H of three separate measurements of three different batches (n=9)±standard deviation (SD). Size of NPs stored in the dark at 4°C for 3 months was monitored too. The morphology of the NPs was examined by transmission electron microscopy (CM 12 Philips, Eindhoven, The Netherlands) using samples stained with a 2% phosphotungstic acid solution. Zeta potential was determined by analyzing a NP dispersion in water on a Zetasizer Nano Z (Malvern Instruments Ltd.). Results are reported as mean of three separate measurements of three different batches (n=9)±SD.

Steady State and Time-resolved Fluorescence Spectroscopy

Fluorescence emission spectra were carried out on ZnPc-loaded NPs and ZnPc/DTX-loaded NPs based on AB and ABA copolymers dispersed in ultra pure water (Galenica Senese, V=20 mL) and sonicated for 10 min. In all the experiments ZnPc was set at 0.07 μg/mL. Steady-state fluorescence measurements were performed on Jasco model FP-750 spectrofluorimeter with an excitation wavelength of 600 nm and using 1 cm path length quartz. Fluorescence spectra are not corrected for the absorbance of the samples. Depolarized fluorescence spectra were measured by using Equation (1)[24]:

$$r = \frac{I_{VV}I_{HH} - I_{VH}I_{HV}}{I_{VV}I_{HH} + 2I_{VH}I_{HV}} \qquad (1)$$

where r is the anisotropy and I_{VV}, I_{HH}, I_{VH}, and I_{HV} are the fluorescence intensities registered with different polarizer orientations (V=vertical, H=horizontal).

Time-resolved fluorescence measurements were carried out by a time-correlated-single-photon-counting (TCSPC) home-made apparatus[25]. The excitation source was a synchronously mode-locked rhodamine 6G dye laser (Spectra Physics 375B) which provided excitation pulses of about 2 ps full width at half-maximum at a repetition rate of 82 MHz. An excitation wavelength of 570 nm was used. The fluorescence pulses were detected with a microchannel-plate photomultiplier (Hamamatsu R1645U-01, about 200 ps rising-time) and the decay profiles were collected with a computer-controlled multichannel analyzer card (EG&G Ortec Trump-8k/2k). The collected data were then analyzed using the nonlinear least-squares iterative reconvolution procedures based on the Marquardt algorithm[26]. In the case of total fluorescence decay curves, the fitting was performed on the basis of the multiexponential decay law[24],

$$I(t) = I_0 \sum_i \alpha_i \exp(-t/\tau_i) \quad (2)$$

where I(t) is the total fluorescence decay curve, I_0 is the intensity at time zero, and α_i and τ_i are, respectively, the relative amplitudes and lifetimes of the ith component (the normalization condition is $\sum_i \alpha_i = 1$). In the case of time-resolved anisotropy measurements, the reconvolution fitting procedure was based on two steps. Fluorescence anisotropy r(t) is defined using the following expression:

$$r(t) = \frac{I_{VV}(t) - I_{VH}(t)}{I_{VV}(t) + 2I_{VH}(t)} = \frac{D(t)}{S(t)} \quad (3)$$

where the sum data, S(t), must be equal to the total intensity I(t). In some cases, an additive constant r_∞ to r(t) was introduced to take into account a long decay contribution due to static interaction with large clusters. In the simple case of spherical molecules, each rotational correlation time, τ_{Rj}, is related to

138

the volume (V_j) of the rotating unit (or of the equivalent sphere) by the following equation [27]:

$$\tau_{Rj} = \frac{\eta V_j}{k_B T} \quad (4)$$

where η is the microviscosity of the medium, T is the temperature in kelvin, and k_B is the Boltzmann constant.

DTX analysis

DTX was analyzed by HPLC on a Shimadzu apparatus equipped with a LC-10ADvp pump, a SIL-10ADvp autoinjector, a SPD-10Avp UV–Vis detector and a C-R6 integrator. The analysis was performed on a Phenosphere-NEXT 5 μm, C18 column (250×4.6 mm, Å) (Phenomenex, USA). The mobile phase was a 40:60 (v/v) mixture of 20 mM phosphate buffer at pH 4.5 and acetonitrile pumped at a flow rate of 1 mL/min. The UV detector was set at 227 nm. A calibration curve for DTX in ethanol was constructed in the concentration range 0.980–196 μg/mL. The limits of quantification (LOQ) and detection (LOD) were 1.29 and 0.39 μg/mL.

ZnPc analysis

ZnPc quantification was carried out by spectrofluorimetry on a Shimadzu RF-1501 at EX=610 nm and EM=668 nm. The concentration of ZnPc was calculated by means of a standard calibration curve derived for THF solutions of ZnPc at known concentrations (7.2–720 ng/mL). The limits of quantification (LOQ) and detection (LOD) in THF were 3.70 and 1.11 ng/mL. Potential interference of DTX on ZnPc emission was preliminarily assessed spiking a ZnPc solution in THF with different amount of DTX.

DTX and ZnPc entrapment efficiency

DTX loading inside NPs was assessed by dissolving 1 mg of NPs in 500 μL of acetonitrile under stirring for 1 h. Thereafter, 500 μL of water was added and the sample stirred for 1 h further and analyzed as reported above. The sample was filtered through a 0.45 μm filter (RC, Chemtek, Italy). ZnPc encapsulation efficiency was evaluated by dissolving a known amount of freeze-dried NPs (1 mg) in 1 mL of THF under magnetic stirring for 1 h and analyzing the solution as described above. To verify a possible interference of copolymers on ZnPc

quantitative analysis, an amount of DTX-loaded NPs was dissolved in THF and analyzed in the same conditions reported for ZnPc.

In vitro release studies

In vitro release of DTX from NPs was assessed in 10 mM phosphate buffer containing NaCl (137 mM) and KCl (2.7 mM) at pH 7.4 (PBS) by a dialysis method. A known amount of NPs (2 mg) was dispersed in 0.5 mL of PBS and placed in a dialysis bag (MWCO=3500 Da, Spectra/Por®). The sample was plunged in 5 mL of PBS (sink condition) and kept at 37 °C. In vitro release of ZnPc from NPs was evaluated as described above in 3 mL of PBS containing 10% v/v of polysorbate 80 in order to ensure sink conditions and to avoid ZnPc aggregation. In both cases, at selected time intervals, 1 mL of release medium was withdrawn and replaced with an equal volume of fresh medium. DTX or ZnPc quantitative analysis was performed as described above. Release profile of free DTX and ZnPc (76 μg and 3.6 μg, respectively dissolved in 0.1 mL of 1:1 ethanol/THF) is reported for comparison. Results are expressed as release % over time±SD of three experiments.

Singlet oxygen generation from NPs

The capacity of NPs to generate singlet oxygen was monitored over time by measuring photobleaching of the radical quencher ADPA[28]. Briefly, 40 μl of a 5 mM ADPA solution in NaOH 0.01 M was added to 2 mL of a ZnPc solution in water/THF 100:1 v/v or a NP water dispersion ([ZnPc]=2 μg/mL; [NPs]=1 mg/mL). The sample was irradiated at 610 nm using a 150 W ozone-free xenon-arc lamp (JobinYvon) with a slit width of 10 nm for different times (15, 30 and 45 min). Sample containing NPs was centrifuged at 16,090 ×g (Mikro 20, Hettich) for 30 min. The supernatant was collected and analyzed by spectrophotometry at 400 nm to evaluate ADPA absorption. Singlet oxygen generation was monitored by the decrease of OD at 400 nm as a function of the irradiation time.

Hemolytic activity of NPs

Hemolysis studies were carried out on unloaded NPs, ZnPc/DTX-loaded NPs and HPβCD as control. After centrifugation of EDTA-treated human blood at 880 ×g for 5 min, a red blood cells (RBC) dispersion was obtained and diluted with 0.1 M PBS up to a concentration of 10% v/v. The RBC dispersion (0.1 mL) was added to 0.9 mL of a NP dispersion, with NP concentrations ranging from 0.01 to 2.0 mg/mL. The sample was incubated at 37 °C for 30 min and

centrifuged at 1000 ×g for 10 min. The supernatant was collected and analyzed for hemoglobin release by spectrophotometry at 416 nm. To obtain 0 and 100% hemolysis, 0.1 mL of RBC dispersion was added to 0.9 mL of PBS and distilled water, respectively. The degree of hemolysis was determined by the following equation: Hemolysis (%)=(ABS–ABS_0)/(ABS_{100}–ABS_0)×100, where ABS_{100} and ABS_0 are the absorbance of the solution at 100% and 0% hemolysis, respectively.

NP stability in the presence of blood components

To determine the stability of NPs under physiologically relevant conditions, a known amount of freeze-dried NPs was dispersed in PBS containing 2% w/v of human serum albumin (HSA) or in human plasma (NP concentration was 4.5 and 1.3 mg/mL, respectively) and incubated at 37 °C for different times. Human plasma was obtained by centrifugation of EDTA-treated human blood at 880 ×g for 5 min. Size measurements of the samples were taken by PCS after 24, 48 and 72 h of incubation. The stability of NPs was demonstrated by the absence of macroscopic aggregates and unchanged of initial particle size.

NP behavior in cell culture medium

The behavior of NPs prepared from AB copolymer in the medium employed for in vitro PDT studies (RPMI with 10% FBS) was evaluated by different methods. DTX concentration in NP dispersions was measured according to a method described elsewhere[29]. Briefly, 2.5 mg of ZnPc/DTX-loaded NPs were dispersed in 1.5 mL of RPMI enriched with FBS 10% v/v and incubated at 37 °C. At 24 h the samples were treated with 1.5 mL of acetonitrile and stirred overnight to promote protein precipitation. Then, the samples were centrifuged at 1000 ×g and 4 °C for 15 min. Supernatant was filtered through a 0.45 μm RC filter and dried under a nitrogen stream at 40 °C. After complete solvent evaporation, the sample was reconstituted in 1 mL of acetonitrile–water 50:50 v/v and analyzed by HPLC for DTX content. Recovery of DTX in the extraction process was 95±1%. Decrease of DTX concentration along time was considered indicative of NP aggregation and precipitation. Results are expressed as % decrease of DTX concentration as compared to the initial DTX content of the samples. For release studies, 2.5 mg of NPs were dispersed in RPMI with10% FBS (0.5 mL) and placed in a dialysis bag. The sample was plunged in 5 mL of PBS (sink condition) and kept at 37 °C up to 72 h. At selected time intervals, 1 mL of release medium was withdrawn and replaced with an equal volume of fresh medium. DTX analysis was performed as described above. Results are expressed as release % over time±SD of three

experiments. Absorption spectra of ZnPc/DTX-loaded and ZnPc-loaded NPs dispersed in PBS or RPMI ([ZnPc]=0.4 μg/mL, [NPs]=0.2 mg/mL) were collected on a Shimadzu UV-1800 spectrophotometer using a 1 cm path length quartz cuvette. As control, a solution of ZnPc in DMSO or diluted in RPMI (1:50 v/v, [ZnPc]=0.4 μg/mL) was analyzed.

In vitro PDT

HeLa cells were obtained from the American Type Culture Collection and propagated at 1:6 ratio in RPMI supplemented with 100 units/mL of penicillin and 10% fetal bovine serum. Cells were grown to confluence in 6 well plates and after 24 h they were treated with free drugs and drug-loaded NPs based on AB copolymer up to 72 h at 37 °C. Free DTX and ZnPc were in DMSO respectively ([DTX]=1 μg/mL, [ZnPc]=0.054 μg/mL). ZnPc/DTX-loaded NPs, DTX-loaded NPs, ZnPc-loaded NPs, unloaded NPs were all dispersed in water ([NPs]=10 μg/mL). The cells were subsequently detached from the substrate using trypsin, transferred in polystyrene tubes and centrifuged. After washing in PBS, cell pellets were resuspended in PBS and placed separately in a spectrophotometric cuvette to be irradiated with a halogen lamp for 30 min. The irradiating beam was filtered through an UV filter (Hoya glass type UV-34, cut-off: 340 nm) in order to cut the UV component and through a 1-cm cell filled with water, to remove the IR-component. A light dose of 5 joule/cm^2 was estimated.

Cell viability assay

Cells (6×10^4) were placed in 96-well plates with 100-μL RPMI-1640 medium. After 24 h cells were treated with free drugs and drug-loaded NPs at the correspondent final concentration (as above reported). Cells were incubated and collected at 24 and 72 h, before the addition of the presence of tetrazolium compound [3-(4,5-dimethylthiazol-2-yl)-5-(3-carboxymethoxyphenyl)-2(4-sulfophenyl)-2H-tetrazolium, inner salt;MTS, Promega] and an electron coupling reagent phenazine methosulfate (PMS) dye (MTS 20 μL per well). As a control, the same cells were exposed to the vehicle alone (DMSO), in amounts corresponding to those employed for dissolving the compounds. After further incubation (1 h), the absorbance was read at 490 nm in a microplate reader (Labsystem Multiskan Bichromatic). The percentage of cell viability (%) was calculated according to the equation:

$$\text{Cell viability (\%)} = [(\text{OD}_{\text{before lamp}} - \text{OD}_{\text{after lamp}})/\text{OD}_{\text{before lamp}}]\times100$$

142

Immunofluorescence assay

To analyze nuclear morphology and the distribution of structural protein tubulin immunofluorescence assay was performed. Non-irradiated and irradiated samples were collected at 24 and 72 h post-treatment, layered on slides treated with polylysine. After fixing in PBS (pH 7.4) with 4% paraformaldehyde (pH 7.4) for 15 min at room temperature, a volume of 0.1% Triton X-100 in PBS was added and left for 15 min. After washing three times in PBS, permeabilized cells were incubated with a fluorescein-conjugated monoclonal anti- body against human tubulin for 1 h at room temperature, followed by FITC-conjugated goat anti-mouse IgG. The cells were than stained with Hoechst 33342 fluorescent DNA-binding dye. Samples were analyzed on a Biomed Fluorescence microscope (Letiz,Wetzlar, Germany; magnification 63×) by using a DAPI (blue emission) and FITC filter (green emission), respectively.

Evaluation of apoptosis

Analysis of apoptosis was carried out at single cell level using the TUNEL technique. Labeling of DNA strand breaks with fluorescein-dUTP by terminal deoxynucleotidyl transferase was performed using a commercial kit ("In situ cell death detection kit, fluorescein", Boehringer Mannheim, Mannheim, Germany) according to the manufacturer's instructions. To evaluate DNA fragmentation (Ladder), treated cells were washed in PBS and then lysed in 0.5 ml of lysis buffer (10 mM Tris, pH 7.4, 1 mM EDTA, pH 8.0, 0.2% Triton X-100) containing proteinase K (100 mg/ml) for 1 h at room temperature. Samples were then centrifuged at 16,000 ×g for 15 min. DNA in the supernatants was precipitated with 5 N NaCl in 1 volume of isopropanol for 1 h at −20 °C. DNA precipitates were recovered by centrifugation at 16,000 × g, air dried for 15 min at room temperature, resuspended in TE buffer (10 mM Tris, pH 7.4, 1 mM EDTA, pH 8.0) containing RNase (100 mg/ml) and incubated for 1 h at 37 °C. Before electrophoresis, loading buffer (2% SDS, 15 mM EDTA, 0.25% w/v bromophenol blue, 50% v/v glycerol) was added to each sample. DNA was electrophoresed on 1.5% agarose gel stained with Gel Star (Lonza Rockland, Inc.) and visualized by UV light transillumination.

In vivo antitumor activity

The antitumor effects of NPs containing both DTX and ZnPc were tested in an orthotopic mouse model of amelanotic melanoma. The experimental procedures performed in this study followed the specific guidelines of the

Italian (N. 116/1992) and European Council law (N.86/609/CEE) for animal care. Eight-week old female athymic Nu/Nu nude mice were purchased from Harlan, Italy. Mice were housed 5 for cages and maintained on a light/dark cycle in a temperature-controlled room. To produce tumor, A375 cell line (human amelanotic melanoma cells) were harvested from subconfluent cultures. A375 human amelanotic melanoma cells were obtained from the American Type Culture Collection. A375 cells were grown in Dulbecco's modified Eagle's medium (DMEM) (Invitrogen, San Diego, CA) at pH 7.4, supplemented with 10% FCS (Gibco, UE), 100 units/ml penicillin and 100 μg/ml streptomycin. Cultures were maintained at 37 °C in a humidified atmosphere with 5% CO_2. Only cells with 90% viability were used for the injections. Each mouse underwent subcutaneous injections of 2×10^6 cells, suspendedin a volume of 100 μl of PBS, directly into the right-side flank area. When tumor volume was around 100 mm 465 3, mice were randomizedinto 5 different groups and treated by injection into the caudal vein (5 mice per group) with: saline alone, empty NP_{AB}, free DTX (Polysorbate 80: EtOH: water, 20:13:67), DTX_5-NP_{AB}, ZnPc/DTX_5-NP_{AB}. DTX dose was 3.5 mg/kg whereas ZnPc dose was 0.2 mg/kg. After 24 h mice were anesthetized and exposed to 15 min (149 J) of 172 mW/cm^2 light from a PDT-CLD100 system emitting red light at 618 nm $\pm$5% (EPEM, Greece). Surrounding skin tissue was protected from light using a light impenetrable fabric. The day of NP treatment was designated as day 0 and observation continued until day 21. The size of tumors was measured along time by using a digital caliper. Normally distributed data were represented as mean$\pm$S.E.M. Two-way ANOVA and Bonferroni post-hoc analysis were used to examine the significance of differences among groups (Graph pad Prism 5.0). A probability value with *P<0.05 and **P<0.01 was considered to be statistically significant.

Results

Properties of NPs

PEO_{2000}–PCL_{4300} diblock (AB) and PEO_{2000}–PCL_{6800}–PEO_{2000} triblock (ABA) copolymers with unimodal and narrow molecular weight distributions (PI=1.16, AB, and 1.32, ABA) were employed to prepare unloaded, DTX-loaded, ZnPc-loaded and ZnPc/DTX-loaded NPs (Table 1). The recovery yield for all the formulations was very high highlighting that neither drug precipitation nor NP aggregation occurred during MeSo. Hydrodynamic diameters of NPs were below 100 nm. All formulations showed a negative zeta potential, slightly more negative for AB NPs. Entrapment of both drugs did not influence significantly surface properties and zeta potential of AB and ABA NPs, whereas a slight increase of polydispersity index was observed when ZnPc was loaded. The addition of trehalose at different mass ratio with copolymer (10–40:1) did not prevent the aggregation of NPs after freeze-drying, while the presence of HPβCD at 10:1 mass ratio with ZnPc-loaded NPs allowed no collapsing of NPs during freeze-drying and storage at 4 °C up to three months (supplementary material, Table S1 and Fig. S1).

The spherical morphology and the absence of aggregation of freeze-dried ZnPc/DTX-loaded NPs were confirmed by TEM (Fig. 1). Also NP size was in line with the data obtained by PCS.
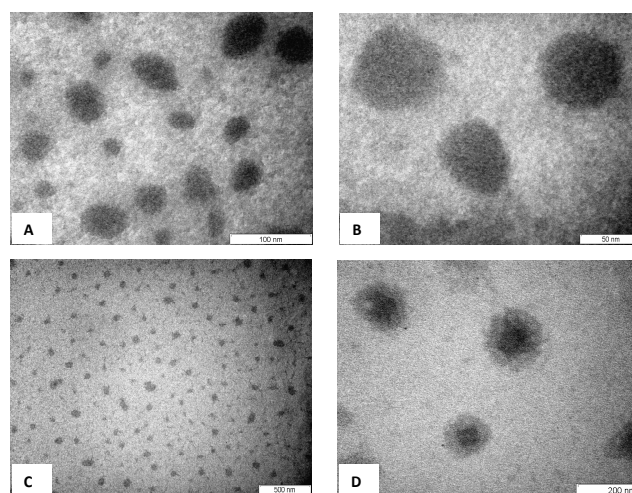
Figure 1. TEM images of ZnPc/DTX$_5$-NP$_{AB}$ (A-B) and ZnPc/DTX$_5$-NP$_{ABA}$ (C-D).

Table 1. Composition and properties of NPs produced. SD were calculated on three different batches.

Code	DTX (% w/w)	ZnPc (% w/w)	Yield (%)	Mean D_H (nm ± SD)	P.I.	Zeta Potential (mV ± SD)	ZnPc Actual loading[a] (Entrapment efficiency[b])	DTX Actual loading[a] (Entrapment efficiency[b])
NP_{AB}	-	-	93	57.8 ±6.1	0.217	-10.3±3.3	-	-
$DTX\text{-}NP_{AB}$	10	-	85	54.0 ±3.0	0.217	-8.8±4.0	-	6.3 ± 0.4 (71.2 ± 4.8)
$ZnPc\text{-}NP_{AB}$	-	0.2	86	67.4 ±5.7	0.279	-11.7±4.6	0.172 ± 0.01 (98.1 ± 1.9)	-
$ZnPc/DTX_{10}\text{-}NP_{AB}$	10	0.2	89	69.3 ±4.3	0.329	-13.4±1.3	0.095 ± 0.03 (49.8 ± 10.5)	5.5 ± 1.1 (57.7 ± 8.3)
$ZnPc/DTX_{5}\text{-}NP_{AB}$	5	0.2	83	61.0 ± 1.6	0.342	-13.7±1.8	0.196 ± 0.03 (92.5 ± 8.4)	3.7 ± 0.1 (75.8 ± 4.1)
NP_{ABA}	-	-	93	76.8±2.2	0.259	-7.9±0.7	-	-
$DTX\text{-}NP_{ABA}$	10	-	88	84.7±5.5	0.276	-8.5±3.3	-	8.8 ± 0.6 (94.1 ± 3.3)
$ZnPc\text{-}NP_{ABA}$	-	0.2	83	89.4±6.0	0.317	-8.0±1.5	0.171 ± 0.01 (94.0 ± 5.2)	-
$ZnPc/DTX_{10}\text{-}NP_{ABA}$	10	0.2	80	90.6 ±7.3	0.332	-9.0±5.3	0.09 ± 0.02 (56.7 ± 8.4)	4.3 ± 0.5 (47.6 ± 4.8)
$ZnPc/DTX_{5}\text{-}NP_{ABA}$	5	0.2	81	96.8 ± 8.1	0.339	-10.4±0.7	0.185 ± 0.01 (94.9 ± 7.0)	4.6 ± 0.3 (95.4 ± 4.1)

[a]Actual loading is expressed as the amount (mg) of drug encapsulated *per* 100 mg of NPs (corresponding to 1g of freeze-dried powder due to the presence of HPβCD at 10:1 mass ratio with copolymer).
[b]Ratio between actual and theoretical loading x 100.

The entrapment efficiencies of DTX and ZnPc inside both formulations are summarized in Table 1. When NPs were loaded with a single drug, entrapment efficiency was higher than 70% independently of the drug employed and type of copolymer used. When DTX and ZnPc were loaded simultaneously, at 10 and 0.2% theoretical loading respectively, a significant decrease in entrapment efficiencies was observed for NPs prepared with both copolymers. When the theoretical loading of DTX was reduced at 5%, the entrapment efficiency of NPs for both drugs increased.

Release profiles of drugs from ZnPc/DTX-loaded AB and ABA NPs in PBS at pH 7.4 and 37 °C were evaluated up to 70 days and compared with free drugs in combination. In Fig. 2, it is possible to note that both AB and ABA NPs assure a sustained release pattern of DTX characterized by two phases, an initial burst followed by a much slower diffusion-erosion phase, completed in around 70 days, compared with the free drug in the same conditions (inset). In these conditions, no ZnPc release was found. To observe a ZnPc release, it was necessary to enrich the phosphate buffer with Polysorbate 80 as surfactant which ensured both sink conditions in the release medium and prevented ZnPc aggregation. Nevertheless, ZnPc precipitation occurred in the dialysis bag resulting in an incomplete release of the PS (Supplementary material, Fig. S2).
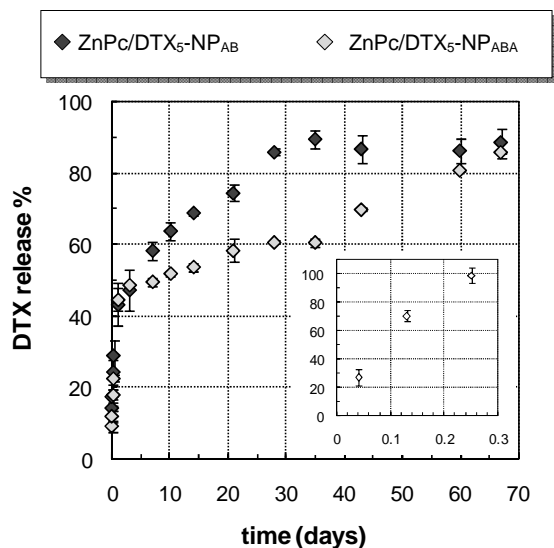
Figure 2. Release profile of DTX from ZnPc/DTX-loaded NPs in 10 mM phosphate buffer at pH 7.4 and 37°C. Release profile of DTX is reported for comparison (inset). Data are reported as mean of three independent experiments ± SD. For key legend see table 1.

Fluorescence properties and singlet oxygen generation of NPs

The interaction of ZnPc with the copolymers inside NPs was investigated by steady-state and time-resolved fluorescence emission. Fluorescence emission spectra were carried out on samples prepared by dispersing an appropriate amount of powder tominimize the scattering contribute. ZnPc is poorly soluble in aqueous solution and needed DMSO to be solubilized. The spectrum in aqueous solution of ZnPc-loaded NPs exhibits bands centered at 680, 710 and 740 nm (type AB copolymer is reported as representative) both in the absence (curve a) and in the presence (curve b) of DTX. The fluorescence bands are characteristic of metal – phthalocyanines dispersed in aqueous solution. The anisotropy value, which is around zero for free ZnPc (see inset of Fig. 3, trace c), is increasing at around 0.2–0.3 in ZnPc-NP$_{AB}$ (trace a) and in ZnPc/DTX$_5$-NP$_{AB}$ (trace b). ZnPc entrapped in NPs based on ABA copolymers both alone or in combination with DTX showed similar results (data not shown).
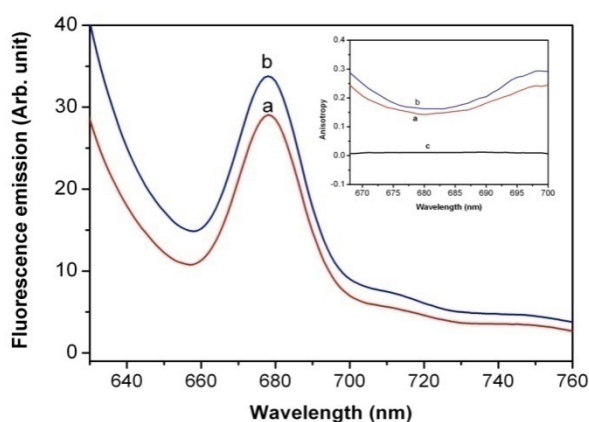
Figure 3. Steady-state fluorescence emission spectra and, in the inset, correspondent anisotropy of ZnPc in ZnPc-NP$_{AB}$ (traces a) and ZnPc/DTX$_5$-NP$_{AB}$ (traces b) dispersed in water ([ZnPc]=0.07 μg/mL, λex=600 nm). Trace c in the inset is the anisotropy of free ZnPc in DMSO.

From fluorescence time decay (Fig. 4A), it results that free ZnPc in DMSO has a lifetime of 3±0.4 ns, and this value remains unaffected when ZnPc is entrapped in NPs based on AB and ABA copolymers both in absence and in combination with DTX. To focus on the dynamic interaction between ZnPc and polymeric NPs, time-resolved fluorescence anisotropy experiments were carried out. These investigations provide detailed information on photosensitizer structural changes in the colloidal microenvironment.

148
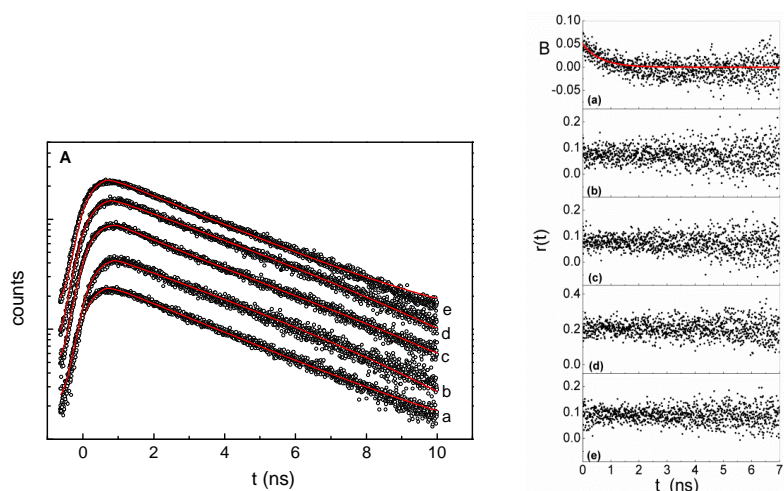
Figure 4. Fluorescence time decay (A), and time-resolved fluorescence anisotropy (B): ZnPc in DMSO (a); ZnPc-loaded NPs (b,d), ZnPc/DTX$_5$-loaded NPs (c, e) water dispersion (b and c traces refer to NPs of AB copolymer, d and e to NPs of ABA copolymer). In A the decays are scaled for a multiplicative factor in order to make easier the visualization. The continuous curves are the fit resulting from the convolution of the fluorescence decay and the excitation. In B the continuous curve is the best fit according to an exponential law.

Anisotropy fluorescence time decay (Fig. 4B) established a rotational correlation time of $\tau R \cong 0.6$ ns and a limiting anisotropy of 0.05, whereas in the aqueous dispersion of ZnPc-loaded NPs, r(t) of ZnPc appears as a plateau, indicating a much longer rotational correlation time (>20 ns).The generation of singlet oxygen from free ZnPc or ZnPc-loaded NPs dispersed in water was evaluated by monitoring the photobleaching of ADPA, a singlet oxygen quencher, occurring along time (Fig. 5). Comparable time-dependent production of singlet oxygen by ZnPc was found for free drug and ZnPc-loaded NPs also when DTX was co-entrapped, suggesting that the presence of DTX did not interfere with the photochemical properties of ZnPc.
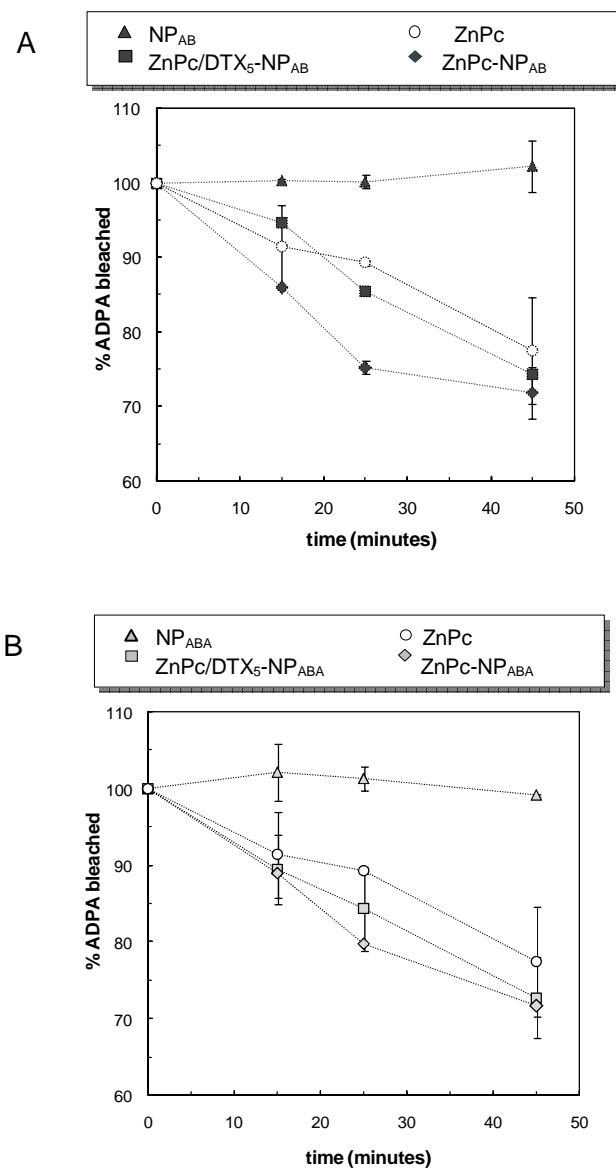
Figure 5. Photobleaching of ADPA by singlet oxygen generated from AB (A) and ABA (B)NPs. Data are reported as mean of three independente xperiments±SD. For key legend see Table 1.

Hemolytic activity of NPs

To investigate cytotoxicity toward red blood cells, hemolysis studies were carried out ondeveloped NPs (Fig. 6). Hemolysis was assessed in the NP concentration range from 0.01 to 2.0 mg/mL, with and without HPβCD as cryoprotector. As shown in Fig. 6A, NPs did not display significant hemolysis whereas hemolysis up to 70% occurred for NPs cryoprotected by HPβCD (Fig. 6B). This effect was related to HPβCD which, as such, showed a dose-dependent cytotoxicity.
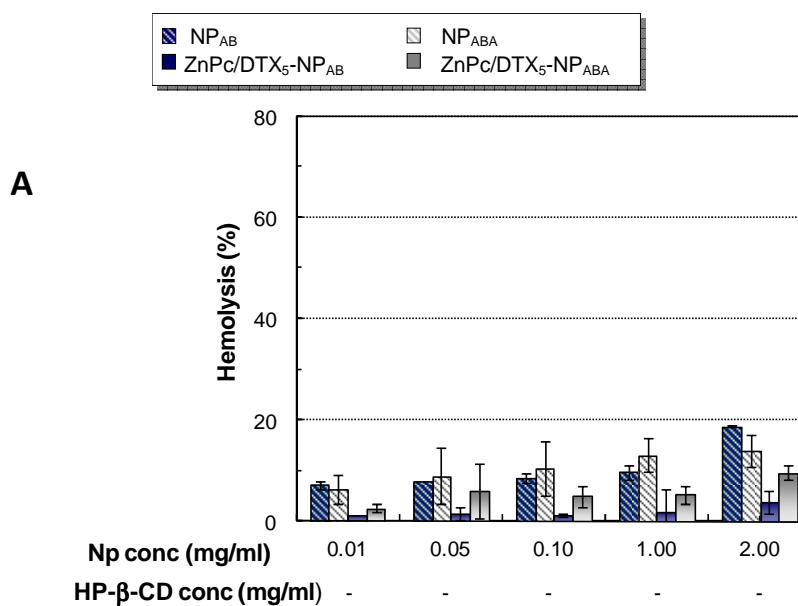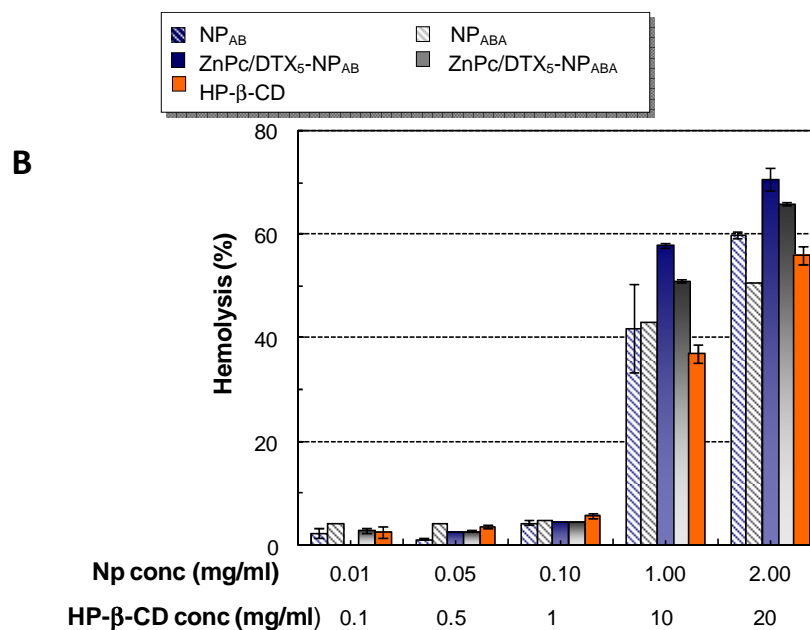
Figure 6. Haemolysis of red blood cells after incubation with NPs at different concentrations. NPs were tested immediately after preparation (A) or after freeze-drying with HPβCD (B). Free HPβCD was used at the same concentration present in the NPs formulations as control. Data are reported as mean of three independent experiments ± SD. For key legend see table 1.

Stability of NPs in the presence of serum proteins

In order to verify the absence of aggregation due to eventual interactions of NPs with serum proteins, NPs were incubated in PBS supplemented with 2% (w/v) of human serum albumin or in human plasma (Fig. 7). Hydrodynamic diameters of NP dispersions were monitored up to 72 h of incubation by PCS. Both ZnPc/DTX-loaded AB and ABA NPs displayed a comparable behavior in the presence of proteins and serum components, showing a slight increase of their size, which remained still lower than 200 nm. On the other hand, these results suggest that NPs do not undergo disassembly in biologically- relevant conditions. It is likely that protein-repelling properties of NPs were imparted by the presence of an external hydrophilic PEG shell with a thickness around 2 nm (Supplementary material, Fig. S3).
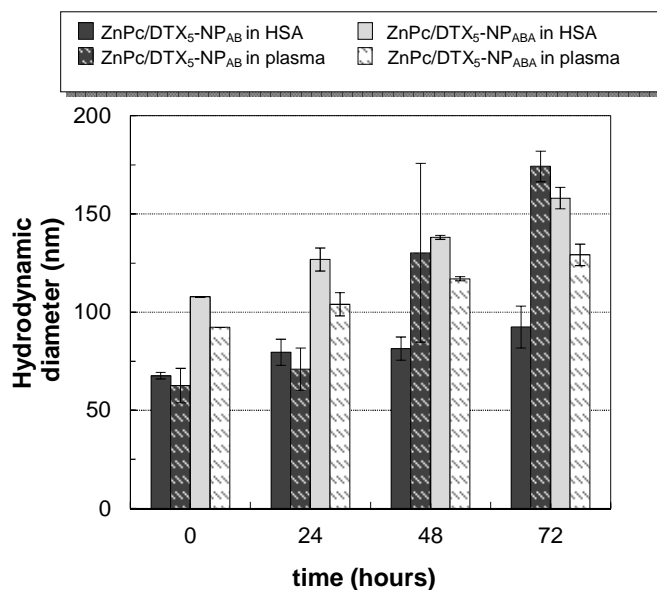
Figure 7. Stability of NPs in the presence of 2% w/v Human Serum Albumin and human plasma. Data are reported as mean of three independent experiments ± SD. For key legend see table 1.

NP behavior in cell culture medium

Behavior of AB NPs in RPMI culture medium was assessed by different methods (Fig. 8). Stability of NPs in RPMI culture medium was monitored analyzing DTX content in the supernatant of NP dispersions after centrifugation to eliminate eventual aggregates (Fig. 8A). After 24 h of incubation, DTX amount in the supernatant was kept around 100%, which corresponded to the actual DTX loaded in the NPs, suggesting that both formulations displayed no tendency to aggregation. Release of DTX from NPs dispersed in RPMI (Fig. 8B) occurred at a rate slower than both NPs and free DTX dispersed in PBS. Finally, UV spectra of free ZnPc in DMSO showed a Q band centered at 674 nm which is both blue-and hypocromically shifted in the spectra of ZnPc-NPs and ZnPc/DTX-NPs dispersion in PBS. The spectra of all the dispersions in RPMI remained almost unaltered as compared to PBS. A fair red-shift and hypochromicity of Q band was only registered for ZnPc/DTX-NPs dispersion in RPMI.
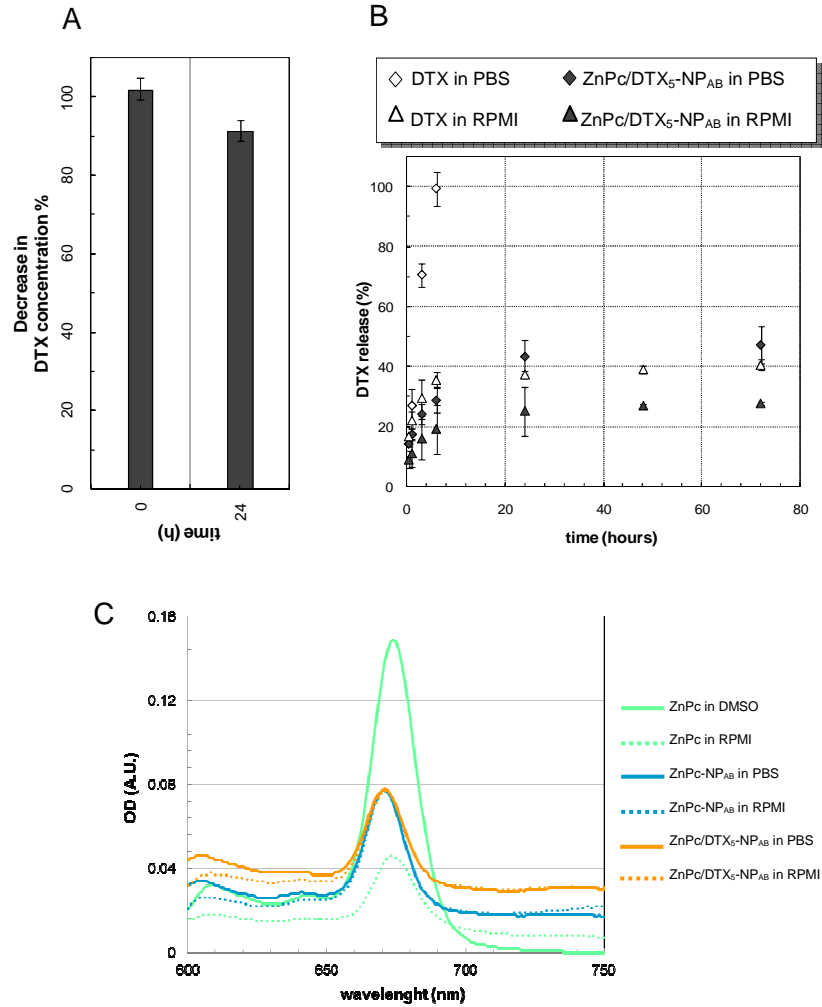
Figure 8. Behavior of AB NPs in RPMI with FBS 10%. (A) Decrease of DTX concentration in NP dispersions (1.6 mg/mL) prepared in RPMI+FBS 10% after 24 h of incubation. (B) Release of DTX from NPs dispersed in RPMI with FBS 10% at 37 °C. The external medium used for dialysis was PBS at pH 7.4. Release of DTX from NPs dispersed in PBS at pH 7.4 is reported again for comparison purpose. (C) UV spectra of ZnPc dissolved in DMSO and diluted in RPMI ([ZnPc]=0.4 µg/mL), ZnPc-NPs and ZnPc/DTX-NPs dispersions in PBS and RPMI ([ZnPc]=0.4 µg/mL, [NPs]=0.2 mg/mL, 1 cm path length). Data are reported as mean of three independent experiments±SD. For key legend see Table 1.

In vitro PDT

To evaluate cytotoxicity, the percentage of viable HeLa cells at 24 and 72 h of treatment was measured (Fig. 9). Experiments were performed on NPs made of AB copolymer. No reduction in terms of vitality was detected in samples incubated with unloaded NPs at all experimental times tested. In addition no significant reduction in cells viability was detected in cells treated with DTX-loaded NPs and free DTX at 24 h after treatment, respectively (Fig. 9A). On the contrary the percentage of mortality was significantly higher in cells treated with DTX-loaded NPs at 72 h of treatment, as compared to those treated with free DTX. At 24 h and upon irradiation, a marked decline in cell viability was evident in samples treated with ZnPc-loaded and ZnPc/DTX-loaded NPs. No relevant variation in terms of cell viability before and after irradiation was found at 72 h after treatment with free ZnPc and ZnPc-loaded NPs (Fig. 9B).
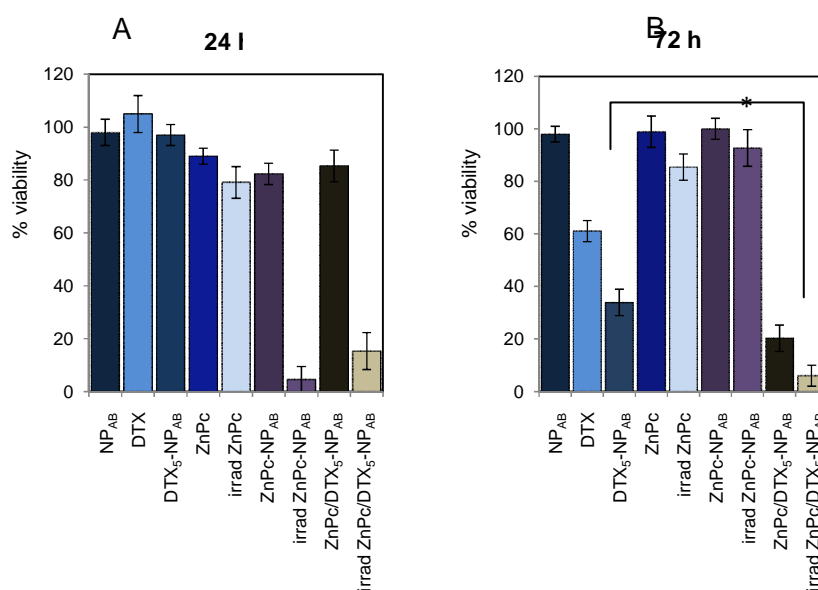
Figure 9. Effects of different NPs on cell viability in HeLa cells after 24 h (A) and 72 h (B) treatment ("*irrad*" refers to samples irradiated as described above). HeLa cells were treated with a control vehicle (DMSO) or with drug-loaded and unloaded NPs. Data are reported as mean of three separate experiments ± SD. Free ZnPc and DTX were used at the same concentration present in the NPs ([ZnPc]= 0.054 µg/mL, [DTX]= 1 µg/mL). Cell viability was quantified using MTT assay. * p <0.0003.

At 72 h, the cells treated with both DTX-loaded NPs and ZnPc/DTX-loaded NPs showed a higher percentage of mortality before irradiation as compared to those observed after 24 h treatment. However, cytotoxic activity related to the presence of ZnPc was observed in cells treated with ZnPc/DTX-loaded NPs, after irradiation.

In order to establish the effect of DTX on cellular DNA and detect modifications at nuclear level, cells were stained with the fluorescent DNA binding dye Hoechst 33342. Fig. 10 shows microscopy images from HeLa cells mock-treated or treated with NPs. Staining with Hoechst 33342 allowed us to identify cells undergoing aberrant mitosis. At 24 h, cells treated with DTX-loaded NPs and ZnPc/DTX-loaded NPs show morphological characteristics of mitotic catastrophe. No nuclear damage was detected in cells treated with ZnPc-loaded NPs. At 72 h the DNA damage initiated by DTX revealed the presence of apoptotic nuclei after staining with Hoechst fluorescent DNA-binding dye.
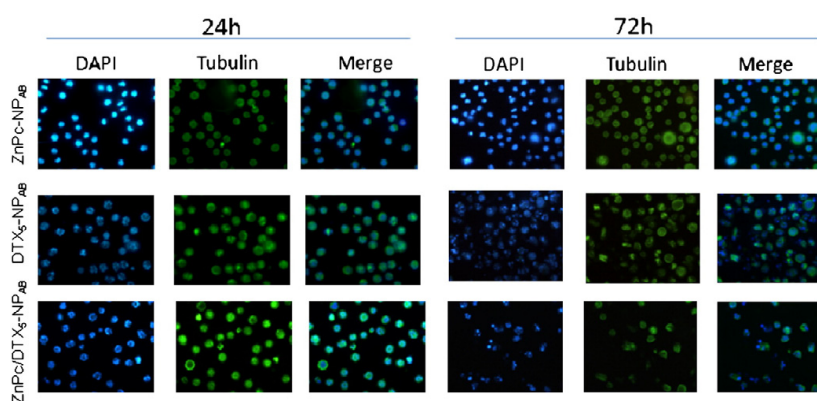
Figure 10. Microscopy analysis of HeLa treated with DTX-, ZnPc- and ZnPc/DTX-loaded NPs and analyzed at 24 h and 72 h post exposure. To distinguish the subcellular location, dual staining for simultaneous detection of chromatin and cellular protein-positive cells was performed with Hoechst 33342 fluorescent DNA-binding dye and a fluorescein-conjugated monoclonal antibody against human tubulin, respectively. Cells were analyzed by DAPI filter and FITC filter to detect chromatin and tubulin respectively, and the images obtained were merged (63× objective).

This occurrence was more marked in cells treated with ZnPc/DTX-loaded NPs as compared with those treated with DTX-loaded NPs. Due to the affinity of DTX for cellular tubulin, distribution of tubulin was also assessed by staining

treated samples with an antibody against human tubulin. In addition, apoptosis was monitored by detection of apoptotic bodies at single cell level using the TUNEL technique or at culture level by DNA gel electrophoresis (Ladder). As shown in Fig. 11A, a higher numbers of HeLa cells in apoptotic stage was found following treatment for 72 h with ZnPc/DTX$_5$-NP$_{AB}$ or DTX-NP$_{AB}$ when compared to the mock cells. As can be seen in Fig. 11B, the presence of the typical apoptotic DNA ladder was found in cells treated with ZnPc/DTX$_5$-NP$_{AB}$ or DTX-NP$_{AB}$, whereas it was absent in control sample.
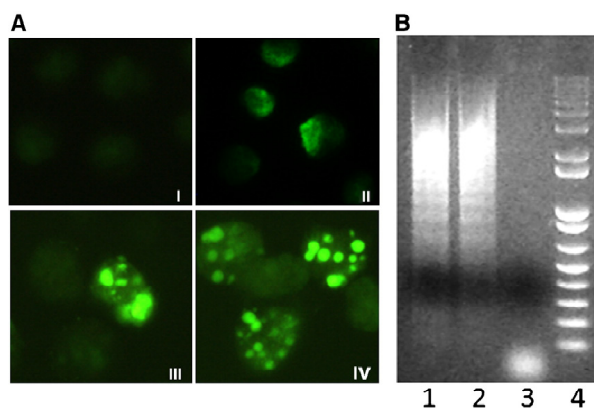
Figure 11. Analysis of cell death in HeLa cells after 72 h of treatment. (A) HeLa cells were incubated with DTX-NP$_{AB}$ (image III), ZnPc/DTX$_5$-NP$_{AB}$ (image IV) or mock treated (image I) and analyzed by labeling of DNA strand breaks with fluorescein-dUTP TUNEL assay at single cell level. Positive control consisted of HeLa treated with DNase 1 (2U samples, Ambion Life Technology) for 1 h at 37 °C (image II). Analysis of labeled cells was performed by fluorescence microscopy (63× objective). (B) Analysis of DNA fragmentation by gel electrophoresis after HeLa cells treatment with DTX-NP$_{AB}$ (lane 1), ZnPc/DTX$_5$-NP$_{AB}$ (lane 2) or mock treated (lane 3). Lane 4: 1-Kb Plus DNA ladder (Invitrogen).

In vivo antitumor activity

In vivo experiment was carried out by xenografting nu/nu mice with the human amelanotic melanoma cell line A375. Results are reported in Fig. 12 as tumor growth along time and survival. At 17 days post NPs injection, tumor growth in animals that received free DTX was significantly slower than that in control group (*P<0.05). DTX-NPs displayed tumor growth inhibition similar to thatof DTX at the same drug dose (CTR vs DTX$_5$-NP$_{AB}$, *P<0.05). Tumor growth in the group treated with the combination of DTX/ZnPc in NPs and PDT was significantly slower than that in animals that received other treatments (CTR vs ZnPc/DTX$_5$-NP$_{AB}$**P<0.01). Group treated with empty

NPs did not show statistically different effects as compared with the control group. Survival of animals closely followed the tumor growth profile. Mice treated with combined NPs under light exposure survived longer compared to those that received other treatments.
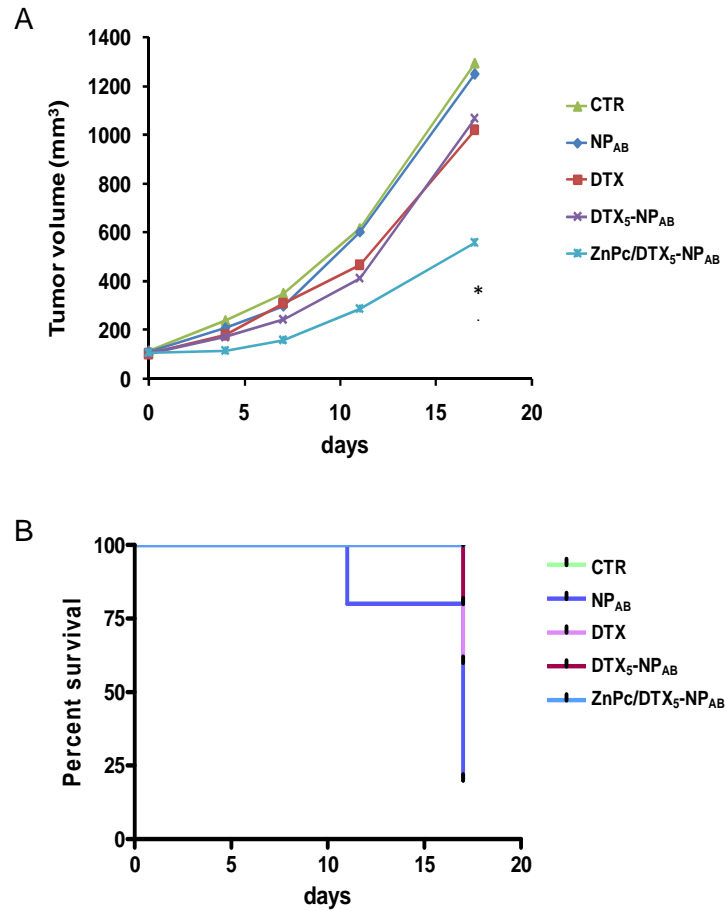
Figure. 12. (A) Tumor growth inhibition and (B) Kaplan–Meier survival plot of female athymic Nu/Nu nude mice bearing subcutaneous A375 tumor. Mice received an i.v. injection of saline (CTR), free DTX, empty NPs (NP$_{AB}$), DTX$_5$-NP$_{AB}$, ZnPc/DTX$_5$-NP$_{AB}$. DTX dose was 3.5 mg/kg whereas ZnPc dose was 0.2 mg/kg After 24 h mice were anesthetized and exposed to 15 min (149 J) of 172 mW/cm^2 light. *P<0.05 DTX$_5$NP$_{AB}$ vs ZnPc/DTX$_5$-NP$_{AB}$ at 17 days post injection; **P<0.01 CTR vs ZnPc/DTX$_5$-NP$_{AB}$ at 17 days post injection; **P<0.01 NP$_{AB}$ vs ZnPc/DTX$_5$-NP$_{AB}$ at 17 days post injection. Kaplan–Meier results showed an increased median survival for the ZnPc/DTX$_5$-NP$_{AB}$ treated mice with respect to the control groups (CTR and NP$_{AB}$) at 17 days (P=0.008 determined using log-rank test).

158

Discussion

An emerging concept in modern oncology relies on combination of different therapeutic strategies. A great advantage of associating PDT to conventional chemotherapy is the synergic PDT cytotoxicity that can be elicited at pathological site, without risking non-target effects. On the other hand, it has been demonstrated that sustained release of chemotherapeutics (sustained chemotherapy), offers superior antitumor efficacy and prevents induction of MDR in chemosensitive and chemoresistant diseases[30,31]. With this idea in mind, in this study we have developed a biodegradable system for the combined photo- and chemo-therapy of cancer. In the effort to develop a translational system, we focused on two types of core-shell NPs made of amphiphilic biodegradable block copolymers of PEO–PCL able to deliver a taxan and a cyanine at sustained rates in the body. PEO–PCL of specific composition was selected on the basis of recent evidences highlighting that PEO:PCL molecular weight ratio is a key determinant for stability in biologically relevant media[32]. Furthermore, we have recently demonstrated that entrapment of DTX in NPs of PEO–PCL preserves DTX cytotoxicity while attenuating drug toxicity in vivo, in analogy to similar PEO–PLA block copolymer micelles[33]. Nevertheless, this last type of micelles has shown disassembly in the bloodstream[34] which could explain an activity profile of DTX-loaded PEO-b-PLA micelles similar to free drug[33]. Making advantage of the low melting temperature and amphiphilic properties of PEO–PCL copolymers, the formation of a solid-like semicrystalline structure[23] with potentially high stability in biologically relevant conditions, we combined DTX with ZnPc in PEO–PCL NPs to obtain a multifunctional system for cancer therapy.

A preliminary formulation study was devoted to evaluate the best conditions to obtain NPs i) with a suitable size for i.v. injections; ii) able to entrap both molecules with high efficiency; iii) stable in different complex media; iv)with a good storage stability; v) able to preserve PS photobiological activity; vi) releasing chemotherapeutic agent at a controlled rate. Results highlight the formation of spherical, non-aggregated NPs with a quite small size useful to escape RES and kidney excretion[35,36]. Dual molecules entrapment is feasible and controlled by the total amount of the most abundant drug i.e. DTX. In fact, lipophilic molecules accommodate between polymeric chains in the amorphous regions of PCL and once these domains are saturated, drug crystallizes outside polymeric NPs and a decrease of entrapment efficiency is experienced[23]. Considering the very low solubility of ZnPc in water, it can be reasonably hypothesized that when entrapping both drugs a mutual impairment

of drug solubilization in the melted copolymer may occur at high DTX theoretical loading. Thus, this effect is attenuated by decreasing the loading of the most abundant DTX at 5%. In analogy to previous papers drug-copolymer ratio is found again a critical parameter to control encapsulation efficiency[37]. For all the formulations tested, both DTX and ZnPc loadings are considered suitable for a therapeutically relevant system. Dual release of drugs from NPs show that while DTX was released from the carrier, ZnPc remains substantially entrapped along time. Different release rates are clearly attributed to different aqueous solubility of ZnPc and DTX. In fact, release from PEO–PCL-based systems is activated by drug dissolution in the medium diffusing inside the polymer. Due to the fact that ZnPc is practically insoluble in water, it remains entrapped in both NP types while DTX is released at a sustained rate. It is worth of note that sink conditions realized by adding a surfactant in the release medium allow ZnPc release but induce also its precipitation during release. In order to avoid NP aggregation phenomena during freeze-drying, HPβCD was selected as cryoprotector and added to NP dispersion before freeze-drying. As demonstrated in the literature, HPβCD is able to increase collapse temperature during freeze-drying process, preventing aggregation of different nanocarriers based on PCL polymers[38,39]. NP formulations exhibit excellent long-term size stability upon storage at 4 °C and allow efficient NP dispersion in aqueous phase.

The proof that the fluorophore is intercalated in the polymeric matrix is the significant change both in the steady-state and time-resolved fluorescence anisotropy of ZnPc-loaded NPs. In particular the longer rotational correlation time (longer than 20 ns) in ZnPc-loaded NPs as compared to ZnPc is due to the fact that the dye is rotating together with larger particles. The presence of DTX does not cause further changes in the fluorescence anisotropy decay. It is worth noting that there is a significant background in the fluorescence decay profile of ZnPc free in DMSO, mainly due to much longer lifetime of the triplet state emission. This background is still present for all the samples investigated, indicating that, despite being embedded in the polymer matrix, ZnPc maintains its phosphorescence properties useful for applications in PDT. The similar fluorescence lifetime of ZnPc (3±0.4 ns) in organic solvents (i.e., both in DMSO and in THF used in the preparation) and when PS is incorporated in NPs suggests that clusters of residual organic solvent could remain entangled in the mesoporous structure of NPs forming nanodomains able to host and stabilize both drugs[39,40]. On the other hand, steady-state fluorescence emission spectra and the correspondent anisotropy values suggest the strong interaction between ZnPc and NPs. While free ZnPc in aqueous solution is poorly soluble

(no emission spectra was observed), ZnPc-NPs and ZnPc/DTX-NPs exhibit emission fluorescence bands which are characteristic of ZnPc fluorophore highly dispersed in an aqueous solution, confirming the increased solubility of ZnPc incorporated in NPs. The similar amount of singlet oxygen generated from ZnPc-loaded NPs, alone or in combination with DTX, as compared to free ZnPc highlights that ZnPc generates singlet oxygen inside the polymeric matrix and suggests that, unlike conventional drug delivery systems, PS does not require to be released from PEO–PCL NPs to induce a photodynamic reaction[28]. This result is in line with previous findings where PCL was demonstrated to be permeable to singlet oxygen[41]. Photophysical investigations have shown also that association of ZnPc to NPs does not necessarily alter its excited-state properties nor its singlet oxygen generation. Presumably, a similar yield of singlet oxygen demonstrates also that NPs prevent ZnPc aggregation phenomena in water[42].

NP interaction with plasma proteins and blood components can be responsible of aggregation, charge neutralization, dissociation and, in some cases, may trigger clearance mechanisms in the body[16]. Several efforts have been devoted to understand how NP surface features drive protein-NPs interactions which, if properly handled, can be regarded as a very simple tool to control NP biodistribution[16]. Our results suggest that the steric hindrance conferred by a PEO corona on NPs offers efficient protection against NP aggregation in both HSA and plasma making the system suitable for intravenous injection. On the other hand, the fact that NP size is kept in the presence of serum suggests also that this type of NPs is not prone to dissociation once in the blood circulation, a phenomenon that has been demonstrated recently for PEO-polylactide NPs[34]. Interaction of NPs with proteins is regarded as a critical factor also in cell culture studies since it has been demonstrated that NPs can aggregate/dissociate in complex media altering photobiological results[32]. Combination of DTX with ZnPc inside NPs does not affect stability profile of NPs in RPMI, the medium employed for cell studies, and allow ZnPc to maintain its monomeric form. Furthermore, since amount of drugs free to pass through cell membranes cannot be derived directly from release studies in PBS[43], release rate in RPMI highlights a sustained DTX release from NPs whereas ZnPc remains substantially entrapped in NPs and maintains its monomeric form. Since we experienced no relevant difference in the behavior of AB and ABA NPs, we decided to focus on AB copolymer due to its simpler architecture as compared to ABA copolymer.

On a biological standpoint, in vitro results obtained here on HeLa cells highlight that DTX can benefit from the combined action of ZnPc in inducing

161

cell mortality. The results show firstly that unloaded NPs are highly biocompatible in the in vitro model. Furthermore, they indicate that upon photo-activation there is an immediate action (within 24 h) of ZnPc in ZnPc-loaded NPs with or without DTX. On the contrary, along the time of treatment and upon irradiation ZnPc efficacy decreases and DTX starts evidencing severe cytotoxicity. The increase of cell mortality observed after 72 h of treatment suggests that ZnPc/DTX-loaded NPs are exerting a combined action under irradiation. The higher phototoxicity displayed by ZnPc-NPs as compared to free ZnPc well correlates with a significant aggregation of free ZnPc in RPMI, likely contributed by its very poor aqueous solubility. Conversely, the insufficient activity of ZnPc-NP$_{AB}$ at 72 h in the absence of DTX can be related to a decreased phototoxicity typical of lipophilic phthalocyanines such as ZnPc which, even if entrapped in NPs, could aggregate along time[44]. However these mechanistic aspects are still under investigation.

DTX cytotoxic activity is exerted by promoting and stabilizing microtubule assembly, causing the inhibition of mitotic cancer cell division. It is noteworthy that in specific cancer cells microtubules do not disassemble in the presence of DTX, and accumulate inside cells causing initiation of apoptosis[45]. Apoptotic cell death was unequivocally shown by using different techniques and here it is proven that most of the cells treated with DTX-NPs, as well as with ZnPc/DTX-loaded NPs, display chromatin condensation, apoptotic body formation and DNA ladder. Nevertheless it is notable that only DTX-loaded NPs display a significant reduction in term of cell viability. Thus, association of DTX and ZnPc, both entrapped in polymeric NPs, should be required to improve the therapy effectiveness at all the stage of treatment. However further investigation are needed to understand the mechanisms involved in the compartmentalization of drugs and the induction of cytotoxicity by apoptosis.

The encouraging findings obtained in a conventional cell line used for testing photodynamic effects were validated in an orthotopic mouse model of amelanotic melanoma to reinforce their translational potential in clinical practice. Results show again no cytotoxic effect of empty NPs and a slower tumor growth for DTX-loaded NPs in the presence of ZnPc. This effect is shown in the case of combined NPs, suggesting that alteration of drug biodistribution exerted by NPs does not impair pharmacological effect. It is worth noting that schedule of photodynamic treatment as well as dose regimen can be further revised to optimize treatment.

Conclusions

This study has demonstrated that it is possible to construct a nanoassembly for combining sustained release chemotherapywith photodynamic therapy. NPs are especially useful to compatibilize the lipophilic ZnPc with an aqueous environment without altering photophysic properties. Under photoirradiation, NPs generate singlet oxygen and in parallel sustain the release of the chemotherapeutic resulting in dual cytotoxic effects,with ZnPc playing a fundamental role in the early stage of the treatment, followed by a delayed DTX action. On the basis of the preliminary in vivo data, this type of approach may be of clinical interest for the treatment of accessible solid tumors.

References

(1) D.E. Dolmans, D. Fukumura, R.K. Jain, Photodynamic therapy for cancer, Nat. Rev. Cancer 3 (2003) 380–387.

(2) P. Agostinis, K. Berg, K.A. Cengel, T.H. Foster, A.W. Girotti, S.O. Gollnick, S.M.Hahn,M.R. Hamblin, A. Juzeniene, D. Kessel, M. Korbelik, J. Moan, P.Mroz, D. Nowis, J. Piette, B.C. Wilson, J. Golab, Photodynamic therapy of cancer: an update, CA Cancer J. Clin. 61 (2011) 250–281.

(3) S.B. Brown, E.A. Brown, I. Walker, The present and future role of photodynamic therapy in cancer treatment, Lancet Oncol. 5 (2004) 497–508.

(4) Z. Huang, A review of progress in clinical photodynamic therapy, Technol. Cancer Res. Treat. 4 (2005) 283–293.

(5) R.R. Allison, C.H. Sibata, Oncologic photodynamic therapy photosensitizers: a clinical review, Photodiagn. Photodyn. Ther. 7 (2010) 61–75.

(6) M.F. Zuluaga, N. Lange, Combination of photodynamic therapy with anti-cancer agents, Curr. Med. Chem. 15 (2008) 1655–1673.

(7) A.E. O'Connor, W.M. Gallagher, A.T. Byrne, Porphyrin and nonporphyrin photosensitizers in oncology: preclinical and clinical advances in photodynamic therapy, Photochem. Photobiol. 85 (2009) 1053–1074.

(8) A. Rück, R. Steiner, Basic reaction mechanisms of hydrophilic and lipophilic photosensitisers in photodynamic tumour treatment, Minim. Invasive Ther. Allied Technol. 7 (1998) 503–509.

(9) Y.N. Konan, R. Gurny, E. Allemann, State of the art in the delivery of photosensitizers for photodynamic therapy, J. Photochem. Photobiol. B 66 (2002) 89–106.

(10) E. Paszko, C. Ehrhardt, M.O. Senge, D.P. Kelleher, J.V. Reynolds, Nanodrug applications in photodynamic therapy, Photodiagn. Photodyn. Ther. 8 (2011) 14–29.

(11) W.T. Li, Nanotechology-based strategies to enhance the efficacy of photodynamic therapy for cancers, Curr. Drug Metab. 10 (2009) 851–860.

(12) D. Bechet, P. Couleaud, C. Frochot, M.L. Viriot, F. Guillemin, M. Barberi-Heyob, Nanoparticles as vehicles for delivery of photodynamic therapy agents, Trends Biotechnol. 26 (2008) 612–621.

(13) Y.E. Lee, R. Kopelman, Polymeric nanoparticles for photodynamic therapy, Methods Mol. Biol. 726 (2011) 151–178.

(14) D.K. Chatterjee, L.S. Fong, Y. Zhang, Nanoparticles in photodynamic therapy: an emerging paradigm, Adv. Drug Deliv. Rev. 60 (2008) 1627–1637.

(15) S.M. da Volta, M.R. Oliveira, E.P. dos Santos, G.L. de Brito, G.M. Barbosa, C.H. Quaresma, E. Ricci-Junior, Nanostructured delivery system for zinc phthalocyanine: preparation, characterization, and phototoxicity study against human lung adenocarcinoma A549 cells, Int. J. Nanomedicine 6 (2011) 227–238.

(16) N. Bertrand, J.C. Leroux, The journey of a drug-carrier in the body: an anatomo-physiological perspective, J. Control Release (2011).

(17) E. Allemann, N. Brasseur, O. Benrezzak, J. Rousseau, S.V. Kudrevich, R.W. Boyle, J.C. Leroux, R. Gurny, J.E. van Lier, PEG-coated poly(lactic acid) nanoparticles for the delivery of hexadecafluoro zinc phthalocyanine to EMT-6 mouse mammary tumours, J. Pharm. Pharmacol. 47 (1995) 382–387.

(18) M.J. Bovis, J.H.Woodhams,M. Loizidou, D. Scheglmann, S.G. Bown, A.J.MacRobert, Improved in vivo delivery of m-THPC via pegylated liposomes for use in photodynamic therapy, J. Control. Release 157 (2012) 196–205.

(19) G. Palumbo, Photodynamic therapy and cancer: a brief sightseeing tour, Expert Opin. Drug Deliv. 4 (2007) 131–148.

(20) A. Khdair, D. Chen, Y. Patil, L. Ma, Q.P. Dou, M.P. Shekhar, J. Panyam, Nanoparticle-mediated combination chemotherapy and photodynamic

165

therapy overcomes tumor drug resistance, J. Control. Release 141 (2010) 137–144.

(21) E. Pasquier, M. Kavallaris, N. Andre,Metronomic chemotherapy: new rationale for new directions, Nat. Rev. Clin. Oncol. 7 (2010) 455–465.

(22) L. Ostacolo, M. Marra, F. Ungaro, S. Zappavigna, G. Maglio, F. Quaglia, A. Abbruzzese, M. Caraglia, In vitro anticancer activity of docetaxel-loaded micelles based on poly(ethylene oxide)-poly(epsilon-caprolactone) block copolymers: do nanocarrier properties have a role? J. Control. Release 148 (2010) 255–263.

(23) F.Ungaro, C. Conte, L.Ostacolo,G.Maglio, A. Barbieri, C. Arra, G.Misso, A. Abbruzzese, M. Caraglia, F. Quaglia, Core-shell biodegradable nanoassemblies for the passive targeting of docetaxel: features, antiproliferative activity and in vivo toxicity, Nanomedicine (in press).

(24) J.R. Lackowicz, Principles of Fluorescence Spectroscopy, Kluwer Academic, Plenum Publisher, New York, 1999.

(25) N. Angelini, N. Micali, V. Villari, P. Mineo, D. Vitalini, E. Scamporrino, Interactions between water soluble porphyrin-based star polymer and amino acids: spectroscopic evidence of molecular binding, Phys. Rev. E 71 (2005).

(26) D.W. Marquardt, An algorithm for least squares estimation of nonlinear parameters,J. Soc. Ind. Appl. Math. 11 (1969) 431–441.

(27) A. Mazzaglia, N. Micali, L. Monsù Scolaro, Structural characterization of colloidal cyclodextrins: molecular recognition by means of photophysical investigation, in:Abderrazzak Douhal (Ed.), Cyclodextrins Materials: Photochemistry, Photophysicsand Photobiology, Elsevier, Amsterdam, 2006, pp. 203–222.

(28) W. Tang, H. Xu, R. Kopelman, M.A. Philbert, Photodynamic characterization and in vitro application of methylene blue-containing nanoparticle platforms, Photochem.Photobiol. 81 (2005) 242–249.

(29) L. Ostacolo, M. Marra, F. Ungaro, S. Zappavigna, G. Maglio, F. Quaglia, A. Abbruzzese, M. Caraglia, In vitro anticancer activity of docetaxel-loaded micelles based on poly(ethylene oxide)-poly(epsilon-caprolactone) block copolymers: do nanocarrier properties have a role? J. Control. Release 148 (2010) 255–263.

(30) R. De Souza, P. Zahedi, R.M. Badame, C. Allen, M. Piquette-Miller, Chemotherapy dosing schedule influences drug resistance development in ovarian cancer, Mol. Cancer Ther. 10 (2011) 1289–1299.

(31) P. Zahedi, J. Stewart, R. De Souza, M. Piquette-Miller, C. Allen, An injectable depotsystem for sustained intraperitoneal chemotherapy of ovarian cancer results infavorable drug distribution at the whole body, peritoneal and intratumoral levels, J. Control. Release 158 (2012) 379–385.

(32) R. Savic, T. Azzam, A. Eisenberg, D. Maysinger, Assessment of the integrity of poly(caprolactone)-b-poly(ethylene oxide) micelles under biological conditions:a fluorogenic-based approach, Langmuir 22 (2006) 3570–3578.

(33) S.W. Lee, M.H. Yun, S.W. Jeong, C.H. In, J.Y. Kim, M.H. Seo, C.M. Pai, S.O. Kim, Development of docetaxel-loaded intravenous formulation, Nanoxel-PM™ using polymer-based delivery system, J. Control. Release 155 (2011) 262–271.

(34) H. Chen, S. Kim, W. He, H. Wang, P.S. Low, K. Park, J.X. Cheng, Fast release of lipophilic agents from circulating PEG-PDLLA micelles revealed by in vivo forster resonance energy transfer imaging, Langmuir 24 (2008) 5213–5217.

(35) F. Alexis, E. Pridgen, L.K. Molnar, O.C. Farokhzad, Factors affecting the clearance and biodistribution of polymeric nanoparticles, Mol. Pharm. 5 (2008) 505–515.

(36) A.S. Mikhail, C. Allen, Block copolymer micelles for delivery of cancer therapy: transport at the whole body, tissue and cellular levels, J. Control. Release 138 (2009) 214–223.

(37) H.M. Aliabadi, A. Mahmud, A.D. Sharifabadi, A. Lavasanifar, Micelles of methoxy poly(ethylene oxide)-b-poly(epsilon-caprolactone) as vehicles for the solubilization and controlled delivery of cyclosporine A, J. Control. Release 104 (2005) 301–311.

(38) W. Abdelwahed, G. Degobert, S. Stainmesse, H. Fessi, Freeze-drying of nanoparticles: formulation, process and storage considerations, Adv. Drug Deliv. Rev. 58 (2006) 1688–1713.

(39) M.A. Moretton, D.A. Chiappetta, A. Sosnik, Cryoprotection-lyophilization and physical stabilization of rifampicin-loaded flower-like polymeric micelles, J. R. Soc. Interface 9 (2012) 487–502.

(40) R. Stancanelli, M. Guardo, C. Cannavá, G. Guglielmo, P. Ficarra, V. Villari, N. Micali, A. Mazzaglia, Amphiphilic cyclodextrins as nanocarriers of genistein: a spectroscopic investigate on pointing out the structural properties of the host/drug complex system, J. Pharm. Sci. 99 (2010) 3141–3149.

(41) S. Jesenská, L. Plístil, P. Kubát, K. Lang, L. Brozová, Š. Popelka, L. Szatmáry, J.Mosinger, Antibacterial nanofiber materials activated by light, J. Biomed. Mater. Res. 99 (2011) 676–683.

(42) B. Zhao, J.J. Yin, P.J. Bilski, C.F. Chignell, J.E. Roberts, Y.Y. He, Enhanced photodynamic efficacy towards melanoma cells by encapsulation of Pc4 in silica nanoparticles, Toxicol. Appl. Pharmacol. 241 (2009) 163–172.

(43) E. Gullotti, Y. Yeo, Beyond the imaging: limitations of cellular uptake study in the evaluation of nanoparticles, J. Control. Release 164 (2012) 170–176.

(44) P. Margaron, M.J. Gregoire, V. Scasnar, H. Ali, J.E. vanLier, Structure-photodynamic activity relationships of a series of 4-substituted zinc phthalocyanines, Photochem. Photobiol. 63 (1996) 217–223.

(45) K. Fukuoka, N. Saijo, Antimitotic agents, Gan To Kagaku Ryoho 24 (1997) 1519–1525.

GENERAL CONSIDERATIONS

The journey of a NP from injection to the site of action is often fraught with a sequence of substantial obstacles that adversely impact therapeutic indices in cancer. A translational anticancer nanomedicine intended for iv administration of anticancer drugs should:

- ✓ be not toxic and biocompatible;
- ✓ encapsulate a variety of therapeutic agents, improving their solubility and stability;
- ✓ release the entrapped drug in a controlled manner over time to maintain a drug concentration within the therapeutic window;
- ✓ offer a prolonged blood circulation half-life and a limited clearance by RES;
- ✓ overcome biological barriers and reach selectively tumor sites, reducing the systemic toxicity of the therapeutic agent as well as increasing its concentration in the area of interest;
- ✓ achieve cellular uptake by targeted tissues.

To fulfill all these requirements is a demanding task and several approaches with specific advantages/disadvantages have been devoped.

As base material for biomimetic core-shell nanomedicines, the use of amphiphilic materials, especially amphiphilic block copolymers, which spontaneously organize in supramolecular highly ordered core-shell systems, has received increasing interest. This special arrangement makes them suitable as long-circulating drug nanocontainers able to deliver drugs in different body compartments. Being loaded in the hydrophobic core, the drug is well protected from biological inactivation of surroundings and is distributed according to the pharmacokinetics of the carrier system. Furthermore, the external flexible fringe of hydrophilic blocks allows a steric stabilization against the opsonisation by RES, thus prolonging the in vivo fate into the bloodstream of the entrapped drugs. In spite of these advantages, a great drawback associated to these kind of systems widely discussed in the literature, resides in the poor stability they often show in biological environment. To this respect, properties of the hydrophobic core are of utmost importance in controlling precocious nanocarrier disassembly in the blood stream.

On this rationale, we focused our work on the development of core-shell nanoassemblies based on PCL–PEO copolymers for the iv administration of small lipophilic and hydrophilic anticancer drugs, testing also the possibility to further combine different chemotherapeutics and obtain a synergic antitumor effect.

At a polymer level, results of this research project highlight that PCL–PEO are very promising materials to be used in iv delivery of anticancer drugs. Since copolymer architecture is critical in driving self-assembly properties, in the first part of this work, we investigated the ability of PCL–PEO block copolymers to assemble in nanocarriers with different structures (nanocapsules, NPs) to be used in the delivery of both lipophilic and hydrophilic molecules. In particular, we pointed at studying the impact of architecture rather than hydrophobic-hydrophilic balance indriving the organization and morphology of corresponding nanostructures and in controlling their stability, size, drug-loading capacity and release rate. Independently of the structure (micelle, NP, nanocapsule) the hydrophilic blocks of PEO impart steric stability and biomimetic properties to nanoassemblies, providing them with all the features for prolonged blood circulation.

To produce nanocapsules with a aqueous core, which is in theory very challenging, we set up an emulsion/melting-sonication (EMeSo) technique forming nanocapsules with an inner aqueous core on an emulsion template. Novel amphiphilic Y-shaped miktoarm PCL–PEO block copolymers gave nanocapsules with size around 150 nm, low polydispersity index, high encapsulation efficiency and release rate. These properties together with an excellent toxicity profile suggest their potential use for further application as iv carrier.

On the other hand, linear PCL–PEO triblock and PCL–PEO diblock copolymers formed, besides micelles, NPs in the range 50-80 nm which can be used as carriers for lipophilic drugs. NPs of PCL–PEO block copolymers entrapping the lipophilic drug DTX could be obtained by a MeSo method set up in our labs. Experimental conditions for MeSo had to be adapted when ZnPc was co-encapsulated inside NPs. In particular drug loading of both drugs was greatly affected by DTX to polymer and drug to drug ratio. A core-shell structure with highly mobile hydrated PEO segments forming the corona (around 2 nm), conferring stealth properties of the system, and PCL segments forming a solid-like core, was evidenced. Concerning a possible pharmaceutical application, PCL–PEO NPs could be freeze-dried giving powders with good stability along time. The use of cryoprotectants was needed depending on the entrapped drug. Thus, a stable formulation with a good shelf life to reconstitute in an aqueous medium before administration was obtained.

PCL-PEO core-shell NPs with different architectures were found to be stable in complex protein-rich environments such as cell culture media and plasma. Furthermore, PCL-PEO NPs showed no toxicity toward human blood cells,

172

thus highlighting the suitability of these system as translational iv nanoplatform.

Cytotoxicity studies on DTX-loaded PCL-PEO NPs in several human cancer cell lines (prostate carcinoma DU145 and LnCaP and breast cancer MDA-MB231 and MCF-7) have demonstrated that entrapment in nanocarriers results in an improvement of DTX activity which is very relevant at low drug doses. Potentiation of drug activity was mainly related to slow extracellular drug release. When ZnPc was combined to DTX, interpretation of cytotoxicity results was much more complicate. Indeed, ZnPc/DTX-NPs gave severe activity on HeLa cells upon irradiation as compared to DTX-NPs highlighting that ZnPc/DTX-loaded NPs are exerting a combined action in inducing cell mortality.

Some tasks of this research aimed to clarify the cellular biofate encompassing mechanisms involved in the molecular events controlling cellular response, focusing on apoptosis and/or autophagy. It is well know that the type and dose of stress within the cellular context after a pharmacological treatment dictate the cellular outcome, which is intimately converted to complex pathways mediating control of cell-cycle and cell death. Cells treated with DTX-loaded NPs showed a highly condensed chromatin, which was also, marginated or fragmented. These data were confirmed by ladder analysis. It is possible that prolonged mitotic arrest triggered by DTX can lead to activation of apoptotic cell death. Nevertheless, initiation of autophagic pathway by accumulation of p62 protein was assessed. Data obtained in our experimental model showed that a consistent generation of autophagosome in HeLa cells treated with nanoparticles, was observed. Thus, autophagy dysfunction is recognized as a potential mechanism of cell death which accompains apoptosis. However, further studies should be addressed to understanding in depth these mechanisms also in light of a proper safety assessment of nanoassemblies.

Finally, from a preclinical point of view, the in vivo antitumor activity of NPs as carrier for DTX was tested in different animal models. First of all, the empty carrier did not show toxicity, suggesting the possibility of employment as safe parenteral formulation. Studies are in progress to assess pharmacokinetics of PCL-PEO NPs in healthy mice as well as in a breast cancer orthotopic model.

Combined effect of DTX and ZnPc was demonstrated also in vivo in a ortotopic model of amelanotic melanoma. The ability to sustain the release of DTX along time and to induce singlet oxygen generation under PDT treatment generate a better antitumor response of PCL-PEO NPs as compared to free drugs at the same doses.

CONCLUSIONS

The experimental work enclosed in this manuscript was aimed to design novel PCL-PEO nanocarriers for the iv administration of anticancer drugs.

The conclusions extracted from the results were the following:

CHAPTER 2: Nanocapsules Based on Linear and Y Shaped 3-Miktoarm Star Block PEO-PCL Copolymers as Sustained Delivery System for Hydrophilic Molecules:

1. Nanocapsules with an aqueous core can be obtained by a novel emulsion-melting-sonication techniques employing novel amphiphilic Y-shaped miktoarm PCL-PEO block copolymers.
2. Nanocapsules showed high entrapment efficiency of hydrophilic macromolecules and their controlled release was realized.
3. An excellent cell toxicity profile makes these *stealth* nanocapsules very promising as iv nanoplatform for passive delivery of hydrophiphilic drugs in solid tumors.

CHAPTER 3: Core-shell biodegradable nanoassemblies for the passive targeting of docetaxel: features, antiproliferative activity and in vivo toxicity:

1. Core-shell PCL-PEO NPs for the delivery of highly lipophilic anticancer drugs can be obtained by the novel MeSo technique.
2. NPs were able to entrap high amounts of DTX related to copolymer properties, thus sustaining its release along time and not toxicity toward red blood cells was evidenced.
3. A strong efficiency in inhibiting cell growth of breast and prostate cancer cells and not toxicity in experimental animal models were highlighed.
4. These nanocarriers are attractive carriers for the passive targeting and sustained release of different lipophilic drugs in solid tumors able to maintain activity and strongly decrease treatment toxicity linked to free drugs.

CHAPTER 4: Biodegradable core-shell nanoassemblies for the delivery of docetaxel and Zn(II)-phthalocyanine inspired by combination therapy for cancer:

1. Biodegradable PCL-PEO block copolymers gave a nanoassembly for combining sustained release chemotherapy with PDT.
2. NPs provided high DTX and ZnPc loadings, a slow release of the chemotherapeutic drug and high efficacy of the PS in the singlet oxygen generation.
3. Their high stability in biological environments and the encouraging results obtained by the in vivo data suggested the possibility to employ this system as a translational injactable nanomedicine for the synergistic combination of chemotherapy and PDT.

ANNEXES:

ANNEX-1:

Core/shell poly(ɛ-caprolactone)-polyethyleneoxide nanoparticles for skin sustained delivery of poorly water soluble drugs

ANNEX-2:

Lipidic nanoemulsions for intravenous administration of nucleic acids

ANNEX-1: Core/shell poly(ε-caprolactone)-polyethyleneoxide nanoparticles for skin sustained delivery of poorly water soluble drugs

C. Conte[1], G. Costabile[1], I. d'Angelo[1], P. Tirino[2], G. Maglio[2], R. Palumbo[2], F. Ungaro[1], F. Quaglia[1]

[1]Dip. di Chimica Farmaceutica e Tossicologica, [2]Dip. di Chimica "Paolo Corradini" – Università di Napoli Federico II, Italy

Abstract

The aim of this work was to evaluate if small pegylated biodegradable nanoparticles (NPs) can be a possible carrier for skin delivery of lipophilic drugs. An amphiphilic and biodegradable diblock copolymer of poly(ϵ-caprolactone) (PCL= 4.2 kDa) and poly(ethylene oxide)(PEO=2 kDa) (PEO-b-PCL) was employed to produce NPs entrapping Zinc(II)phtalocyanine (ZnPc), a highly lipophilic photosensitizer, by using the *melting/sonication technique*. NPs displayed a hydrodynamic diameter around 60 nm, a slightly negative zeta potential and a high ZnPc entrapment efficiency (0.2 mg/100 mg NPs). ZnPc-loaded NPs or free ZnPc was then incorporated in Sepigel 305. To evaluate skin transport of ZnPc, *in vitro* permeation studies on porcine skin were carried out in non-occlusive conditions through porcine ear skin on Franz-type diffusion cells. In all cases, no permeation of ZnPc in the receptor compartment was observed despite its solubility in the filling medium. Since ZnPc was not released from NPs, permeation of NPs should be followed. Results showed that ZnPc dissolved in PEG_{400} (which acts also as permeation enhancer) was retained mainly in stratum corneum likely due to high affinity of ZnPc for SC lipids. In the case of ZnPc-loaded NPs, ZnPc reached dermis in an extent depending on the type of dispersing medium (water, PEG_{400}, Sepigel 305).

Taken together, these results highlight PEO-b-PCL NPs as a novel vehicle for the skin delivery of highly lipophilic compounds, such as photosensitizing agents, with potential in photodynamic therapy as well as in other different applications.

181

Introduction

Due to its peculiar composition, stratum corneum (SC) represents the main barrier limiting percutaneous transport of chemical species [1]. Recently, research has been focused on the design of strategic approaches to improve topical delivery of different drugs, in order to propose innovative and non-invasive treatment modalities for several skin diseases. It is well recognized that small and highly lipophilic molecules are unable to cross SC and reach the water-rich viable epidermis. On these bases, several chemical and physical strategies have been proposed so far to improve drugs transport encompassing the use of permeation enhancers [2'3], surfactants and organic solvents, as well as the application of iontophoresis [4] and electroporation [5].

Novel drug delivery strategies aimed at increasing the topical permeation of lipophilic drugs, without injuring or modifying the physiological skin composition have been recently proposed with particular emphasis on nanosized carriers [6'7][8]. Vesicular systems (liposomes, surfactant), lipid-based colloidal carriers (lipid nanocapsules and solid lipid nanoparticles), micelles and microemulsion are currently investigated for their potential in driving a drug through the skin [9'10]. The masking of a drug in a nanosized carrier allows effective hindering of the interactions with biological environment, thus overcoming intrinsic unfavorable properties of the drug (molecular weight, lipophilicity, ionization). If suitably engineered, nanocarrier properties such as size, surface charge and structure can be a valuable tool to control drug distribution in the skin layers [11]. As compared to other nanocarriers, nanoparticles based on biodegradable polymers, such as poly(lactic-co-glycolic acid) (PLGA) [12'13], polylactic acid (PLA)[14] and poly(ε-caprolactone) (PCL) [15-17] could offer a further advantage of sustained drug release in the skin.

Recent studies have shown that polymeric nanocapsules or nanoparticles with a core-shell structure, based on amphiphilic block copolymers of PLA, PLGA and PCL with various architectures, can assemble in nanostructures able to entrap hydrophilic and lipophilic molecules with different molecular weight. These NPs have been found to drive DNA and minoxidil to the viable epidermis and oridonin even the intravascular sites [18-20], pointing to their possible application as transdermal delivery platforms. This special behaviour is ascribed to the presence of the hydrophilic external shell with deformable characteristics [21], that allows overcoming of the stratum corneum barrier. It has been reported, in fact, that elastic particles, for example with an external hydrophilic PEG shell are able to distribute through the epidermis faster, while rigid particles were found to remain on the surface of the upper stratum

corneum [22]. However, it has been highlighted also that the composition and the molecular weight of the base copolymer, as well as the number of amphiphilic arms or the ratio between the blocks, can strongly modify the behavior and the fate of a nanocarrier through the skin [23[,]24].

The aim of this work was to highlight the potential of core-shell NPs based on a diblock PCL-PEO copolymer in skin delivery of drugs. To this purpose, NPs entrapping the second generation photosensitizer Zn(II)-phthalocyanine (ZnPc) as a model of highly lipophilic drug were developed. ZnPc is an active drug, mainly investigated for its possible application in photodynamic therapy, for both systemic and topical diseases [25[,]26]. Up to now, due its high lipophilicity and its disadvantageous chemical profile, no strategy has been still selected to allow its clinical administration. For these reasons, many studies have been focus on more hydrophilic phthalocyanine derivates and on the design of different delivery devices to achieve their possible application, especially in the treatment of topical lesions [27-31]. NPs were prepared by melting/sonication (MeSo), characterized and their distribution in the skin assessed on porcine skin.

Experimental part

Materials

Sepigel 305 (polyacrylamide, C13-14 isoparaffin, laureth-7) was purchased from Farmalabor, sodium propyl parahydroxybenzoate and methylparahydroxybenzoate sodium were provided from New Fa.Dem. Zinc(II) phthalocyanine (ZnPc, MW= 577.91), (2-hydroxypropyl)-β-cyclodextrin (DS 0.6) (HPβCD), polysorbate 80, polyethylene glycol 400 (PEG), potassium phosphate dibasic and potassium phosphate monobasic, sodium azide and sodium chloride were purchased from Sigma-Aldrich. Potassium hydroxide was provided from Delchimica Scientific Glassware. Ethanol 96°, phosphoric acid (85%), acetonitrile and tetrahydrofuran were purchased from Carlo ErbaReagenti (Milan, Italy). α-Methoxy,ω-hydroxy poly(ethyleneoxide) with M_n = 2.0 kDa, $mPEO_{2000}$-OH, (Aldrich) was dried by azeotropic distillation from toluene. ε-Caprolactone, CL, (Aldrich) was distilled over CaH_2 under vacuum before use. Tin(2-ethylhexanoate)$_2$, Sn(Oct)$_2$, (Aldrich), 4-(dimethylamino) pyridine, DMAP (Fluka), 1,3-dicyclohehylcarbodiimide, DCCI (Fluka), and N-hydroxysuccinimide, NHS (Fluka) were used as received.

Synthesis and characterization of block copolymers

A PEO_{2000}-PCL_{4300} diblock copolymer was prepared [32]. Briefly, $mPEO_{2000}$-OH and Sn(Oct)$_2$ were used as initiator and catalyst, respectively, in the bulk ring-opening polymerization (ROP) of CL at 120 °C; CL/initiator molar ratio = 38 ($\eta_{inh.}$= 0.28 dL xg^{-1} ; M_w /M_n = 1.16).

ZnPc quantitative analysis

ZnPc quantification was carried out by spectrofluorimetry on a Shimadzu RF-1501 at EX= 610 nm and EM=668 nm**.** The concentration of ZnPc was calculated by means of a standard calibration curve obtained on THF solutions of known ZnPc concentrations (7.2–720 ng/ml). The limits of quantification (LOQ) and detection (LOD) in THF were 3.70 and 1.11 ng/mL, respectively.

Solubility determination of ZnPc

Saturated solution of ZnPc were prepared by stirring an excess of ZnPc in PBS at pH 7.4 with different amounts of Polysorbate 80 and in PEG_{400} at room temperature for 72 h. The samples were then filtered through a RC (Chemtek,

Italy) membrane (pore size 0.22 μm) and analyzed by UV spectrophotometry at 666 nm.

Preparation of NPs

NPs were prepared by a slightly modified *melting/sonication* procedure previously described. Ten mg of copolymer were added to 1.8 mL of filtered water in a vial and poured in a water bath heated at $72\pm2°C$ to allow copolymer melting. ZnPc (0.2% of copolymer weight) was dissolved in 0.2 mL of ethanol/THF 1:1 volume ratio and the solution obtained added to water containing melted copolymer. The mixture was sonicated for 10 min at 3 W (Sonicator 3000, Misonix, USA) by a microtip probe and finally cooled at room temperature. The organic solvent was removed under vacuum by a rotary evaporator for 30 min and NPs were finally collected (ZnPc-NPs). The same procedure was employed to prepare unloaded NPs as control. NPs were filtered through 0.45 μm filters (RC, Chemtek, Italy), freeze-dried for 24 h and kept at 4°C. HPβCD was added as excipient (10:1 mass ratio with NPs) to yield ZnPc/CD-NPs in powder. Recovery yield of production process was evaluated on an aliquot of NP dispersion (without cryoprotectant) by weighting the solid residue after freeze-drying. Results are expressed as the ratio of the actual NPs weight to the theoretical polymer weight x 100.

Characterization of NPs

Hydrodynamic diameter (D_H) and polydispersity index (PI) of NPs were determined by Photon Correlation Spectroscopy (PCS) using a N5 Submicron Particle Size Analyzer (Beckman-Coulter). An NP dispersion was diluted in Milli-Q water at intensities in the range 10^4-10^6 counts/s and measurements were performed at 25°C on 90° angle. Results are reported as mean D_H of three separate measurements of three different batches (n=9) ± standard deviation (SD). Size of NPs stored in the dark at 4 °C for 3 months was monitored too.

The morphology of the nanoparticles was examined by transmission electron microscopy (CM 12 Philips, Eindhoven, The Netherlands) using samples stained with a 2% phosphotungstic acid solution.

Zeta potential was determined by analysing a NP dispersion in water on a Zetasizer Nano Z (Malvern Instruments Ltd). Results are reported as mean of three separate measurements on three different batches (n=9) ± SD.

ZnPc encapsulation efficiency was evaluated by dissolving a known amount of freeze-dried NPs (1 mg) in 1 mL of THF under magnetic stirring for 1 hour. Results are reported as actual loading, i.e. the amount (mg) of drug

encapsulated per 100 mg of nanoparticles, and entrapment efficiency, i.e. the ratio between actual and theoretical loading x $100 \pm SD$ (n=6)

Singlet oxygen generation

The capacity of NPs to generate singlet oxygen was monitored over time by measuring photobleaching of the radical quencher ADPA [33]. Briefly, 40 µl of a 5 mM ADPA solution in NaOH 0.01 M was added to 2 mL of a ZnPc solution in water/THF 100:1 v/v, in water/PEG$_{400}$ 10:1 or a NP water dispersion ([ZnPc]=2 µg/mL; [NPs]=1 mg/mL). The sample was irradiated at 610 nm using a 150 W ozone-free xenon-arc lamp (JobinYvon) with a slit width of 10 nm for different times (15, 30 and 45 min). Sample containing NPs was centrifuged at 16,090 $\times$g (Mikro 20, Hettich) for 30 min. The supernatant was collected and analyzed by spectrophotometry at 400 nm to evaluate ADPA absorption. Singlet oxygen generation was monitored by the decrease of OD at 400 nm as a function of the irradiation time.

Preparation of ZnPc-NPs dispersions in PEG

A known amount of ZnPc-loaded NP water dispersion ([NPs] = 3.75 mg [ZnPc] = 7.5 µg) was centrifuged at 573340 xg for 40 minutes and dispersed in PEG$_{400}$ (0.2 mL). As control, a PEG$_{400}$ stock solution containing the same amount of ZnPc was prepared.

Preparation of ZnPc-loaded NPs in Sepigel 305

Sepigel 305 of medium viscosity (3% w/v) was prepared by adding preserved water containing sodium propyl parahydroxybenzoate (0.14% w/w) and sodium methyl parahydroxybenzoate (0.06% w/w) to Sepigel 305 (30 mg) under gentle stirring until gel formation. A known amount of ZnPc-NPs water dispersion obtained by MeSo ([NPs] = 3.75 mg, [ZnPc] = 7.5 µg) was mixed with preserved water and then added to Sepigel under gentle stirring. Another gel was prepared by dispersing freeze dried ZnPc/CD-NPs in preserved water and adding Sepigel. The control formulations with free ZnPc were prepared by adding 0.35 mL of PEG$_{400}$ stock solution containing the same amount of ZnPc in the preserved water employed for Sepigel preparation.

In vitro release studies

In vitro release of ZnPc from NPs was assessed in 10 mM phosphate buffer containing NaCl (137 mM) and KCl (2.7 mM) at pH 7.4 (PBS) or in PEG$_{400}$ by

a dialysis method. A known amount of NP water dispersion (corresponding to 2.5 mg of NPs) was centrifuged at 573340 xg for 40 minutes, redispersed in 0.5 mL of PBS or PEG_{400} and placed in a dialysis bag (MWCO=3500 Da, Spectra/Por®). The sample was plunged in 3 mL of PBS containing 10 % v/v of polysorbate 80 or in 5 mL of PEG_{400} respectively, in order to ensure sink conditions and to avoid ZnPc aggregation. At selected time intervals, 1 mL of release medium was withdrawn and replaced with an equal volume of fresh medium. ZnPc quantitative analysis in the sample was performed as described above. To understand the contribution of HPβCD on ZnPc release profile, the experiment was repeated on freeze dried ZnPc/CD-NPs (25 mg) dispersed in 0.5 mL of PBS according to the above reported method.

Release from Sepigel 305 containing ZnPc-NPs was performed on modified Franz diffusion cells using regenerated cellulose membranes (MWCO=3500 Da, Spectra/Por®). A weighted amount of gel (0.5 g) was applied in the donor compartment. At predetermined time intervals, 1 mL of release medium in the receptor phase (PBS enriched with 10 % v/v of polysorbate 80) was withdrawn and replaced with an equal volume of fresh medium. Results are expressed as release % over time ± SD of three experiments.

Permeation studies

Permeation studies were carried out on free ZnPc dissolved in PEG_{400} or in Sepigel, and on ZnPc-NPs dispersed in water, with or without the addition of HPβCD (10:1 mass ratio with copolymer), in PEG_{400} or incorporated in Sepigel 305.

Drug transport through porcine ear skin was assessed on Franz-type diffusion cells (diffusion area 0.785 cm^2). Porcine ear skin was obtained from a freshly killed pig weighing about 100 kg slaughtered on the day of the experiment. After removal, the tissue was stored at 4°C and used within 2 h. The skin was separated from the underlying tissue using surgical scissors and mounted between the donor and receiver chambers of diffusion cell with stratum corneum (SC) facing the formulation tested. Non-occlusive conditions were adopted for all samples whereas for ZnPc/CD-NPs the experiment was carried out also in occlusive conditions. The receptor compartment was filled with a 10 mM PBS at pH 7.4 containing 10% v/v of polysorbate 80 maintained at 32 ± 1 °C under gentle stirring. At predetermined times, 1 mL of receiving medium was sampled and replaced by an equivalent volume of fresh medium. ZnPc concentration in the receiving medium was evaluated as described above. Results are reported as μg/cm^2 of permeated ZnPc ± SD of three experiments.

Skin distribution of ZnPc

At the end of the permeation experiment (24 h), skin was collected, washed with a NaCl solution 0.9% w/v to eliminate any residue of the formulation and tape-stripped by applying a 3M-Scotch magic^{TM} tape roll (1.5 cm × 1.5 cm). Complete removal of SC from the viable epidermis was indicated by the appearance of a white and shiny surface. First strip was separately analysed whereas the other 15 samples were pooled. ZnPc was extracted from the tape by treating the sample with 3 mL THF under magnetic stirring overnight. After centrifugation at 16090 xg for 30 minutes, the sample was filtered through 0.22 µm filters (PTFE, Chemtek, Italy), and analysed for ZnPc content as reported above.

The remaining skin membrane (epidermis without SC) was treated under a hot air flow for 60 sec. Through a surgical blade, epidermis and derma were separated by aid of a surgical blade and placed in separate vials. Tissues were hydrolyzed in KOH 1 M (2 mL) under stirring at 37°C, and then ZnPc was extracted in THF (2 mL) for 2 hours. Samples were centrifuged at 224 xg for 30 minutes, and the supernatant filtered through a 0.45 µm filter before ZnPc quantitative analysis. Extraction technique was validated by placing known amounts of drug solubilized in THF in contact with tape, epidermis and derma, and extracting the drug. Recovery higher than 85% was always obtained.

Fluorescence microscopy

At the end of the permeation experiments, the excess formulation was removed from the skin surface. The skin was then washed three times with saline and dried gently with a cotton swab. The skin samples were fixed in 4% paraformaldehyde and examined without additional tissue processing. Sections of 20µm thickness were prepared from each sample using a microtome (ACCU-CUT®SRM™200 rotary microtome, Sakura Finetek, USA). Cutting was performed with fresh blades from the dermis side towards the epidermis in order to avoid dislocation of NPs from the skin surface on the section. Sections were finally observed by fluorescence microscopy (Leica DMRB) and a Leica *application suite program* v 2.8.1. was used for imaging.

To ensure proper visual comparison, the exposure time was the same for all samples examined, including the control samples.

Results

NPs based on biodegradable amphiphilic block copolymers of poly(ε-caprolactone) (PCL) and poly(ethyleneoxide) (PEO) were prepared by a modified MeSo technique previously described.[32] In particular, we selected as base material a simple linear diblock copolymer (PEO_{2000}-PCL_{4300}) with unimodal and narrow molecular weight distribution (PI = 1.16). The second generation photosensitizer ZnPc was selected as fluorescence lipophilic probe and incorporated in NPs at 0.2% theoretical loading.

In table 1, composition and overall properties of NPs are summarized. Significant differences between unloaded and ZnPc-loaded NPs were not observed. NPs displayed a hydrodynamic diameter around 60 nm with a low polydispersity index and a slightly negative zeta potential.

Table 1. Composition and properties of NPs produced.

Code	Unloaded NPs	ZnPc-NPs
ZnPc (% w/w)	-	0.2
Yield (%)	93	86
Mean D_H (nm ± SD)	57.8 ±6.1	67.4 ±5.7
P.I.	0.217	0.279
Zeta Potential(mV ± SD)	-10.3±3.3	-11.7±4.6
ZnPc Actual loading[a]	-	0.172 ± 0.01
(EE [b]**)**		(98.1 ± 1.9)

[a] Actual loading is expressed as the amount (mg) of drug encapsulated per 100 mg of nanoparticles
[b] EE (entrapment efficiency) is calculated from the ratio between actual and theoretical loading x 100.

In the case of nanoparticles, their storage stability is a key parameters to consider, in order to ensure that native technological properties are maintained along time. Strong aggregation of ZnPc-NPs occurred after freeze-drying which needed a cryoprotector to be stored in solid form. The addition of HPβCD to NP dispersion was effective to avoid NP collapsing and to give original NP size after sample dispersion in an queous phase [34]. It is possible to note from TEM image (fig. 1) the spherical and non-aggregated morphology

of freeze-dried ZnPc/CD-NPs dispersed in filtered water Also the sizes of NPs found in TEM was in line with PCS measurements acquired immediately after MeSo.
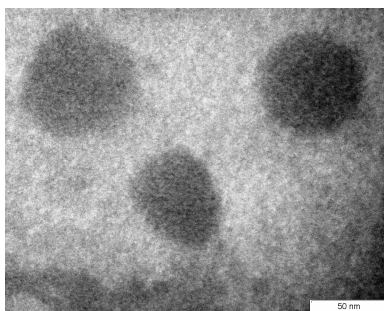
Figure 1. TEM image of freeze-dried ZnPc-NPs in HPβCD.

Concerning drug loading properties of NPs, PEO-b-PCL NPs well adapt to the entrapment of highly lipophilic molecules giving encapsulation efficiency of the initial ZnPc amount around 100%.

Due the poorly water solubility of ZnPc, we preliminarly assessed its solubility in different media with the final aim to find the optimized conditions to monitor release and carry out transport studies. The solubility of ZnPc in PEG_{400} was high whereas in PBS at pH 7.4 containing Polysorbate 80 depended on surfactant concentration. In particular, as evident in fig. 2, UV spectra of ZnPc in polysorbate 80 showed an intense and sharp Q-band in the red visible region between 678 and 710 nm highlighting the absence of ZnPc aggregation, thus promoting its solubilization, as demonstrated for other cyanines [35].

	Medium	Solubility (µg/ml)
A		
	PEG$_{400}$	22.71
	PBS+Polysorbate 80 1% v/v	0.54
	PBS+Polysorbate 80 5% v/v	1.25
	PBS+Polysorbate 80 10% v/v	2.64

B
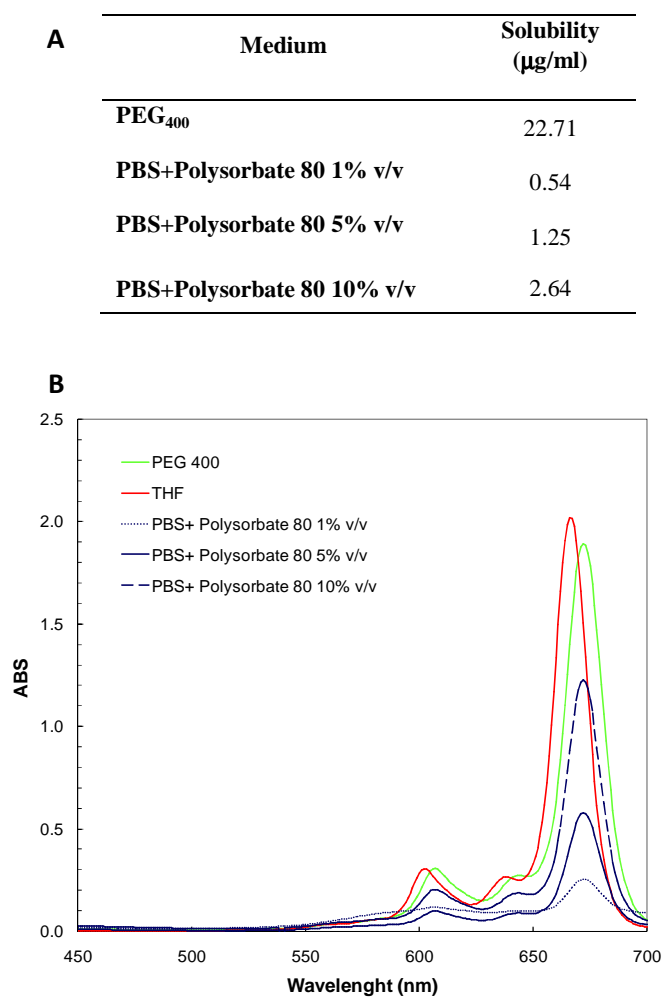
Figure 2. (A) Solubility of ZnPc in PBS enriched with different amounts of Polysorbate 80 and in PEG$_{400}$. (B) UV spectra of ZnPc in THF, in PEG$_{400}$ (diluition factor 5X) and PBS pH 7.4 enriched with different amounts of Polysorbate 80. ZnPc concentration in THF was 4 µg/mL.

On the bases of our previous findings about the ability of PEO-PCL diblock NPs to slowly release poorly water soluble drugs, we performed several in vitro experiments to assess ZnPc release from formulations assigned to skin application. First of all, we monitored ZnPc release from NPs in PBS at pH 7.4 enriched with Polysorbate 80 at 10% v/v to ensure sink conditions, thus

191

avoiding ZnPc precipitation. No detectable amount of ZnPc was found in the release medium after 24 hours (data not shown) thus suggesting that ZnPc was strongly fixed to NPs. Afterwards the experiment was repeated employing NPs freeze-dried with HPβCD to find out a possible influence of the excipient on NP release properties. Nevertheless, no ZnPc was released in the medium (data not shown). When incorporated in Sepigel, ZnPc was not released from NPs (data not shown). Conversely, when NPs were dispersed in PEG$_{400}$, about 10% of entrapped drug was released after 24 hours (time-frame of transport experiment), as shown in figure 3.
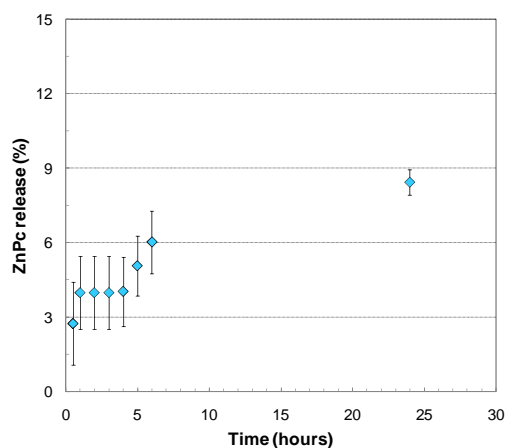
Figure 3. Release profile of ZnPc from NPs dispersed in PEG$_{400}$. Results are the mean of three experiments ± SD.

In order to test the photodynamic activity of ZnPc dissolved in THF or PEG$_{400}$ or entrapped in NPs, singlet oxygen studies were carried out. As evidenced in figure 4, comparable time-dependent production of singlet oxygen was found for free drug both in THF (employed as control) and in PEG$_{400}$ whereas for ZnPc-NPs, a faster ADPA bleaching was observed.
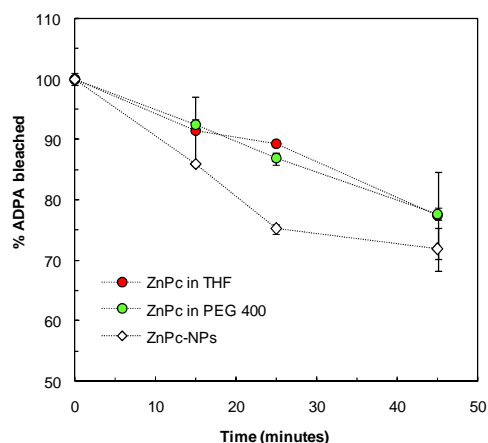
Figure 4. Photobleaching of ADPA by singlet oxygen generated from ZnPc-NPs and ZnPc free in THF or in PEG$_{400}$ after photoirradiation at 610 nm ([ZnPc]=2 μg/mL). Data are reported as mean of three independent experiments±SD.

To analyze the potential of core-shell PEO-b-PCL nanoparticles in skin trasport of ZnPc, *in vitro* permeation studies were carried out in non-occlusive conditions through porcine ear skin on Franz-type diffusion cells. Furthermore, ZnPc skin distribution was then evaluated in SC and skin layers (epidermis and dermis) after 24 h of permeation. In particular, we monitored the variation of NP deposition across the skin depending on the NP vehicle employed for the experiment (water, gel) or the presence of some permeation enhancers (PEG$_{400}$, HPβCD).

The composition of all formulations tested is reported in table 2.

Table 2. Composition of formulations tested.

Formulation code	ZnPc (μg)	PEG$_{400}$ (μl)	Water (μl)	Sepigel (g)	NPs (mg)
ZnPc-PEG	7.5	720	-	-	-
ZnPc-gel	7.5	375	-	1	-
ZnPc-NPs/W	7.5	-	800	-	3.75
ZnPc/CD-NPs/W	7.5	-	100	-	3.75
ZnPc-NPs/PEG	7.5	200	-	-	3.75
ZnPc-NPs/gel	7.5	-	-	1	3.75

In all the transport experiments, ZnPc was not detected in the receptor compartment despite its solubility in the receptor filling medium. Concerning ZnPc deposition through the skin, different results were obtained depending on the formulation type.

Skin distribution of ZnPc-NPs dispersed in water or PEG$_{400}$ was compared with that obtained from ZnPc dissolved in PEG$_{400}$ at same concentration. As reported in figure 5, when ZnPc was dissolved in PEG$_{400}$, a similar drug amount was extracted by SC and E/D. Dipersion of ZnPc-NPs in PEG, instead gave higher accumulation in SC. In the case of ZnPc-NPs dispersed in water the lowest accumulation of the drug both in the SC and in E/D was detected after 24 h of permeation. Finally, skin permeation from ZnPc/CD-NPs resulted in a total skin accumulation of ZnPc even higher as compared to ZnPc dissolved in PEG, especially when occlusive conditions were adopted.
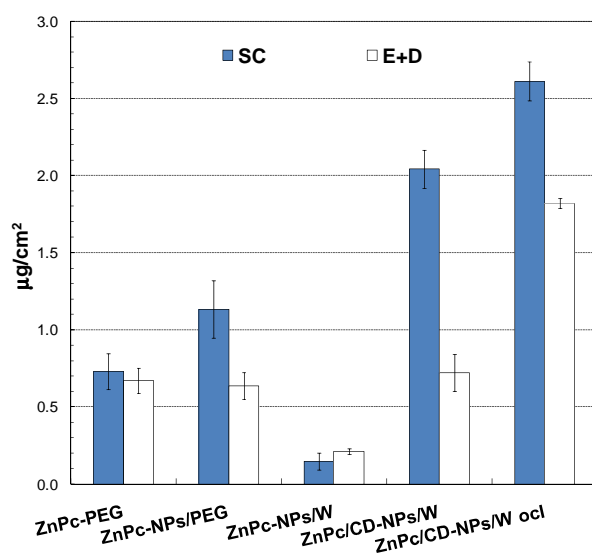
Figure 5. ZnPc amount found in porcine ear skin after 24 h of ex vivo permeation experiment. ZnPc amounts in stratum corneum (SC) and in skin layers (epidermis (E) and derma (D)). Results are the mean of three experiments ± SD.

In a second step, ZnPc accumulation in the skin after gel application was assessed (figure 6). ZnPc-NPs incorporated in Sepigel 305 at medium viscosity allowed a strong accumulation of ZnPc in the stratum corneum, which was similar to that observed for gel loaded with free ZnPc. The accumulation of

ZnPc in deeper skin layer was not very different as compared to the control, thus suggesting that Sepigel did not modify NPs transport through the skin.
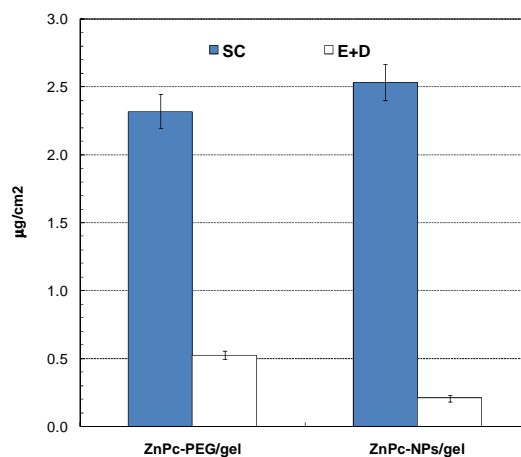
Figure 6. ZnPc amount found in porcine ear skin after 24 h of ex vivo permeation experiment. ZnPc amounts in stratum corneum (SC) and in skin deeper layers (epidermis (E) and derma (D)). Results are the mean of three experiments ± SD.

To confirm the data obtained in the permeation studies, fluorescence microscopy studies of skin sections treated with the different formulations for 24 hours were carried out. As reported in figure 7, a more marked fluorescence in the deeper skin layers was evident in the case of ZnPc-NPs dispersed in PEG$_{400}$ and in a HPβCD-containing medium, whereas conversely the permeation of NPs dispersed in water did not induce a high skin deposition of the fluorescent drug.
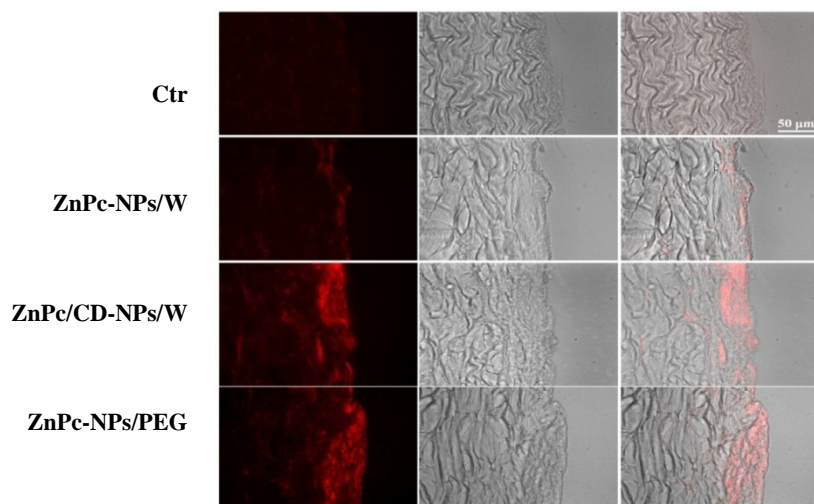
Figure 7. Fluorescence microscopy of sections of in porcine ear skin treated with ZnPc-NP formulations after 24 h of ex vivo permeation experiment.

Discussion

In this study, we investigated the suitability of small core/shell nanoparticles based on a linear amphiphilic diblock copolymer (PEO-b-PCL) as carrier system of lipophilic drugs in the skin. The second generation photosensitizer Zn(II)-phthalocyanine (ZnPc) was selected as model lipophilic drug and fluorescent tag. In fact, ZnPc has been proposed for the photodynamic treatment of skin diseases, such as for example cancerous lesions.

It is generally accepted that highly lipophilic drugs are unable to cross the stratum corneum due to therir high affinity with lipids. As a consequence, to date several technological approaches encompassing also nanotechnologies have emerged in order to promote skin penetration of different molecules with the aim to reach deeper layers. Since skin turn-over is around 30 days, NPs with sustained release properties can be also beneficial to exert long-term effect, which is useful in long-term therapies. In this scenario, biodegradable polymeric nanoparticles received remarkable attention as potential drug vehicle through the skin, recognizing their ability to protect the drugs, sustain its release and eventually reach also deeper skin layers, depending on compositions and properties.

Spherical PEO-b-PCL core-shell nanoparticles with a small size were formed by the melting/sonication technique, exploiting the amphiphilic profile of PEO–PCL block copolymer. On the basis of our recent findings, ZnPc remains substantially intercalated in the polymeric matrix of NPs in monomeric form which is a key feature to maintain its photophysical and photodynamic properties. Furthermore, the addition of HPβCD to NP dispersion before freeze-drying, allowed to obtain a good storage stability of NPs, preventing their aggregation. [36]

Since it was demonstrated that the ZnPc was not released from NPs after 24 hours, it was assumed that the drug coul act as probe of NP transport in the skin.[36] Furthermore, the effect of aqueous vehicles containing different excipients, namely HPβCD, PEG$_{400}$ and Sepigel 305, and used to disperse NPs was evaluated. In particular, HPβCD and PEG$_{400}$ were selected for their ability to act as permeation enhancers, whereas Sepigel 305 was chosen for its well known ability to incorporate lipophilic components. In all cases, no permeation of ZnPc occurred, in line with previous results [16] whereas a significantly different distribution in skin layers was evident, depending of the dispersing vehicle used. In particular, the accumulation of NPs dispersed in water soon after MeSo in the skin was very poor. This result can be easy explained by the continuous Brownian motion of NPs in water resulting in their weak transport through the skin. On the contrary, when using PEG$_{400}$ as dispersing medium

for ZnPc-NPs, ZnPc was found in SC, viable epidermis and dermis likely due to transport of both free ZnPc released from NPs and ZnPc-NPs by themselves. This observation is in line with previous findings highlighting the permeation enhancing activity of PEG$_{400}$ in the skin for several lipophilic drugs, including photosensitizing agents and phthalocyanines[37]. The comparable UV spectra of ZnPc in THF and in PEG$_{400}$, in fact, highlight the absence of aggregation phenomena and the preservation of its monomeric form, suggesting the suitability of this medium for topical administration. Furthermore, PEG$_{400}$ did not alter the photophysical properties of ZnPc which produced a similar yield of singlet oxygen as compared to an aqueous monomeric formulation. At the same time, previous photophysical investigations and a similar yield of singlet oxygen demonstrate also that NPs prevent ZnPc aggregation phenomena in water [36]. In spite of these advantages, the ZnPc amount that can be apply in a topical formulation employing PEG$_{400}$ is strongly limited by its restricted solubility profile in this medium, thus reducing the dose that can be administered.

The most remarkable result of this study refers to the role played by HPβCD. In fact dispersion of ZnPc-NPs in a medium containing HPβCD, allowed a very high accumulation of ZnPc in the deeper skin layers. Since ZnPc as not released from NPs, it is likely that this accumulation refers to actual NP penetration in the skin. This permeation enhancer activity of HPβCD on NPs is presumably related to HPβCD ability to extract SC lipids, behaving as classical chemical permeation enhancer [38,39]. To our knowledge, this is the first time that HPβCD is found to promote also nanocarrier transport through the skin.

To improve the applicability of NPs to skin surface, we decided to incorporate this nanosystem in a gel, commonly employed in pharmaceutical and cosmetic topical formulations. In this way, a higher accumulation of the drug in the external stratum corneum was detected, due to the longer residence time of the formulation to the shin surface, without modifying the transport of NPs through the skin deep layers.

Conclusion

In light of our results, we can suppose that PEO-PCL NPs can be a promising alternative for topical application of ZnPc, especially if dispersed in HPβCD carrier. First of all, we can apply high amounts of NPs on skin surface (corresponding to higher ZnPc dosages) for their inert character. The addition of HPβCD can then improve the carrier permeation containing the active molecule, without increasing its release from NPs. Finally Sepigel could be easy used to disperser NPs and to achieve a longer residence time on skin surface than an aqueous vehicle, due its stronger viscosity.

References

1, J.A.Bouwstra, P.L.Honeywell-Nguyen, G.S.Gooris and M.Ponec, Prog.Lipid Res. 42 (2003) 1-36.

2, I.Som, K.Bhatia and M.Yasir, J.Pharm Bioallied.Sci. 4 (2012) 2-9.

3, A.C.Williams and B.W.Barry, Adv.Drug Deliv.Rev 56 (2004) 603-618.

4, Y.Wang, R.Thakur, Q.Fan and B.Michniak, Eur.J.Pharm Biopharm. 60 (2005) 179-191.

5, N.A.Charoo, Z.Rahman, M.A.Repka and S.N.Murthy, Curr Drug Deliv. 7 (2010) 125-136.

6, A.O.Hassan and A.H.Elshafeey, J.Biomed.Nanotechnol. 6 (2010) 621-633.

7, T.W.Prow, J.E.Grice, L.L.Lin, R.Faye, M.Butler, W.Becker, E.M.Wurm, C.Yoong, T.A.Robertson, H.P.Soyer and M.S.Roberts, Adv.Drug Deliv.Rev 63 (2011) 470-491.

8, M.Kreilgaard, Adv.Drug Deliv.Rev 54 Suppl 1 (2002) S77-S98.

9, B.Baroli, J.Pharm Sci. 99 (2010) 21-50.

10, M.Schafer-Korting, W.Mehnert and H.C.Korting, Adv.Drug Deliv.Rev 59 (2007) 427-443.

11, A.N.Jatariu, M.Popa and C.A.Peptu, J.Drug Target 18 (2010) 243-253.

12, P.P.Shah, P.R.Desai, A.R.Patel and M.S.Singh, Biomaterials 33 (2012) 1607-1617.

13, W.Zhang, J.Gao, Q.Zhu, M.Zhang, X.Ding, X.Wang, X.Hou, W.Fan, B.Ding, X.Wu, X.Wang and S.Gao, Int.J.Pharm 402 (2010) 205-212.

14, F.Rancan, D.Papakostas, S.Hadam, S.Hackbarth, T.Delair, C.Primard, B.Verrier, W.Sterry, U.Blume-Peytavi and A.Vogt, Pharm Res. 26 (2009) 2027-2036.

15, R.varez-Roman, A.Naik, Y.N.Kalia, R.H.Guy and H.Fessi, Pharm Res. 21 (2004) 1818-1825.

16, Y.S.Nam, J.W.Kim, J.Park, J.Shim, J.S.Lee and S.H.Han, Colloids Surf.B Biointerfaces. 94 (2012) 51-57.

17, C.Rosado, C.Silva and C.P.Reis, Pharm.Dev.Technol. (2012).

18, J.Shim, K.H.Seok, W.S.Park, S.H.Han, J.Kim and I.S.Chang, J.Control Release 97 (2004) 477-484.

19, P.W.Lee, S.H.Hsu, J.S.Tsai, F.R.Chen, P.J.Huang, C.J.Ke, Z.X.Liao, C.W.Hsiao, H.J.Lin and H.W.Sung, Biomaterials 31 (2010) 2425-2434.

20, B.Xue, Y.Wang, X.Tang, P.Xie, Y.Wang, F.Luo, C.Wu and Z.Qian, J.Biomed.Nanotechnol. 8 (2012) 80-89.

21, Z.Teixeira, C.A.Dreiss, M.J.Lawrence, R.K.Heenan, D.Machado, G.Z.Justo, S.S.Guterres and N.Duran, J.Colloid Interface Sci. 382 (2012) 36-47.

22, L.W.Zhang, W.W.Yu, V.L.Colvin and N.A.Monteiro-Riviere, Toxicol.Appl.Pharmacol. 228 (2008) 200-211.

23, D.E.Poree, M.D.Giles, L.B.Lawson, J.He and S.M.Grayson, Biomacromolecules 12 (2011) 898-906.

24, H.K.Cho, J.H.Cho, S.W.Choi and I.W.Cheong, J.Microencapsul. (2012).

25, P.G.Calzavara-Pinton, M.Venturini and R.Sala, J.Eur.Acad.Dermatol.Venereol. 21 (2007) 293-302.

26, C.Fabris, M.Soncin, G.Miotto, L.Fantetti, G.Chiti, D.Dei, G.Roncucci and G.Jori, J.Photochem. Photobiol.B 83 (2006) 48-54.

27, F.C.Rossetti, L.B.Lopes, A.R.Carollo, J.A.Thomazini, A.C.Tedesco and M.V.Bentley, J.Control Release 155 (2011) 400-408.

28, J.G.Souza, G.M.Gelfuso, P.S.Simao, A.C.Borges and R.F.Lopez, Anticancer Drugs 22 (2011) 783-793.

29, E.R.da Silva, Z.M.de Freitas, L.B.Gitirana and E.Ricci-Junior, Drug Dev.Ind.Pharm 37 (2011) 569-575.

30, M.E.Rodriguez, V.E.Diz, J.Awruch and L.E.Dicelio, Photochem.Photobiol. 86 (2010) 513-519.

31, M.Lam, A.H.Hsia, Y.Liu, M.Guo, A.R.Swick, J.C.Berlin, T.S.McCormick, M.E.Kenney, N.L.Oleinick, K.D.Cooper and E.D.Baron, Clin Exp.Dermatol. 36 (2011) 645-651.

32, F.Ungaro, C.Conte, L.Ostacolo, G.Maglio, A.Barbieri, C.Arra, G.Misso, A.Abbruzzese, M.Caraglia and F.Quaglia, Nanomedicine. 8 (2012) 637-646.

33, W.Tang, H.Xu, R.Kopelman and M.A.Philbert, Photochem.Photobiol. 81 (2005) 242-249.

34, W.Abdelwahed, G.Degobert, S.Stainmesse and H.Fessi, Adv.Drug Deliv.Rev. 58 (2006) 1688-1713.

35, J.Pietkiewicz, K.Zielinska, J.Saczko, J.Kulbacka, M.Majkowski and K.A.Wilk, Eur.J.Pharm.Sci. 39 (2010) 322-335.

36, C.Conte, F.Ungaro, G.Maglio, P.Tirino, G.Siracusano, M.T.Sciortino, N.Leone, G.Palma, A.Barbieri, C.Arra, A.Mazzaglia and F.Quaglia, J.Control Release (2013).

37, F.C.Rossetti, L.B.Lopes, A.R.Carollo, J.A.Thomazini, A.C.Tedesco and M.V.Bentley, J.Control Release 155 (2011) 400-408.

38, T.Loftsson and M.Masson, Int.J.Pharm 225 (2001) 15-30.

39, P.Zi, X.Yang, H.Kuang, Y.Yang and L.Yu, Int.J.Pharm. 358 (2008) 151-158.

ANNEX-2: Lipidic nanoemulsions for intravenous administration of nucleic acids

Conte C[1], de la Fuente M[2], Garcia-Fuentes M[2], Csaba N[2], Alonso MJ[2]

[1]Dip. di Farmacia,–Università di Napoli Federico II, Italy , [2]NanoBioFar Group, Center for Research in Molecular Medicine and Chronic Diseases- University of Santiago de Compostela (USC), Spain.

Introduction

Gene therapy has been regarded as a promising and the ultimate cure for many acquired and inherited life-threatening diseases, such as cancer, genetic disorders, etc [1]. Despite the obvious promise shown by nucleic acids as therapeutic agents for cancer, such as small interfering RNA (siRNA), plasmid DNA (pDNA) and oligonucleotides (ODN), a number of problems need to be solved before their use can become commercial therapies. These are essentially their instability in biological media and their poor penetration into cells [2'2-4]. Their mechanism of action, in fact, requires that they reach the cytoplasm, but also on a cellular level, these molecules suffer of a strong degradation by lysosomal hydrolytic enzymes. Lysosomal escape is therefore an important factor for therapeutic effect [5]. Extensive efforts have been focused on overcoming these barriers, and some strategies have been reviewed lately. One approach is a chemical strategy that consists in synthesizing nucleic acids with variations in the natural structure, which give them better resistance in physiological media while conserving the specificity of binding to the target [6'7]. The second is a pharmaceutical technology approach that aims to associate the nucleic acid with appropriate delivery systems, which can protect it from degradation and modify its tissue and cellular distribution to reach the target [8-10]. The vectors for gene delivery are usually divided into two categories: viral and non-viral (or synthetic) vectors. Viruses offer greater efficiency of gene delivery; however, non-viral vectors are preferred due to safety concerns with the viral vectors [11-13]. DNA/cationic lipid (lipoplexes), DNA/cationic polymer (polyplexes) and DNA/cationic polymer/cationic lipid (lipopolyplexes) electrostatic complexes were proposed as non-viral nucleic acids delivery systems [14-16]. The complexes protect the genetic material from degradation by nucleases. Moreover, cellular and local delivery strategies have to deal with the need for internalization, release, and distribution in the proper subcellular compartment. Nevertheless, they have had limited success for in vivo gene downregulation, they have also exhibited a dose-dependent toxicity, and a low colloidal stability under physiological conditions with poor intracellular release of the oligonucleotides.

On these bases, the aim of this work was to design a delivery system with a low toxicity profile that could be applied for a broad range of gene delivery applications, such as pDNA or siRNA delivery. For this purpose, we chose specific biomaterials, which have shown beneficial properties not only from the biocompatibility point of view, but also from the perspective of their efficacy for pDNA delivery.

Lecithin is a mixture of phospholipids with phosphatidylcholine (PC) as a main component (up to 98% w/w). Egg or soy lecithin as well as purified phospholipids aroused for pharmaceutical purposes as components of liposomes, mixed micelles and submicron emulsions [17-19]. Cui et al have proposed the use of lecithin for the design of nucleic acid delivery systems; they have achieved a significant improvement in the stability of a previously reported nanoparticle-based DNA delivery system using the cationic tensioactive CTAB (Cetyltrimethylammonium bromide). A plasmid was adsorbed onto the surface of the lecithin nanoparticles and was successfully transfected to cultured cells; however, this formulation resulted very toxic for the presence of the cationic surfactant [20]. The idea of the present work was to take advantage of lecithin's biocompatibility along with its physicochemical properties for the preparation of lecithin nanoemulsions; these dispersions would be used then as nanocarriers for pDNA and siRNA delivery.

Methods

Preparation of blank nanoemulsion

Blank nanoemulsions were obtained by a modification of the solvent displacement technique. Briefly, an organic phase was formed by dissolving 2 mg of Epikuron 80 (PC 80) or a synthetic lysophospholipid (SLP-1-octadecyl-2-O-methyl-glycero-3-phosphocholine) in 3.2 mL of ethanol, followed by 84 μL of Mygliol 812 with or without the addition of different amounts of Cholesterol and/or DC-cholesterol. This organic phase was added drop by drop to 10 mL of water under magnetic stirring. After 30 minutes of agitation, nanoemulsions were evaporated under vacuum to a final constant volume of 10 mL.

Characterization of nanoemulsion

The hydrodynamic diameter (D_H) and polydispersity index (PI) of nanoemulsions were determined by Photon Correlation Spectroscopy (PCS) using Zetasizer Nano ZS (Malvern Instruments, Malvern, UK). A nanoemulsion dispersion was diluted in Milli-Q water at intensity in the range 10^4-10^6 counts/s and measurements were performed at 25°C on 173° angle. Results are reported as mean D_H of three separate measurements of three different batches (n=9) ± standard deviation (SD). Size of nanoemulsions stored in the dark at 4 °C for 15 days was monitored too.

Zeta potential was determined by analysing NP dispersion in water on a Zetasizer Nano ZS (Malvern Instruments, Malvern, UK). Results are reported as mean of three separate measurements of three different batches (n=3) ± SD.

Haemolysis studies

Haemolysis studies were carried out on blank nanoemulsions based on PC 80 and SLP with or without the presence of Cholesterol and/or DC-cholesterol. After centrifugation of EDTA-treated human blood at 880 x*g* for 5 min, a red blood cells (RBC) dispersion was obtained and diluted with 0.1 M PBS up to a concentration of 10% v/v. The RBC dispersion (0.1 mL) was added to 0.9 mL of the nanoemulsion suspension. The concentrations of the nanoemulsion suspensions varied from 0.01 to 0.7 mg/mL. The sample was incubated at 37 °C for 30 minutes and centrifuged at 1000 x*g* for 10 minutes. The supernatant was collected and analysed for haemoglobin release by spectrophotometry at 416 nm. To obtain 0 and 100% haemolysis, 0.1 mL of RBC dispersion was added to 0.9 mL of PBS and distilled water, respectively. The degree of haemolysis was determined according to the following equation: Haemolysis

(%)= (ABS-ABS_0)/(ABS_{100}-ABS_0) x 100, where ABS_{100} and ABS_0 are the absorbance of the solution at 100% and 0% haemolysis, respectively. Results are reported as mean of three separate measurements of three different batches (n=9) ± SD.

Nanoemulsion stability in human plasma

To determine the stability of nanoemulsion under physiologically relevant conditions, a known amount of nanoemulsion (0.15 mL) was dispersed in 0.5 mL of human plasma and incubated at 37 °C up to 48 hours. Human plasma was obtained by centrifugation of EDTA-treated human blood at 880 x*g* for 5 min. Size measurements of the samples were taken by PCS. The stability of nanoemulsion was demonstrated by the absence of macroscopic aggregates and unchanged of initial particle size.

pDNA and siRNA Association Efficiency

Plasmid DNA (pDNA) or small interfering DNA (siRNA) was adsorbed on the surface of nanoemulsions at 1%, 2.5%,5%, 7.5% or 10% loadings, defined as the percentage between the mass of pDNA and the total mass of lipids (Epikuron 80 and Cholesterol and/or DC-cholesterol) in the formulation (mg of pDNA /100 mg of lipids). For the adsorption procedure, a pDNA solution was added to an isolated nanoemulsion suspension (200 μl) and subsequently vortexed for 30 seconds. Eventually, nanoemulsions were concentrated by vacuum evaporation. Formulations were left at room temperature under magnetic stirring for 1 hour to achieve an optimal interaction of the pDNA with the nanoemulsions.

pDNA- and siRNA-associated nanoemulsions were characterized according to size and zeta potential as detailed previously. Additionally, the association of pDNA to the nanoemulsions was studied by a conventional agarose gel electrophoresis assay (1% agarose, 50 V, 120 min, Sub-Cell GT 96/192, Bio-Rad Laboratories Ltd., England). In order to displace the pDNA adsorbed to the nanoemulsions, a far excess of heparin (12.5 mg/mL) was added to the suspension and the mixture was incubated for 2 hours. pDNA was stained with SYBR Gold by adding 2 μL.

Results and discussion

Preparation and characterization of nanoemulsions

In the last few years, research on the field of gene therapy has focused on the design of several safe non-viral vectors, which are typically based on cationic lipids or polymers, in order to improve the delivery efficiency and therapeutic effect of different nucleic acids. With this idea in mind, in this work we developed a lipidic nanoemulsion intended for intravenous administration, thus testing its properties as potential carrier system of plasmid DNA and small interfering RNA.

For the preparation of nanoemulsions we employed as base materials two different lipids, the amphiphilic phospholipid lecithin (PC 80), widely employed as carrier system, and a synthetic lysophospholipid (SLP) in order to investigate first of all their differences concerning the toxicity profile. Furthermore, we incorporated in the system different amounts of Cholesterol or/and a cationic cholesterol (DC-Chol) in order to obtain formulations with different surface properties. The employment of Chol is due to the recent findings about its ability to enhance the serum stability of lipidic formulations, thus improving resistance to aggregation after intravenous administration [21]. DC-Chol, indeed, is the most widely used cationic lipid in liposome preparation and has been classified as one of the most efficient vectors for the transfection of pDNA into cells and in clinical trials [22,23]. It was widely note, in fact, that the inclusion of cationic lipids in lipid formulations improves the association with polyanionic nucleic acids. Moreover, the presence of a positive surface charge on nucleic acid/lipid particles facilitates binding and uptake by cells in vitro [24,25]. However, in using cationic lipids it is often not clear whether all of the nucleic acid is encapsulated inside a bilayer envelope or whether small complexes of cationic liposome/nucleic acid are formed. Furthermore,when delivery systems bearing a net cationic charge are administered intravenously (i.v.), they exhibit rapid plasma clearance, distribute into lung, liver and spleen [26], and often exhibit liver and hemodynamic toxicities, such as activation of complement and prolongation of clotting times [27,28]. For these reasons, we decided to develop various nanoemulsions with different amounts of Chol and DC-Chol, thus understanding the optimized conditions for an efficient gene binding and delivery as well as a minimal toxicity profile.

Unloaded nanoemulsions based on PC 80 or SLP were prepared by a modified solvent displacement technique, as previously described.

They were characterized for their size, polydispersity index and zeta potential (Table 1).

Table 1. Composition and some properties of unloaded PC 80 and SLP nanoemulsions.

Code	PC 80 (mg)	SLP (mg)	Chol (mg)	DC-Chol (mg)	Mean D_H (nm ± [a]SD)	P.I.	ZP (mV ± [a]SD)
CH: PC 1:5	2	-	0.4	-	191.9±3.9	0.1	-37.7±2.3
CH⁺: PC 1:5	2	-	-	0.4	192.2±5.0	0.1	+40.4±3.9
CH⁺: PC 1:10	2	-	-	0.2	259.8±63.9	0.2	+15.0±5.6
CH/CH⁺: PC A	2	-	0.2	0.2	205.9±11.5	0.2	+19.5±4.7
CH/CH⁺: PC B	2	-	0.3	0.1	precipitation	-	-
CH/CH⁺: PC C	2	-	0.15	0.25	194.8±7.5	0.1	+25.6±5.3
CH/CH⁺: PC D	2	-	0.25	0.15	232.7±5.3	0.2	+22.0±1.4
CH/SLP 1:5	-	2	0.4	-	191.5±2.5	0.1	-26.2±4.5
CH⁺:SLP 1:5	-	2	-	0.4	192.4±5.5	0.1	+26.6±3.2
CH⁺:SLP 5:1	-	0.4	-	2	183.4±5.6	0.1	+24.1±1.8
CH/CH⁺:SLP	-	2	0.25	0.15	192.2±6.5	0.1	+19.7±1.5
SLP	-	2	-	-	206.3±4.1	0.1	-20.5±3.3

[a]SD calculated on three different batches

All the formulations displayed monodispersed populations with a hydrodynamic diameter of around 200 nm. As expected, their zeta potential values were dependent on the type and the amount of Cholesterol used. The presence of Cholesterol induced the formation of an anionic nanoemulsion, whereas the addition of DC-Cholesterol allowed an inversion of the surface charge.

Hemolysis studies

Being designed as injectable nanomedicines, we investigated the cytotoxicity of developed nanoemulsions towards human red blood cells in order to evidence the different behavior of the two lipids. Hemolysis studies on developed unloaded PC and SLP with Cholesterol and/or DC-Cholesterol were carried out. Hemolysis was assessed in the NE concentration range from 0.01 to 0.7 mg/mL. As shown in fig. 1, all the nanoemulsions based on PC did not display significant hemolysis, whereas, a strong hemolytic activity occurred for NE based on SLP. In particular, it's possible to note that the presence of

DC-Chol in the formulations, can control and reduce the toxicity of SLP, probably for the interaction of the cationic cholesterol with the phosphate groups of the synthetic lysophospholipid.
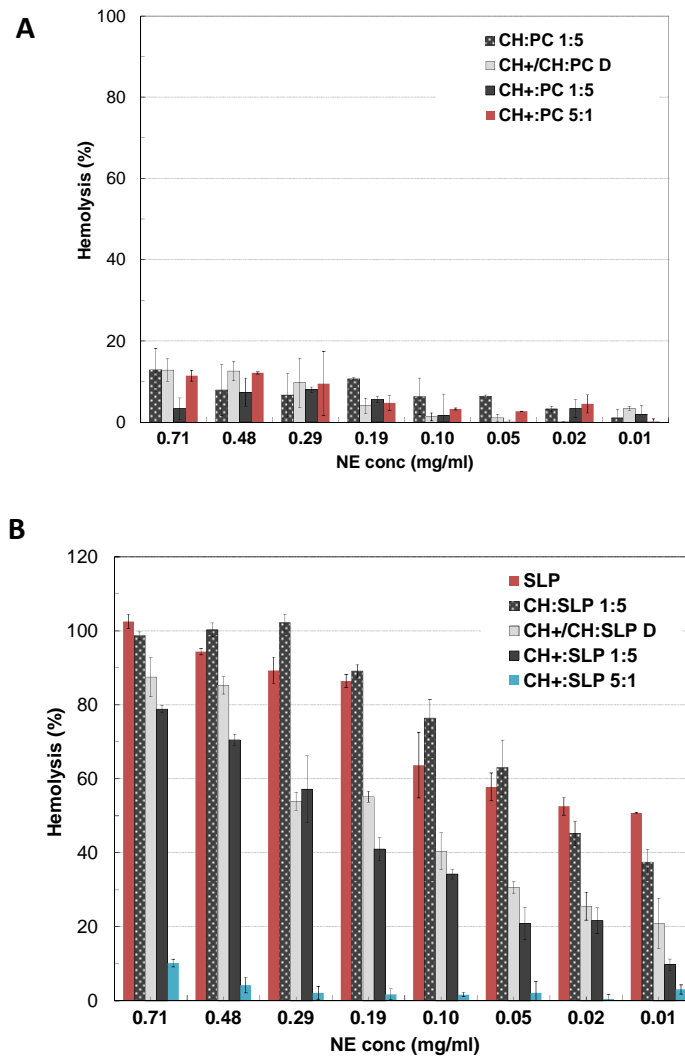
Figure 1 . Hemolysis of red blood cells after incubation with different concentrations of NE based on Epikuron 80 (A) or a synthetic lysophospholipid (B). Data are reported as mean of three independent experiments ± SD.

210

Nanoemulsion stability

On the bases of the results toxicity and the charge of the NEs we selected only formulations based on PC 80 with some specific compositions for evaluating the stability and later studying the association of both pDNA and siRNA. In particular, we selected only three formulations, CH: PC 1:5, CH$^+$: PC 1:5 and CH/CH$^+$: PC D. Their stability in the dark at 4 °C was analyzed. As shown in figure 2, all the formulations displayed a high stability concerning their size and surface properties up to 15 days.
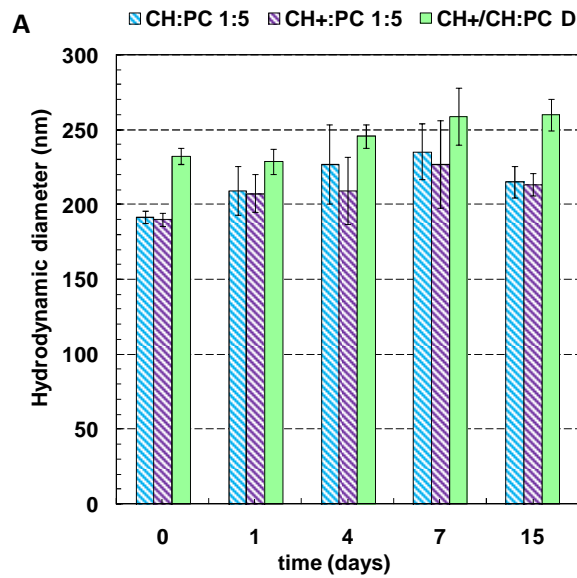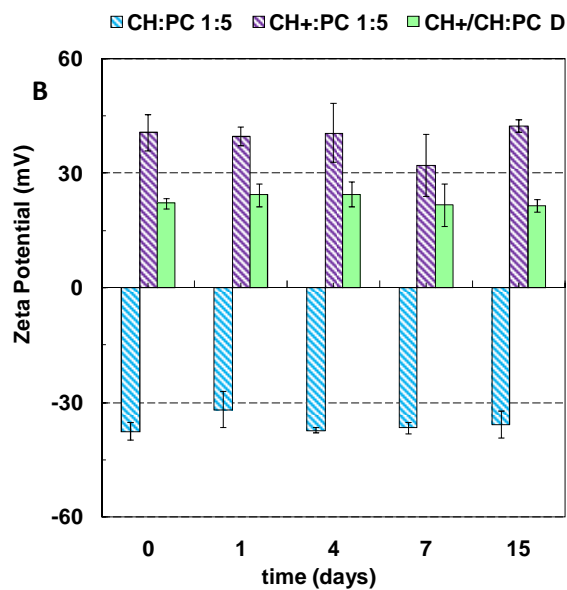
Figure 2. Stability of unloaded PC-nanoemulsions in terms of size (panel A) and zeta potential (B) in the dark at 4 °C.Data are reported as mean of three independent experiments ± SD.

Nanoemulsion stability in human plasma

One of the strongest drawback of a nanomedicine following intravenous administration, is the stability in the biological fluids. In fact, nanocarriers tend to adsorb plasma components such as opsonins, which mediate nanoparticle recognition by monocytes and subsets of tissue macrophages and opsonized nanoparticles tend to be rapidly cleared from the circulation by phagocytic cells of RES.

For this reason, we investigated the stability of NE dispersions in human plasma monitoring the change of their hydrodinamic diameters up to 72 hours of incubation by PCS. The experiment was carry out only on cationic nanoemulsions, being eventually employed in the adsorption of nucleic acids.
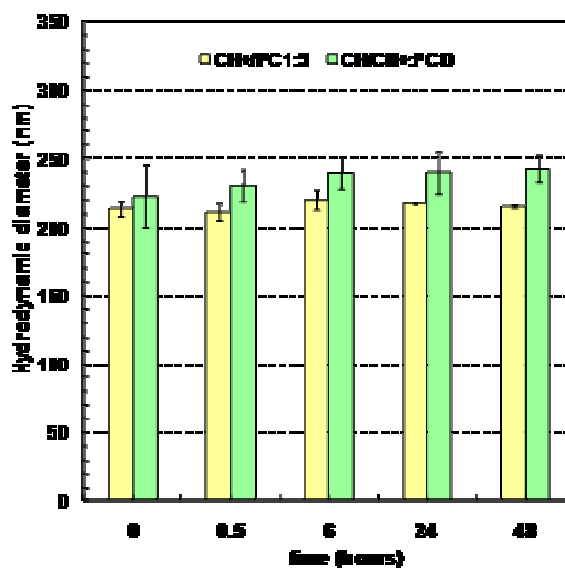
Figure 3. Stability of nanoemulsions in the presence in human plasma (70 µg/mL). Data are reported as mean of three independent experiments ± SD.

As clearly shown in figure 3, both unloaded CH^+:PC and CH/CH^+:PC D nanoemulsions displayed a comparable behavior in the presence of proteins, showing a slight increase of their size, which remained always around 200 nm. On the other hand, results are suggestive that NE do not undergo aggregation or disassembly in biologically-relevant conditions.

pDNA Association Efficiency

Following, the ability of nanoemulsions to interact with plasmid DNA (pDNA) was tested. In particular, pDNA was adsorbed on the surface of the systems at different loadings. pDNA-associated nanoemulsions were then characterized in term of size and zeta potential, whereas the association of the pDNA was determined by gel electrophoresis assays.

Table 2. Properties of pDNA-associated PC 80-nanoemulsions.

Code	pDNA (% w/w)	Mean D_H (nm ± SD)	P.I.	Zeta Potential (mV ± SD)
CH: PC pDNA 5%	5	211.2±6.2	0.2	-27.0±3.5
CH: PC pDNA 7.5%	7.5	215.4±7.1	0.1	-29.4±2.3
CH: PC pDNA 10%	10	216.3±4.0	0.1	-31.4±6.4
CH$^+$: PC pDNA 5%	5	precipitation	-	-
CH$^+$: PC pDNA 7.5%	7.5	213.0±2.4	0.1	-11.9±4.3
CH$^+$: PC pDNA 10%	10	218.7±11.7	0.1	-16.8±5.4
CH/CH$^+$: PC D pDNA 5%	5	233.6±5.5	0.2	-14.2±0.1
CH/CH$^+$: PC D pDNA 7.5%	7.5	223.4±7.6	0.3	-15.4±7.2
CH/CH$^+$: PC D pDNA 10%	10	230.4±26.4	0.1	-19.4±3.0

[a]SD calculated on three different batches

Concerning PC-nanoemulsions containing only Cholesterol, the addition of pDNA did not modify the size and the polydispersity index of the nanodroplets, as shown in Table 2, whereas a strongly inversion of zeta potential was observed, depending of the amount of the pDNA added. Nevertheless, pDNA was not adsorbed on the surface of nanemulsion, as evidenced by gel electrophoresis assay (fig.4).
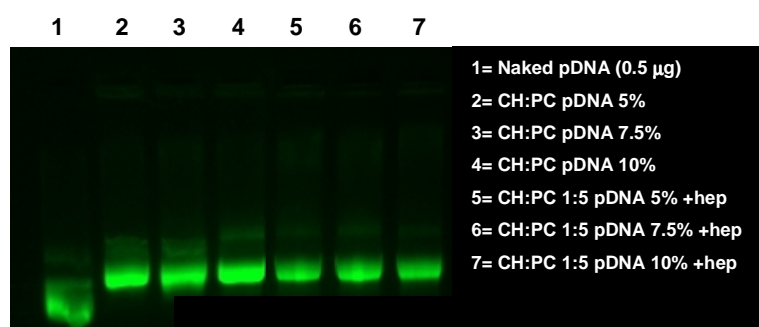
Figure 4. Gel electrophoresis of naked pDNA, pDNA-loaded CH:PC nanoemulsions and at 5%, 7.5% and 10% loading pDNA/nanoemulsions, without and after treatment with heparin.

214

On the contrast, the presence of cationic DC-Cholesterol, as shown in the figure 5, allowed the interaction of pDNA: in particular a slight adsorption at 7.5% theoretical loading, and a complete association at 5% theoretical loading on NE surface was observed, due to the electrostatic binding between the cationic charge of the DC-Chol and the negative charge of the phosphate group of the pDNA. In spite of these results, the addition of pDNA at 5% theoretical loading induced a strong precipitation of the system (table 2).
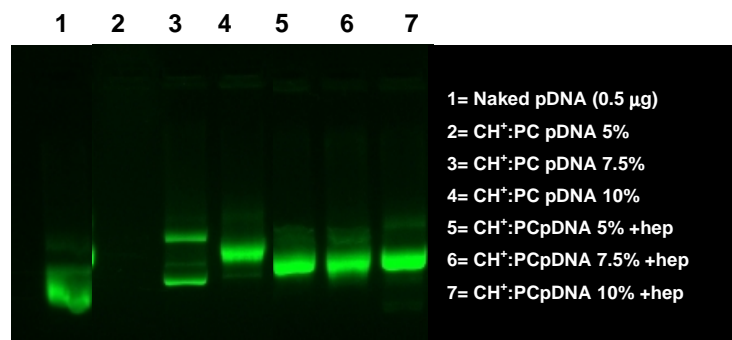
Figure 5. Gel electrophoresis of naked pDNA, pDNA-loaded CH$^+$:PC nanoemulsions and at 5%, 7.5% and 10% loading pDNA/nanoemulsions, without and after treatment with heparin.

Finally, we tested the nanoemulsion containing both Cholesterol and DC-Cholesterol. In this case, we observed good properties in all cases (table 2) and some delay on the pDNA migration that suggest a slight but not complete association of pDNA at 5% theoretical loading (fig. 6).
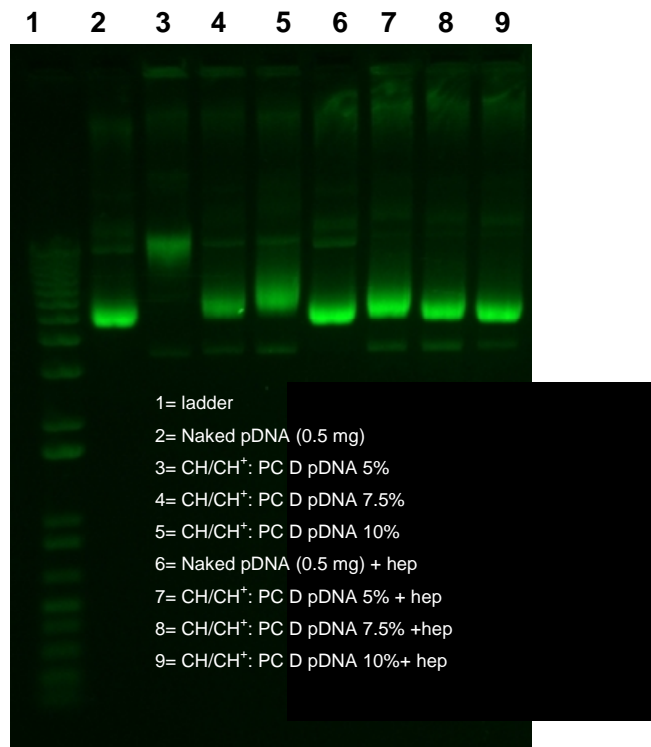
Figure 6. Gel electrophoresis of naked pDNA, pDNA-loaded CH/CH⁺:PC D nanoemulsions and at 5%, 7.5% and 10% loading pDNA/nanoemulsions, without and after treatment with heparin.

On the bases of these preliminary results, we selected the combined CH/CH⁺:PC D nanoemulsion as possible formulation to deliver nucleic acids. Then, we decided to analyze the stability of the pDNA-associated complex. It displayed a high stability in terms of size and zeta potential up to 15 days, as the unloaded formulation (fig. 7).

216
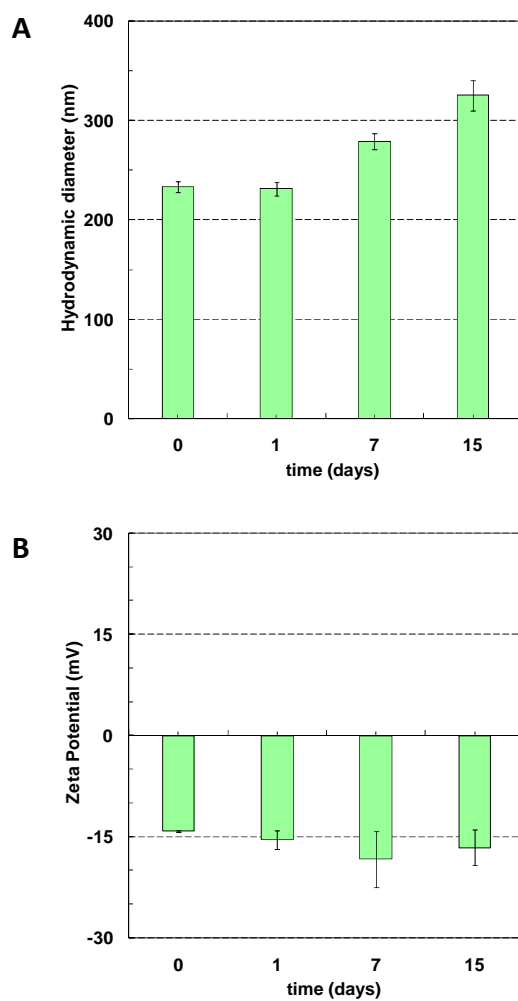
Figure 7. Stability of unloaded CH/CH[+]:PC D pDNA 5% nanoemulsions in terms of size (panel A) and zeta potential (B) in the dark at 4 °C. Data are reported as mean of three independent experiments ± SD.

siRNA-associated nanoemulsions

Small interfering RNAs face similar pharmacokinetic and cell penetration limitations of plasmid DNA. Besides the common delivery tasks, structural and chemical aspects of the pDNA and siRNA molecules also need to be considered. Both are double-stranded nucleic acids with anionic phosphodiester backbones. The negative charge allows electrostatic interactions with cationic polymers or lipids that condense the nucleic acids into polyplexes or lipoplexes with nanometric sizes. However, the ability to form these stable complexes differs greatly because of different properties regarding size, structure and chemistry of the pDNA and siRNA molecules. Plasmid DNA has a size of several kilobp, while siRNA has only about 21 to 23 bp and consequently shows less electrostatic interactions with polycations [29]. Thus, a preliminary formulation study was devoted to test the association of siRNA on PC nanoemulsions and the technological properties of the complexes were evaluated. On the basis of results obtained by the association of pDNA, we selected only the formulations containing the cationic DC-cholesterol, trying to adsorb five different amounts of siRNA.

Table 3. Properties of siRNA-associated PC 80-nanoemulsions.

Code	pDNA (% w/w)	Mean D_H (nm ± [a]SD)	P.I	Zeta Potential (mV ± [a]SD)
CH[+]: PC siRNA 1%	1	210.8±4.7	0.2	24.7±3.9
CH[+]: PC siRNA2.5%	2.5	203.1±2.0	0.1	14.7±3.4
CH[+]: PC siRNA 5%	5	precipitation	-	-
CH[+]: PC siRNA 7.5%	7.5	precipitation	-	-
CH[+]: PC siRNA 10%	10	precipitation	-	-
CH/CH[+]: PC D siRNA 1%	1	precipitation	-	-
CH/CH[+]: PC DsiRNA 2.5%	2.5	precipitation	-	-
CH/CH[+]: PC D siRNA 5%	5	precipitation	-	-
CH/CH[+]: PC DsiRNA 7.5%	7.5	precipitation	-	-
CH/CH[+]: PC DsiRNA 10%	10	precipitation	-	-

[a]SD calculated on three different batches

As evidenced in the table 4, only the CH$^+$:PC nanoemulsion allowed the adsorption of siRNA but at low theoretical loading (1% and 2.5%). In the other cases, in fact, a fast precipitation of the nanoemulsions was observed.

Conclusions

We demonstrated that lipidic nanoemulsions based on the amphiphilic phospholipid lecithin are suitable for iv administration for their high stability in human plasma and the safe profile toward human red blood cells. However, in spite of the presence of a cationic surface, the association of plasmid DNA and small interfering RNA is not too high. Thus, for an eventual clinical application in gene therapy more work still needs to be done to optimize the formulations.

References

1, P.Lam, G.Khan, R.Stripecke, K.M.Hui, N.Kasahara, K.W.Peng and B.A.Guinn, Cancer Gene Ther. (2013).

2, W.Guo, W.Chen, W.Yu, W.Huang and W.Deng, Chin J.Cancer (2013).

3, C.Scholz and E.Wagner, J.Control Release 161 (2012) 554-565.

4, S.D.Li and L.Huang, Gene Ther. 13 (2006) 1313-1319.

5, J.Soutschek, A.Akinc, B.Bramlage, K.Charisse, R.Constien, M.Donoghue, S.Elbashir, A.Geick, P.Hadwiger, J.Harborth, M.John, V.Kesavan, G.Lavine, R.K.Pandey, T.Racie, K.G.Rajeev, I.Rohl, I.Toudjarska, G.Wang, S.Wuschko, D.Bumcrot, V.Koteliansky, S.Limmer, M.Manoharan and H.P.Vornlocher, Nature 432 (2004) 173-178.

6, G.F.Deleavey, J.K.Watts and M.J.Damha, Curr.Protoc.Nucleic Acid Chem. Chapter 16 (2009) Unit.

7, X.Chen, N.Dudgeon, L.Shen and J.H.Wang, Drug Discov.Today 10 (2005) 587-593.

8, C.Y.Hsu and H.Uludag, J.Drug Target 20 (2012) 301-328.

9, K.C.Petkar, S.S.Chavhan, S.Agatonovik-Kustrin and K.K.Sawant, Crit Rev.Ther.Drug Carrier Syst. 28 (2011) 101-164.

10, J.Nguyen and F.C.Szoka, Acc.Chem.Res. 45 (2012) 1153-1162.

11, M.Jafari, M.Soltani, S.Naahidi, D.N.Karunaratne and P.Chen, Curr.Med.Chem. 19 (2012) 197-208.

12, Y.K.Oh and T.G.Park, Adv.Drug Deliv.Rev. 61 (2009) 850-862.

13, E.Wagner, J.BUON. 12 Suppl 1 (2007) S77-S82.

14, d.Tros, I, Y.Sun and N.Duzgunes, Eur.J.Pharm.Sci. 40 (2010) 159-170.

15, S.L.Hart, Cell Biol.Toxicol. 26 (2010) 69-81.

16, K.K.Ewert, A.Zidovska, A.Ahmad, N.F.Bouxsein, H.M.Evans, C.S.McAllister, C.E.Samuel and C.R.Safinya, Top.Curr.Chem. 296 (2010) 191-226.

17, S.Hoeller, A.Sperger and C.Valenta, Int.J.Pharm. 370 (2009) 181-186.

18, F.Bruxel, S.Cojean, A.Bochot, H.Teixeira, C.Bories, P.M.Loiseau and E.Fattal, Int.J.Pharm. 416 (2011) 402-409.

220

19, I.Venkateshwarlu, K.Prabhakar, M.Ali and V.Kishan, PDA.J.Pharm.Sci.Technol. 64 (2010) 233-241.

20, Z.Cui, F.Qiu and B.R.Sloat, Int.J.Pharm. 313 (2006) 206-213.

21, S.Y.Yang, Y.Zheng, J.Y.Chen, Q.Y.Zhang, D.Zhao, D.E.Han and X.J.Chen, Colloids Surf.B Biointerfaces. 101 (2013) 6-13.

22, L.Wasungu and D.Hoekstra, J.Control Release 116 (2006) 255-264.

23, Y.Zhang, H.Li, J.Sun, J.Gao, W.Liu, B.Li, Y.Guo and J.Chen, Int.J.Pharm. 390 (2010) 198-207.

24, C.Lonez, M.Vandenbranden and J.M.Ruysschaert, Prog.Lipid Res. 47 (2008) 340-347.

25, S.Zhang, Y.Xu, B.Wang, W.Qiao, D.Liu and Z.Li, J.Control Release 100 (2004) 165-180.

26, D.C.Litzinger, J.M.Brown, I.Wala, S.A.Kaufman, G.Y.Van, C.L.Farrell and D.Collins, Biochim.Biophys.Acta 1281 (1996) 139-149.

27, L.G.Barron, L.S.Uyechi and F.C.Szoka, Jr., Gene Ther. 6 (1999) 1179-1183.

28, P.Delepine, C.Guillaume, T.Montier, J.C.Clement, J.J.Yaouanc, A.H.Des, F.Berthou, P.A.Le and C.Ferec, J.Gene Med. 5 (2003) 600-608.

29, C.Scholz and E.Wagner, J.Control Release 161 (2012) 554-565.